

A Comparative Study of Long and Short GRBs. I. Overlapping Properties

Ye Li, Bing Zhang, Hou-Jun Lü¹

Department of Physics and Astronomy, University of Nevada, Las Vegas, NV 89154, USA

ABSTRACT

Gamma ray bursts (GRBs) are classified into long and short categories based on their durations. Broad band studies suggest that these two categories of objects roughly correspond to two different classes of progenitor systems, i.e. compact star mergers (Type I) vs. massive star core collapse (Type II). However, the duration criterion sometimes leads to mis-identification of the progenitor systems. We perform a comprehensive multi-wavelength comparative study between duration-defined long GRBs and short GRBs as well as the so-called “consensus” long GRBs and short GRBs (which are believed to be more closely related to the two types of progenitor systems). The parameters we study include two parts: the prompt emission properties including duration (T_{90}), spectral peak energy (E_p), low energy photon index (α), isotropic γ -ray energy ($E_{\gamma,\text{iso}}$), isotropic peak luminosity ($L_{p,\text{iso}}$), and the amplitude parameters (f and f_{eff}); and the host galaxy properties including stellar mass (M_*), star formation rate (SFR), metallicity ([X/H]), half light radius (R_{50}), angular and physical (R_{off}) offset of the afterglow from the center of the host galaxy, the normalized offset ($r_{\text{off}} = R_{\text{off}}/R_{50}$), and the brightness fraction F_{light} . For most parameters, we find interesting overlapping properties between the two populations in both 1D and 2D distribution plots. The three best parameters for the classification purpose are T_{90} , f_{eff} , and F_{light} . However, no single parameter alone is good enough to place a particular burst into the right physical category, suggesting a need of multiple criteria for physical classification.

Subject headings: gamma-ray burst

¹Current address: GXU-NAOC Center for Astrophysics and Space Sciences, Department of Physics, Guangxi University, and Guangxi Key Laboratory for Relativistic Astrophysics, Nanning 530004, China

1. Introduction

The Gamma-Ray Burst (GRB) duration has a bimodal distribution. It had been seen in the early GRB data (Mazets et al. 1981), and was more clearly seen in the GRB sample collected by Burst And Transient Source Experiment (BASTE) on board the Compton Gamma Ray Observatory (CGRO) (Kouveliotou et al. 1993). The division line between the long-duration GRBs (LGRBs) and short-duration GRBs (SGRBs) is around 2 seconds in the BATSE 50 – 300 keV band. Although the significance of this bimodality and the division line depend on the sensitivity and energy band of the detectors (Richardson et al. 1996; Bissaldi et al. 2011; Zhang et al. 2012; Qin et al. 2013), the authenticity of the bimodal T_{90} distribution is confirmed not only with a larger BATSE sample (Meegan et al. 1996; Paciesas et al. 1999), but also by GRB data collected from other instruments such as BeppoSAX (Frontera et al. 2009), INTEGRAL (Foley et al. 2008; Savchenko et al. 2012; Bošnjak et al. 2014), Swift (Sakamoto et al. 2011b) and Fermi (Paciesas et al. 2012; von Kienlin et al. 2014). The existence of two phenomenological classes of GRBs is firmly established. The connection between these two phenomenological classes of GRBs with two physically distinct progenitor systems are theoretical motivated and observationally confirmed through observations of afterglow and host galaxies of both LGRBs and SGRBs.

LGRBs, typically with duration $T_{90} > 2$ s, are supposed to originate from core-collapse of massive stars (Woosley 1993; Paczyński 1998; MacFadyen & Woosley 1999). A direct observational support comes from the associations of some LGRBs with Type Ic supernovae (SNe) (Galama et al. 1998; Hjorth et al. 2003a; Stanek et al. 2003; Woosley & Bloom 2006; Hjorth & Bloom 2012; Xu et al. 2013b). It strongly suggests that LGRBs are related to the death of massive stars, $> 30 M_\odot$ in general. Also, host galaxies of LGRBs are generally dwarf star-forming galaxies with low metallicity, sometimes interacting with other galaxies (Sahu et al. 1997; Bloom et al. 1998, 2002; Chary et al. 2002; Christensen et al. 2004; Savaglio et al. 2009; Krühler et al. 2015). Within their host galaxies, LGRBs are also located in bright star-forming regions with a small offset from the center of the host galaxy (Bloom et al. 2002; Fruchter et al. 2006; Blanchard et al. 2016). Both galactic and subgalactic environments of LGRBs are consistent with an association of LGRBs with recent star formation, supporting the massive star origin of LGRBs.

SGRBs, typically with duration $T_{90} < 2$ s, are believed to be products of compact star mergers, i.e., neutron star - neutron star (NS-NS) or neutron star - black hole (NS-BH) mergers (Paczynski (1986); Eichler et al. (1989); Narayan et al. (1992), see Berger (2014) for a review). Contrary to LGRBs, so far no SN was found associated with any SGRB and the limits for the existence of a SN are 2-7 magnitudes deeper than typical SNe associated with LGRBs (Fox et al. 2005; Hjorth et al. 2005a,b; Kann et al. 2011; Berger et al. 2013).

The absence of SN associations strongly disfavors a massive star origin, but is consistent with the compact star origin of SGRBs. Also, SGRBs reside in diverse types of galaxies, including both late-type galaxies and early-type galaxies, e.g. GRB 050509B (Gehrels et al. 2005) and GRB 050724 (Berger et al. 2005b). The offset of SGRBs from the center of their host galaxy is generally large, which is generally consistent with theoretical prediction of compact star mergers (Fong et al. 2010; Kann et al. 2011; Fong & Berger 2013). The compact star merger origin is also supported by the putative discovery of r-process-powered “kilonovae/macronovae” associated with SGRBs 130603B, 060614, and probably 080503, 050709 as well (Li & Paczyński 1998; Metzger et al. 2010; Tanvir et al. 2013b; Berger et al. 2013; Yang et al. 2015; Gao et al. 2015; Jin et al. 2016).

However, the duration criterion alone is not always reliable to reveal the physical origin of individual GRBs, i.e., a massive star collapsar or a compact star merger. GRB 060614 is classified as a LGRB by duration since its prompt emission shows 4.5-s hard spikes followed by \sim 190 s extended emission (Gehrels et al. 2006; Norris et al. 2010b). However, no SN was found down to hundreds of times less luminous than SN 1998bw, the Type Ic SN associated with GRB 980425 (Gal-Yam et al. 2006; Della Valle et al. 2006; Fynbo et al. 2006). Moreover, its host galaxy is much more passive than normal LGRB host galaxies, and its afterglow is located at a relatively faint position within the host galaxy (Gal-Yam et al. 2006; Fynbo et al. 2006; Blanchard et al. 2016). There is even a putative kilonova associated with it (Yang et al. 2015). The analogy of GRB 060614 with some SGRBs with extended emission allows Zhang et al. (2007) to suggest a compact star merger origin of this apparently long duration GRB. Another nearby long-duration GRB 060505 also showed a similar puzzle: stringent SN limit, low sSFR host galaxy and large offset (Fynbo et al. 2006; Blanchard et al. 2016). On the other hand, GRB 090426 is classified as a SGRB by duration $T_{90} = 1.24$ s. However, it has a blue, star-forming and interacting host galaxy, its afterglow had a small offset with respect to the galaxy, and it is located in the LGRB region in $E_{\text{p,rest}} - E_{\gamma,\text{iso}}$ plot (Antonelli et al. 2009; Levesque et al. 2010b). All these indicate that it might be of a collapsar origin. Indeed, it can be understood as a long GRB with a short-duration “tip-of-iceberg” detected above the background level (Lü et al. 2014).

Motivated by these observations, Zhang (2006) suggested to separate the phenomenological classification scheme (short vs. long) from the physical classification scheme (compact star origin or Type I vs. massive star origin or Type II). Zhang et al. (2009) presented a detailed study of observational and theoretical motivations of connecting various observational properties with progenitor systems, and suggested that one should apply multi-wavelength criteria (including properties of prompt emission, afterglow emission and host galaxy) to judge the physical category of individual GRBs.

In order to apply these multi-wavelength criteria, the first task is to investigate how different/similar the two phenomenological types of GRBs are from each other for each individual observational property. In previous papers, some individual properties of LGRBs and SGRBs have been compared, such as prompt emission properties (Zhang et al. 2012), afterglow properties (Gehrels et al. 2008, 2009; Kann et al. 2010, 2011), and host galaxy properties (Fong & Berger 2013). However, these studies mostly focus on one particular type of properties. In order to get a global understanding of the differences and similarities between LGRBs and SGRBs, we need a comprehensive comparative study of multiple criteria, especially between prompt emission properties and host galaxy properties, both carry important information to diagnose the physical origin of GRBs.

In this paper, we gather prompt emission and host galaxy properties for a large sample of LGRBs and SGRBs detected/observed before June 30th, 2014, and examine how much LGRBs and SGRBs properties overlap with each other. We compare the properties of T_{90} -defined LGRBs and SGRBs, and also the “consensus” LGRBs and SGRBs. The latter are based on the definition in Jochen Greiner’s online catalog,² with SGRBs labeled as ‘S’.³ Some of the bursts in consensus SGRB sample have T_{90} longer than 2 s, so the classification is not based on duration only. It reflects the consensus from the community, which already takes into account multi-wavelength criteria (e.g. spectral lag, host galaxy type, offset) in the definition. In a sense, the consensus classification of short vs. long GRBs are more analogous to physical classification scheme of Type I vs. Type II by Zhang et al. (2009).

The cosmological parameters $H_0 = 71 \text{ km s}^{-1} \text{ Mpc}^{-1}$, $\Omega_m = 0.27$, and $\Omega_\Lambda = 0.73$ are adopted in this paper. The sample and the observational properties we are interested in are presented in Section 2. Section 3 shows the 1D distributions of each parameter for both LGRBs and SGRBs, which show overlapping behaviors. In Section 4, we show a series of 2-D distribution plots, each with a pair of prompt emission vs. host galaxy parameters, and quantify their overlapping properties. We conclude and discuss the implications of these distributions for GRB classification schemes in Section 5.

²<http://www.mpe.mpg.de/~jcg/grbgen.html>

³One exception is GRB 061210, which has a 0.13s spike with a 77s extended emission. It does not have a label ‘S’ in Greiner’s catalog, while other catalogs such as Sakamoto et al. (2011b) classify it as SGRB with extended emission. We use it as a SGRB hereafter.

2. Samples

Our main sample includes 375 GRBs with spectroscopic redshift measurements in the literature before June 30th, 2014. Also included are 32 GRBs with host galaxy information, even though no spectroscopic redshifts have been reported for these bursts. Altogether we have 407 GRBs in total.

Column 2–4 of Table 1 show the redshift, the method of redshift measurement/estimate, and the reference for each GRB in our sample. They are obtained from refereed papers when possible, otherwise GCN circulars. The redshifts of GRBs are usually measured/estimated via host galaxy emission lines (E), afterglow absorption lines (A), or broad band SED fitting based on photometric properties (P). For a few objects such as GRB 050509B, host galaxies spectra are obtained and only absorption lines are detected. They are indicated by ‘HA’. Redshifts measured with emission lines are favored when possible, since absorption lines strictly speaking only give the lower limit of the redshift. When no emission line is detected, we adopt the highest redshift in absorption line systems if no conflict with photometric redshift is claimed. There are 187 GRBs with emission line redshifts, and 188 GRBs with absorption line redshifts. For those GRBs whose spectroscopic redshift is not available but are included in our sample due to their host galaxy information, we list their photometric redshifts (16 GRBs) if available. One object, GRB 080123, has a redshift reported in Leibler & Berger (2010), but no measurement/estimate method is given. There are 15 GRBs included in our sample that do not have any redshift information.

2.1. Prompt Emission properties

2.1.1. Duration

The most basic prompt emission property of GRBs is duration T_{90} , the timescale during which 5% to 95% of its γ -ray fluence is detected. It shows a clear bimodal distribution in the BATSE 50 - 300 keV Band (Kouveliotou et al. 1993), which is used as the criterion to classify SGRBs and LGRBs. Column 6 and 7 of Table 1 present the observed duration the T_{90} and related reference for each GRB. Also shown in Column 5 is the GRB detector from which the T_{90} is derived. For Swift GRBs, T_{90} values are derived in the 15 – 150 keV band, which are obtained from Sakamoto et al. (2011b) when possible, otherwise from the Swift GRB table⁴. For Fermi GRBs without Swift detections, the T_{90} (10 – 1000 keV) values from

⁴http://swift.gsfc.nasa.gov/archive/grb_table/

the Fermi GRB table (von Kienlin et al. 2014) are presented. For GRBs before the Swift era, the T_{90} values from BeppoSAX (Frontera et al. 2009) and HETE-2 (Pé langeon et al. 2008) are adopted when possible. Some GRBs were detected from other detectors, e.g. Konus-Wind, INTEGRAL and Suzaku. Their T_{90} values are obtained from GRB GCN circulars or related publications when available.

2.1.2. Spectral parameters, fluence and flux

The broad band spectra of GRB prompt emission are usually fitted with the so-called “Band function” (Band et al. 1993), which is a smoothly joint broken power law defined by

$$N(E) = \begin{cases} A \left(\frac{E}{100 \text{ keV}} \right)^\alpha \exp \left(-\frac{E}{E_0} \right), & E < (\alpha - \beta)E_0 \\ A \left(\frac{E}{100 \text{ keV}} \right)^\beta \left[\frac{(\alpha - \beta)E_0}{100 \text{ keV}} \right]^{\alpha - \beta} \exp(\beta - \alpha), & E \geq (\alpha - \beta)E_0 \end{cases} \quad (1)$$

where α is low energy photon index, β is high energy photon index and E_0 is the break energy. Instead of E_0 , more frequently quoted is E_p , the peak energy in the energy spectrum $E^2 N$, where $E_p = (2 + \alpha)E_0$. The spectral parameters α , β , and E_p in time-integrated spectra are provided in columns 4 – 6 of Table 2 when Band function fitting is available (Amati et al. 2002; Goldstein et al. 2013). Sometimes not all of these parameters are well constrained, due to the narrowness of the detector’s energy band (Swift/BAT, Sakamoto et al. (2011b)), and the low fluence of the bursts. In these cases, a cutoff power law (CPL) model, which is essentially the first half of Eq.(1), or a simple power law (PL) model

$$N(E) = AE^{-\Gamma}$$

are used for spectral fitting instead. If a CPL fitting is available, the parameters α and E_p are recorded. If the spectrum can be fitted with a PL model without an E_p estimation, the PL index Γ is recorded in the third column of Table 2. The PL Γ shows a systematic difference from Band α (Virgili et al. 2012). For sake of fair comparison, Γ is presented whenever available, regardless of whether α is provided or not.

Table 2 also shows fluence S_γ and peak flux F_p of each GRB, as well as the respective energy band and the detector used to derive them. The fluence S_γ is given as energy fluence, in units of erg cm^{-2} . If not specified, the peak flux is energy flux at the peak time t_p , in units of $\text{erg s}^{-1} \text{ cm}^{-2}$, with a time bin of 1 second. The photon peak flux P_p , in units of photons $\text{s}^{-1} \text{ cm}^{-2}$, is shown with superscript ‘P’. Peak flux from Konus-Wind is usually not binned in 1 second. The binning timescale is labelled in Table 2 using the following convention: 1) 0.004 s; 2) 0.016 s; 3) 0.064 s; 4) 0.128 s; 5) 0.256 s; 6) 2.944 s; 7) 3 s, respectively.

Parameters of BeppoSAX are obtained from Amati et al. (2002) and Frontera et al. (2009) in general. Parameters from BASTE are obtained from Yonetoku et al. (2004) and 5B BASTE catalogue (Goldstein et al. 2013). The 5B BASTE catalogue does not come with traditional GRB names, so we match 5B BASTE catalogue burst IDs with traditional GRB names by requiring the positional difference smaller than 10 degree and a close temporal match (typically the difference less than a few seconds). Spectral parameters from HETE-II are obtained from Sakamoto et al. (2005a) and Pélangeon et al. (2008), covering 2-400 keV in general. Spectral parameters from INTEGRAL are obtained from Bošnjak et al. (2014) and Foley et al. (2008), covering a time span from 2002 to 2012. While Bošnjak et al. (2014) makes a joint IBIS/SPI spectral fit covering 20-1000 keV, spectral fitting in Foley et al. (2008) uses data from IBIS only, covering 20-200 keV. So data from Bošnjak et al. (2014) are favored if parameters of a same burst are provided in both catalogs. Spectral parameters from Fermi/GBM are obtained from the Fermi GRB catalog (Gruber et al. 2014), typically covering 10 - 1000 keV. Sometimes, parameters from Konus-Wind, RHESSI or Suzaku/WAM are used, obtained from GCN circulars in general. Otherwise, Swift BAT parameters are presented, including Γ , fluence and flux for those with PL as the best fit model, and α , E_p , fluence and flux for those with CPL as the best fit model.

2.1.3. $E_{\gamma,\text{iso}}$ and $L_{p,\text{iso}}$

The isotropic gamma-ray energy $E_{\gamma,\text{iso}}$ and peak luminosity $L_{p,\text{iso}}$ in the cosmological rest frame $1 - 10^4$ keV are estimated with parameters presented in the previous sections. The estimated value are shown in Column 8 and 9 of Table 1.

The isotropic energy $E_{\gamma,\text{iso}}$ is estimated as

$$E_{\gamma,\text{iso}} = 4\pi D_L^2 S_\gamma k / (1 + z), \quad (2)$$

where S_γ is the γ -ray fluence, in units of erg cm $^{-2}$, D_L is the luminosity distance estimated with redshift, and k is a k -correction factor from the lab frame to the bolometric rest frame, defined as

$$k = \frac{\int_{1/(1+z)}^{10^4/(1+z)} EN(E)dE}{\int_{e_{\min}}^{e_{\max}} EN(E)dE}. \quad (3)$$

Here e_{\max} and e_{\min} are the observational energy range of fluence, presented in Column 8 of Table 2, $N(E)$ denotes the photon spectrum of GRBs. All the GRB spectra are assumed to be a Band function as shown in Eq. 1, with the spectral parameters listed in Table 2. For those GRBs fitted with a CPL, $\beta = -2.3$ is assumed. For the GRBs with PL fitting only,

the rough correlation between power law index Γ and the peak energy E_p , i.e.

$$\log E_p = (4.34 \pm 0.48) - (1.32 \pm 0.13)\Gamma$$

is used to estimate E_p (Zhang et al. 2007; Sakamoto et al. 2009; Virgili et al. 2012). For bursts without α and β , $\alpha = -1.0$ and $\beta = -2.3$ are assumed for LGRBs, and $\alpha = -0.5$, $\beta = -2.3$ for SGRBs (Band et al. 1993; Preece et al. 2000). For the bursts without redshift estimation, $z = 2$ is assumed for LGRBs, and $z = 0.5$ for SGRBs. One exception is GRB 020410, for which $z = 0.5$ is assumed according to the redshift estimation based on the possible SN detection in Levan et al. (2005).

The peak luminosity $L_{p,\text{iso}}$ is estimated as

$$L_{p,\text{iso}} = 4\pi D_L^2 F_p k, \quad (4)$$

with the same k correction as $E_{\gamma,\text{iso}}$ estimation, and the peak flux F_p in units of $\text{erg s}^{-1} \text{cm}^{-2}$. For GRBs with photon peak flux P_p (in units of $\text{photon s}^{-1} \text{cm}^{-2}$) reported only, F_p is estimated from P_p

$$F_p = P_p \frac{\int_{e_{\min}}^{e_{\max}} EN(E)dE}{\int_{e_{\min}}^{e_{\max}} N(E)dE}, \quad (5)$$

where e_{\max} and e_{\min} define the observational energy range of flux, presented in Column 10 of Table 2.

2.1.4. Amplitude f and f_{eff}

Lü et al. (2014) introduced the amplitude parameters f and f_{eff} to assist classification of GRBs. The f parameter is defined as the ratio between 1-s peak flux and background flux $f = \frac{F_p}{F_B}$, which measures how bright the brightest peak of a burst is above the background level. The effective amplitude parameter is defined as $f_{\text{eff}} = \frac{F'_p}{F_B}$, which is the amplitude of a pseudo GRB which was scaled down from the original burst until the new duration T_{90} is shorter than 2 s. It reflects the measured f value for an intrinsically long GRB to be confused as a short GRB when the bulk of the emission is buried below the background. Since short GRBs already have $T_{90} < 2$ s, their f_{eff} parameter is the same as the f parameter. Lü et al. (2014) showed that the f_{eff} values of long GRBs are typically smaller than 2, which means that the “tip-of-iceberg” effect cannot give very high-amplitude short GRBs. In contrast, short GRBs typically have $f_{\text{eff}} = f$ greater than 2. As a result, the f and f_{eff} parameters are useful parameters to diagnose the physical origin of a burst. We include all the f and f_{eff}

parameters published in Lü et al. (2014)⁵ in our analysis. The f and f_{eff} values of later Swift GRBs are also calculated using the same method of Lü et al. (2014). They are presented in the last two columns of Table 1.

2.2. Host Galaxy Properties

In general, GRB host galaxies can be detected with deep observations after the GRB afterglows fade away. With images of the host galaxies, morphological properties such as galaxy size R_{50} , angular and physical offsets of GRBs from the center of host galaxies, in units of arcsec θ_{off} and kpc R_{off} , as well as normalized offset $r_{\text{off}} = R_{\text{off}}/R_{50}$, can be obtained. If multi color photometric properties are available, especially if the rest frame 4000 Å is covered, the host galaxy stellar mass M_* may be estimated through stellar population syntheses. With emission lines, which are quite common for GRB host galaxies, physical properties such as SFR and metallicity [X/H] can be studied. Together with the stellar mass information, one can estimate specific SFR (sSFR), average SFR per unit stellar mass. We go through the refereed papers and GCN reports related to each GRB to gather host galaxy property information and present them in this section. For each GRB with redshift, we use ADS⁶ to search for papers and reports with the GRB name in the title and abstract, and use SIMBAD⁷ to search for papers and reports that refer to the burst, regardless of in which parts of the paper and reports it is mentioned.

2.2.1. Stellar mass, Star formation rate, and Metallicity

Stellar mass, M_* , which is the main control of luminosity, SFR and metallicity of a galaxy, is the most important host galaxy parameter. It is also used to estimate the specific SFR (sSFR), defined as SFR per unit stellar mass (SFR/M_*), which shows the intrinsic star formation status of a galaxy. Broad band spectral energy distribution (SED) fitting to stellar population synthesis models is the most common method to estimate M_* . For most of the bursts in our sample, the SED-fitted M_* is collected from the catalogs of Savaglio et al. (2009) and Leibler & Berger (2010). Others are obtained from individual papers. When SED estimated M_* is not available, a single band luminosity such as the K band magnitude

⁵ Available at <http://grb.physics.unlv.edu/f/data.txt>

⁶ http://adsabs.harvard.edu/abstract_service.html

⁷ <http://simbad.u-strasbg.fr/simbad/>

(Svensson et al. 2010) or infrared magnitude (Laskar et al. 2011) is used as the indicator of stellar mass. In these cases, the uncertainty is larger than one order of magnitude. For GRBs from Laskar et al. (2011), upper limits of M_* are used when only upper limits are available. For those with detections, $M_{70\text{Myr}}$ are used since 70 Myr is a typical age of LGRB hosts at $z \sim 1$ (Leibler & Berger 2010). The values of M_* and the method to estimate them are presented in column 4 and 5 of Table 3.

SFR indicates average rate of star formation in a “recent” time range. It can be estimated with emission lines, ultra-violet (UV) light, infared (IR), radio, and X-rays (see Kennicutt (1998) and Kennicutt & Evans (2012) for reviews). Among different diagnostics, emission lines such as $\text{H}\alpha$, $\text{H}\beta$, and [OII] represent the most recent 0-10 Myr SFR, best matching the life of LGRB progenitor, stars with $> 30 M_\odot$ (Kennicutt & Evans 2012). Among different emission lines, $\text{H}\alpha$ is the best indicator of SFR, due to its relative strength, small dust extinction and independence of metallicity. However, for objects with redshift larger than 0.4, $\text{H}\alpha$ shifts out of the optical band and requires an infared detection. For these cases, $\text{H}\beta$ and [OII] emission lines become good indicators instead in the optical band, which are applicable up to the redshift 0.9 and 1.4, respectively. The benefit of $\text{H}\beta$ over [OII] is its independence of metallicity. Moustakas et al. (2006) shows that the dependence of [OII] estimated SFR on metallicity is weak in the range of $8.2 < 12+\log(\text{O/H}) < 8.7$, but is significant in the range of $12+\log(\text{O/H}) < 8.2$ and $12+\log(\text{O/H}) > 8.7$. Since a lot of GRB hosts show $12+\log(\text{O/H}) < 8.2$ (Savaglio et al. 2009; Krühler et al. 2015), $\text{H}\beta$ is in general a better indicator than [OII]. However, [OII] is usually stronger than $\text{H}\beta$. So [OII] is more frequently used as the SFR indicator for galaxies with redshifts as high as 1.4. For objects with redshifts higher than 2, the $\text{Ly}\alpha$ emission line shifts into optical and may be used as an SFR indicator (Milvang-Jensen et al. 2012). The SFR and the method used to estimate it are shown in column 6 and 7 of Table 3, with column 3 presenting the instrument offering the spectrum. For those without SFR information, column 3 gives the instruments of spectral observations that provide redshift information. The criteria mentioned above are used.

The two largest LGRB SFR catalogs are from Savaglio et al. (2009) and Krühler et al. (2015). Savaglio et al. (2009) summarized emission line information of GRBs before Dec 2006 and presented a systematic estimation of SFR using $\text{H}\alpha$, $\text{H}\beta$, [OII] and UV, respectively. We record the SFR of each GRB host according to the criteria mentioned above. Krühler et al. (2015) estimated the host galaxy SFR for GRBs later than April 2005, with emission line luminosities obtained from the VLT/X-Shooter spectra. Due to the infared coverage of VLT/X-Shooter, Krühler et al. (2015) extended $\text{H}\alpha$ detection to $z \sim 2.5$. It enables SFR estimation with $\text{H}\alpha$ and better dust extinction A_V estimation. There are only two objects presented in both of these two catalog, GRB 050416A and GRB 051022A, with redshift

0.653 and 0.807 respectively. Krühler et al. (2015) showed that their Balmer decrement estimated A_V are $1.62_{-0.36}^{+0.36}$ mag and $1.86_{-0.13}^{+0.17}$ mag, respectively, and made dust extinction correction with these values. It turns out that the estimated SFR of these two bursts by Krühler et al. (2015) are around two times larger than those estimated by Savaglio et al. (2009), who applied a mean $A_V = 0.53$ to their LGRB sample due to the lack of A_V estimate for both of bursts. As both of GRB 050416A and GRB 051022A have dust extinction A_V much larger than $A_V = 0.53$, the diversity between these two papers can be easily accounted for by the discrepancy of the A_V applied. On the other hand, the average A_V and SFR for the same redshift range are consistent with each other between Krühler et al. (2015) and Savaglio et al. (2009), so that these two GRBs do not indicate statistically inconsistency between these two catalogs.

Two largest SGRB SFR catalogs are from Savaglio et al. (2009) and Berger (2009), each presenting 5 bursts. Three of their host galaxies, GRB 051221, GRB 050709 and GRB 061006, show active star formation with emission lines and their emission-line-estimated SFRs show consistency between these two papers. The other two, GRB 050509B and GRB 050724, have passive hosts without emission lines. While the emission-line-estimated SFR upper limits are < 0.1 and $< 0.05 M_\odot \text{ yr}^{-1}$, respectively (Berger 2009), their UV-estimated SFRs are as high as 16.87 and $18.76 M_\odot \text{ yr}^{-1}$, respectively (Savaglio et al. 2009). The discrepancy could be understood by the difference of the age of stars that emission lines and UV light trace, i.e., $0 - 10$ Myr for emission lines and $10 - 200$ Myr for UV light. Since LGRBs originate from stars with mass $> 30 M_\odot$ and age ~ 10 Myr, emission lines are better diagnostics than UV light. As a result, we do not include UV SFRs in our analysis even though we still list them in Table 3 for completeness.

Metallicity, abundance of elements other than hydrogen and helium, is generally described by the number density ratio between a specific element and hydrogen. It may be estimated with absorption lines or emission lines. Although these two methods provide metallicity estimation for somewhat different regimes in GRB host galaxies, they show consistency in GRB 121024A, which has both emission- and absorption-line estimated metallicities (Friis et al. 2015). The two methods also cover complementary redshift ranges, so we include both of them here. We caution that one needs more objects with both absorption lines and emission lines to provide metallicity estimates to confirm the consistency between the two methods. Metallicities estimated by absorption lines are generally described by $[X/H] = \log(N_X/N_H) - \log(N_{X_\odot}/N_{H_\odot})$, where N_X indicates column density of element X. Metallicities estimated by emission lines, on the other hand, are generally described by $12 + \log(O/H)$, with solar value $12 + \log(O/H)_\odot = 8.69$. In order to be consistent with each other, we convert $12 + \log(O/H)$ to $[X/H]$ with $X = O$ by $12 + \log(O/H) - 8.69$ (Asplund et al. 2009). The estimated values as well as corresponding methods are presented in column 8

and 9 of Table 3.

Emission line ratios are the most common diagnostics for late type galaxy metallicity (Kewley & Dopita 2002; Kobulnicky & Kewley 2004; Pettini & Pagel 2004). This method estimates the metallicities in HII regions of the host galaxy. It is based on photoionisation models (Kewley & Dopita 2002) and local HII region and galaxies observations (Pettini & Pagel 2004). If the host galaxy redshift is larger than 0.2, it is hard to obtain a spatially resolved spectrum of a specific point. Since most GRBs have redshifts greater than 0.2, emission-line-estimated metallicity is generally the luminosity-weighted metallicity of the hosts.

The largest two LGRB samples with metallicity measurements are Savaglio et al. (2009) and Krühler et al. (2015). Savaglio et al. (2009) used different emission line diagnostics for different GRBs, due to different available emission lines. A direct estimation comes from electron temperature T_e , which requires a comparison of different ionization lines with the same elements (Izotov et al. 2006). This is only valid for a few cases where both $[\text{OIII}]\lambda 4363$ and $[\text{OIII}]\lambda 4959, 5007$ are available. For most cases, other indicators with higher uncertainties are generally used. If $\text{H}\alpha$ is detected, for GRBs with $z < 0.4$ in general, $\text{O3N2} = \log\{([\text{OIII}]\lambda 5007/\text{H}\beta)/([\text{NII}]\lambda 6583/\text{H}\alpha)\}$ is used, with (Pettini & Pagel 2004)

$$12 + \log(\text{O/H}) = 8.73 - 0.32 \times \text{O3N2}.$$

If $\text{H}\alpha$ is not available, for most high redshift GRBs,

$$\log R_{23} = \log\{([\text{OII}]\lambda 3727 + [\text{OIII}]\lambda 4959, 5007)/\text{H}\beta\}$$

are used for metallicity estimation, with

$$\log O_{32} = \log\{([\text{OIII}]\lambda 4959, 5007)/([\text{OII}]\lambda 3727)\}$$

as an indicator of the ionization parameter. However, the relation between R_{23} and $12 + \log(\text{O/H})$ is double-valued. Following Kewley & Ellison (2008), equation (18) of Kobulnicky & Kewley (2004) is applied for the upper branch and Kewley & Dopita (2002) for the lower branch. These R_{23} metallicities are corrected to O3N2 values as suggested by Kewley & Ellison (2008). Due to the lack of $[\text{NII}]$, which is usually needed to decouple the double value effect, the two values are sometimes both listed (Savaglio et al. 2009). Krühler et al. (2015) used a combination of the methods by estimating the probability density profile (PDF) of metallicities for each GRB. Benefiting from IR spectra with $\text{H}\alpha$ lines and $[\text{NII}]$ lines, their values do not encounter the double value problem.

The largest SGRB sample is from Berger (2009). The R_{23} method is used and only the upper branch is presented, as suggested by Kobulnicky & Kewley (2004). However, the event

available for O3N2, i.e. GRB 061210, shows $12+\log(\text{O/H})=8.47$ by the method applied in Savaglio et al. (2009), which is 0.35 smaller than the value $12+\log(\text{O/H})=8.82$ estimated with the upper R_{23} branch. It indicates that the upper R_{23} branch method may overestimate the metallicities of SGRB host galaxies, and the diversity of SGRB and LGRB metallicities may not be as significant as shown. However, due to the complexity of metallicity estimation and the lack of $\text{H}\alpha$ and [NII] line information of other three events, GRB 061006, GRB 070724 and GRB 051221A, we still present the values of Berger (2009) in Table 3. We notice here that the true metallicities may be a factor of 0.4 smaller than the listed values. More observations, especially of the IR spectra, are required to verify the metallicities of these SGRBs.

With the absorption line equivalent width (EW) and line profile, column densities of various elements N_X along the line of sight can be estimated (Draine 2011). By comparing with hydrogen column density N_H obtained from $\text{Ly}\alpha$, metallicities $[\text{X}/\text{H}]=\log(N_X/N_H)-\log(N_{X_\odot}/N_{H_\odot})$ can be estimated for various elements X, such as Oxygen. The condition to produce absorption lines is that the probed regions are cooler than those probed with emission lines. These absorption line regions are estimated to be around 100 pc away from GRBs (Vreeswijk et al. 2012; Krühler et al. 2013; D’Elia et al. 2014), so that they can reveal the properties of local environment of GRBs. Since generally the detection of $\text{Ly}\alpha$ absorption line is needed, the absorption line metallicity estimation is generally valid for high redshift GRBs, i.e. $z > 1.8$ in general. If metallicity is estimated for more than one element, the value for most abundant element is recorded, e.g., in the order of O, C, N, Mg, Si, Fe, S (Asplund et al. 2009). The largest absorption line estimated metallicity catalog is from Cucchiara et al. (2015), and other cases are obtained from individual papers. These values are labelled as ‘A’ in the metallicity method column and the specific elements used to estimate it is also recorded. Lower limits for metallicity is usually due to saturation of the absorption lines, e.g., in GRB 140515A. Although these values are lower limits in definition, they are generally used as the metallicity in the literature, so we treat them as the measured metallicity in the rest of the paper. The upper limits are usually due to non-detection of metal lines, e.g. in GRB 140518A.

2.2.2. Morphological properties: galaxy size and offset

Morphological properties of GRB host galaxies are obtained from optical images. Due to the faintness of GRB hosts, it usually requires deep and high angular resolution photometric observations, e.g. with Hubble Space Telescope (HST). The identification of a GRB host galaxy is not straightforward (Bloom et al. 2002; Berger 2010; Church et al. 2011;

Tunnicliffe et al. 2014). If the position uncertainty is large, there might be many galaxies within the error box. Sometimes, especially for SGRBs, the offset of the GRB location from the center of host galaxy may be larger than the size of host galaxy itself, so that it is not straightforward to identify the host galaxy without a probability argument. It is also possible that the host galaxy of a particular GRB is too faint to be detected, but there is a galaxy near the afterglow location by chance, so that it may be mis-identified as the GRB host. Following Bloom et al. (2002), a chance coincidence probability P_{cc} is usually defined as the possibility of a non-host galaxy identified as the host galaxy by chance

$$P_{cc} = 1 - \exp(-\pi r^2 \sigma(\leq m_i)),$$

where $\sigma(\leq m_i)$ is the surface densities of the galaxies with magnitude $\leq m_i$, and r is the effective radius, which is a function of position uncertainty, offset and the size of a candidate host galaxy. In order to indicate how much the candidate host galaxy is trustable, we list the instrument used to take the image, and P_{cc} in column 3 and 4 in Table 4 when possible.

The basic morphological property of host galaxies is size, represented by the half brightness radius R_{50} , which indicates the semi-major axis of the ellipse within which half flux of the entire galaxy is enclosed. Sometimes the host surface brightness is fitted with the Sérsic profile

$$\Sigma(r) = \Sigma_e \exp\{-k_n[(r/r_e)^{1/n} - 1]\},$$

with the effective radius r_e as the size indicator (Wainwright et al. 2007; Fong et al. 2010; Fong & Berger 2013). Sometimes, the size of a host galaxy is defined as the eighty-percent radius R_{80} (Fruchter et al. 2006; Svensson et al. 2010), which is the major axis radius of a similar ellipse that encloses 80 percent of flux. For these cases, we convert R_{80} to R_{50} by assuming that the surface brightness profile of the galaxy is an Sérsic profile. Since nearly all LGRB host galaxies and most SGRB host galaxies are disk (spiral) galaxies, $n = 1$ is assumed. This is equivalent to an exponential profile, which is consistent with the disk galaxy surface density profile. For $n = 1$, one has $R_{50} = R_{80}/1.79$, and $R_{50} = r_e$. The host galaxies of three SGRBs, GRB 050509B, GRB 050724 and GRB 100117A, are obviously elliptical galaxies with $n \sim 4$, so that the conversion factor $R_{50} = 0.968r_e$ is applied. If R_{50} of more than one band is given, the value for the band mostly close to optical is used since the blue band may be affected by dust extinction. Sometimes, no precisely defined radius is available, and only vaguely defined “size” or “radius” are quoted in the literature. In these cases, we treat them as R_{80} which covers most flux of galaxy. R_{50} in units of arcsec and kpc are presented in column 5 and 6 of Table 4. The parameter n is also presented in column 7 when possible. Some GRBs with angular R_{50} values do not have redshift detections. For these cases, $z = 0.5$ for SGRBs and $z = 2.0$ for LGRBs are assumed to estimate physical size of the galaxy.

Angular and physical offsets, the angular/physical separation of a GRB from the center of its host galaxy, are given in column 8 and 9 of Table 4, in units of arcseconds and kpc, respectively. If an offset is smaller than the positional uncertainty of the GRB or host galaxy, an upper limit is given. The largest samples of LGRB offsets are from Bloom et al. (2002) and Blanchard et al. (2016), and the largest SGRB offset samples are from Fong et al. (2010) and Fong & Berger (2013). For GRBs from Table 2 of Perley et al. (2013), the angular distance between the afterglow and the host galaxy is used to define the offset. Similar to R_{50} , $z = 0.5$ for SGRB and $z = 2.0$ for LGRB are also assumed for those without redshift detections. In some problems, one cares more about the relative offset with respect to the size of the host galaxy. The normalized offset (the true offset normalized to R_{50} of the host galaxy) is shown in column 10 of Table 4.

Many GRB hosts are irregular and interacting galaxies. For these, the size R_{50} , the center, and hence, the offset of the galaxy are not well defined. In these cases, the fraction of brightness F_{light} , which is the ratio between the area of the host fainter than the GRB position and the area of the entire host galaxy, is defined. It delineates how bright the GRB location is relative to the other regions of the host galaxy, and reveals the local SFR, especially if the UV band image is used. The largest LGRB F_{light} samples are from Fruchter et al. (2006), Svensson et al. (2010) and Blanchard et al. (2016), and the largest SGRB F_{light} samples are from Fong et al. (2010) and Fong & Berger (2013). Others are collected from individual papers. The parameter F_{light} is given in column 11 of Table 4. $F_{\text{light}} = 1$ indicates that the GRB is located in the brightest region of the host, and $F_{\text{light}} = 0$ indicates that the GRB is in the faintest region of the host.

3. Distribution of properties

With the comprehensive prompt and host galaxy properties in Table 1, 2, 3 and 4, we are able to study the differences and similarities of LGRBs and SGRBs. We present the distributions of both LGRBs and SGRBs for each property in this section. The histograms are shown in Fig. 1, and the statistical results are presented in Table 5 and Table 6. In all the figures, LGRBs are shown in red and SGRBs in blue. In Fig. 1, the histograms of all the GRBs are presented in black. Dotted lines show objects with redshift $z < 1.4$, within which most SGRBs are located. Inspecting this sample allows one to compare SGRBs to LGRBs in the similar redshift range, and examine the influence of redshift on each parameter. In the left column of all the figures, LGRBs and SGRBs are defined by the “consensus” criteria, i.e., GRBs with label “S” in Greiner’s catalog are defined as SGRBs, otherwise LGRBs. Their statistical results are shown in Table 5. In the right column of all figures, LGRBs and

SGRBs are defined by T_{90} only, i.e., GRBs with $T_{90} < 2$ s are defined as SGRBs, otherwise LGRBs. Their statistical results are shown in Table 6. In Table 5 and 6, the numbers of LGRBs and SGRBs with each parameter are given in column 2 and 4. The median values and dispersion of them are given in column 3 and 5.

In order to investigate how different the LGRB sample is from the SGRB sample, we employ the Kolmogorov-Smirnov test (KS test), and examine the fraction of LGRBs and SGRBs overlapping with each other. Column 6 of Table 5 and 6 show the null probability P_{KS} of KS test between LGRBs and SGRBs for these two definitions of SGRBs and LGRBs, respectively. The smaller P_{KS} is, the more different LGRBs and SGRBs are from each other for that particular property. The overlapping range of each parameter is shown in column 7 of both tables. The fractions of LGRBs and SGRBs located in the overlapping region (defined as “overlapping fraction” hereafter) are presented in column 8 and 9. In the following, we discuss each property in detail.

The redshift distributions of the consensus and T_{90} -defined LGRBs and SGRBs are presented in the left and right column of Fig. 1, Row 1. Photometric redshifts are not included. It is apparent that SGRBs show a much lower redshift distribution than LGRBs, with $z_{\text{SGRB}} = 0.45 \pm 0.51$ as compared with $z_{\text{LGRB}} = 1.64 \pm 1.30$. The highest-redshift GRB in our sample is GRB 090423, with $z = 8.23$ obtained from absorption lines (Tanvir et al. 2009a; Salvaterra et al. 2009). GRB 090429B has a photometric redshift $z = 9.2$ (Cucchiara et al. 2011c) without absorption/emission lines, and there is no host galaxy information available. It is not included in our sample according to our primary selection criteria given in Section 2. The highest redshift SGRB is GRB 090426, which is an ambiguous event with $T_{90} = 1.24$ s (Antonelli et al. 2009; Levesque et al. 2010b). If it is considered as a short GRB based on the duration criterion, the overlapping fraction of LGRB redshift is as large as 72 %. If it is classified as a Type II GRB based on other information (and hence join the LGRB sample), the LGRB overlapping fraction in redshift is 29 %. Consensus SGRBs have less high redshift objects than T_{90} -defined SGRBs, which results in a smaller P_{KS} and indicates more significant difference between the two groups. Note that even with a redshift cut $z < 1.4$, LGRBs still show a higher median redshift than SGRBs, due to the dominance of high redshift events over low redshift events in this LGRBs sub-sample.

3.1. Prompt emission properties

Duration T_{90} denotes the (observed) time scale of GRB explosions. Physically, Type I GRBs, which have a neutron-star dense accretion torus from the debris of NS-NS or NS-BH mergers, have a small free-fall time scale to allow short-duration GRBs. Type II GRBs,

on the other hand, having an extended stellar envelop with stellar density, have a free-fall time scale longer than several seconds, which is natural to explain long-duration GRBs. The distributions of T_{90} for the consensus and T_{90} -defined LGRBs and SGRBs are presented in the left and right panels of Figure 1, Row 2, respectively. The T_{90} distribution of the entire GRB population (both LGRBs and SGRBs) (black lines) show a peak around 50 s and a flat tail in the range smaller than 2 s. The bimodality is not as significant as in the BATSE sample (Kouveliotou et al. 1993), due to the dominance of LGRBs. The dominance of LGRBs is a result of the dominance of the Swift sample, since 325/407 events in our sample are discovered by Swift, and Swift is dominated by LGRBs due to its insensitivity to SGRBs (Sakamoto et al. 2011b; Qin et al. 2013). For T_{90} -defined LGRBs (red solid line) and SGRBs (blue solid line), the T_{90} criterion gives the lowest P_{KS} among all the parameters as shown in Table 5 and 6, i.e. $\sim 10^{-27}$. This is simply because the definitions of LGRBs and SGRBs are based on the duration criterion. For the consensus LGRB and SGRB samples, the SGRB T_{90} distribution extends to as long as 5.66 s, GRB 090510, and the LGRB T_{90} distribution extends to as short as 1.30 s, GRB 000926. Such an overlap increases P_{KS} by one order of magnitude but still allows a very low P_{KS} value, suggesting that the T_{90} criterion is truly a good indicator to separate the two physically distinct populations. The significant overlap in the T_{90} properties (7% in LGRBs and 20% in SGRBs), on the other hand, suggests that other properties are needed to correctly place a certain GRB into the right physical category (Type I vs. Type II).

Isotropic gamma-ray energy $E_{\gamma,\text{iso}}$ gives a rough indicator of the energy budget of a GRB. In the BH central engine scenario, the total energy budget is related to the total material available for accretion. Type II GRBs, having plenty of fuel from the massive star progenitor ($M > 30M_{\odot}$ for the total mass budget), are expected to be more energetic than Type I GRBs, which are related to compact star mergers ($M \sim (2 - 3)M_{\odot}$ for the total mass budget). In the magnetar scenario, some energy from a NS-NS merger may be released in the form of gravitational waves (GWs) or falls into the collapsed BH, resulting in less energetic Type I GRBs than Type II GRBs (e.g. Gao et al. 2016). Observationally, our sample shows that the $E_{\gamma,\text{iso}}$ distribution of LGRBs is nearly a Gaussian, with an extremely low energy tail extending to 10^{47} erg. The LGRBs with $E_{\gamma,\text{iso}} < 10^{49}$ erg are usually defined as low luminosity GRBs (llGRBs), probably with a somewhat different physical origin from normal LGRBs (Campana et al. 2006; Soderberg et al. 2006b; Liang et al. 2007; Virgili et al. 2009; Bromberg et al. 2011; Sun et al. 2015). Due to their rareness, the inclusion of llGRBs does not significantly influence the median $E_{\gamma,\text{iso}}$ and the overlapping fraction of LGRBs. Nearly all SGRBs have $E_{\gamma,\text{iso}} > 10^{49}$ erg, so the inclusion of llGRBs does not influence the overlapping fraction with SGRBs much, either. The median $E_{\gamma,\text{iso}}$ of SGRBs is about 1.6 dex lower than the entire sample of LGRBs, and P_{KS} of the $E_{\gamma,\text{iso}}$ criterion is as significant

as 10^{-14} . However, the low redshift LGRBs shows a 0.5 dex smaller $E_{\gamma,\text{iso}}$, making P_{KS} eight orders of magnitude larger (but still small) if one focuses on the $z < 1.4$ sample. Due to their wide distributions ($\sigma=1.0$ dex), the SGRBs and LGRBs show significant overlap in the $E_{\gamma,\text{iso}}$ domain. If there were no duration information, SGRBs look like the low energy tail of LGRBs, suggesting that the $E_{\gamma,\text{iso}}$ property alone is not a good criterion to differentiate between the two populations.

The typical peak luminosity $L_{\text{p},\text{iso}}$ of LGRBs is about 0.8 dex larger than that of SGRBs. However, due to the large dispersion, 1.1 dex, the difference between these two samples is not significant, either, with $P_{\text{KS}} = 0.007$. LGRBs at $z < 1.4$ have 0.6 dex smaller $L_{\text{p},\text{iso}}$ than the entire LGRB sample, making it more difficult to apply the $L_{\text{p},\text{iso}}$ criterion for classification. This is consistent with Zhang et al. (2009) and Ghirlanda et al. (2009), who showed that LGRBs and SGRBs have similar $L_{\text{p},\text{iso}}$, and their differences in $E_{\gamma,\text{iso}}$ is mostly due to different durations.

It has been long known that LGRBs have softer spectra than SGRBs. Theoretically, such a connection is not straightforward and is model dependent (e.g. Zhang et al. 2009 for a detailed discussion), but it may be somewhat related to a possible higher Lorentz factor in SGRBs, originating from a relatively cleaner environment of Type I GRBs. The hardness of a spectrum is a combination effect of the peak energy E_{p} , and the low energy photon index α . Consistent with previous work, LGRB α is -1.01 ± 0.34 , softer than that of SGRBs, $\alpha = -0.60 \pm 0.25$. The difference between them is moderately strong, with $P_{\text{KS}} = 10^{-7}$. The E_{p} center value of LGRBs is 0.49 dex smaller than SGRBs, and the two samples have about 80% overlaps, which shows a moderately strong difference between LGRBs and SGRBs.

The amplitude parameter f shows 43% LGRBs and 100% SGRBs within the overlap region, The K-S test gives $P_{\text{KS}} \sim 10^{-7}$, indicating a moderately strong difference between LGRBs and SGRBs. As suggested by Lü et al. (2014), the f_{eff} is expected to be a better indicator. Our analysis shows $P_{\text{KS}} \sim 10^{-20}$ between LGRBs and SGRBs, which is indeed a good indicator. It is still not as significant as the T_{90} criterion, due to the smaller sample of f_{eff} than T_{90} . The LGRB and SGRB overlapping fractions of f_{eff} are 7% and 79% in the consensus samples. GRB 130427A, which has the largest $f_{\text{eff}} = 4.75$ is an obvious outlier. It shows an intense initial pulse with a weak tail in Swift/BAT while the peak is not significant in Fermi/GBM. If excluding it from the LGRB sample, The LGRB and SGRB overlapping fractions of f_{eff} are 7% and 48%, respectively.

3.2. Host galaxy properties

3.2.1. Stellar mass, Star formation rate, and metallicity

The properties of galaxies are mainly controlled by their stellar mass M_* (van der Wel et al. 2014; Ilbert et al. 2015). Host galaxy masses of the consensus and T_{90} -defined LGRBs and SGRBs are presented in the left and right columns of Fig. 1, Row 9. In order to be consistent, only stellar masses obtained with SED fitting are used here. Most SGRB and LGRB host galaxies are smaller than the turnover mass of galaxies extending to redshift 3 (Mortlock et al. 2015). Although the median of SGRB hosts is 0.6 dex larger than that of all LGRB hosts, their difference is not statistically significant. LGRB hosts with $z < 1.4$ show a 0.2 dex lower stellar mass than the whole sample. It may be a selection effect, since the galaxies with larger stellar masses are brighter and easier to be observed at high redshifts. It makes the low- z LGRBs more significantly different from SGRBs. Since the median redshift of low- z LGRBs is still larger than that of SGRBs, a true same-redshift comparison between LGRB and SGRB host stellar masses should show even more significant differences. Also, it indicates that there should be more small stellar mass host galaxies that are not been discovered yet, especially in the high redshift range. The overlapping fractions are around 90% for both LGRBs and SGRBs. The results of the consensus and T_{90} -defined LGRB and SGRB samples are consistent with each other.

The SFR represents the global star formation status of the entire galaxy. It is expected to be large in LGRB hosts, since LGRBs are presumed to be massive star collapsars and are expected to be associate with star formation. SGRBs are believed to be related to compact star mergers, so at least some of them are expected to be associated with the old stellar populations and no recent star formation is required for the presence of SGRBs. SFR of consensus and T_{90} -defined LGRBs and SGRBs are presented in Fig. 1, Row 10. In order to be consistent, only SFRs obtained with emission lines are used. The median SFR of LGRBs is around 0.4 dex larger than that of SGRBs, although their difference is not statistically significant, due to the large dispersion, both around 0.8 dex. It may be also due to the generally more massive host galaxies of SGRBs, since SFR is proportional to the stellar mass of the galaxies. The low- z LGRB hosts are similar to those of low- z SGRBs. It may be a result of the decrease of the LGRB host mass at low redshifts. Both LGRBs and SGRBs show around 90% overlapping fraction for SFR. The T_{90} -defined samples show even less difference and larger overlaps, suggesting the limitation of T_{90} to define the physical category of GRBs.

In the sample of the consensus SGRBs, the one with an extremely large SFR is GRB 100816A. Its T_{90} is reported to be 2.9 s in the Swift GRB table and 1.99 s in Pérez-Ramírez et al.

(2013). With a small spectral lag 10 ± 25 ms(Norris et al. 2010a), it is suggested to be a SGRB in Greiner’s catalog. Considering its high SFR (Kröhler et al. 2015) and possible interacting nature of the host galaxy (Tanvir et al. 2010b), we would suggest it to be still a Type II GRB. We still keep it in the consensus SGRB sample based on our sample selection criterion. Changing it to the consensus LGRB sample makes the median log(SFR) of SGRB to be 0.08, i.e., $1.2 M_{\odot} \text{ yr}^{-1}$, with a dispersion 0.71, and results in a lower P_{KS} 0.04 for this criterion.

For the bursts with both SFR and stellar mass M_* , specific SFR ($\text{sSFR} = \text{SFR}/M_*$) of the host galaxy is available. Since sSFR describes SFR per unit stellar mass, it is a more relevant parameter to describe the star formation status in the GRB location. The distributions of sSFRs are presented in Fig. 1, Row 11. sSFR shows a more significant difference between LGRBs and SGRBs than SFR. In general, the sSFR of LGRBs is 0.5 dex higher than SGRBs. The redshift evolution of the sSFR for the LGRB host is not significant, even though the redshift evolution of sSFR of the entire universe is apparent, with a peak at $z = 2 - 3$. This may indicate that sSFR is directly related to the LGRB rate. Another factor might be the selection effects. Since the massive hosts with less sSFRs are easier detected, high redshift samples should on average show smaller sSFRs relative to the true distribution. The T_{90} -defined sample shows a 0.3 dex less difference than the consensus sample, again indicating the limitation of the T_{90} -only criterion.

In the consensus LGRB sample, the GRB with the lowest sSFR, 0.006 Gyr^{-1} , is GRB 050219A (Rossi et al. 2014). Its host was discovered by GROND and confirmed by VLT. No HST image is available. It is an elliptical galaxy $4.6''$ away from the GRB XRT location, with a $1.9''$ positional uncertainty. The estimated chance coincide probability is $P_{\text{cc}} = 0.8\%$. If we exclude GRB 050219, the LGRB sSFR becomes $0.05 \pm 0.62 \text{ Gyr}^{-1}$ and $P_{\text{KS}} = 0.01$. The overlap range becomes $(-1.17, 1.05)$ and the overlapping fraction becomes 90% and 78% for the consensus LGRBs and SGRBs, respectively.

LGRB progenitor models prefer a low metallicity environment, since it would keep enough angular momentum in the core the star to launch a jet. On the other hand, no metallicity limitation is required for SGRBs. The distributions of metallicity [X/H] of the consensus and T_{90} -defined LGRBs and SGRBs are presented in the left and right columns of Fig. 1, Row 12. If one event has double values, the average value is plotted. For the consensus samples, SGRBs show a 0.5 dex richer metallicity than LGRBs, and are consistent with the highest end of the consensus LGRBs. The P_{KS} value is 0.0007, indicating a relatively significant difference. The overlapping fractions are 47% and 100% for LGRBs and SGRBs, respectively, which is as low as that of the amplitude parameter f . However, the $z < 1.4$ LGRB sample is much metal richer than the whole LGRB sample. In this redshift range, the

difference between median LGRBs and SGRBs becomes 0.3 dex, and the overlapping fraction of LGRBs increases to 73%. Since the average redshift of low- z LGRBs is still higher than SGRBs, and metallicity from Berger (2009) may overestimate the SGRB metallicity, the difference between SGRBs and LGRBs in the same redshift bin may be even milder. This makes metallicity not a good indicator of the physical origin of individual GRBs.

3.2.2. Morphological properties: galaxy size and Offset

Galaxy size is correlated with stellar mass, according to the galaxy types (van der Wel et al. 2014). The R_{50} distributions of the consensus and T_{90} -defined LGRB and SGRB samples are presented in Fig. 1, Row 13. The LGRB host size is typically 0.31 dex smaller than that of SGRBs in the consensus samples, with a small $P_{\text{KS}} = 4 \times 10^{-4}$. The overlapping fraction of LGRBs is $\sim 69\%$. For $z < 1.4$, the R_{50} distribution of LGRB hosts is consistent with that of the whole sample, only 0.06 index larger. However, due to shrinkage of the sample size, The P_{KS} value is one order of magnitude larger. The T_{90} defined SGRB sample includes more small size hosts, again indicating the limitation of the T_{90} criterion.

SGRB offsets are expected to be larger than LGRBs, since the explosion of SNe that formed the NSs and BHs in the merger systems would have given the system two kicks, so that the system may have a large offset from the original birth location in the host galaxy. The cumulative offset distribution of SGRBs indeed differ from that of LGRBs (Fong et al. 2010; Fong & Berger 2013; Berger 2014). Our analysis shows that the typical physical offset of SGRBs, in units of kpc, is 0.77 dex larger than that of LGRBs. The KS test gives $P_{\text{KS}} = 10^{-4}$. However, the overlapping fractions of both LGRBs and SGRBs are as large as 80%. Only 5 of the 28 SGRBs show offsets larger than all LGRBs. The redshift evolution of the offsets is not significant. At $z < 1.4$, LGRBs have the same median physical offset as the whole sample.

The offset normalized to the host size R_{50} is a more physical parameter to delineate the location of a SGRB within the host galaxy. Also, normalized offset does not require the measurements of the absolute values of the offset and host size, so one can include events without redshift measurements as well. The normalized offset distributions are presented in Fig. 1, Row 15. In general, SGRBs are 0.27 dex larger than LGRBs, and mildly different with $P_{\text{KS}}=0.02$. No redshift evolution is seen. Only 3 SGRBs have normalized offset larger than all LGRBs, and only 8 LGRBs have normalized offset smaller than all SGRBs. The overlapping fractions are as high as 90%.

The surface brightness fraction F_{light} is expected to be large for LGRBs since they are

believed to be associated with the highest local SFR in the galaxy. The F_{light} of SGRBs is expected to be small since compact star mergers usually are expected to be kicked from the star forming regions by the time the merger happens. It is also a parameter that does not require a redshift measurement. They are presented in the last row of Fig. 1. It can be seen that SGRBs tend to be located in the faint regions of their hosts and LGRBs tend to be located in the bright regions of their hosts. A SGRB within the brightest region of its host is the ambiguous GRB 090426, which has $F_{\text{light}} = 0.82$. Although the numbers of both consensus SGRBs and LGRBs with F_{light} measurement are relatively small, F_{light} shows the most significant difference between the two types of GRBs in the host galaxy properties, with $P_{\text{KS}} = 7 \times 10^{-5}$. The regions where LGRBs are located are 60% fraction brighter than the regions where SGRBs reside. Excluding GRB 090426, the overlapping fractions become 48% and 100% for LGRB and SGRBs. At $z < 1.4$, LGRBs are located in even brighter regions of their hosts, and SGRBs are located in even fainter regions due to the exclusion of ambiguous GRB 090426. It makes the difference between LGRBs and SGRBs even more significant, and the overlapping fractions are as low as 40%. It is one of the best physical origin indicator candidates. Similar to other parameters, T_{90} -defined samples show less difference between LGRBs and SGRBs.

3.3. Simulated 1-D distribution

The KS test provides a statistical judgement about how different two groups of data are. By definition, it is sensitive to the sample size, the number of objects within each group. T_{90} has the largest sample size among all the tested properties, with 403 in total, so it is easier to show more significant differences, with very small P_{KS} values. Physically, however, we want to examine how efficient each property of GRB is for distinguishing SGRBs from LGRBs. It is a fair comparison only if we use equal sample size for each property. We then simulate 400 GRBs (which is roughly the T_{90} sample size) for each property, based on the observational sample we already have.

The simulated numbers of LGRBs and SGRBs, median and dispersion of each property, and null probability of the KS test are presented in Table 7.⁸ For each property, the sum of the LGRB and SGRB numbers are 400. The median and dispersion of each property are generally the same as the observed sample. According to P_{KS} , f_{eff} shows the most significant difference between LGRB and SGRBs, $P_{\text{KS}} \sim 10^{-38}$. This suggests that f_{eff} is the most

⁸Although the absolute P_{KS} value depends on the seed of random generator, the relative significance of difference physical parameters do not change.

efficient criterion for LGRB and SGRB classification, even better than T_{90} . Besides T_{90} and f_{eff} , two prompt emission properties, the host galaxy property F_{light} shows $P_{\text{KS}} = 4 \times 10^{-19}$, In the $z < 1.4$ sample, F_{light} shows an even more significant difference between LGRBs and SGRBs, with $P_{\text{KS}} = 4 \times 10^{-32}$. It suggests that F_{light} , as a representative of the host galaxy properties, is also a good indicator of LGRB and SGRB classification. Besides these, f , α , $E_{\gamma,\text{iso}}$, physical offsets, and size of the host galaxy R_{50} also show significant differences between LGRBs and SGRBs. However, opposite to common sense, SFR does not show a significant difference between the two classes. This may be due to the generally larger mass of SGRB host galaxies, which compensate their relatively low sSFR. On the other hand, the 8% to 100% overlapping fractions of each parameter do not change with the sample size. As a result, multiple parameters are always needed to tell the physical categories of GRBs.

4. 2-D distributions of the properties

Two-dimensional distributions of properties play an important role in classifications of astronomical objects. A famous example is the Hertzsprung - Russell diagram for stars. In GRBs, the duration - hardness ratio plot played an important role of defining LGRBs and SGRBs (e.g. Kouveliotou et al. 1993).

Since in this paper we perform a joint analysis between prompt emission properties and host galaxy properties of GRBs, it is interesting to investigate these two types of properties in pairs in 2-D distribution plots. This would allow us to investigate whether there are distinct 2-D distribution plots that can clearly separate two physical classes of GRBs. In the following, we examine the difference between LGRBs and SGRBs in different combinations of prompt emission properties vs. host galaxy properties. Redshift vs. host galaxy property plots are also presented, in order to study the selection effects and possible redshift evolution. Since the eventual goal is to investigate the differences between Type I and Type II GRBs using these plots, we use the consensus SGRB and LGRB samples (which already considered multiple criteria other than T_{90}) in the analysis. All the 2-D distribution plots are presented in Figure 2, and the statistical results are presented in Table 8. The numbers of LGRBs and SGRBs for each pair of parameters are shown in column 2,7,12,17 of Table 8.

Since the standard 2-D KS test only works well for samples without correlations, and since some of our 2-D plots show mild to significant correlations, we perform a rotated KS test to investigate how different LGRB and SGRB samples are from each other. For each 2-D plot, we rotate the axis with 180 trial angles from 0 – 180 degrees and calculate the P_{KS} along the new x -axis for each angle. We then choose the lowest P_{KS} as the P_{KS} of that particular 2-D plot. The angle with the lowest P_{KS} and the corresponding P_{KS} value are presented in

Table 8 for each plot. The black line segment in the circle at the lower left corner of each plot shows the direction of the x -axis with the lowest P_{KS} . We also test the possible correlation among LGRB sample between each parameter pair with the Spearman correlation. The Spearman correlation ρ_s and the null probability of the Spearman correlation P_S are also presented in Table 8.

Since T_{90} defines LGRBs and SGRBs, plots related to T_{90} have LGRBs and SGRBs are well separated and show low P_{KS} values, with the lowest P_{KS} angle at about 90° , especially if the host galaxy parameters do not show significant difference between LGRBs and SGRBs. There is generally no correlation between T_{90} and the host galaxy parameters.

In the plots with gamma-ray spectral parameters α and E_p , in general SGRBs have harder α , larger E_p and show mild difference from LGRBs. However, the overlap is still significant, and one cannot clearly distinguish the two classes by any of these plots.

In the plots with $E_{\gamma,\text{iso}}$, LGRBs and SGRBs show obvious differences but still overlap with each other. The P_{KS} value is not as significant as the 1D plots due to about two thirds reduction of the total number. The best separated plot is $E_{\gamma,\text{iso}}$ vs. offset. Plots with $L_{p,\text{iso}}$ do not show as significant difference between LGRBs and SGRBs as $E_{\gamma,\text{iso}}$ plots. There are some correlations for LGRBs in $E_{\gamma,\text{iso}}/L_{p,\text{iso}}$ vs M_*/SFR plots, as is also shown in Rhoads (2010). Some anticorrelations are also shown in $E_{\gamma,\text{iso}}/L_{p,\text{iso}}$ vs [X/H] plots.

The 2D plots involving f and f_{eff} are similar to those involving T_{90} . In particular, those involving f_{eff} show significant differences between LGRBs and SGRBs, even though significant overlapping is observed.

In several plots involving redshift, LGRBs show apparent correlations between z and other parameters. Most of these correlations may be partially attributed to observational selection effects. In the plots of $\log M_*$ vs. z and SFR vs. z , LGRB hosts with higher redshifts generally have larger stellar masses and larger SFRs. This is likely due to a selection effect, since galaxies with larger stellar masses are usually brighter and therefore detectable at higher redshifts, and since SFR is mainly determined by stellar mass. However, this selection effect is not obvious for SGRBs. SGRB hosts are generally more massive than LGRB hosts at a same redshift, while having nearly the same SFR. This results in a smaller sSFR for SGRB hosts, as shown in the plot of sSFR vs. z , as expected. In the plot of sSFR vs. z , the influence of stellar mass on SFR is generally removed and no significant redshift evolution is shown. A strong evolution of metallicity can be seen in the [X/H] vs. z plot, which also shows higher metallicity of SGRB hosts relative to the LGRB hosts at the same redshift.

The host sizes R_{50} of SGRBs are generally larger than those of LGRBs at all redshifts,

even though much overlap is seen. A mild, negative correlation between galaxy size R_{50} and redshift can be noticed. Since selection effects may create a positive correlation, this negative correlation should be intrinsic, even though it is not significant. There is also a mild, negative correlation between F_{light} and redshift. F_{light} of SGRBs shows a tentative positive correlation with redshift despite of a wide spread. SGRBs and LGRBs are generally more separated at $z < 1$ than at $z > 1$.

5. Conclusions and Discussion

In this paper, we present a sample of 407 GRBs detected before June 30th, 2014, with both prompt emission and host galaxy properties. Most GRBs (375) have spectroscopic redshift measurements. The other 32 bursts are included because of their host galaxy information. The prompt emission properties include duration T_{90} , spectral peak energy E_p , low energy photon index α , isotropic γ -ray energy $E_{\gamma,\text{iso}}$, peak luminosity $L_{p,\text{iso}}$, amplitude parameters f and f_{eff} . The host galaxy properties include star formation rate SFR, stellar mass M_* , specific star formation rate sSFR, metallicity [X/H], galaxy size R_{50} , physical offsets of GRBs from the center of the host R_{off} , normalized offset $r_{\text{off}} = R_{\text{off}}/R_{50}$, and brightness fraction F_{light} . We pay special attention to the comparison between T_{90} -defined SGRBs and LGRBs, and more importantly, the physically defined Type I vs. Type II GRBs. For the latter, we compare the “consensus” samples of SGRBs and LGRBs as listed in Jochen Greiner’s catalog, in which the definition of each SGRB was based on multiple criteria, with some of them having T_{90} longer than 2 s. For both definitions of SGRB/LGRB samples, we present the one-dimensional (1D) histograms of the two types, compare their distributions, and quantify their overlapping fractions. For the consensus samples, we further presented series two-dimensional (2D) scatter plots between prompt emission properties and host galaxy properties, aiming at identifying good parameters to separate the two types of bursts. Our results can be summarized as follows.

1. In 1D diagrams, all the prompt emission properties and host galaxy properties show more or less overlaps between SGRBs and LGRBs. No property shows a clear separation between consensus SGRBs and LGRBs. The duration T_{90} and the effective amplitude parameter f_{eff} are two parameter that have the lowest overlaps. The overlapping fractions for the f_{eff} histograms are 7% for LGRBs and 20% for SGRBs. The overlapping fractions for the f_{eff} histograms are 7% for LGRBs and 79%⁹ for SGRBs, respectively. Other parameters have much larger overlapping fractions, typically 50%-80% for LGRBs and 80%-100% for

⁹48% if the outlier GRB 130427A is excluded.

SGRBs. This suggests that no single parameter alone is good enough to place a particular burst into the right physical category.

2. The T_{90} -defined LGRB and SGRB samples show more overlaps than the consensus LGRBs and SGRBs in most properties other than T_{90} , especially in host galaxy properties. This indicates that the T_{90} -only criterion mis-classifies some GRBs. Other properties are needed as supplementary criteria to classify GRBs physically.

3. None of the 2D prompt emission vs host galaxy property plots show a clear separation between the consensus LGRBs and SGRBs. It suggests that simple 2D plots are not good enough for Type I and Type II GRB classifications.

4. The three best parameters to classify GRBs are the effective amplitude f_{eff} , T_{90} , and the brightness fraction F_{light} . They show the smallest overlapping fractions and the smallest null probability P_{KS} in the simulated 1-D distributions.

5. Some correlations between prompt emission properties and host galaxy properties are found in some 2D plots, such as $L_{\text{p,iso}}/E_{\gamma,\text{iso}}$ vs. M_* , $L_{\text{p,iso}}/E_{\gamma,\text{iso}}$ vs. SFR, $L_{\text{p,iso}}/E_{\gamma,\text{iso}}$ vs. [X/H], etc. (see Fig. 2 and Table 8). However, all these parameters show even more significant correlation with redshift, indicating that the correlations may be significantly subject to observational selection effects.

The significant overlapping nature of the observed properties suggests that it is not always easy to identify the correct physical category of GRBs. Multiple observational criteria are needed to give more robust judgement, as suggested by Zhang et al. (2009). This first paper in a series presents all the observational data and 1-D and 2-D overlapping properties. In a follow-up paper, we will develop a quantitative method to apply the multiple observational criteria to classify GRBs into the Type I vs. Type II physical categories.

This work is partially supported by NASA through grants NNX14AF85G and NNX15AK85G. We thank the anonymous referee for detailed review and very useful suggestions, and Antonion Cucchiara, Wenfai Fong, T. Krühler, Sandra Savaglio and Qiang Yuan for helpful discussion. We also acknowledge the public data available at the Swift catalog (<http://swift.gsfc.nasa.gov/archive/>) and the SIMBAD database, operated at CDS, Strasbourg, France.

REFERENCES

Afonso, P., Schady, P., Kruehler, T., & Greiner, J. 2010, GRB Coordinates Network, 10782,

- Amati, L., Frontera, F., Tavani, M., et al. 2002, A&A, 390, 81
- Amati, L., Frontera, F., in't Zand, J. J. M., et al. 2004, A&A, 426, 415
- Andersen, M. I., Hjorth, J., Pedersen, H., et al. 2000, A&A, 364, L54
- Antonelli, L. A., D'Avanzo, P., Perna, R., et al. 2009, A&A, 507, L45
- Arabsalmani, M., Møller, P., Fynbo, J. P. U., et al. 2015, MNRAS, 446, 990
- Asplund, M., Grevesse, N., Sauval, A. J., & Scott, P. 2009, ARA&A, 47, 481
- Band, D., Matteson, J., Ford, L., et al. 1993, ApJ, 413, 281
- Barraud, C., Olive, J.-F., Lestrade, J. P., et al. 2003, A&A, 400, 1021
- Barth, A. J., Sari, R., Cohen, M. H., et al. 2003, ApJ, 584, L47
- Basa, S., Cuby, J. G., Savaglio, S., et al. 2012, A&A, 542, A103
- Bellm, E., Bandstra, M., Boggs, S., et al. 2006, GRB Coordinates Network, 5867, 1
- Berger, E. 2006a, GRB Coordinates Network, 5952, 1
- . 2006b, GRB Coordinates Network, 5962, 1
- . 2009, ApJ, 690, 231
- . 2010, ApJ, 722, 1946
- . 2014, ARA&A, 52, 43
- Berger, E., Foley, R., Simcoe, R., & Irwin, J. 2008a, GRB Coordinates Network, 8434, 1
- Berger, E., Fong, W., & Chornock, R. 2013, ApJ, 774, L23
- Berger, E., & Fox, D. B. 2009, GRB Coordinates Network, 9156, 1
- Berger, E., Fox, D. B., & Cucchiara, A. 2007a, GRB Coordinates Network, 6470, 1
- Berger, E., Fox, D. B., Cucchiara, A., & Cenko, S. B. 2008b, GRB Coordinates Network, 8335, 1
- Berger, E., Fox, D. B., Kulkarni, S. R., Frail, D. A., & Djorgovski, S. G. 2007b, ApJ, 660, 504
- Berger, E., & Gladders, M. 2006, GRB Coordinates Network, 5170, 1

- Berger, E., Morrell, N., & Roth, M. 2007c, GRB Coordinates Network, 7154, 1
- Berger, E., Penprase, B. E., Cenko, S. B., et al. 2006, ApJ, 642, 979
- Berger, E., & Rauch, M. 2008, GRB Coordinates Network, 8542, 1
- Berger, E., Kulkarni, S. R., Fox, D. B., et al. 2005a, ApJ, 634, 501
- Berger, E., Price, P. A., Cenko, S. B., et al. 2005b, Nature, 438, 988
- Berger, E., Fox, D. B., Kulkarni, S. R., et al. 2005c, ApJ, 629, 328
- Berger, E., Fox, D. B., Price, P. A., et al. 2007d, ApJ, 664, 1000
- Bissaldi, E., von Kienlin, A., Kouveliotou, C., et al. 2011, ApJ, 733, 97
- Blanchard, P. K., Berger, E., & Fong, W.-f. 2016, ApJ, 817, 144
- Bloom, J. S., Berger, E., Kulkarni, S. R., Djorgovski, S. G., & Frail, D. A. 2003a, AJ, 125, 999
- Bloom, J. S., Djorgovski, S. G., Kulkarni, S. R., & Frail, D. A. 1998, ApJ, 507, L25
- Bloom, J. S., Foley, R. J., Kocevski, D., & Perley, D. 2006a, GRB Coordinates Network, 5217, 1
- Bloom, J. S., Fox, D., van Dokkum, P. G., et al. 2003b, ApJ, 599, 957
- Bloom, J. S., Kulkarni, S. R., & Djorgovski, S. G. 2002, AJ, 123, 1111
- Bloom, J. S., Perley, D., Kocevski, D., et al. 2006b, GRB Coordinates Network, 5238, 1
- Boer, M., Ricker, G., Atteia, J.-L., et al. 2005, GRB Coordinates Network, 3653, 1
- Bošnjak, Ž., Götz, D., Bouchet, L., Schanne, S., & Cordier, B. 2014, A&A, 561, A25
- Bromberg, O., Nakar, E., & Piran, T. 2011, ApJ, 739, L55
- Burns, E. 2014, GRB Coordinates Network, 16363, 1
- Burud, I., Rhoads, J., Fruchter, A., & Hjorth, J. 2001, GRB Coordinates Network, 1213, 1
- Butler, N., Ricker, G., Atteia, J.-L., et al. 2004, GRB Coordinates Network, 2701, 1
- Cabrera Lavers, A., de Ugarte Postigo, A., Castro-Tirado, A. J., et al. 2011, GRB Coordinates Network, 12234, 1

- Campana, S., Mangano, V., Blustin, A. J., et al. 2006, *Nature*, 442, 1008
- Cano, Z., Bersier, D., Guidorzi, C., et al. 2011, *MNRAS*, 413, 669
- Cano, Z., de Ugarte Postigo, A., Pozanenko, A., et al. 2014, *A&A*, 568, A19
- Cano, Z., de Ugarte Postigo, A., Perley, D., et al. 2015, *MNRAS*, 452, 1535
- Castro, S., Galama, T. J., Harrison, F. A., et al. 2003, *ApJ*, 586, 128
- Castro-Tirado, A. J., Sokolov, V. V., Gorosabel, J., et al. 2001, *A&A*, 370, 398
- Castro-Tirado, A. J., Møller, P., García-Segura, G., et al. 2010, *A&A*, 517, A61
- Cenko, S. B., Berger, E., Djorgovski, S. G., Mahabal, A. A., & Fox, D. B. 2006a, GRB Coordinates Network, 5155
- Cenko, S. B., Cucchiara, A., Fox, D. B., Berger, E., & Price, P. A. 2007a, GRB Coordinates Network, 6888, 1
- Cenko, S. B., Fox, D. B., Cucchiara, A., et al. 2007b, GRB Coordinates Network, 6556, 1
- Cenko, S. B., Hora, J. L., & Bloom, J. S. 2011a, GRB Coordinates Network, 11638, 1
- Cenko, S. B., Kasliwal, M., Cameron, P. B., Kulkarni, S. R., & Fox, D. B. 2006b, GRB Coordinates Network, 5946, 1
- Cenko, S. B., Levan, A. J., & Cucchiara, A. 2013, GRB Coordinates Network, 14762, 1
- Cenko, S. B., Perley, D. A., Junkkarinen, V., et al. 2009, GRB Coordinates Network, 9518, 1
- Cenko, S. B., Perley, D. A., Morgan, A. N., et al. 2010, GRB Coordinates Network, 10752, 1
- Cenko, S. B., Prochaska, J. X., Cucchiara, A., Perley, D. A., & Bloom, J. S. 2011b, GRB Coordinates Network, 11736, 1
- Cenko, S. B., Fox, D. B., Penprase, B. E., et al. 2008a, *ApJ*, 677, 441
- Cenko, S. B., Berger, E., Nakar, E., et al. 2008b, ArXiv e-prints, arXiv:0802.0874
- Cenko, S. B., Frail, D. A., Harrison, F. A., et al. 2011c, *ApJ*, 732, 29
- Cenko, S. B., Urban, A. L., Perley, D. A., et al. 2015, *ApJ*, 803, L24

- Chaplin, V. 2012, GRB Coordinates Network, 13737
- Chary, R., Becklin, E. E., & Armus, L. 2002, ApJ, 566, 229
- Chary, R., Berger, E., & Cowie, L. 2007, ApJ, 671, 272
- Chen, H.-W., Prochaska, J. X., Bloom, J. S., & Thompson, I. B. 2005, ApJ, 634, L25
- Chen, H.-W., Perley, D. A., Pollack, L. K., et al. 2009, ApJ, 691, 152
- Chornock, R., & Berger, E. 2011, GRB Coordinates Network, 11518, 1
- Chornock, R., Berger, E., & Fox, D. 2011a, GRB Coordinates Network, 12537, 1
- Chornock, R., Berger, E., Fox, D., et al. 2010a, GRB Coordinates Network, 11164, 1
- Chornock, R., Berger, E., & Fox, D. B. 2011b, GRB Coordinates Network, 11538, 1
- Chornock, R., Berger, E., Fox, D. B., et al. 2013a, ApJ, 774, 26
- Chornock, R., Cenko, S. B., Griffith, C. V., et al. 2009a, GRB Coordinates Network, 9151, 1
- Chornock, R., Cucchiara, A., Fox, D., & Berger, E. 2010b, GRB Coordinates Network, 10466, 1
- Chornock, R., Fox, D. B., & Berger, E. 2014a, GRB Coordinates Network, 16269, 1
- Chornock, R., Fox, D. B., Cucchiara, A., Perley, D. A., & Levan, A. 2014b, GRB Coordinates Network, 16301, 1
- Chornock, R., Fox, D. B., Tanvir, N. R., & Berger, E. 2014c, GRB Coordinates Network, 15966, 1
- Chornock, R., Lunnan, R., & Berger, E. 2013b, GRB Coordinates Network, 15307, 1
- Chornock, R., Perley, D. A., Cenko, S. B., & Bloom, J. S. 2009b, GRB Coordinates Network, 9243, 1
- Chornock, R., Perley, D. A., Cenko, S. B., et al. 2009c, GRB Coordinates Network, 8994, 1
- Chornock, R., Perley, D. A., & Cobb, B. E. 2009d, GRB Coordinates Network, 10100, 1
- Chornock, R., Berger, E., Levesque, E. M., et al. 2010c, ArXiv e-prints, arXiv:1004.2262
- Christensen, L., Hjorth, J., & Gorosabel, J. 2004, A&A, 425, 913

- . 2005, ApJ, 631, L29
- Church, R. P., Levan, A. J., Davies, M. B., & Tanvir, N. 2011, MNRAS, 413, 2004
- Cobb, B. E., Bailyn, C. D., van Dokkum, P. G., Buxton, M. M., & Bloom, J. S. 2004, ApJ, 608, L93
- Collazzi, A. C., & Connaughton, V. 2013, GRB Coordinates Network, 14972
- Crew, G., Ricker, G., Atteia, J.-L., et al. 2005, GRB Coordinates Network, 4021, 1
- Cucchiara, A. 2012, GRB Coordinates Network, 13213, 1
- Cucchiara, A., Bloom, J. S., & Cenko, S. B. 2011a, GRB Coordinates Network, 12202, 1
- Cucchiara, A., & Cenko, S. B. 2013, GRB Coordinates Network, 15624, 1
- Cucchiara, A., Fox, D., & Tanvir, N. 2009a, GRB Coordinates Network, 10065, 1
- Cucchiara, A., & Fox, D. B. 2008, GRB Coordinates Network, 7654, 1
- . 2010, GRB Coordinates Network, 10606, 1
- Cucchiara, A., Fox, D. B., & Cenko, S. B. 2007a, GRB Coordinates Network, 7124, 1
- Cucchiara, A., Fox, D. B., Cenko, S. B., & Berger, E. 2008a, GRB Coordinates Network, 8346, 1
- . 2008b, GRB Coordinates Network, 8713, 1
- Cucchiara, A., Fox, D. B., Cenko, S. B., et al. 2007b, GRB Coordinates Network, 6665
- Cucchiara, A., Fox, D. B., Cenko, S. B., & Price, P. A. 2007c, GRB Coordinates Network, 6083, 1
- Cucchiara, A., Fox, D. B., Cenko, S. B., Tanvir, N., & Berger, E. 2009b, GRB Coordinates Network, 10031, 1
- Cucchiara, A., Fox, D. B., Tanvir, N., & Berger, E. 2009c, GRB Coordinates Network, 9873, 1
- Cucchiara, A., & Fumagalli, M. 2013, GRB Coordinates Network, 14207, 1
- Cucchiara, A., Fumagalli, M., Rafelski, M., et al. 2015, ApJ, 804, 51
- Cucchiara, A., Levan, A. J., & Tanvir, N. 2011b, GRB Coordinates Network, 12777, 1

- Cucchiara, A., & Perley, D. 2013, GRB Coordinates Network, 15144, 1
- Cucchiara, A., Perley, D., & Cenko, S. B. 2013, GRB Coordinates Network, 14748, 1
- Cucchiara, A., & Tanvir, N. R. 2013, GRB Coordinates Network, 14621, 1
- Cucchiara, A., Tanvir, N. R., Perley, D., & Levan, A. J. 2012, GRB Coordinates Network, 13512, 1
- Cucchiara, A., Levan, A. J., Fox, D. B., et al. 2011c, ApJ, 736, 7
- Cummings, J., Barbier, L., Barthelmy, S., et al. 2005, GRB Coordinates Network, 3339, 1
- D’Avanzo, P., Malesani, D., Covino, S., et al. 2009, A&A, 498, 711
- D’Avanzo, P., Perri, M., Fugazza, D., et al. 2010, A&A, 522, A20
- De Cia, A., Jakobsson, P., Björnsson, G., et al. 2011, MNRAS, 412, 2229
- De Cia, A., Ledoux, C., Fox, A. J., et al. 2012, A&A, 545, A64
- de Ugarte Postigo, A., Castro-Tirado, A. J., & Gorosabel, J. 2011a, GRB Coordinates Network, 11978, 1
- de Ugarte Postigo, A., Castro-Tirado, A. J., Tello, J. C., Cabrera Lavers, A., & Reverte, D. 2011b, GRB Coordinates Network, 11993, 1
- de Ugarte Postigo, A., Gorosabel, J., Fynbo, J. P. U., Wiersema, K., & Tanvir, N. 2009a, GRB Coordinates Network, 9771, 1
- de Ugarte Postigo, A., Gorosabel, J., Malesani, D., Fynbo, J. P. U., & Levan, A. J. 2009b, GRB Coordinates Network, 9383, 1
- de Ugarte Postigo, A., Jakobsson, P., Malesani, D., et al. 2009c, GRB Coordinates Network, 8766, 1
- de Ugarte Postigo, A., Tanvir, N., Sanchez-Ramirez, R., et al. 2013a, GRB Coordinates Network, 14437, 1
- de Ugarte Postigo, A., Thoene, C. C., Gorosabel, J., et al. 2013b, GRB Coordinates Network, 15470, 1
- de Ugarte Postigo, A., Xu, D., Malesani, D., et al. 2013c, GRB Coordinates Network, 15187, 1

- de Ugarte Postigo, A., Campana, S., Thöne, C. C., et al. 2013d, *A&A*, 557, L18
- de Ugarte Postigo, A., Gorosabel, J., Xu, D., et al. 2014a, GRB Coordinates Network, 16310, 1
- de Ugarte Postigo, A., Thöne, C. C., Rowlinson, A., et al. 2014b, *A&A*, 563, A62
- D'Elia, V., Covino, S., & D'Avanzo, P. 2008a, GRB Coordinates Network, 8438, 1
- D'Elia, V., Thoene, C. C., de Ugarte Postigo, A., et al. 2008b, GRB Coordinates Network, 8531, 1
- D'Elia, V., Fynbo, J. P. U., Goldoni, P., et al. 2014, *A&A*, 564, A38
- Della Valle, M., Chincarini, G., Panagia, N., et al. 2006, *Nature*, 444, 1050
- Djorgovski, S. G., Bloom, J. S., & Kulkarni, S. R. 2003, *ApJ*, 591, L13
- Djorgovski, S. G., Frail, D. A., Kulkarni, S. R., et al. 2001, *ApJ*, 562, 654
- Djorgovski, S. G., Kulkarni, S. R., Bloom, J. S., & Frail, D. A. 1999, GRB Coordinates Network, 289, 1
- Djorgovski, S. G., Kulkarni, S. R., Bloom, J. S., et al. 1998, *ApJ*, 508, L17
- Dominik, M., Berti, E., O'Shaughnessy, R., et al. 2015, *ApJ*, 806, 263
- Draine, B. T. 2011, Physics of the Interstellar and Intergalactic Medium
- Eichler, D., Livio, M., Piran, T., & Schramm, D. N. 1989, *Nature*, 340, 126
- Elliott, J., Krühler, T., Greiner, J., et al. 2013a, *A&A*, 556, A23
- . 2013b, ArXiv e-prints, arXiv:1308.5520
- Fatkullin, T., Gorosabel, J., de Ugarte Postigo, A., et al. 2009, GRB Coordinates Network, 9712, 1
- Ferrero, P., Klose, S., Kann, D. A., et al. 2009, *A&A*, 497, 729
- Flores, H., Covino, S., de Ugarte Postigo, A., et al. 2013, GRB Coordinates Network, 14493, 1
- Flores, H., Fynbo, J. P. U., de Ugarte Postigo, A., et al. 2010, GRB Coordinates Network, 11317, 1

- Foley, S., McGlynn, S., Hanlon, L., McBreen, S., & McBreen, B. 2008, A&A, 484, 143
- Fong, W., & Berger, E. 2013, ApJ, 776, 18
- Fong, W., Berger, E., & Fox, D. B. 2010, ApJ, 708, 9
- Fong, W., Berger, E., Chornock, R., et al. 2011, ApJ, 730, 26
- . 2013, ApJ, 769, 56
- Fox, A. J., Ledoux, C., Vreeswijk, P. M., Smette, A., & Jaunsen, A. O. 2008, A&A, 491, 189
- Fox, D. B., Frail, D. A., Price, P. A., et al. 2005, Nature, 437, 845
- Frederiks, D. 2013, GRB Coordinates Network, 14578
- Frederiks, D. D., Hurley, K., Svinkin, D. S., et al. 2013, ApJ, 779, 151
- Friis, M., De Cia, A., Krühler, T., et al. 2015, MNRAS, 451, 167
- Frontera, F., Guidorzi, C., Montanari, E., et al. 2009, ApJS, 180, 192
- Fruchter, A., Pattel, S., Kouveliotou, C., et al. 2002, GRB Coordinates Network, 1268, 1
- Fruchter, A. S., Levan, A. J., Strolger, L., et al. 2006, Nature, 441, 463
- Fugazza, D., Thoene, C. C., D'Elia, V., et al. 2009, GRB Coordinates Network, 8892, 1
- Fynbo, J. P. U., Møller, P., Thomsen, B., et al. 2002, A&A, 388, 425
- Fynbo, J. P. U., Jakobsson, P., Möller, P., et al. 2003, A&A, 406, L63
- Fynbo, J. P. U., Gorosabel, J., Smette, A., et al. 2005, ApJ, 633, 317
- Fynbo, J. P. U., Watson, D., Thöne, C. C., et al. 2006, Nature, 444, 1047
- Fynbo, J. P. U., Jakobsson, P., Prochaska, J. X., et al. 2009, ApJS, 185, 526
- Fynbo, J. P. U., Tanvir, N. R., D'Elia, V., et al. 2012, GRB Coordinates Network, 14120, 1
- Fynbo, J. P. U., Krühler, T., Leighly, K., et al. 2014, A&A, 572, A12
- Gal-Yam, A., Fox, D. B., Price, P. A., et al. 2006, Nature, 444, 1053
- Galama, T. J., Groot, P. J., van Paradijs, J., et al. 1997, IAU Circ., 6655, 1
- Galama, T. J., Vreeswijk, P. M., van Paradijs, J., et al. 1998, Nature, 395, 670

- Galama, T. J., Reichart, D., Brown, T. M., et al. 2003, *ApJ*, 587, 135
- Galassi, M., Ricker, G., Atteia, J.-L., et al. 2004, GRB Coordinates Network, 2770, 1
- Galli, A., & Piro, L. 2006, *A&A*, 455, 413
- Gao, H., Ding, X., Wu, X.-F., Dai, Z.-G., & Zhang, B. 2015, *ApJ*, 807, 163
- Gao, H., Zhang, B., & Lü, H.-J. 2016, *Phys. Rev. D*, 93, 044065
- Gehrels, N., Ramirez-Ruiz, E., & Fox, D. B. 2009, *ARA&A*, 47, 567
- Gehrels, N., Sarazin, C. L., O'Brien, P. T., et al. 2005, *Nature*, 437, 851
- Gehrels, N., Norris, J. P., Barthelmy, S. D., et al. 2006, *Nature*, 444, 1044
- Gehrels, N., Barthelmy, S. D., Burrows, D. N., et al. 2008, *ApJ*, 689, 1161
- Gendre, B., Stratta, G., Atteia, J. L., et al. 2013, *ApJ*, 766, 30
- Ghirlanda, G., Nava, L., Ghisellini, G., Celotti, A., & Firmani, C. 2009, *A&A*, 496, 585
- Goldoni, P., de Ugarte Postigo, A., & Fynbo, J. P. U. 2013, GRB Coordinates Network, 15571, 1
- Goldoni, P., Flores, H., Malesani, D., et al. 2010, GRB Coordinates Network, 10684, 1
- Goldstein, A., Preece, R. D., Mallozzi, R. S., et al. 2013, *ApJS*, 208, 21
- Golenetskii, S., Aptekar, R., Frederiks, D., et al. 2013a, GRB Coordinates Network, 14958, 1
- . 2013b, GRB Coordinates Network, 15145, 1
- . 2013c, GRB Coordinates Network, 15203, 1
- . 2013d, GRB Coordinates Network, 15413, 1
- . 2014a, GRB Coordinates Network, 15889, 1
- Golenetskii, S., Aptekar, R., Mazets, E., et al. 2004, GRB Coordinates Network, 2754, 1
- . 2005a, GRB Coordinates Network, 3660, 1
- . 2005b, GRB Coordinates Network, 3179, 1
- . 2005c, GRB Coordinates Network, 3474, 1

- . 2005d, GRB Coordinates Network, 4030, 1
- . 2005e, GRB Coordinates Network, 4078, 1
- . 2005f, GRB Coordinates Network, 4150, 1
- . 2005g, GRB Coordinates Network, 4238, 1
- . 2005h, GRB Coordinates Network, 4394, 1
- . 2006a, GRB Coordinates Network, 5837, 1
- . 2006b, GRB Coordinates Network, 4564, 1
- . 2006c, GRB Coordinates Network, 4599, 1
- . 2006d, GRB Coordinates Network, 4881, 1
- . 2006e, GRB Coordinates Network, 5264, 1
- . 2006f, GRB Coordinates Network, 5460, 1
- . 2006g, GRB Coordinates Network, 5722, 1
- . 2006h, GRB Coordinates Network, 5748, 1
- . 2006i, GRB Coordinates Network, 5890, 1
- . 2006j, GRB Coordinates Network, 5710, 1
- . 2007a, GRB Coordinates Network, 6049, 1
- . 2007b, GRB Coordinates Network, 6230, 1
- . 2007c, GRB Coordinates Network, 6459, 1
- . 2007d, GRB Coordinates Network, 6615, 1
- . 2007e, GRB Coordinates Network, 6849, 1
- . 2007f, GRB Coordinates Network, 6879, 1
- . 2007g, GRB Coordinates Network, 6960, 1
- . 2007h, GRB Coordinates Network, 7155, 1
- . 2008a, GRB Coordinates Network, 7482, 1

- . 2008b, GRB Coordinates Network, 7487, 1
- . 2008c, GRB Coordinates Network, 7589, 1
- . 2008d, GRB Coordinates Network, 7784, 1
- . 2008e, GRB Coordinates Network, 7812, 1
- . 2008f, GRB Coordinates Network, 7854, 1
- . 2007i, GRB Coordinates Network, 6403, 1
- . 2007j, GRB Coordinates Network, 7114, 1
- . 2009a, GRB Coordinates Network, 10045, 1
- . 2009b, GRB Coordinates Network, 9647, 1
- . 2008g, GRB Coordinates Network, 7862, 1
- . 2008h, GRB Coordinates Network, 7995, 1
- . 2008i, GRB Coordinates Network, 8611, 1
- Golenetskii, S., Aptekar, R., Frederiks, D., et al. 2009c, GRB Coordinates Network, 9679, 1
- Golenetskii, S., Aptekar, R., Mazets, E., et al. 2009d, GRB Coordinates Network, 8878, 1
- Golenetskii, S., Aptekar, R., Frederiks, D., et al. 2010a, GRB Coordinates Network, 10833, 1
- . 2010b, GRB Coordinates Network, 10882, 1
- . 2010c, GRB Coordinates Network, 11470, 1
- Golenetskii, S., Aptekar, R., Mazets, E., et al. 2011a, GRB Coordinates Network, 11659, 1
- . 2011b, GRB Coordinates Network, 11722, 1
- . 2011c, GRB Coordinates Network, 11971, 1
- Golenetskii, S., Aptekar, R., Frederiks, D., et al. 2011d, GRB Coordinates Network, 12008, 1
- . 2011e, GRB Coordinates Network, 12135, 1
- . 2011f, GRB Coordinates Network, 12166, 1

- . 2011g, GRB Coordinates Network, 12270, 1
- . 2011h, GRB Coordinates Network, 12362, 1
- . 2011i, GRB Coordinates Network, 12433, 1
- Golenetskii, S., Aptekar, R., Mazets, E., et al. 2011j, GRB Coordinates Network, 12663, 1
- . 2011k, GRB Coordinates Network, 12676, 1
- Golenetskii, S., Aptekar, R., Frederiks, D., et al. 2012, GRB Coordinates Network, 13382
- . 2013e, GRB Coordinates Network, 14368, 1
- . 2013f, GRB Coordinates Network, 14417, 1
- . 2013g, GRB Coordinates Network, 14487, 1
- . 2013h, GRB Coordinates Network, 14575, 1
- . 2013i, GRB Coordinates Network, 14771, 1
- Golenetskii, S., Aptekar, R., Mazets, E., et al. 2013j, GRB Coordinates Network, 14808, 1
- Golenetskii, S., Aptekar, R., Frederiks, D., et al. 2014b, GRB Coordinates Network, 16134,
1
- Gorosabel, J., Fynbo, J. P. U., Fruchter, A., et al. 2005, A&A, 437, 411
- Götz, D., Covino, S., Hascoët, R., et al. 2011, MNRAS, 413, 2173
- Graziani, C., Shirasaki, Y., Matsuoka, M., et al. 2003, GRB Coordinates Network, 1956, 1
- Greiner, J., Rau, A., Schady, P., Saviane, I., & Cenko, B. 2012, GRB Coordinates Network,
13493, 1
- Greiner, J., Klose, S., Salvato, M., et al. 2003, ApJ, 599, 1223
- Greiner, J., Krühler, T., McBreen, S., et al. 2009, ApJ, 693, 1912
- Greiner, J., Krühler, T., Klose, S., et al. 2011, A&A, 526, A30
- Greiner, J., Yu, H.-F., Krühler, T., et al. 2014, A&A, 568, A75
- Greiner, J., Fox, D. B., Schady, P., et al. 2015, ApJ, 809, 76
- Groot, P., Kaper, L., Ellerbroek, L., et al. 2010, GRB Coordinates Network, 10441, 1

- Gruber, D., & Goldstein, A. 2012, GRB Coordinates Network, 13498
- Gruber, D., Krühler, T., Foley, S., et al. 2011, A&A, 528, A15
- Gruber, D., Goldstein, A., Weller von Ahlefeld, V., et al. 2014, ApJS, 211, 12
- Guidorzi, C., Kobayashi, S., Perley, D. A., et al. 2011, MNRAS, 417, 2124
- Han, X. H., Hammer, F., Liang, Y. C., et al. 2010, A&A, 514, A24
- Hartoog, O. E., Malesani, D., Wiersema, K., et al. 2012, GRB Coordinates Network, 13730, 1
- Hartoog, O. E., Xu, D., Malesani, D., et al. 2013, GRB Coordinates Network, 15494, 1
- Hartoog, O. E., Malesani, D., Fynbo, J. P. U., et al. 2015, A&A, 580, A139
- Hashimoto, T., Perley, D. A., Ohta, K., et al. 2015, ApJ, 806, 250
- Heise, J., in't Zand, J. J. M., Kulkarni, S. R., & Costa, E. 2001, GRB Coordinates Network, 1138, 1
- Hjorth, J., & Bloom, J. S. 2012, The Gamma-Ray Burst - Supernova Connection, 169–190
- Hjorth, J., Sollerman, J., Møller, P., et al. 2003a, Nature, 423, 847
- Hjorth, J., Møller, P., Gorosabel, J., et al. 2003b, ApJ, 597, 699
- Hjorth, J., Sollerman, J., Gorosabel, J., et al. 2005a, ApJ, 630, L117
- Hjorth, J., Watson, D., Fynbo, J. P. U., et al. 2005b, Nature, 437, 859
- Holland, S. T., Soszyński, I., Gladders, M. D., et al. 2002, AJ, 124, 639
- Holland, S. T., Sbarufatti, B., Shen, R., et al. 2010, ApJ, 717, 223
- Hunt, L. K., Palazzi, E., Michałowski, M. J., et al. 2014, A&A, 565, A112
- Hurley, K., & Cline, T. 1999, GRB Coordinates Network, 450, 1
- Hurley, K., Cline, T., & Mazets, E. 2000a, GRB Coordinates Network, 529, 1
- Hurley, K., Cline, T., Mazets, E., & Golenetskii, S. 2000b, GRB Coordinates Network, 791, 1
- Hurley, K., Cline, T., Mazets, E., et al. 2000c, ApJ, 534, L23

- Hurley, K., Cline, T., Ricker, G., et al. 2002a, GRB Coordinates Network, 1263
- . 2002b, GRB Coordinates Network, 1507, 1
- Ilbert, O., Arnouts, S., Le Floc'h, E., et al. 2015, A&A, 579, A2
- in't Zand, J., Reali, F., Granata, S., Lowes, P., & Piro, L. 2002, GRB Coordinates Network, 1383, 1
- Izotov, Y. I., Stasińska, G., Meynet, G., Guseva, N. G., & Thuan, T. X. 2006, A&A, 448, 955
- Jakobsson, P., de Ugarte Postigo, A., Gorosabel, J., et al. 2009, GRB Coordinates Network, 9797, 1
- Jakobsson, P., Malesani, D., Fynbo, J. P. U., et al. 2007a, GRB Coordinates Network, 6997, 1
- Jakobsson, P., Hjorth, J., Fynbo, J. P. U., et al. 2004, A&A, 427, 785
- Jakobsson, P., Frail, D. A., Fox, D. B., et al. 2005, ApJ, 629, 45
- Jakobsson, P., Levan, A., Fynbo, J. P. U., et al. 2006a, A&A, 447, 897
- Jakobsson, P., Fynbo, J. P. U., Ledoux, C., et al. 2006b, A&A, 460, L13
- Jakobsson, P., Fynbo, J. P. U., Andersen, M. I., et al. 2007b, GRB Coordinates Network, 6398, 1
- Jakobsson, P., Hjorth, J., Malesani, D., et al. 2012, ApJ, 752, 62
- Jaunsen, A. O., Andersen, M. I., Hjorth, J., et al. 2003, A&A, 402, 125
- Jenke, P. 2013, GRB Coordinates Network, 15331, 1
- Jenke, P., & Xiong, S. 2014, GRB Coordinates Network, 15644, 1
- Jensen, B. L., Fynbo, J. U., Gorosabel, J., et al. 2001, A&A, 370, 909
- Jeong, S., Sanchez-Ramirez, R., Gorosabel, J., & Castro-Tirado, A. J. 2014a, GRB Coordinates Network, 15936, 1
- Jeong, S., Castro-Tirado, A. J., Bremer, M., et al. 2014b, A&A, 569, A93
- Jimenez, R., Band, D., & Piran, T. 2001, ApJ, 561, 171

- Jin, Z.-P., Covino, S., Della Valle, M., et al. 2013, ApJ, 774, 114
- Jin, Z.-P., Hotokezaka, K., Li, X., et al. 2016, ArXiv e-prints, arXiv:1603.07869
- Kaneko, Y., Bostancı, Z. F., Göğüş, E., & Lin, L. 2015, MNRAS, 452, 824
- Kann, D. A., Klose, S., Zhang, B., et al. 2010, ApJ, 720, 1513
- . 2011, ApJ, 734, 96
- Kawai, N., Kosugi, G., Aoki, K., et al. 2006, Nature, 440, 184
- Kelly, P. L., Filippenko, A. V., Fox, O. D., Zheng, W., & Clubb, K. I. 2013, ApJ, 775, L5
- Kennicutt, R. C., & Evans, N. J. 2012, ARA&A, 50, 531
- Kennicutt, Jr., R. C. 1998, ARA&A, 36, 189
- Kewley, L. J., & Dopita, M. A. 2002, ApJS, 142, 35
- Kewley, L. J., & Ellison, S. L. 2008, ApJ, 681, 1183
- Klose, S., Greiner, J., Rau, A., et al. 2004, AJ, 128, 1942
- Knust, F., Kruehler, T., Klose, S., & Greiner, J. 2012, GRB Coordinates Network, 13810, 1
- Kobulnicky, H. A., & Kewley, L. J. 2004, ApJ, 617, 240
- Kohn, S. A., Michałowski, M. J., Bourne, N., et al. 2015, MNRAS, 448, 1494
- Kouveliotou, C., Meegan, C. A., Fishman, G. J., et al. 1993, ApJ, 413, L101
- Krimm, H. A., Barthelmy, S. D., Baumgartner, W. H., et al. 2012, GRB Coordinates Network, 14123, 1
- Kruehler, T., Fynbo, J. P. U., Milvang-Jensen, B., Tanvir, N., & Jakobsson, P. 2012, GRB Coordinates Network, 13134, 1
- Kruehler, T., Xu, D., Sanchez-Ramirez, R., et al. 2013, GRB Coordinates Network, 14390, 1
- Krühler, T., Schady, P., Greiner, J., et al. 2011a, A&A, 526, A153
- Krühler, T., Greiner, J., Schady, P., et al. 2011b, A&A, 534, A108
- Krühler, T., Ledoux, C., Fynbo, J. P. U., et al. 2013, A&A, 557, A18

- Kröhler, T., Malesani, D., Fynbo, J. P. U., et al. 2015, A&A, 581, A125
- Kuin, N. P. M., Landsman, W., Page, M. J., et al. 2009, MNRAS, 395, L21
- Kulkarni, S. R., Djorgovski, S. G., Ramaprakash, A. N., et al. 1998, Nature, 393, 35
- Kulkarni, S. R., Djorgovski, S. G., Odewahn, S. C., et al. 1999, Nature, 398, 389
- Laskar, T., Berger, E., & Chary, R.-R. 2011, ApJ, 739, 1
- Lazzarotto, F., Del Monte, E., Donnarumma, I., et al. 2011, GRB Coordinates Network, 12666
- Le Floc'h, E., Duc, P.-A., Mirabel, I. F., et al. 2002, ApJ, 581, L81
- Leibler, C. N., & Berger, E. 2010, ApJ, 725, 1202
- Levan, A., Nugent, P., Fruchter, A., et al. 2005, ApJ, 624, 880
- Levan, A. J., Fynbo, J. P. U., Hjorth, J., et al. 2009a, GRB Coordinates Network, 9958, 1
- Levan, A. J., Tanvir, N. R., Wiersema, K., & O'Brien, P. T. 2011, GRB Coordinates Network, 12414
- Levan, A. J., Malesani, D., Tanvir, N. R., et al. 2009b, GRB Coordinates Network, 8856, 1
- Levan, A. J., Tanvir, N. R., Starling, R. L. C., et al. 2014a, ApJ, 781, 13
- Levan, A. J., Tanvir, N. R., Fruchter, A. S., et al. 2014b, ApJ, 792, 115
- Levesque, E., Chornock, R., Kewley, L., et al. 2009, GRB Coordinates Network, 9264, 1
- Levesque, E. M., Berger, E., Soderberg, A. M., & Chornock, R. 2011, ApJ, 739, 23
- Levesque, E. M., Chornock, R., Soderberg, A. M., Berger, E., & Lunyan, R. 2012, ApJ, 758, 92
- Levesque, E. M., Kewley, L. J., Berger, E., & Zahid, H. J. 2010a, AJ, 140, 1557
- Levesque, E. M., Bloom, J. S., Butler, N. R., et al. 2010b, MNRAS, 401, 963
- Li, L.-X., & Paczyński, B. 1998, ApJ, 507, L59
- Liang, E., Zhang, B., Virgili, F., & Dai, Z. G. 2007, ApJ, 662, 1111
- Lü, H.-J., Zhang, B., Lei, W.-H., Li, Y., & Lasky, P. D. 2015, ApJ, 805, 89

- Lü, H.-J., Zhang, B., Liang, E.-W., Zhang, B.-B., & Sakamoto, T. 2014, MNRAS, 442, 1922
- MacFadyen, A. I., & Woosley, S. E. 1999, ApJ, 524, 262
- Maiorano, E., Masetti, N., Palazzi, E., et al. 2006, A&A, 455, 423
- Malesani, D., Fynbo, J. P. U., Christensen, L., et al. 2009a, GRB Coordinates Network, 9761, 1
- Malesani, D., Fynbo, J. P. U., D’Elia, V., et al. 2009b, GRB Coordinates Network, 9457, 1
- Malesani, D., Xu, D., D’Avanzo, P., Palazzi, E., & Perna, D. 2014a, GRB Coordinates Network, 16229, 1
- Malesani, D., Xu, D., Fynbo, J. P. U., et al. 2014b, GRB Coordinates Network, 15800, 1
- Mannucci, F., Salvaterra, R., & Campisi, M. A. 2011, MNRAS, 414, 1263
- Masetti, N., Palazzi, E., Pian, E., et al. 2003, A&A, 404, 465
- . 2005, A&A, 438, 841
- Mazets, E. P., Golenetskii, S. V., Ilinskii, V. N., et al. 1981, Ap&SS, 80, 3
- McBreen, S., Krühler, T., Rau, A., et al. 2010, A&A, 516, A71
- McGlynn, S., Foley, S., McBreen, S., et al. 2008, A&A, 486, 405
- McGuire, J. T. W., Tanvir, N. R., Levan, A. J., et al. 2015, ArXiv e-prints, arXiv:1512.07808
- Meegan, C. A., Pendleton, G. N., Briggs, M. S., et al. 1996, ApJS, 106, 65
- Melandri, A., Bernardini, M. G., D’Avanzo, P., et al. 2015, A&A, 581, A86
- Metzger, B. D., Martínez-Pinedo, G., Darbha, S., et al. 2010, MNRAS, 406, 2650
- Michałowski, M. J., Gentile, G., Hjorth, J., et al. 2015, A&A, 582, A78
- Milne, P. A., & Cenko, S. B. 2011, GRB Coordinates Network, 11708, 1
- Milvang-Jensen, B., Fynbo, J. P. U., Malesani, D., et al. 2012, ApJ, 756, 25
- Mirabal, N., Halpern, J. P., An, D., Thorstensen, J. R., & Terndrup, D. M. 2006, ApJ, 643, L99
- Mirabal, N., Halpern, J. P., & O’Brien, P. T. 2007, ApJ, 661, L127

- Mirabal, N., Halpern, J. P., Kulkarni, S. R., et al. 2002, ApJ, 578, 818
- Möller, P., Fynbo, J. P. U., Hjorth, J., et al. 2002, A&A, 396, L21
- Morgan, A. N., Perley, D. A., Cenko, S. B., et al. 2014, MNRAS, 440, 1810
- Mortlock, A., Conselice, C. J., Hartley, W. G., et al. 2015, MNRAS, 447, 2
- Moustakas, J., Kennicutt, Jr., R. C., & Tremonti, C. A. 2006, ApJ, 642, 775
- Nakagawa, Y., Ricker, G., Atteia, J.-L., et al. 2005, GRB Coordinates Network, 3053, 1
- Narayan, R., Paczynski, B., & Piran, T. 1992, ApJ, 395, L83
- Nava, L., Ghirlanda, G., Ghisellini, G., & Firmani, C. 2008, MNRAS, 391, 639
- Nicastro, L., in't Zand, J. J. M., Amati, L., et al. 2004, A&A, 427, 445
- Niino, Y., Hashimoto, T., Aoki, K., et al. 2012, PASJ, 64, 115
- Norris, J., Ukwatta, T. N., Barthelmy, S. D., et al. 2010a, GRB Coordinates Network, 11113, 1
- Norris, J. P., Gehrels, N., & Scargle, J. D. 2010b, ApJ, 717, 411
- Ofek, E. O., Cenko, S. B., Gal-Yam, A., et al. 2007, ApJ, 662, 1129
- Ohno, M., Kokubun, M., Suzuki, M., et al. 2008, GRB Coordinates Network, 7630, 1
- Olivares E., F., Greiner, J., Schady, P., et al. 2015, A&A, 577, A44
- Osip, D., Chen, H.-W., & Prochaska, J. X. 2006, GRB Coordinates Network, 5715, 1
- Paciesas, W. S., Meegan, C. A., Pendleton, G. N., et al. 1999, ApJS, 122, 465
- Paciesas, W. S., Meegan, C. A., von Kienlin, A., et al. 2012, ApJS, 199, 18
- Paczynski, B. 1986, ApJ, 308, L43
- Paczyński, B. 1998, ApJ, 494, L45
- Pal'Shin, V. 2006, GRB Coordinates Network, 5984, 1
- Pal'Shin, V., Golenetskii, S., Aptekar, R., et al. 2008, GRB Coordinates Network, 8256, 1
- . 2009a, GRB Coordinates Network, 9196, 1

- . 2009b, GRB Coordinates Network, 9821, 1
- Pélagéon, A., Atteia, J.-L., Nakagawa, Y. E., et al. 2008, *A&A*, 491, 157
- Pellizza, L. J., Duc, P.-A., Le Floc'h, E., et al. 2006, *A&A*, 459, L5
- Penprase, B. E., Berger, E., Fox, D. B., et al. 2006, *ApJ*, 646, 358
- Pérez-Ramírez, D., Norris, J. P., Gorosabel, J., et al. 2013, in EAS Publications Series, Vol. 61, EAS Publications Series, ed. A. J. Castro-Tirado, J. Gorosabel, & I. H. Park, 345–349
- Perley, D. A. 2014, GRB Coordinates Network, 16181, 1
- Perley, D. A., Bloom, J. S., Modjaz, M., et al. 2008a, GRB Coordinates Network, 7889, 1
- Perley, D. A., Bloom, J. S., & Prochaska, J. X. 2008b, GRB Coordinates Network, 7791, 1
- Perley, D. A., Foley, R. J., Bloom, J. S., & Butler, N. R. 2006, GRB Coordinates Network, 5387, 1
- Perley, D. A., Modjaz, M., Morgan, A. N., et al. 2012a, *ApJ*, 758, 122
- Perley, D. A., Prochaska, J. X., Kalas, P., et al. 2009a, GRB Coordinates Network, 10272, 1
- Perley, D. A., Prochaska, J. X., & Morgan, A. N. 2012b, GRB Coordinates Network, 14059, 1
- Perley, D. A., Li, W., Chornock, R., et al. 2008c, *ApJ*, 688, 470
- Perley, D. A., Bloom, J. S., Butler, N. R., et al. 2008d, *ApJ*, 672, 449
- Perley, D. A., Metzger, B. D., Granot, J., et al. 2009b, *ApJ*, 696, 1871
- Perley, D. A., Cenko, S. B., Bloom, J. S., et al. 2009c, *AJ*, 138, 1690
- Perley, D. A., Levan, A. J., Tanvir, N. R., et al. 2013, *ApJ*, 778, 128
- Perley, D. A., Krühler, T., Schulze, S., et al. 2016, *ApJ*, 817, 7
- Pettini, M., & Pagel, B. E. J. 2004, *MNRAS*, 348, L59
- Piranomonte, S., Vergani, S. D., Malesani, D., et al. 2011, GRB Coordinates Network, 12164, 1
- Piranomonte, S., Japelj, J., Vergani, S. D., et al. 2015, *MNRAS*, 452, 3293

- Piro, L., Frail, D. A., Gorosabel, J., et al. 2002, ApJ, 577, 680
- Preece, R. D., Briggs, M. S., Mallozzi, R. S., et al. 2000, ApJS, 126, 19
- Price, P. A. 2006, GRB Coordinates Network, 5104, 1
- Price, P. A., Kulkarni, S. R., Berger, E., et al. 2002a, ApJ, 571, L121
- Price, P. A., Berger, E., Kulkarni, S. R., et al. 2002b, ApJ, 573, 85
- Prochaska, J. X., Chen, H.-W., Dessauges-Zavadsky, M., & Bloom, J. S. 2007a, ApJ, 666, 267
- Prochaska, J. X., Cooper, M., Newman, J., et al. 2005a, GRB Coordinates Network, 3390
- Prochaska, J. X., Dessauges-Zavadsky, M., Ramirez-Ruiz, E., & Chen, H.-W. 2008, ApJ, 685, 344
- Prochaska, J. X., Ellison, S., Foley, R. J., Bloom, J. S., & Chen, H.-W. 2005b, GRB Coordinates Network, 3332, 1
- Prochaska, J. X., Perley, D. A., Modjaz, M., et al. 2007b, GRB Coordinates Network, 6864, 1
- Prochaska, J. X., Bloom, J. S., Chen, H.-W., et al. 2004, ApJ, 611, 200
- Prochaska, J. X., Chen, H.-W., Bloom, J. S., et al. 2007c, ApJS, 168, 231
- Qin, Y., Liang, E.-W., Liang, Y.-F., et al. 2013, ApJ, 763, 15
- Quimby, R., Fox, D., Hoeflich, P., Roman, B., & Wheeler, J. C. 2005, GRB Coordinates Network, 4221, 1
- Rau, A., Fynbo, J., & Greiner, J. 2010a, GRB Coordinates Network, 10350, 1
- Rau, A., Kruehler, T., & Greiner, J. 2013, GRB Coordinates Network, 15330, 1
- Rau, A., McBreen, S., & Kruehler, T. 2009, GRB Coordinates Network, 9353, 1
- Rau, A., Salvato, M., & Greiner, J. 2005, A&A, 444, 425
- Rau, A., Savaglio, S., Krühler, T., et al. 2010b, ApJ, 720, 862
- Rhoads, J. E. 2010, ApJ, 709, 664

- Richardson, G., Koshut, T., Paciesas, W., & Kouveliotou, C. 1996, in American Institute of Physics Conference Series, Vol. 384, American Institute of Physics Conference Series, ed. C. Kouveliotou, M. F. Briggs, & G. J. Fishman, 87–90
- Ricker, G., Atteia, J.-L., Kawai, N., et al. 2002, GRB Coordinates Network, 1530, 1
- Rossi, A., Piranomonte, S., Savaglio, S., et al. 2014, A&A, 572, A47
- Rowlinson, A., Wiersema, K., Levan, A. J., et al. 2010, MNRAS, 408, 383
- Ruiz-Velasco, A. E., Swan, H., Troja, E., et al. 2007, ApJ, 669, 1
- Sahu, K. C., Livio, M., Petro, L., et al. 1997, Nature, 387, 476
- Sakamoto, T., Barthelmy, S. D., Baumgartner, W. H., et al. 2010, GRB Coordinates Network, 10524, 1
- Sakamoto, T., Lamb, D. Q., Kawai, N., et al. 2005a, ApJ, 629, 311
- Sakamoto, T., Ricker, G., Atteia, J.-L., et al. 2005b, GRB Coordinates Network, 3189, 1
- Sakamoto, T., Sato, G., Barbier, L., et al. 2009, ApJ, 693, 922
- Sakamoto, T., Barthelmy, S. D., Baumgartner, W., et al. 2011a, GRB Coordinates Network, 12276, 1
- Sakamoto, T., Barthelmy, S. D., Baumgartner, W. H., et al. 2011b, ApJS, 195, 2
- Salvaterra, R., Della Valle, M., Campana, S., et al. 2009, Nature, 461, 1258
- Sanchez-Ramirez, R., Gorosabel, J., Castro-Tirado, A. J., Cepa, J., & Gomez-Velarde, G. 2013, GRB Coordinates Network, 14685, 1
- Sanchez-Ramirez, R., Gorosabel, J., de Ugarte Postigo, A., & Gonzalez Perez, J. M. 2012, GRB Coordinates Network, 13723, 1
- Savaglio, S., Glazebrook, K., & Le Borgne, D. 2009, ApJ, 691, 182
- Savaglio, S., Rau, A., Greiner, J., et al. 2012, MNRAS, 420, 627
- Savchenko, V., Neronov, A., & Courvoisier, T. J.-L. 2012, A&A, 541, A122
- Schady, P., Page, M. J., Oates, S. R., et al. 2010, MNRAS, 401, 2773
- Schady, P., Krühler, T., Greiner, J., et al. 2015, A&A, 579, A126

- Schaefer, B. E., Snyder, J. A., Hernandez, J., et al. 1999, ApJ, 524, L103
- Schulze, S., Klose, S., Björnsson, G., et al. 2011, A&A, 526, A23
- Schulze, S., Malesani, D., Cucchiara, A., et al. 2014, A&A, 566, A102
- Serino, M., Sakamoto, T., Kawai, N., et al. 2014, PASJ, 66, 87
- Smette, A., Ledoux, C., Vreeswijk, P., et al. 2013, GRB Coordinates Network, 14848, 1
- Soderberg, A. M., Kulkarni, S. R., Berger, E., et al. 2004, ApJ, 606, 994
- Soderberg, A. M., Kulkarni, S. R., Price, P. A., et al. 2006a, ApJ, 636, 391
- Soderberg, A. M., Kulkarni, S. R., Nakar, E., et al. 2006b, Nature, 442, 1014
- Soderberg, A. M., Berger, E., Kasliwal, M., et al. 2006c, ApJ, 650, 261
- Sparre, M., de Ugarte Postigo, A., Fynbo, J. P. U., et al. 2011a, GRB Coordinates Network, 11607, 1
- Sparre, M., Sollerman, J., Fynbo, J. P. U., et al. 2011b, ApJ, 735, L24
- Sparre, M., Hartoog, O. E., Krühler, T., et al. 2014, ApJ, 785, 150
- Stanek, K. Z., Matheson, T., Garnavich, P. M., et al. 2003, ApJ, 591, L17
- Stanway, E. R., Levan, A. J., Tanvir, N., et al. 2015, MNRAS, 446, 3911
- Stratta, G., Basa, S., Butler, N., et al. 2007, A&A, 461, 485
- Sun, H., Zhang, B., & Li, Z. 2015, ApJ, 812, 33
- Svensson, K. M., Levan, A. J., Tanvir, N. R., Fruchter, A. S., & Strolger, L.-G. 2010, MNRAS, 405, 57
- Svensson, K. M., Levan, A. J., Tanvir, N. R., et al. 2012, MNRAS, 421, 25
- Tanvir, N., Levan, A., Wiersema, K., et al. 2009a, GRB Coordinates Network, 9219
- Tanvir, N. R., & Ball, J. 2012, GRB Coordinates Network, 13532, 1
- Tanvir, N. R., Cucchiara, A., & Cenko, S. B. 2013a, GRB Coordinates Network, 14366, 1
- Tanvir, N. R., Fox, D., Fynbo, J., & Trujillo, C. 2012a, GRB Coordinates Network, 13562, 1

- Tanvir, N. R., Kruehler, T., Schulze, S., & Karjalainen, R. 2014a, GRB Coordinates Network, 15988
- Tanvir, N. R., Levan, A. J., Cucchiara, A., Perley, D., & Cenko, S. B. 2014b, GRB Coordinates Network, 16125, 1
- Tanvir, N. R., Levan, A. J., Fruchter, A. S., et al. 2013b, Nature, 500, 547
- Tanvir, N. R., Levan, A. J., & Matulonis, T. 2012b, GRB Coordinates Network, 14009, 1
- Tanvir, N. R., Levan, A. J., Matulonis, T., & Smith, A. B. 2013c, GRB Coordinates Network, 14567, 1
- Tanvir, N. R., Levan, A. J., Wiersema, K., et al. 2014c, GRB Coordinates Network, 16150, 1
- Tanvir, N. R., Wiersema, K., & Levan, A. J. 2010a, GRB Coordinates Network, 11230, 1
- Tanvir, N. R., Wiersema, K., Levan, A. J., Cenko, S. B., & Geballe, T. 2011, GRB Coordinates Network, 12225, 1
- Tanvir, N. R., Wiersema, K., Levan, A. J., et al. 2012c, GRB Coordinates Network, 13441, 1
- Tanvir, N. R., Wiersema, K., Xu, D., & Fynbo, J. P. U. 2013d, GRB Coordinates Network, 14882, 1
- Tanvir, N. R., Fox, D. B., Levan, A. J., et al. 2009b, Nature, 461, 1254
- Tanvir, N. R., Vergani, S., Hjorth, J., et al. 2010b, GRB Coordinates Network, 11123, 1
- Tanvir, N. R., Rol, E., Levan, A. J., et al. 2010c, ApJ, 725, 625
- Tanvir, N. R., Levan, A. J., Fruchter, A. S., et al. 2012d, ApJ, 754, 46
- Tello, J. C., Sanchez-Ramirez, R., Gorosabel, J., et al. 2012, GRB Coordinates Network, 13118, 1
- Thoene, C. C., de Ugarte Postigo, A., Gorosabel, J., et al. 2012, GRB Coordinates Network, 13628, 1
- Thoene, C. C., Perley, D. A., Cooke, J., et al. 2007, GRB Coordinates Network, 6741, 1
- Thoene, C. C., Jakobsson, P., De Cia, A., et al. 2009, GRB Coordinates Network, 9409, 1

- Thöne, C. C., Kann, D. A., Jóhannesson, G., et al. 2010, A&A, 523, A70
- Thöne, C. C., Fynbo, J. P. U., Goldoni, P., et al. 2013, MNRAS, 428, 3590
- Tinney, C., Stathakis, R., Cannon, R., et al. 1998, IAU Circ., 6896, 3
- Toy, V. L., Cenko, S. B., Silverman, J. M., et al. 2016, ApJ, 818, 79
- Tunnicliffe, R. L., Levan, A. J., Tanvir, N. R., et al. 2014, MNRAS, 437, 1495
- van der Horst, A. J., Levan, A. J., Pooley, G. G., et al. 2015, MNRAS, 446, 4116
- van der Wel, A., Franx, M., van Dokkum, P. G., et al. 2014, ApJ, 788, 28
- Vergani, S. D., D'Avanzo, P., Malesani, D., et al. 2010, GRB Coordinates Network, 10495, 1
- Vergani, S. D., Flores, H., Covino, S., et al. 2011, A&A, 535, A127
- Vergani, S. D., Salvaterra, R., Japelj, J., et al. 2015, A&A, 581, A102
- Villasenor, J. S., Lamb, D. Q., Ricker, G. R., et al. 2005, Nature, 437, 855
- Virgili, F. J., Liang, E.-W., & Zhang, B. 2009, MNRAS, 392, 91
- Virgili, F. J., Qin, Y., Zhang, B., & Liang, E. 2012, MNRAS, 424, 2821
- Volnova, A. A., Pozanenko, A. S., Gorosabel, J., et al. 2014, MNRAS, 442, 2586
- von Kienlin, A., Meegan, C. A., Paciesas, W. S., et al. 2014, ApJS, 211, 13
- Vreeswijk, P., Fruchter, A., Hjorth, J., & Kouveliotou, C. 2003, GRB Coordinates Network, 1785, 1
- Vreeswijk, P. M., Ledoux, C., De Cia, A., & Smette, A. 2012, Memorie della Societa Astronomica Italiana Supplementi, 21, 14
- Vreeswijk, P. M., Rol, E., Hjorth, J., et al. 1999, GRB Coordinates Network, 496, 1
- Vreeswijk, P. M., Fruchter, A., Kaper, L., et al. 2001, ApJ, 546, 672
- Vreeswijk, P. M., Ellison, S. L., Ledoux, C., et al. 2004, A&A, 419, 927
- Vreeswijk, P. M., Smette, A., Fruchter, A. S., et al. 2006, A&A, 447, 145
- Vreeswijk, P. M., Ledoux, C., Smette, A., et al. 2007, A&A, 468, 83
- Wainwright, C., Berger, E., & Penprase, B. E. 2007, ApJ, 657, 367

- Watson, D., Fynbo, J. P. U., Ledoux, C., et al. 2006, ApJ, 652, 1011
- Wiersema, K., Levan, A., Kamble, A., Tanvir, N., & Malesani, D. 2009, GRB Coordinates Network, 9673, 1
- Wiersema, K., van der Horst, A. J., Kann, D. A., et al. 2008, A&A, 481, 319
- Wiersema, K., Flores, H., D'Elia, V., et al. 2011, GRB Coordinates Network, 12431, 1
- Woosley, S. E. 1993, ApJ, 405, 273
- Woosley, S. E., & Bloom, J. S. 2006, ARA&A, 44, 507
- Xiong, S. 2013, GRB Coordinates Network, 14674
- Xu, D., Fynbo, J. P. U., D'Elia, V., & Tanvir, N. R. 2012, GRB Coordinates Network, 13460, 1
- Xu, D., Fynbo, J. P. U., Jakobsson, P., et al. 2013a, GRB Coordinates Network, 15407, 1
- Xu, D., Fynbo, J. P. U., Tanvir, N. R., et al. 2009, GRB Coordinates Network, 10053, 1
- Xu, D., de Ugarte Postigo, A., Leloudas, G., et al. 2013b, ApJ, 776, 98
- Yang, B., Jin, Z.-P., Li, X., et al. 2015, Nature Communications, 6, 7323
- Yonetoku, D., Murakami, T., Nakamura, T., et al. 2004, ApJ, 609, 935
- Younes, G. 2013, GRB Coordinates Network, 15477, 1
- Yu, H.-F., & Goldstein, A. 2014, GRB Coordinates Network, 16224
- Zafar, T., Watson, D. J., Malesani, D., et al. 2010, A&A, 515, A94
- Zauderer, B. A., Berger, E., Margutti, R., et al. 2013, ApJ, 767, 161
- Zhang, B. 2006, Nature, 444, 1010
- Zhang, B., Zhang, B.-B., Liang, E.-W., et al. 2007, ApJ, 655, L25
- Zhang, B., Zhang, B.-B., Virgili, F. J., et al. 2009, ApJ, 703, 1696
- Zhang, F.-W., Shao, L., Yan, J.-Z., & Wei, D.-M. 2012, ApJ, 750, 88

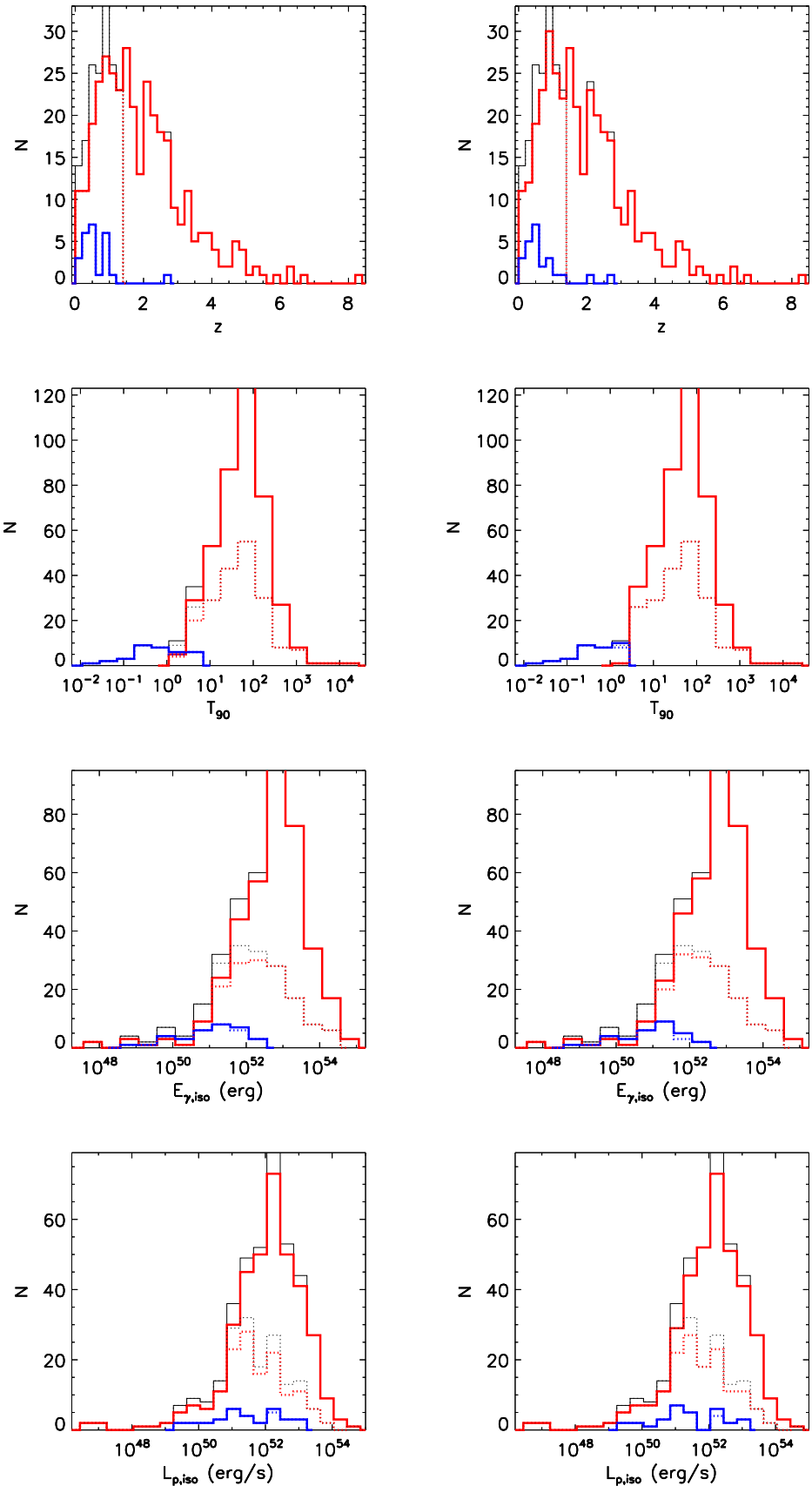


Fig. 1.— Distribution of prompt and host galaxy parameters of LGRBs (red lines) and SGRBs (blue lines). Left panels show distributions with consensus defined LGRBs and SGRBs, and right panels show distributions with T_{90} only defined LGRBs and SGRBs. Dotted lines show distribution of $z < 1.4$ subsamples.

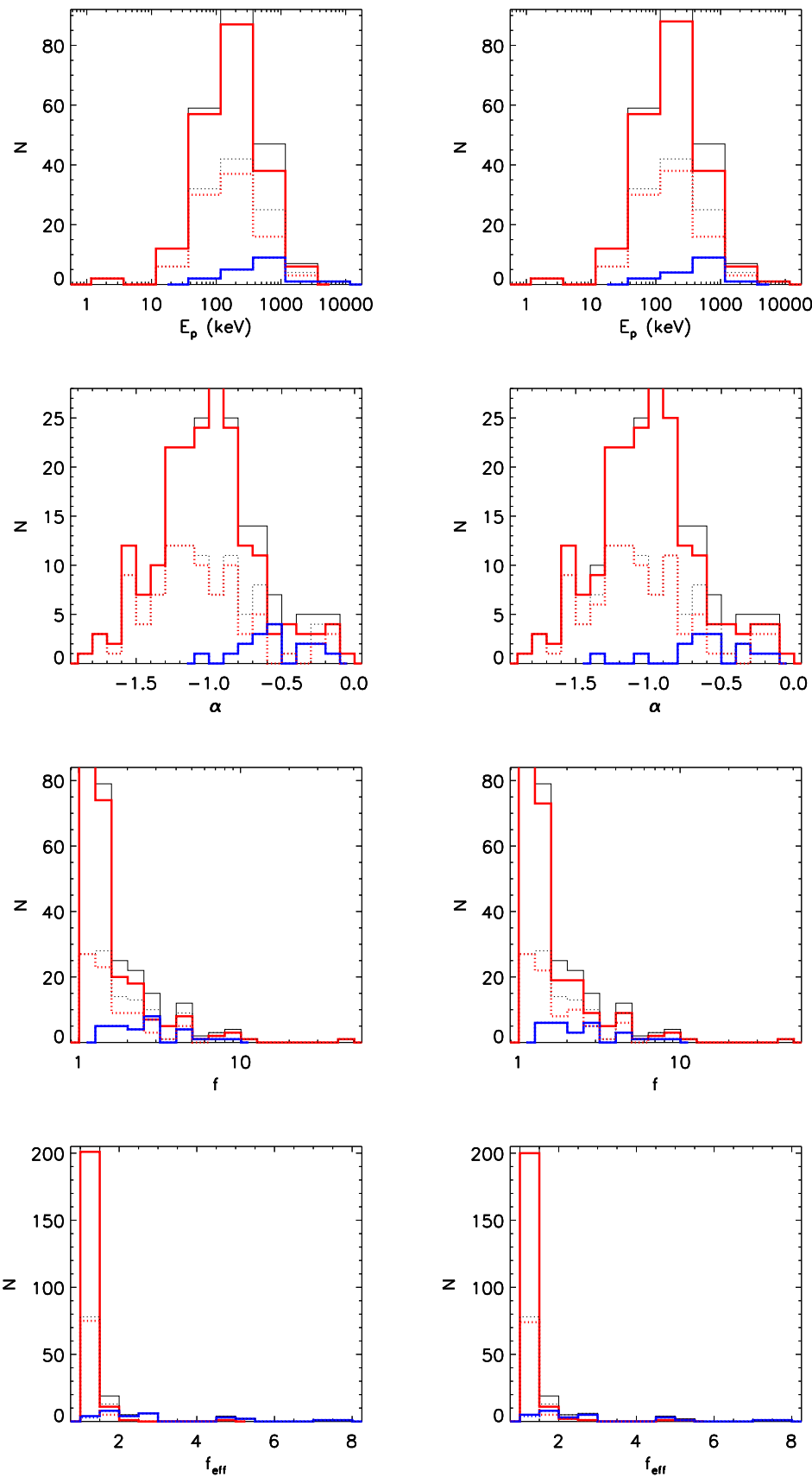


Fig. 1—Continued

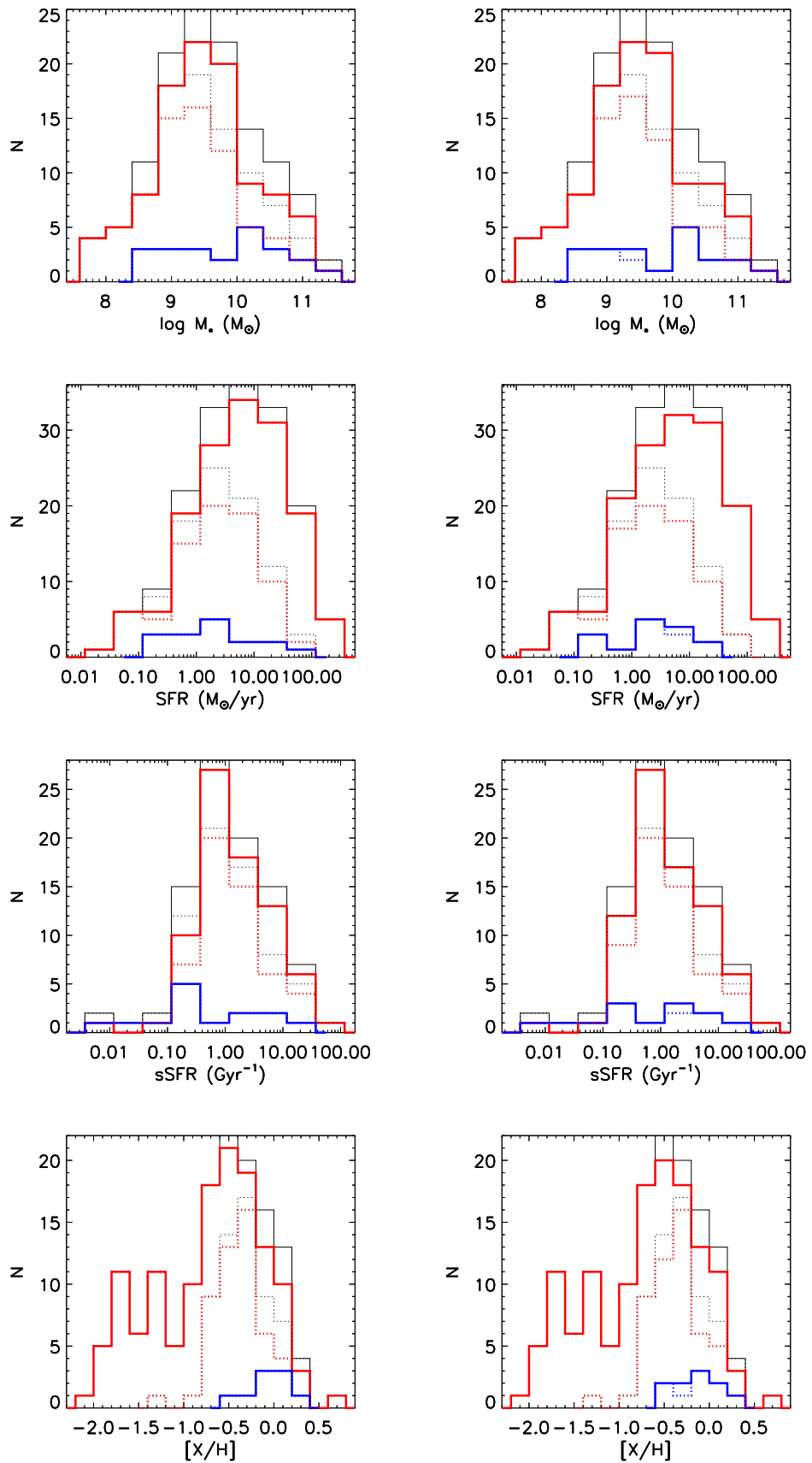


Fig. 1—Continued

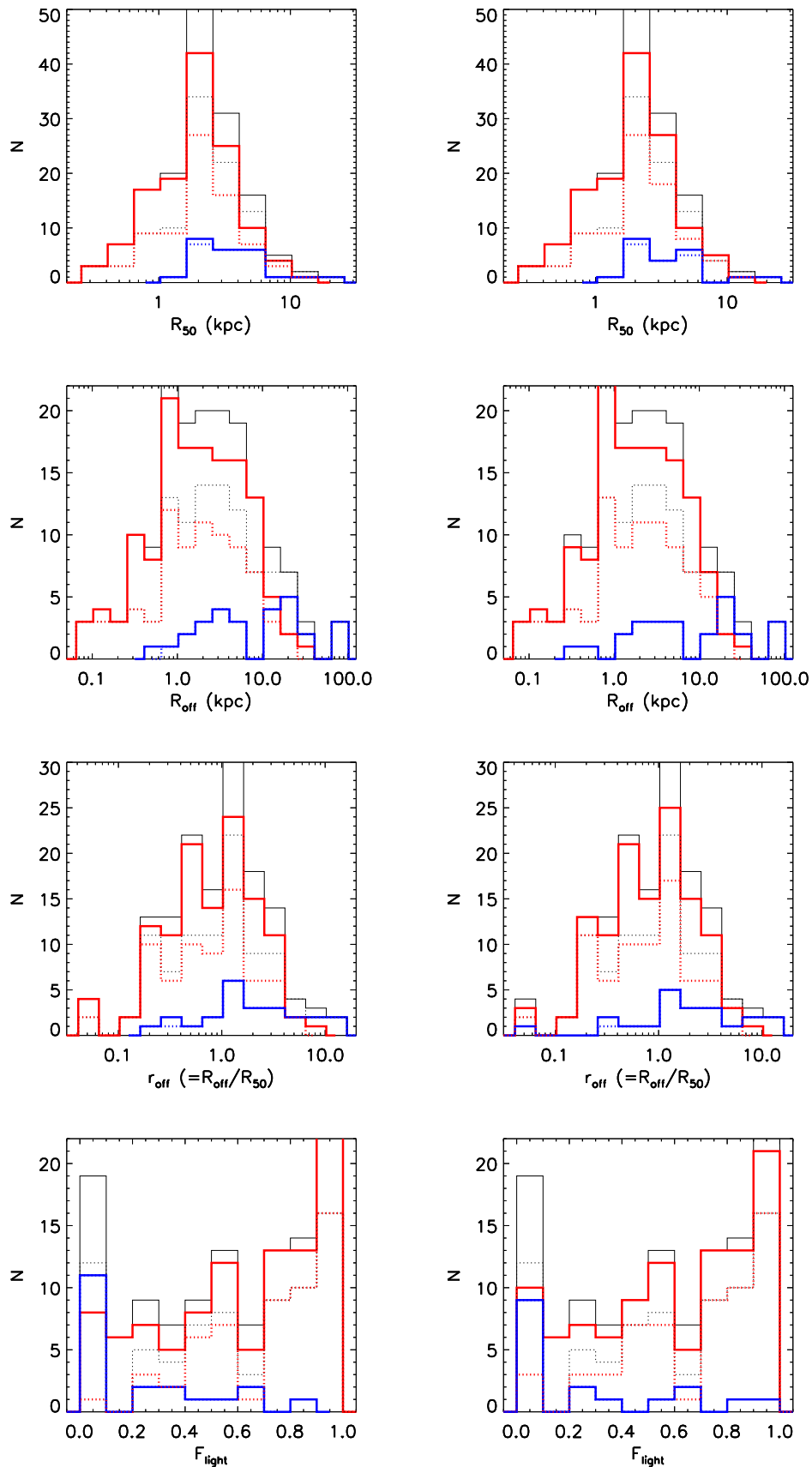


Fig. 1—Continued

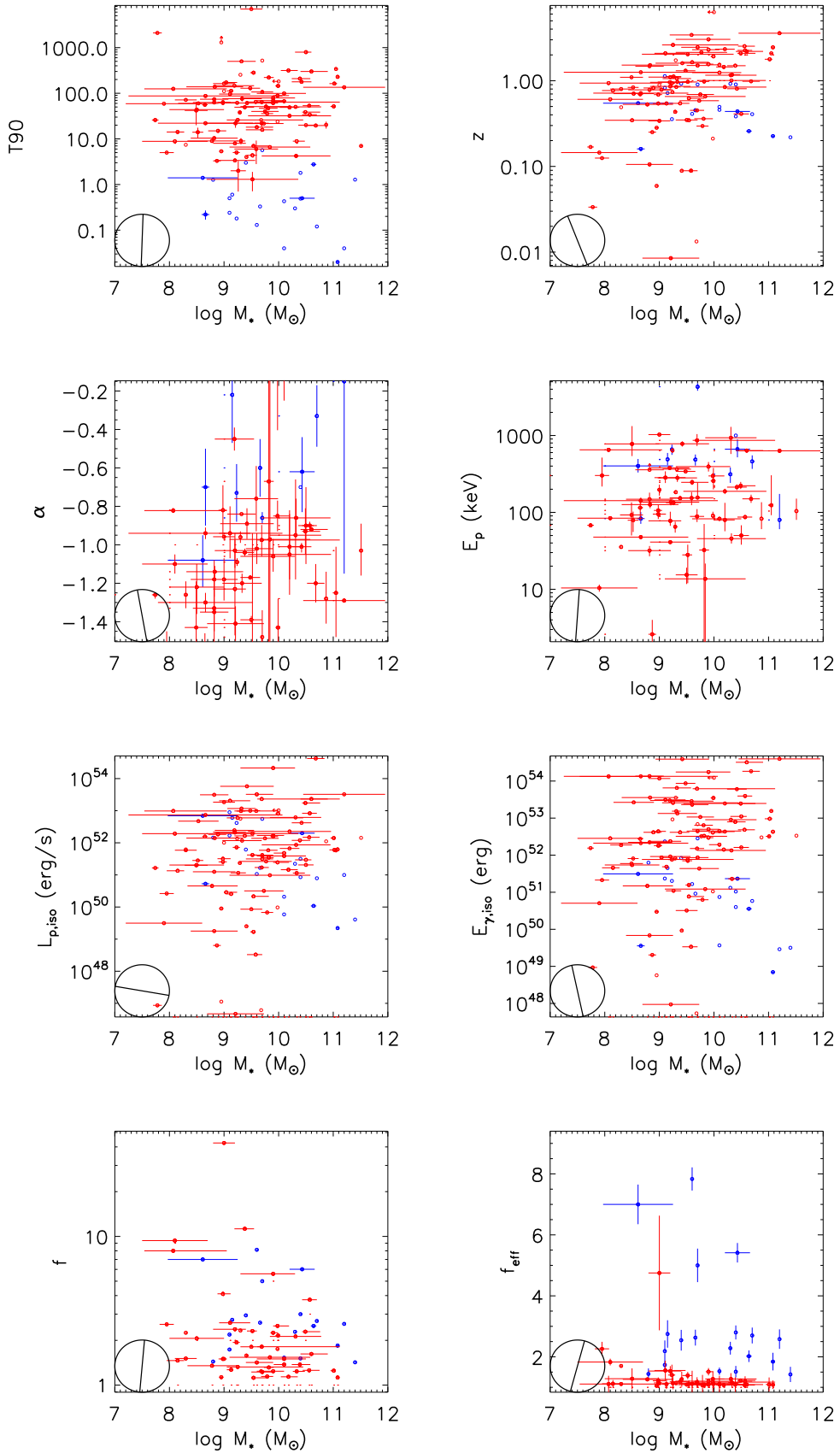


Fig. 2.— Prompt emission VS host galaxy property 2D plots of LGRBs (red dots) and SGRBs (blue dots). Black lines show the rotated new x-axis for the lowest P_{KS} .

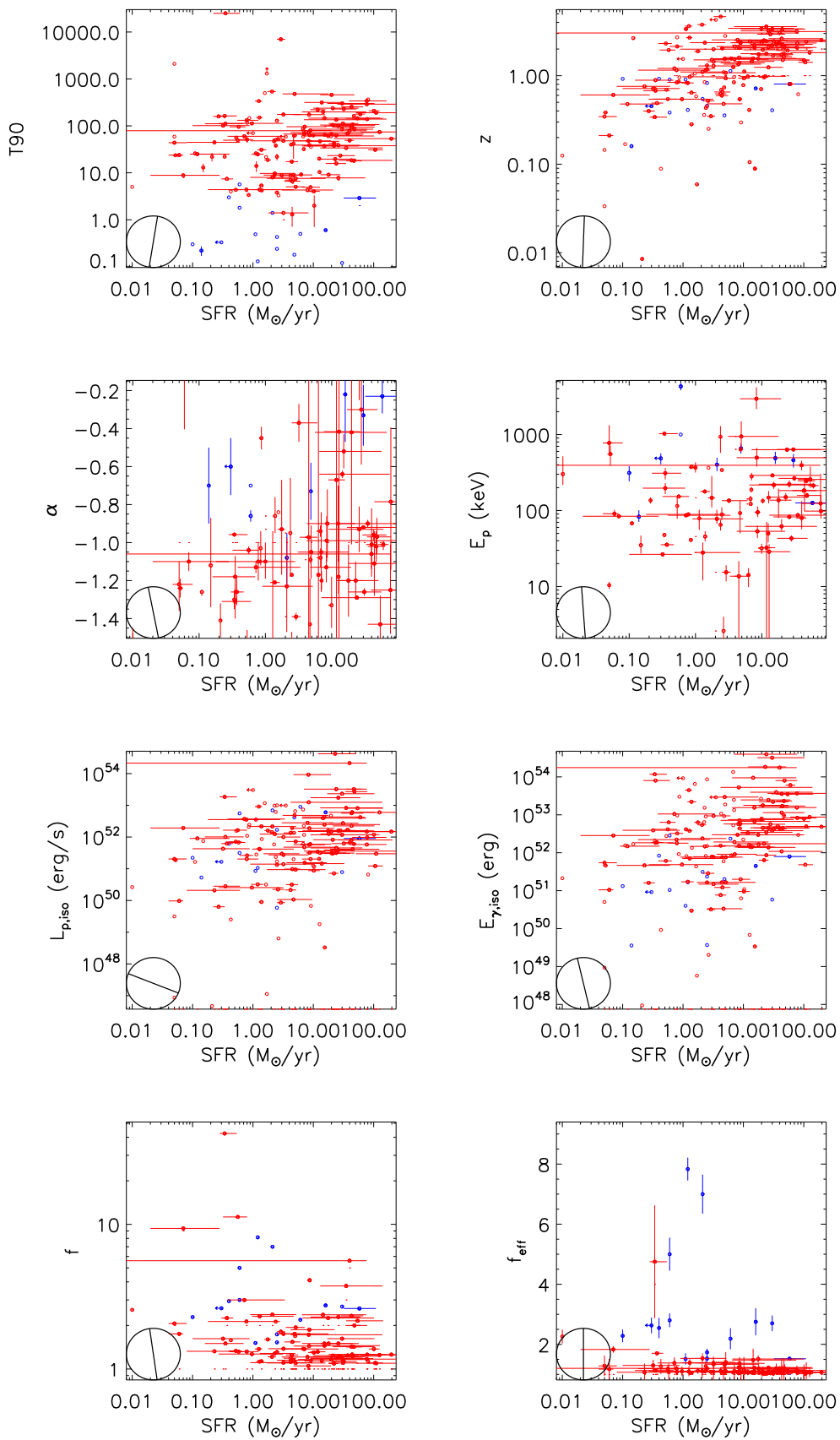


Fig. 2—Continued

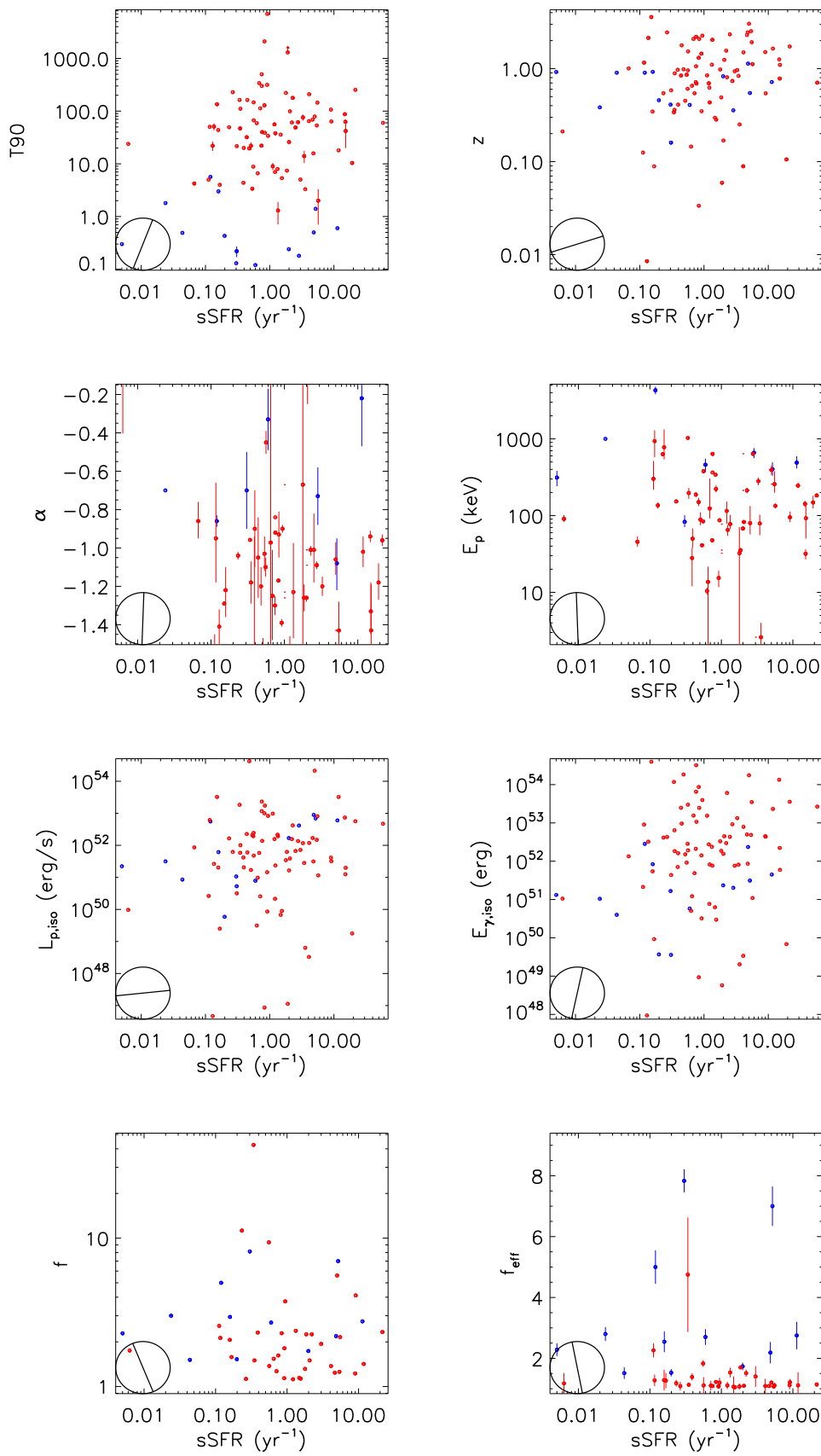


Fig. 2—Continued

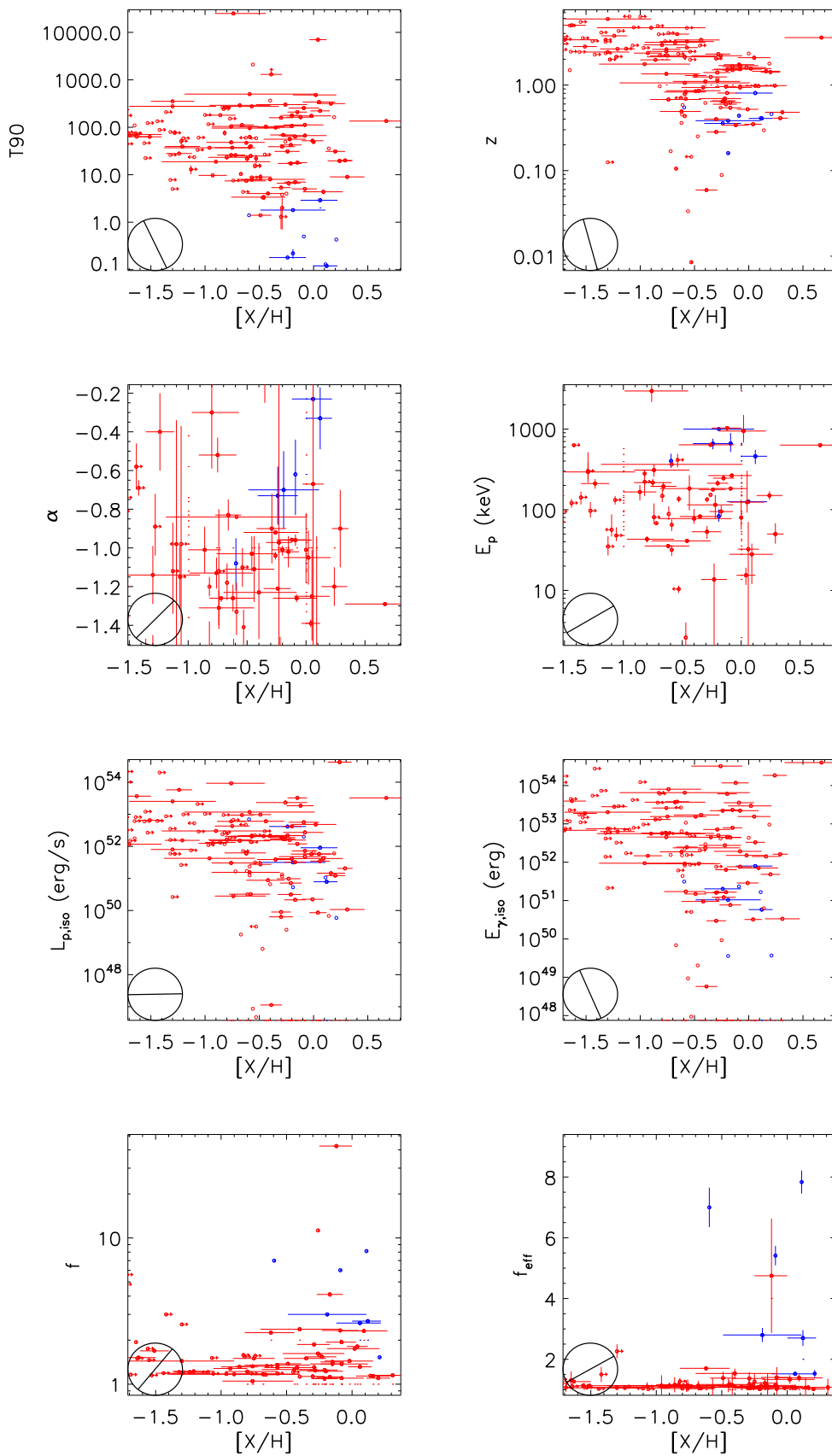


Fig. 2—Continued

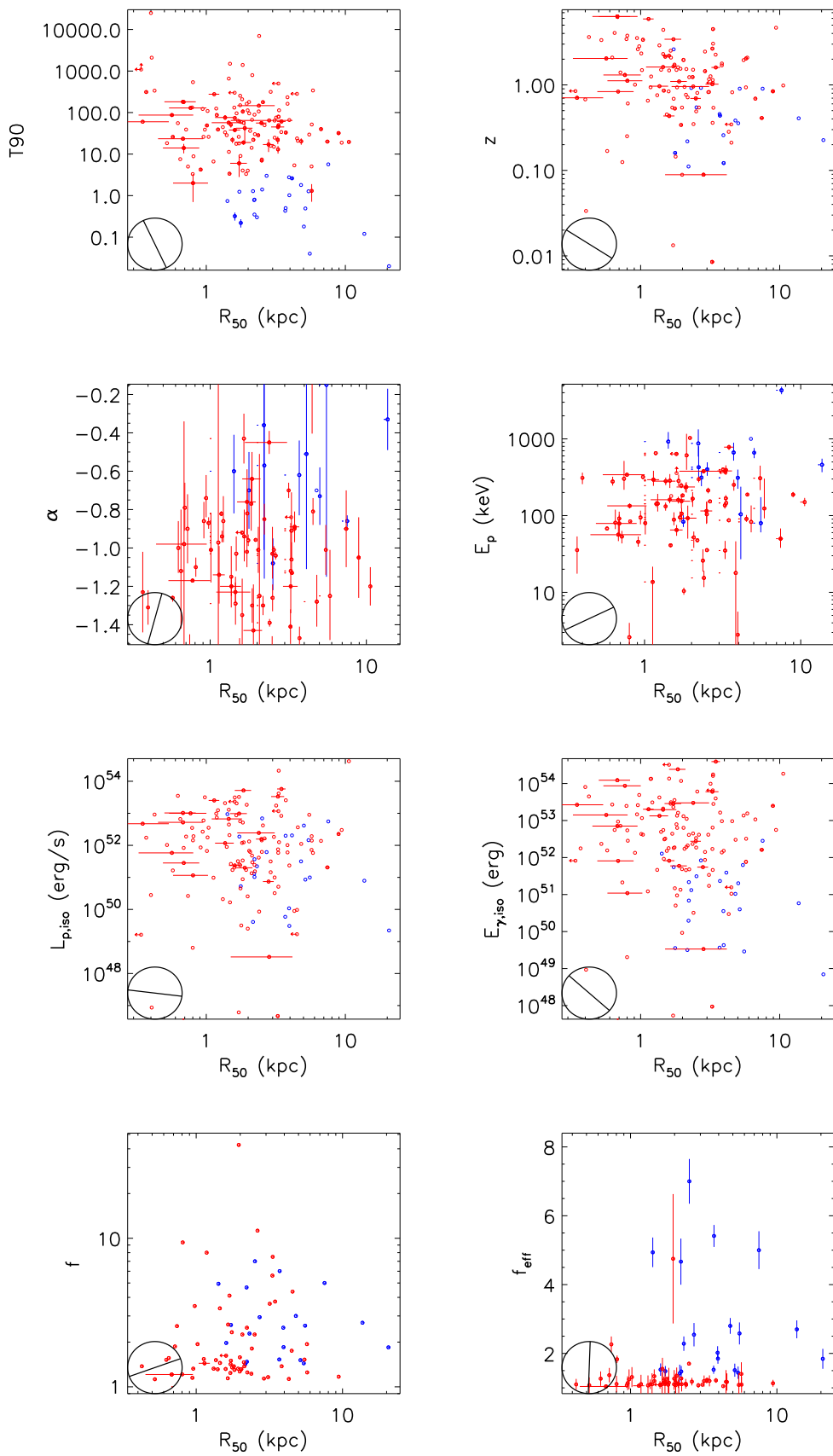


Fig. 2—Continued

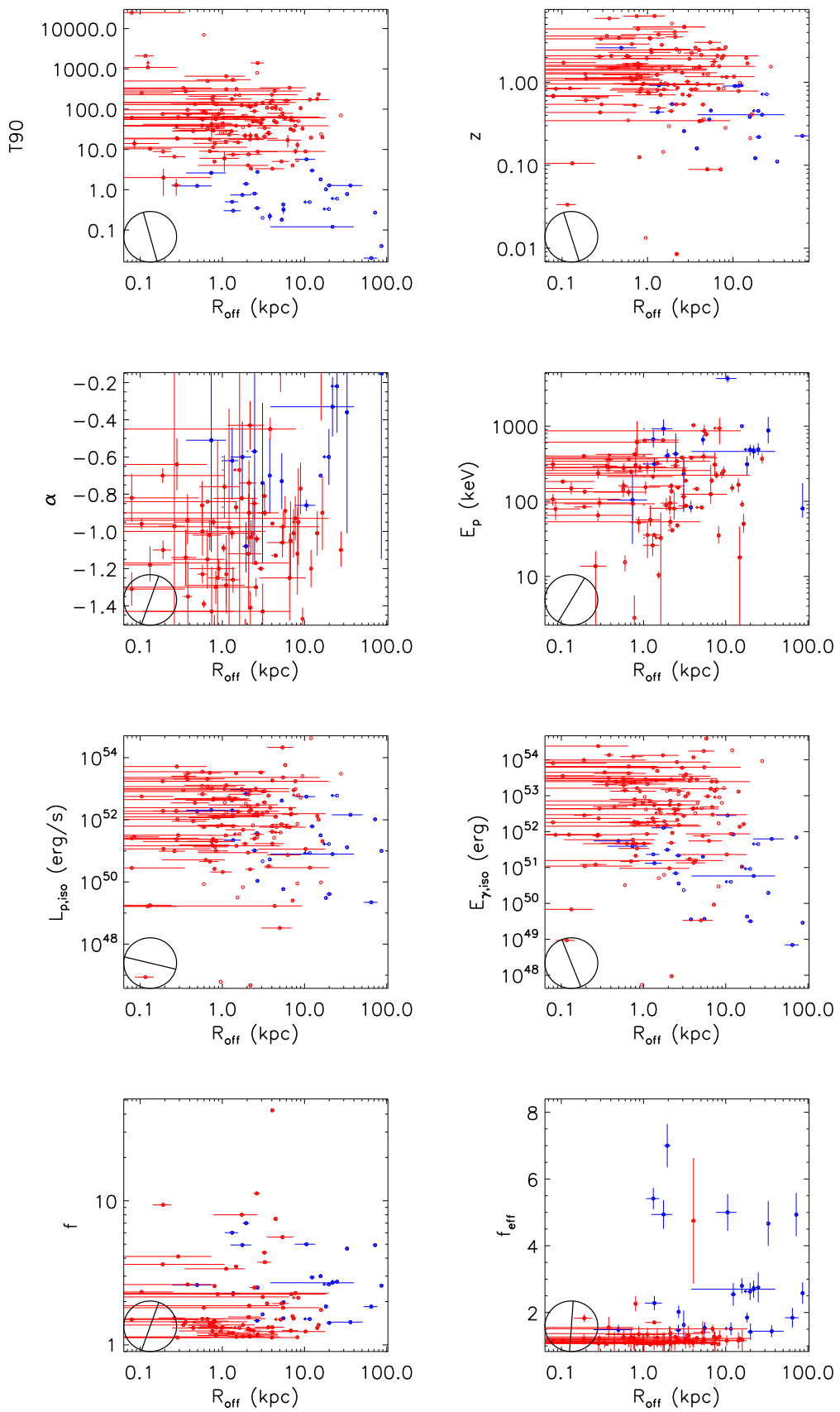


Fig. 2—Continued

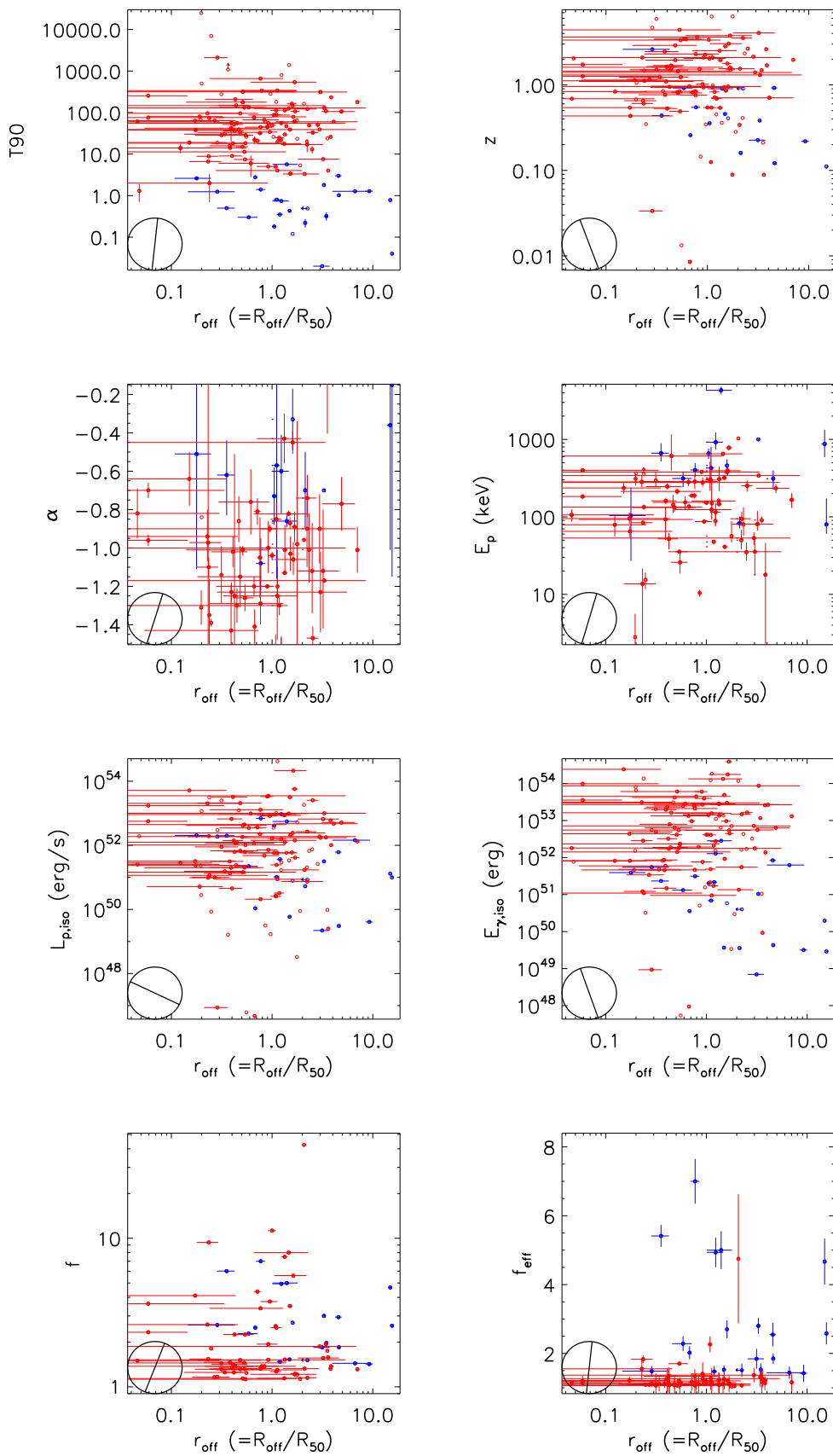


Fig. 2—Continued

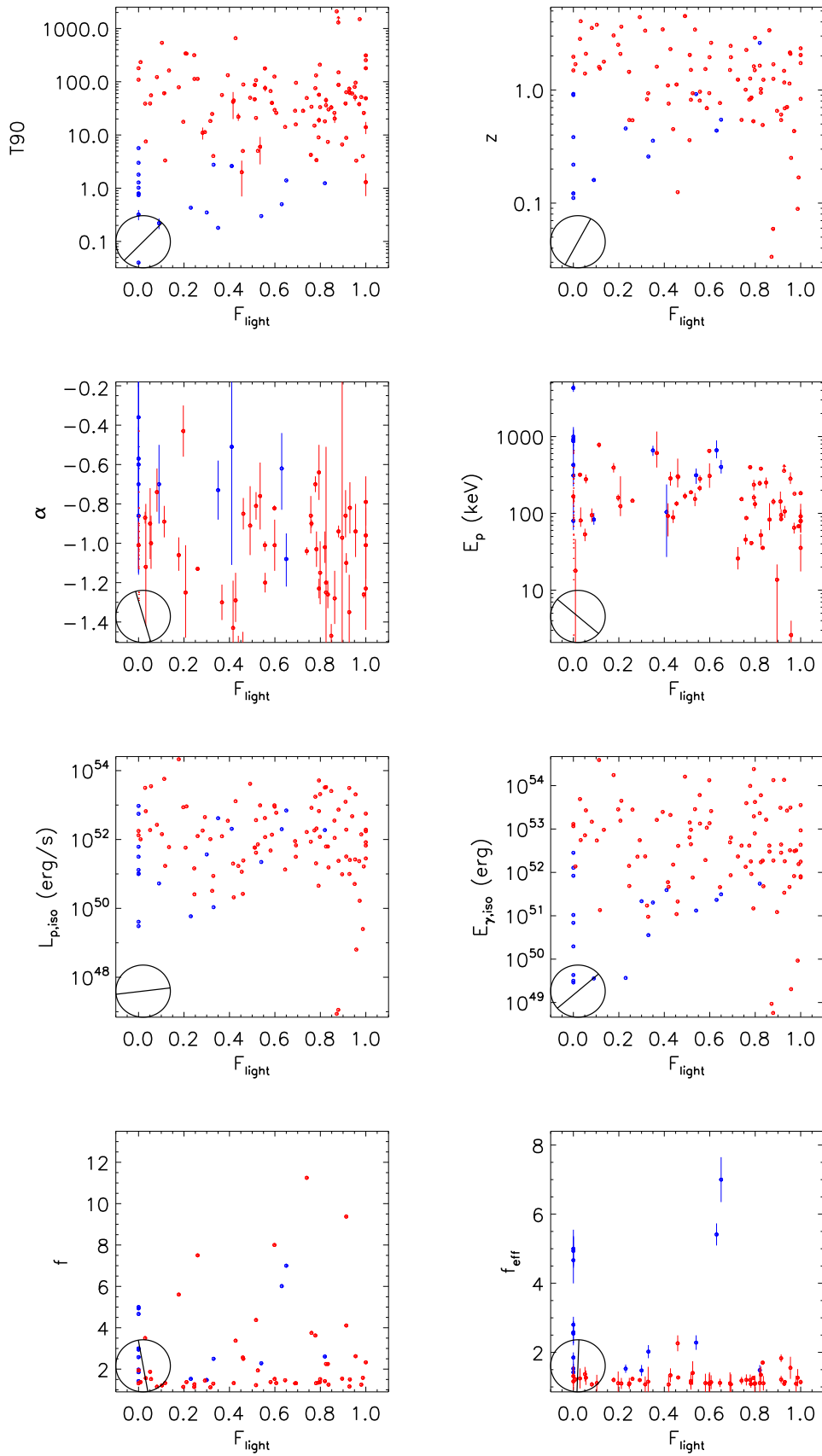


Fig. 2—Continued

Table 1. basic

GRB	redshift				T_{90}			$E_{\gamma,\text{iso}}$	$L_{\text{p},\text{iso}}$	f	f_{eff}
	(1)	(2)	(3)	(4)	Detector	[s]	Ref	[erg cm $^{-2}$]	[erg s $^{-1}$ cm $^{-2}$]	(10)	(11)
140606B	0.384	E	279	Fermi	23.6	39	4.60×10^{51}	1.88×10^{51}
140518A	4.707	A	272	Swift	60.5	42	7.92×10^{52}	2.89×10^{52}	1.18	1.02 ± 0.01	
140515A	6.32	A	271	Swift	23.4	42	7.08×10^{52}	5.23×10^{52}	1.21	1.04 ± 0.02	
140512A	0.725	A	273	Swift	154.8	42	5.63×10^{52}	6.71×10^{51}	1.78	1.25 ± 0.13	
140508A	1.027	A	270	Fermi	44.3	38	2.26×10^{53}	6.74×10^{52}
140506A	0.8893	E	275	Swift	111.1	42	1.83×10^{52}	1.01×10^{52}	1.50	1.13 ± 0.06	
140430A	1.6019	E	275	Swift	173.6	42	1.51×10^{52}	5.73×10^{51}	1.44	1.06 ± 0.03	
140428A	4.7	A	269	Swift	17.42	42	3.69×10^{52}	3.10×10^{52}
140423A	3.26	A	268	Swift	134	42	5.45×10^{53}	6.19×10^{52}	1.19	1.03 ± 0.01	
140419A	3.956	A	267	Swift	94.7	42	1.43×10^{54}	5.73×10^{53}	1.63	1.06 ± 0.03	
140318A	1.02	E	266	Swift	8.43	42	3.49×10^{51}	1.07×10^{51}	1.14	1.04 ± 0.02	
140311A	4.954	A	265	Swift	71.4	42	2.28×10^{53}	6.10×10^{52}
140304A	5.283	A	264	Swift	15.6	42	1.28×10^{53}	1.04×10^{53}	1.30	1.05 ± 0.03	
140301A	1.4155	E	275	Swift	31.0	42	4.82×10^{51}	1.22×10^{51}	1.10	1.02 ± 0.01	
140226A	1.98	A	276	Konus-Wind	15	37	4.81×10^{52}	2.20×10^{52}
140213A	1.2079	E	275	Swift	60.0	42	1.05×10^{53}	3.70×10^{52}	3.00	1.38 ± 0.19	
140206A	2.739	A	263	Swift	93.6	42	3.00×10^{53}	1.86×10^{53}	4.38	1.75 ± 0.38	
140114A	3 ± 0.1	A	275	Swift	139.7	42	1.28×10^{53}	8.96×10^{51}
131231A	0.6427	E	275	Fermi	31	36	2.21×10^{53}	2.18×10^{52}
131227A	5.3	A	258	Swift	18.0	42	1.42×10^{53}	1.03×10^{53}	1.18	1.03 ± 0.01	
131117A	4.042	A	256	Swift	11.00	42	1.44×10^{52}	1.34×10^{52}	1.16	1.04 ± 0.02	
131108A	2.4	A	255	Fermi	19	33	5.95×10^{53}	2.14×10^{53}
131105A	1.6854	E	275	Swift	112.3	42	2.21×10^{53}	2.72×10^{52}	1.10	1.03 ± 0.01	
131103A	0.5960	E	275	Swift	17.3	42	1.65×10^{51}	3.17×10^{50}	1.25	1.09 ± 0.04	
131030A	1.293	A	254	Swift	41.1	42	2.97×10^{53}	1.03×10^{53}	4.63	1.25 ± 0.13	
131011A	1.874	A	253	Fermi	77	32	1.05×10^{53}	1.59×10^{52}
131004A	0.717	E	252	Swift	1.54	42	8.01×10^{50}	1.48×10^{51}	1.94	1.94 ± 0.16	
130925A	0.3483	E	275	Swift	7000	34	3.21×10^{50}	8.56×10^{49}	1.81	1.09 ± 0.04	
130907A	1.238	A	251	Swift	> 360	42	2.98×10^{54}	1.86×10^{53}	4.75	1.38 ± 0.19	
130831A	0.4791	A	250	Swift	32.5	42	6.63×10^{51}	3.23×10^{51}	3.13	1.25 ± 0.13	
130702A	0.145	E	236	Fermi	59	31	5.05×10^{50}	3.15×10^{49}
130701A	1.1548	E	275	Swift	4.38	42	2.22×10^{52}	3.55×10^{52}	2.13	1.19 ± 0.09	
130612A	2.006	A	249	Swift	4.0	42	9.11×10^{51}	9.28×10^{51}	1.23	1.03 ± 0.01	
130610A	2.092	A	248	Swift	46.4	42	5.20×10^{52}	1.33×10^{52}	1.23	1.04 ± 0.02	
130606A	5.913	A	235	Swift	276.58	42	2.02×10^{53}	2.52×10^{53}	1.44	1.06 ± 0.03	
130604A	1.06	E	247	Swift	37.7	42	1.35×10^{52}	1.34×10^{51}	1.13	1.03 ± 0.01	
130528A	1.25	E	260	Swift	59.4	42	5.31×10^{52}	6.09×10^{51}	1.38	1.06 ± 0.03	
130518A	2.49	A	245	Fermi	48	30	1.78×10^{54}	6.01×10^{53}
130511A	1.3033	A	244	Swift	5.43	42	4.18×10^{51}	5.01×10^{51}	1.35	1.05 ± 0.03	
130505A	2.27	A	243	Swift	88	42	2.76×10^{54}	1.99×10^{54}	3.00	1.50 ± 0.25	
130427B	2.78 ± 0.02	A	242	Swift	27.0	42	6.49×10^{52}	3.95×10^{52}	1.31	1.11 ± 0.06	
130427A	0.3401	E	275	Swift	162.83	42	1.17×10^{54}	1.85×10^{53}	42.50	4.75 ± 1.88	
130420A	1.297	A	241	Swift	123.5	42	6.54×10^{52}	5.43×10^{51}	1.38	1.15 ± 0.08	
130418A	1.217	A	240	Swift	> 300	42	9.34×10^{52}	3.30×10^{51}	1.05	1.01 ± 0.01	

Table 1—Continued

GRB	redshift			T_{90}			$E_{\gamma, \text{iso}}$	$L_{\text{P}, \text{iso}}$	f	f_{eff}	
	(1)	(2)	(3)	Ref	Detector	[s]	Ref	[erg cm $^{-2}$]	[erg s $^{-1}$ cm $^{-2}$]		
(4)	(5)	(6)	(7)	(8)	(9)	(10)	(11)				
130408A	3.757	A	239	Swift	28	42	2.80×10^{53}	5.77×10^{53}	1.21	1.06 ± 0.03	
130215A	0.597	A	238	Swift	65.7	42	4.17×10^{52}	2.13×10^{51}	1.08	1.03 ± 0.01	
130131B	2.5393	E	275	Swift	4.30	42	2.98×10^{52}	2.81×10^{52}	1.21	1.08 ± 0.04	
121229A	2.707	A	233	Swift	100	27	1.97×10^{52}	8.70×10^{50}	
121211A	1.023	A	232	Swift	182	42	2.18×10^{51}	2.06×10^{51}	1.19	1.05 ± 0.03	
121209A	2.1 ± 0.3	A	275	Swift	42.7	42	1.09×10^{53}	3.44×10^{52}	1.36	1.05 ± 0.03	
121201A	3.3830	E	275	Swift	85	42	3.81×10^{52}	1.18×10^{52}	1.18	1.08 ± 0.04	
121128A	2.20	A	231	Swift	23.3	42	1.21×10^{53}	5.33×10^{52}	2.75	1.63 ± 0.31	
121027A	1.7732	E	275	Swift	62.6	42	3.46×10^{52}	4.54×10^{51}	1.19	1.02 ± 0.01	
121024A	2.3012	E	275	Swift	69	42	5.00×10^{52}	1.70×10^{52}	1.24	1.09 ± 0.04	
120922A	3.1	P	230	Swift	173	42	2.06×10^{53}	2.56×10^{52}	1.20	1.03 ± 0.01	
120909A	3.93	A	229	Fermi	112	26	3.78×10^{53}	9.46×10^{52}	1.16	1.04 ± 0.02	
120907A	0.970	A	228	Swift	16.9	42	2.55×10^{51}	3.14×10^{51}	1.29	1.06 ± 0.03	
120815A	2.3587	E	275	Swift	9.7	42	1.47×10^{52}	1.24×10^{52}	1.28	1.10 ± 0.05	
120811C	2.671	A	227	Swift	26.8	42	6.24×10^{52}	3.45×10^{52}	1.54	1.06 ± 0.03	
120805A	3.1 ± 0.1	A	275	Swift	48.00	42	8.82×10^{52}	1.47×10^{52}	
120802A	3.796	A	226	Swift	50	42	1.15×10^{53}	5.67×10^{52}	1.35	1.10 ± 0.05	
120729A	0.80	A	225	Swift	71.5	42	1.89×10^{52}	5.87×10^{51}	1.51	1.11 ± 0.05	
120724A	1.48	A	224	Swift	72.8	42	8.10×10^{51}	1.02×10^{51}	
120722A	0.9590	E	275	Swift	42.4	42	6.37×10^{51}	7.16×10^{50}	1.09	1.02 ± 0.01	
120716A	2.486	A	223	Fermi	234	25	2.91×10^{53}	7.96×10^{52}	
120714B	0.3985	E	275	Swift	159	42	1.61×10^{51}	6.33×10^{49}	
120712A	4.1745	A	222	Swift	14.7	42	1.76×10^{53}	1.27×10^{53}	1.41	1.06 ± 0.03	
120711A	1.405	A	221	Fermi	44.033 ± 0.724		35	1.82×10^{54}	1.71×10^{53}
120624B	2.1974	E	275	Konus-Wind	300	24	3.21×10^{54}	2.32×10^{53}	1.62	1.09 ± 0.05	
120422A	0.2826	E	275	Swift	5.35	42	2.97×10^{50}	8.97×10^{49}	1.13	1.05 ± 0.03	
120404A	2.876	A	220	Swift	38.7	42	6.16×10^{52}	1.28×10^{52}	1.09	1.01 ± 0.01	
120327A	2.813	A	219	Swift	62.9	42	1.88×10^{53}	6.53×10^{52}	1.69	1.13 ± 0.06	
120326A	1.798	A	218	Swift	69.6	42	3.19×10^{52}	1.55×10^{52}	1.58	1.06 ± 0.03	
120224A	1.1 ± 0.2	HA	275	Swift	8.13	42	1.75×10^{51}	7.79×10^{50}	
120211A	2.4 ± 0.1	HA	275	Swift	61.7	42	3.38×10^{52}	6.02×10^{51}	1.15	1.05 ± 0.03	
120119A	1.7291	E	275	Swift	253.8	42	3.56×10^{53}	5.64×10^{52}	2.33	1.14 ± 0.07	
120118B	2.9428	E	275	Swift	23.26	42	5.65×10^{52}	1.61×10^{52}	1.22	1.04 ± 0.02	
111229A	1.3805	A	213	Swift	25.4	42	3.68×10^{51}	1.84×10^{51}	1.17	1.13 ± 0.43	
111228A	0.7164	E	275	Swift	101.20	42	3.91×10^{52}	4.27×10^{51}	1.62	1.30 ± 0.19	
111225A	2.012	E	278	Swift	106.8	42	3.08×10^{52}	3.91×10^{51}	1.16	1.13 ± 0.16	
111215A	$2.06^{+0.10}_{-0.16}$	P	278	Swift	796	42	1.11×10^{53}	2.95×10^{51}	
111211A	0.4786	E	275	Konus-Wind	25	23	1.49×10^{52}	9.04×10^{51}	
111209A	0.6770	E	275	Swift	25000	28	8.03×10^{53}	2.82×10^{50}	
111129A	1.0796	E	275	Swift	7.6	42	1.65×10^{51}	9.40×10^{50}	1.10	1.10 ± 0.12	
111123A	3.1513	E	275	Swift	290.0	42	3.68×10^{53}	1.49×10^{52}	1.17	1.13 ± 0.16	
111107A	2.893	A	212	Swift	26.6	42	2.05×10^{52}	2.95×10^{52}	1.21	1.15 ± 0.23	
111008A	4.9898	A	211	Swift	63.46	42	3.93×10^{53}	3.66×10^{53}	1.52	1.27 ± 0.03	
111005A	0.0133	E	210	Swift	26	42	5.39×10^{47}	6.12×10^{46}	1.24	1.16 ± 0.07	

Table 1—Continued

GRB	redshift			Detector	T_{90} [s]	Ref	$E_{\gamma,\text{iso}}$ [erg cm $^{-2}$]	$L_{\text{p},\text{iso}}$ [erg s $^{-1}$ cm $^{-2}$]	f	f_{eff}
	(1)	(2)	(3)							
110918A	0.9843	E	275	Konus-Wind	19.6 ± 0.1	29	1.84×10^{54}	4.23×10^{54}
110818A	3.3609	E	275	Swift	103	42	1.71×10^{53}	6.05×10^{52}	1.26	1.17 ± 0.14
110808A	1.3490	E	275	Swift	48	42	5.74×10^{52}	9.27×10^{53}	1.05	1.08 ± 0.11
110801A	1.858	A	209	Swift	385	42	9.65×10^{52}	5.09×10^{51}	1.09	1.10 ± 0.24
110731A	2.83	A	208	Swift	38.8	42	4.91×10^{53}	3.16×10^{53}	3.50	1.25 ± 0.29
110726A	1.036	A	207	Swift	5.2	42	1.27×10^{51}	7.59×10^{50}	1.25	1.17 ± 0.07
110715A	0.82	A	206	Swift	13.0	42	4.81×10^{52}	4.18×10^{52}	9.70	1.15 ± 0.01
110709B	2.09	E	280	Swift	55.6	42	2.69×10^{53}	3.52×10^{53}	1.52	1.27 ± 0.21
110503A	1.613	A	205	Swift	10.0	42	1.80×10^{53}	1.99×10^{53}	3.12	1.28 ± 0.12
110422A	1.770	A	204	Swift	25.9	42	7.20×10^{53}	2.80×10^{53}	4.00	1.29 ± 0.16
110213B	1.083	A	203	Konus-Wind	50	22	8.08×10^{52}	2.95×10^{51}
110213A	1.46	A	202	Swift	48.0	42	7.34×10^{52}	2.90×10^{52}	1.35	1.21 ± 0.27
110205A	2.22	A	201	Swift	257	42	6.10×10^{53}	2.74×10^{52}	1.54	1.27 ± 0.11
110128A	2.339	A	200	Swift	30.7	42	2.31×10^{52}	9.70×10^{51}	1.12	1.11 ± 0.29
110106B	0.618	E	199	Swift	24.8	42	5.34×10^{51}	6.68×10^{50}	1.15	1.12 ± 0.01
101225A	0.847	E	262	Swift	> 1088	42	8.21×10^{51}	1.62×10^{49}
101219B	0.55185	A	197	Swift	34	42	4.47×10^{51}	2.59×10^{50}
100906A	1.727	A	191	Swift	114.4	42	2.61×10^{53}	5.18×10^{52}	2.35	1.47 ± 0.05
100901A	1.408	A	190	Swift	439	42	3.38×10^{52}	2.61×10^{51}	1.10	1.10 ± 0.2
100814A	1.4392	E	275	Swift	174.5	42	9.39×10^{52}	1.00×10^{52}	1.75	1.34 ± 0.07
100728B	2.106	A	192	Swift	12.1	42	4.86×10^{52}	3.65×10^{52}	1.25	1.17 ± 0.09
100728A	1.5670	E	275	Swift	198.5	42	9.47×10^{53}	3.92×10^{52}	2.37	1.48 ± 0.38
100724A	1.2890	E	275	Swift	1.4	42	1.49×10^{51}	2.74×10^{51}	1.38	1.38 ± 0.21
100621A	0.5426	E	275	Swift	63.6	42	4.39×10^{52}	3.20×10^{51}	4.11	1.21 ± 0.11
100615A	1.3978	E	275	Swift	39	42	7.15×10^{52}	1.88×10^{52}	1.87	1.37 ± 0.21
100606A	1.5545	E	275	Swift	480	42	2.94×10^{53}	4.82×10^{52}	1.75	1.34 ± 0.14
100518A	$4^{+0.3}_{-0.5}$	P	189	INTEGRAL	25	43	5.52×10^{52}	4.95×10^{52}
100513A	4.772	A	188	Swift	84	42	1.40×10^{53}	2.80×10^{52}	1.15	1.12 ± 0.16
100508A	0.5201	E	275	Swift	52	42	2.87×10^{51}	2.24×10^{50}
100425A	1.755	A	187	Swift	37.0	42	9.42×10^{51}	4.23×10^{51}	1.18	1.13 ± 0.34
100424A	2.4656	E	275	Swift	104	42	4.54×10^{52}	3.03×10^{51}
100418A	0.6235	E	275	Swift	7.0	42	7.66×10^{50}	2.15×10^{50}	1.12	1.11 ± 0.12
100414A	1.368	A	186	Fermi	26.497 ± 2.073	35	5.63×10^{53}	3.30×10^{52}
100316D	0.0592	E	275	Swift	> 1300	19	5.74×10^{48}	1.13×10^{47}
100316B	1.180	A	185	Swift	3.8	42	1.65×10^{51}	1.33×10^{51}	1.31	1.19 ± 0.12
100302A	4.813	A	184	Swift	17.9	42	2.82×10^{52}	2.04×10^{52}	1.25	1.17 ± 0.34
100219A	4.6667	A	183	Swift	18.8	42	5.58×10^{52}	3.02×10^{52}	1.17	1.13 ± 0.1
091208B	1.0633	A	157	Swift	14.80	21	2.80×10^{52}	2.03×10^{52}	1.81	1.52 ± 0.16
091127A	0.4904	E	275	Swift	7.42	21	1.86×10^{52}	6.24×10^{51}	2.25	1.70 ± 0.03
091109A	3.076	A	182	Swift	48.03	21	1.42×10^{53}	3.51×10^{52}
091029A	2.752	A	156	Swift	39.18	21	9.50×10^{52}	1.72×10^{52}
091024A	1.092	A	155	Fermi	1020	20	5.15×10^{52}	1.01×10^{52}
091020A	1.71	A	154	Swift	38.92	21	6.85×10^{52}	1.81×10^{52}	1.60	1.09 ± 0.06
091018A	0.9710	E	275	Swift	4.37	21	7.07×10^{51}	4.18×10^{51}	2.31	1.39 ± 0.12

Table 1—Continued

GRB	redshift				T_{90}			$E_{\gamma,\text{iso}}$	$L_{\text{p},\text{iso}}$	f	f_{eff}
	(1)	(2)	method	Ref	(5)	[s]	Ref	[erg cm $^{-2}$]	[erg s $^{-1}$ cm $^{-2}$]	(10)	(11)
091003A	0.8969	E	153	Fermi	20.224 ± 0.362	35	7.17×10^{52}	2.93×10^{52}
090927A	1.37	A	176	Swift	2.16	21	1.83×10^{51}	4.59×10^{51}	1.48
090926B	1.2427	E	275	Swift	99.28	21	4.48×10^{52}	3.89×10^{51}	1.50	1.10 ± 0.05	...
090926A	2.1062	E	180	Fermi	13.760 ± 0.286	35	1.98×10^{54}	6.55×10^{53}
090902B	1.822	A	175	Fermi	19.328 ± 0.286	35	3.05×10^{54}	7.80×10^{53}
090814A	0.696	A	174	Swift	78.22	21	3.68×10^{51}	2.11×10^{50}
090812A	2.452	A	173	Swift	75.09	21	4.45×10^{53}	8.14×10^{52}	1.50	1.11 ± 0.1	...
090809A	2.737	A	172	Swift	7.84	21	2.48×10^{52}	2.16×10^{52}	1.30
090726A	2.71	A	171	Swift	56.68	21	3.17×10^{52}	5.41×10^{51}
090715B	3.00	A	170	Swift	265.39	21	2.10×10^{53}	8.12×10^{52}	1.56	1.09 ± 0.07	...
090709A	1.7 ± 0.6	P	237	Swift	88.73	21	4.09×10^{52}	2.46×10^{51}	2.50	1.27 ± 0.03	...
090618A	0.54	A	169	Swift	113.34	21	2.80×10^{53}	1.26×10^{52}	7.50	1.23 ± 0.03	...
090530A	1.266	A	257	Swift	40.46	21	1.27×10^{52}	5.33×10^{51}	1.50	1.31 ± 0.09	...
090529A	2.625	A	168	Swift	> 70	21	2.19×10^{52}	3.00×10^{51}
090519A	3.85	A	167	Swift	58.26	21	2.66×10^{53}	1.03×10^{53}
090516A	4.109	A	166	Swift	208.00	21	7.31×10^{53}	8.66×10^{52}
090424A	0.544	E	163	Swift	49.47	21	4.14×10^{52}	1.65×10^{52}	11.25	1.18 ± 0.11	...
090423A	8.23	A	178	Swift	9.77	21	7.89×10^{52}	1.14×10^{53}	1.31	1.22 ± 0.11	...
090418A	1.608	A	161	Swift	56.31	21	1.62×10^{53}	1.24×10^{52}
090417B	0.345	E	162	Swift	282.49	21	1.57×10^{51}	1.69×10^{49}
090407A	1.4478	E	275	Swift	315.44	21	1.41×10^{52}	1.45×10^{51}	1.14	1.07 ± 0.07	...
090328A	0.7357	E	196	Fermi	61.697 ± 1.810	35	9.23×10^{52}	1.36×10^{52}
090323A	3.5832 ± 0.004	E	275	Fermi	135.170 ± 1.448	35	3.96×10^{54}	3.24×10^{53}
090313A	3.375	A	160	Swift	70.66	21	6.80×10^{52}	1.16×10^{52}
090205A	4.6497	A	159	Swift	8.80	21	1.54×10^{52}	1.35×10^{52}	1.19
090201A	2.1000	E	275	Swift	84.78	21	8.00×10^{53}	2.70×10^{53}	2.00	1.20 ± 0.14	...
090113A	1.7494	E	275	Swift	9.10	21	1.66×10^{52}	1.25×10^{52}	1.50	1.19 ± 0.16	...
090102A	1.547	A	158	Swift	29.30	21	2.35×10^{53}	4.80×10^{52}
081222A	2.77	A	146	Swift	33.00	21	2.40×10^{53}	1.22×10^{53}	2.31	1.20 ± 0.12	...
081221A	2.2590	E	275	Swift	33.91	21	3.95×10^{53}	8.30×10^{52}	3.75	1.20 ± 0.16	...
081210A	2.0631	E	275	Swift	145.91	21	6.71×10^{52}	2.47×10^{52}	1.45	1.22 ± 0.06	...
081203A	2.05 ± 0.01	A	177	Swift	223.00	21	3.38×10^{53}	3.27×10^{52}	1.50	1.16 ± 0.12	...
081121A	2.512	A	145	Swift	17.67	21	2.84×10^{53}	8.65×10^{52}	1.14	1.11 ± 0.34	...
081118A	2.58	A	144	Swift	49.28	21	3.80×10^{52}	4.12×10^{51}
081109A	0.9785	E	275	Swift	221.49	21	3.31×10^{52}	3.46×10^{51}	1.31	1.07 ± 0.1	...
081029A	3.8479	A	143	Swift	275.05	21	2.03×10^{53}	2.03×10^{52}
081028A	3.038	A	142	Swift	284.42	21	3.51×10^{53}	1.71×10^{52}
081008A	1.967	A	141	Swift	179.52	21	1.30×10^{53}	1.33×10^{52}	1.31	1.16 ± 0.25	...
081007A	0.5295	E	140	Swift	9.01	21	1.48×10^{51}	4.53×10^{50}	1.35	1.26 ± 0.03	...
080928A	1.6919	A	152	Swift	233.66	21	1.37×10^{52}	1.02×10^{52}	1.38	1.22 ± 0.07	...
080916C	4.35	P	194	Fermi	62.977 ± 0.810	35	2.72×10^{54}	7.01×10^{53}
080916A	0.6887	A	152	Swift	61.35	21	1.81×10^{52}	2.55×10^{51}	1.50	1.15 ± 0.03	...
080913A	6.7	A	152	Swift	7.46	21	6.37×10^{52}	1.25×10^{53}	1.26	1.19 ± 0.09	...
080905B	2.3739	A	152	Swift	101.62	21	4.69×10^{52}	1.78×10^{52}	1.26	1.12 ± 0.09	...

Table 1—Continued

GRB	redshift				T_{90}			$E_{\gamma,\text{iso}}$ [erg cm $^{-2}$]	$L_{\text{p,iso}}$ [erg s $^{-1}$ cm $^{-2}$]	f	f_{eff}
	(1)	z (2)	method (3)	Ref (4)	Detector (5)	[s] (6)	Ref (7)				
080810A	3.3604	A	152	Swift	107.67	21	3.54×10^{53}	1.05×10^{53}
080805A	1.5052	E	275	Swift	106.62	21	4.46×10^{52}	4.13×10^{51}	1.23	1.12 ± 0.14	
080804A	2.2059	E	275	Swift	37.19	21	1.55×10^{53}	4.29×10^{52}	1.50	1.10 ± 0.11	
080721A	2.5914	A	152	Swift	176.29	21	1.20×10^{54}	1.00×10^{54}	4.81	1.34 ± 0.07	
080710A	0.8454	A	152	Swift	112.06	21	9.34×10^{51}	1.05×10^{51}	1.11	1.10 ± 0.01	
080707A	1.2322	A	152	Swift	30.17	21	4.79×10^{51}	1.54×10^{51}	1.25	1.11 ± 0.21	
080607A	3.0368	A	152	Swift	78.86	21	1.76×10^{54}	2.13×10^{54}	5.60	1.20 ± 0.07	
080605A	1.6408	E	275	Swift	18.05	21	2.31×10^{53}	3.24×10^{53}	1.42	1.11 ± 0.43	
080604A	1.4171	A	152	Swift	69.16	21	9.49×10^{51}	8.55×10^{50}	
080603B	2.6892	A	152	Swift	59.12	21	9.56×10^{52}	1.18×10^{53}	1.65	1.11 ± 0.19	
080603A	1.688	A	138	INTEGRAL	150	43	1.88×10^{52}	2.39×10^{51}	
080602A	1.8204	E	275	Swift	74.29	21	8.73×10^{52}	5.97×10^{52}	1.25	1.07 ± 0.16	
080520A	1.5457	E	152	Swift	3.32	21	1.35×10^{51}	1.71×10^{51}	1.32	...	
080517A	0.089 ± 0.003	E	277	Swift	64.61	21	3.37×10^{49}	3.29×10^{48}	
080515A	2.47	E	281	Swift	20.91	21	5.43×10^{52}	2.22×10^{52}	1.12	1.07 ± 0.34	
080430A	0.767	A	137	Swift	14.15	21	4.57×10^{51}	1.34×10^{51}	1.46	1.12 ± 0.12	
080413B	1.1012	E	275	Swift	8.00	21	2.37×10^{52}	2.15×10^{52}	2.38	1.53 ± 0.16	
080413A	2.4330	A	152	Swift	46.36	21	1.74×10^{53}	5.98×10^{52}	1.75	1.13 ± 0.06	
080411A	1.0301	A	152	Swift	56.33	21	2.35×10^{53}	9.71×10^{52}	6.85	1.13 ± 0.03	
080330A	1.5119	A	152	Swift	67.05	21	5.77×10^{51}	2.10×10^{51}	1.19	1.11 ± 0.23	
080325A	1.78	E	237	Swift	162.82	21	9.60×10^{52}	6.02×10^{51}	
080319C	1.9492	A	152	Swift	29.55	21	1.36×10^{53}	8.98×10^{52}	1.52	1.09 ± 0.34	
080319B	0.9382	A	152	Swift	124.86	21	1.33×10^{54}	9.80×10^{52}	8.00	1.11 ± 0.27	
080310A	2.4274	A	152	Swift	352.37	21	7.43×10^{52}	7.97×10^{51}	1.19	1.07 ± 0.07	
080210A	2.6419	A	152	Swift	39.36	21	6.33×10^{52}	1.54×10^{52}	1.23	1.09 ± 0.03	
080207A	2.0856	E	275	Swift	340	42	1.56×10^{53}	5.80×10^{51}	
080129A	4.349	A	151	Swift	50.22	21	1.20×10^{53}	1.27×10^{52}	
071122A	1.14	A	131	Swift	80.00	21	4.62×10^{51}	5.11×10^{50}	
071117A	1.3308	E	152	Swift	6.07	21	4.09×10^{52}	1.09×10^{53}	2.40	1.44 ± 0.16	
071112C	0.8227	A	152	Swift	15	42	4.14×10^{52}	1.83×10^{52}	
071031A	2.692	A	152	Swift	150.49	21	3.79×10^{52}	4.25×10^{51}	1.12	1.07 ± 0.09	
071021A	2.4515	E	275	Swift	228.72	21	4.30×10^{52}	6.24×10^{51}	1.12	1.09 ± 0.14	
071020A	2.1462	A	152	Swift	4.30	21	9.38×10^{52}	2.31×10^{53}	2.25	...	
071010B	0.947	A	129	Swift	36.13	21	1.72×10^{52}	6.24×10^{51}	2.25	1.35 ± 0.24	
071010A	0.98	A	128	Swift	6.32	21	1.17×10^{51}	5.15×10^{50}	1.11	1.08 ± 0.29	
071003A	1.60435	A	136	Swift	148.38	21	3.47×10^{53}	2.07×10^{53}	1.57	1.18 ± 0.11	
070810A	2.17	A	127	Swift	9.04	21	1.57×10^{52}	9.36×10^{51}	1.40	1.18 ± 0.14	
070802A	2.4538	E	275	Swift	15.80	21	8.61×10^{51}	3.15×10^{51}	
070721B	3.6298	A	152	Swift	336.86	21	4.48×10^{53}	9.14×10^{52}	1.38	1.10 ± 0.16	
070714A	1.58	E	281	Swift	3.00	21	2.95×10^{51}	4.61×10^{51}	1.50	1.50 ± 0.21	
070612A	0.617	E	125	Swift	365.28	21	2.95×10^{52}	6.57×10^{50}	1.12	1.10 ± 0.06	
070611A	2.0394	A	152	Swift	13.18	21	9.92×10^{51}	5.04×10^{51}	1.14	1.09 ± 0.12	
070529A	2.4996	A	124	Swift	108.90	21	1.52×10^{53}	2.61×10^{52}	
070521A	2.0865	E	275	Swift	38.63	21	2.47×10^{53}	1.74×10^{53}	2.29	1.22 ± 0.05	

Table 1—Continued

GRB	redshift			Detector	T_{90}		$E_{\gamma, \text{iso}}$ [erg cm $^{-2}$]	$L_{\text{p}, \text{iso}}$ [erg s $^{-1}$ cm $^{-2}$]	f	f_{eff}
	(1)	z (2)	method (3)		(5)	[s] (6)	Ref (7)			
070518A	1.161	E	281	Swift	4.35	21	1.23×10^{51}	6.73×10^{50}	1.20	1.12 ± 0.1
070508A	0.82	E	123	Swift	20.90	21	9.60×10^{52}	3.65×10^{52}	4.38	1.17 ± 0.25
070506A	2.3090	A	152	Swift	4.35	21	6.11×10^{51}	7.10×10^{51}	1.33	...
070419B	1.9586	E	275	Swift	238.14	21	1.78×10^{53}	8.21×10^{51}	1.24	1.09 ± 0.16
070419A	0.9705	A	152	Swift	160.00	21	4.19×10^{51}	8.63×10^{49}
070411A	2.9538	A	152	Swift	102.04	21	1.18×10^{53}	1.22×10^{52}	1.11	1.07 ± 0.09
070328A	2.0627	E	275	Swift	72.12	21	5.29×10^{53}	1.24×10^{53}	1.73	1.23 ± 0.14
070318A	0.8401	E	275	Swift	131.52	21	1.79×10^{52}	2.03×10^{51}	1.32	1.09 ± 0.11
070306A	1.4965	E	275	Swift	209.24	21	7.91×10^{52}	1.19×10^{52}	1.38	1.09 ± 0.24
070224A	1.9922	E	275	Swift	48.00	21	7.66×10^{51}	1.40×10^{51}	1.11	1.09 ± 0.29
070223A	1.6295	E	280	Swift	100.00	21	2.49×10^{52}	1.89×10^{51}
070208A	1.165	E	122	Swift	64.00	21	3.40×10^{51}	9.97×10^{50}	1.16	1.09 ± 0.01
070129A	2.3384	E	275	Swift	459.05	21	7.90×10^{52}	3.12×10^{51}
070125A	1.547	A	152	Konus-Wind	70	14	9.21×10^{53}	3.03×10^{53}
070110A	2.3523	E	275	Swift	79.71	21	5.79×10^{52}	5.93×10^{51}
070103A	2.6208	E	275	Swift	18.40	21	1.09×10^{52}	8.07×10^{51}
061222B	3.355	A	110	Swift	37.25	21	1.08×10^{53}	1.81×10^{52}
061222A	2.088	E	149	Swift	96.00	21	3.11×10^{53}	2.04×10^{53}	2.62	1.55 ± 0.32
061202A	2.2543	E	275	Swift	94.19	21	1.14×10^{53}	2.25×10^{52}	1.43	1.09 ± 0.43
061126A	1.1588	E	135	Swift	50.28	21	9.05×10^{52}	6.17×10^{52}	2.12	1.27 ± 0.19
061121A	1.3145	A	152	Swift	81.22	21	2.64×10^{53}	1.38×10^{53}	4.81	1.35 ± 0.16
061110B	3.4344	A	152	Swift	132.76	21	2.48×10^{53}	3.50×10^{52}
061110A	0.7578	E	275	Swift	44.51	21	4.64×10^{51}	2.09×10^{50}	1.32	1.07 ± 0.29
061021A	0.3453	E	275	Swift	43.80	21	5.45×10^{51}	2.03×10^{51}	2.06	1.28 ± 0.34
061007A	1.2622	A	107	Swift	75.74	21	9.84×10^{53}	1.74×10^{53}	3.62	1.20 ± 0.16
060927A	5.4636	A	119	Swift	22.42	21	1.10×10^{53}	1.21×10^{53}	1.46	1.11 ± 0.12
060926A	3.2090	E	275	Swift	7.79	21	1.39×10^{52}	1.59×10^{52}	1.21	...
060923B	1.5094	E	275	Swift	8.95	21	7.85×10^{51}	2.98×10^{51}
060923A	2.6	P	237	Swift	51.54	21	3.22×10^{52}	1.41×10^{52}	1.25	1.09 ± 0.23
060912A	0.9362	E	275	Swift	5.03	21	7.62×10^{51}	7.21×10^{51}	1.94	1.40 ± 0.34
060908A	1.8836	A	216	Swift	18.78	21	6.33×10^{52}	1.61×10^{52}	1.60	1.12 ± 0.1
060906A	3.6856	A	152	Swift	44.58	21	1.22×10^{53}	3.22×10^{52}
060904B	0.7029	E	152	Swift	171.90	21	6.15×10^{51}	1.33×10^{51}	1.50	1.19 ± 0.07
060814A	1.9223	E	275	Swift	144.95	21	3.51×10^{53}	8.12×10^{52}	2.15	1.11 ± 0.09
060805A	2.3633	E	275	Swift	4.93	21	2.00×10^{51}	2.03×10^{51}
060729A	0.5429	E	275	Swift	113.04	21	4.86×10^{51}	2.55×10^{50}	1.27	1.10 ± 0.16
060719A	1.5318	E	275	Swift	66.86	21	1.92×10^{52}	4.79×10^{51}	1.38	1.11 ± 0.27
060714A	2.7108	A	94	Swift	116.04	21	9.66×10^{52}	1.09×10^{52}
060707A	3.4246	E	275	Swift	66.65	21	7.50×10^{52}	1.50×10^{52}	1.16	1.07 ± 0.14
060614A	0.125	E	112	Swift	5/106	40	2.13×10^{51}	2.63×10^{50}	2.56	2.26 ± 0.23
060607A	3.0749	A	134	Swift	102.98	21	1.72×10^{53}	3.47×10^{52}	1.25	1.07 ± 0.11
060605A	3.773	A	148	Swift	539.12	21	5.43×10^{52}	1.43×10^{52}	1.21	1.11 ± 0.24
060604A	2.1355	E	275	Swift	96.00	21	9.14×10^{51}	1.55×10^{51}
060602A	0.787	E	130	Swift	74.68	21	1.54×10^{52}	6.32×10^{50}

Table 1—Continued

GRB	redshift			Detector	T_{90}		$E_{\gamma, \text{iso}}$ [erg cm $^{-2}$]	$L_{\text{p,iso}}$ [erg s $^{-1}$ cm $^{-2}$]	f	f_{eff}
	(1)	(2)	(3)		(5)	(6)	(7)	(8)	(9)	(10)
060526A	3.2213	A	103	Swift	275.20	21	5.63×10^{52}	2.02×10^{52}	1.35	1.09 ± 0.29
060522A	5.11	A	102	Swift	69.12	21	1.35×10^{53}	3.31×10^{52}
060512A	0.4428	E	104	Swift	11.36	21	3.25×10^{50}	9.73×10^{49}	1.15	1.07 ± 0.11
060510B	4.9	A	101	Swift	262.95	21	3.59×10^{53}	2.39×10^{52}
060505A	0.0889	E	117	Swift	4	42	9.24×10^{49}	2.51×10^{49}	1.58	1.27 ± 0.25
060502A	1.5026	A	152	Swift	28.54	21	4.93×10^{52}	8.96×10^{51}	1.31	1.10 ± 0.32
060418A	1.4901	A	114	Swift	109.17	21	1.16×10^{53}	1.77×10^{52}	1.94	1.31 ± 0.29
060319A	1.172	E	237	Swift	8.91	21	2.30×10^{51}	1.14×10^{51}	1.24	1.16 ± 0.16
060306A	1.5597	E	275	Swift	60.94	21	2.97×10^{52}	1.57×10^{52}	2.25	1.51 ± 0.12
060223A	4.406	A	120	Swift	11.32	21	5.53×10^{52}	4.46×10^{52}	1.45	1.20 ± 0.05
060218A	0.03351	E	97	Swift	2100	42	9.33×10^{48}	8.65×10^{46}
060210A	3.9122	A	152	Swift	242.18	21	6.49×10^{53}	9.50×10^{52}	1.58	1.16 ± 0.1
060206A	4.0559	A	152	Swift	7.55	21	5.56×10^{52}	6.63×10^{52}	1.56	...
060204B	2.3393	E	275	Swift	139.46	21	8.31×10^{52}	9.76×10^{51}	1.26	1.07 ± 0.07
060202A	0.785	E	237	Swift	172.16	21	8.66×10^{51}	2.88×10^{50}
060124A	2.3	A	152	Swift	658.2	21	2.11×10^{53}	1.29×10^{53}	3.38	1.34 ± 0.2
060123A	0.56	E	281	Swift	900	42	5.43×10^{50}	7.77×10^{48}
060115A	3.5328	A	152	Swift	122.21	21	1.47×10^{53}	2.67×10^{52}	1.15	1.07 ± 0.07
060111A	2.32	E	281	Swift	13.21	21	3.18×10^{52}	1.17×10^{52}	1.53	1.14 ± 0.16
051117B	0.4805	E	275	Swift	9.01	21	3.34×10^{50}	1.07×10^{50}	1.15	1.08 ± 0.29
051111A	1.55	A	98	Swift	64.00	21	1.12×10^{53}	1.65×10^{52}	1.34	1.07 ± 0.01
051109B	0.080	E	106	Swift	13.38	21	6.78×10^{48}	1.13×10^{48}	1.16	1.08 ± 0.21
051109A	2.346	A	88	Swift	37.20	21	8.28×10^{52}	4.02×10^{52}	1.44	1.12 ± 0.32
051022A	0.8061	E	275	HETE-2	178 ± 8	16	6.06×10^{53}	4.19×10^{52}
051016B	0.9358	E	275	Swift	4.02	21	9.49×10^{50}	8.75×10^{50}	1.30	1.15 ± 0.43
051008A	$2.77^{+0.15}_{-0.2}$	P	274	Swift	64.0	21	6.22×10^{53}	2.31×10^{53}	1.81	1.17 ± 0.16
051006A	1.059	E	215	Swift	26.04	21	1.29×10^{52}	2.71×10^{51}	1.27	1.08 ± 0.29
051001A	2.4295	E	275	Swift	190.63	21	4.94×10^{52}	2.97×10^{51}	1.10	1.06 ± 0.34
050922C	2.1992	A	94	Swift	4.54	21	9.53×10^{52}	1.88×10^{53}	3.29	...
050915A	2.5275	E	275	Swift	53.42	21	4.84×10^{52}	1.48×10^{52}	1.26	1.07 ± 0.06
050908A	3.3467	A	152	Swift	18.29	21	2.34×10^{52}	1.03×10^{52}	1.12	1.07 ± 0.23
050904A	6.295	A	111	Swift	181.70	21	1.23×10^{54}	1.03×10^{53}
050826A	0.296	E	116	Swift	35.73	21	6.27×10^{50}	6.77×10^{49}	1.14	1.07 ± 0.34
050824A	0.8277	E	275	Swift	24.82	21	1.72×10^{51}	3.23×10^{50}
050822A	1.434	E	215	Swift	104.12	21	3.25×10^{52}	3.96×10^{51}	1.29	1.10 ± 0.1
050820A	2.61469	A	121	Swift	26	42	2.59×10^{53}	5.98×10^{52}	1.32	1.14 ± 0.2
050819A	2.5042	E	275	Swift	37.72	21	1.73×10^{52}	3.60×10^{51}
050814A	5.3 ± 0.3	P	91	Swift	144.00	21	1.98×10^{53}	3.25×10^{52}
050802A	1.7102	A	152	Swift	27.46	21	4.41×10^{52}	1.38×10^{52}	1.18	1.08 ± 0.03
050730A	3.96855	A	85	Swift	145.05	21	2.06×10^{53}	1.98×10^{52}	1.16	1.08 ± 0.03
050714B	2.4383	E	275	Swift	46.87	21	1.43×10^{52}	3.16×10^{51}
050525A	0.6063	E	275	Swift	8.84	21	2.84×10^{52}	1.93×10^{52}	9.38	1.83 ± 0.11
050505A	4.2748	A	96	Swift	58.88	21	2.90×10^{53}	9.86×10^{52}
050502A	3.793	A	86	Swift	17.5 ± 0.2	12	9.17×10^{52}	6.32×10^{52}

Table 1—Continued

GRB	redshift				T_{90}			$E_{\gamma,\text{iso}}$	$L_{\text{p},\text{iso}}$	f	f_{eff}
	(1)	z (2)	method (3)	Ref (4)	Detector (5)	[s] (6)	Ref (7)	[erg cm $^{-2}$] (8)	[erg s $^{-1}$ cm $^{-2}$] (9)	(10)	(11)
050416A	0.6542	E	275	Swift	6.62	21	1.22×10^{51}	9.77×10^{50}	1.54
050408A	1.2356	E	84	HETE-2	28.39 ± 0.56	16	2.33×10^{52}
050401A	2.8983	A	100	Swift	33.30	21	4.20×10^{53}	2.08×10^{53}	1.51	1.10 ± 0.14	
050319A	3.2425	A	152	Swift	151.74	21	5.92×10^{52}	1.85×10^{52}	1.19	1.12 ± 0.19	
050318A	1.4436	A	84	Swift	40.0	21	1.23×10^{52}	5.62×10^{51}	1.56	1.17 ± 0.16	
050315A	1.9500	A	84	Swift	95.57	21	6.34×10^{52}	6.76×10^{51}	1.32	1.08 ± 0.29	
050223A	0.584	E	93	Swift	21.68	21	4.36×10^{51}	3.18×10^{50}
050219A	0.211	E	261	Swift	23.84	21	1.05×10^{51}	9.69×10^{49}	1.75	1.18 ± 0.34	
050215B	2.62	E	281	Swift	10.62	21	6.95×10^{51}	6.38×10^{51}	
050126A	1.29002	E	82	Swift	48.00	21	1.59×10^{52}	2.73×10^{51}	
041219A	0.31 ± 0.26	P	214	Swift	520	42	6.88×10^{52}	3.74×10^{51}	
041006A	0.716	E	95	HETE-2	22.08 ± 0.33	16	2.11×10^{52}	
040924A	0.858	E	133	HETE-2	3.37 ± 0.08	16	9.21×10^{51}	2.09×10^{52}	
040912A	1.563	E	113	HETE-2	9.21 ± 0.27	16	8.47×10^{51}	
031203A	0.1055	E	78	HETE-2	10.38 ± 0.29	16	6.84×10^{49}	1.78×10^{49}	
030528A	0.782	E	80	HETE-2	62.8 ± 4.49	16	2.22×10^{52}	1.25×10^{51}	
030429A	2.658 ± 0.004	A	75	HETE-2	12.95 ± 2.69	16	1.70×10^{52}	7.47×10^{51}	
030329A	0.1685	E	73	HETE-2	25.91 ± 0.39	16	1.55×10^{52}	1.65×10^{51}	
030328A	1.5216	A	92	HETE-2	138.27 ± 3.05	16	3.59×10^{53}	1.40×10^{52}	
030323A	3.3736	E	74	HETE-2	26	10	4.14×10^{52}	3.54×10^{52}	
030226A	1.986	A	76	HETE-2	76.23 ± 3.96	16	7.46×10^{52}	5.76×10^{51}	
030115A	2	P	259	HETE-2	20.33 ± 3.54	16	3.01×10^{52}	1.11×10^{52}	
021211A	1.006	E	72	HETE-2	4.23 ± 0.27	16	1.34×10^{52}	8.62×10^{51}	
021004A	2.3351	E	56	HETE-2	48.94 ± 2.5	16	4.33×10^{52}	6.68×10^{51}	
020903A	0.251	E	77	HETE-2	3.3	9	2.03×10^{49}	6.36×10^{48}	
020819B	0.41	E	81	Ulysses	20	8	1.62×10^{52}	2.05×10^{51}	
020813A	1.255	E	67	HETE-2	87.34 ± 0.6	16	1.34×10^{54}	7.36×10^{52}	
020427A	BeppoSAX	66	7	1.52×10^{52}	2.35×10^{51}	
020410A ^a	BeppoSAX	1500	11	3.10×10^{52}	1.66×10^{50}	
020405A	0.6908 ± 0.0017	E	65	BeppoSAX	40.0 ± 2.2	18	1.07×10^{53}	1.38×10^{52}	
020331A	HETE-2	179.4 ± 5.99	16	9.31×10^{52}	8.32×10^{51}	
020322A	BeppoSAX	11.0 ± 2.8	18	2.30×10^{52}	1.82×10^{52}	
020305A	2.8	P	79	HETE-2	39.06 ± 1.17	16	3.09×10^{53}	1.25×10^{53}	
020127A	1.9	P	115	HETE-2	6.99 ± 0.26	16	3.36×10^{52}	1.43×10^{52}	
020124A	3.198 ± 0.004	A	70	HETE-2	51.17 ± 1.55	16	2.09×10^{53}	5.33×10^{52}	
011211A	2.14	A	57	BeppoSAX	51.0 ± 7.6	18	3.23×10^{52}	2.63×10^{51}	
011121A	0.36	E	71	BeppoSAX	47.0 ± 3.2	18	6.42×10^{52}	5.86×10^{51}	
011030A	< 3	P	63	BeppoSAX	1400	6	1.35×10^{53}	3.37×10^{51}	
010921A	0.4509	E	58	BeppoSAX	22.0 ± 3.6	18	1.51×10^{52}	1.70×10^{51}	
010222A	1.47688	A	61	BeppoSAX	74.0 ± 4.1	18	1.36×10^{54}	3.13×10^{53}	
000926A	2.0379	A	68	BeppoSAX	1.30 ± 0.59	18	7.66×10^{51}	1.93×10^{52}	
000911A	1.0585	E	59	Uly/Ko/NE	500	4	6.53×10^{53}	1.17×10^{53}	
000418A	1.1181	E	66	BeppoSAX	2.0 ± 1.3	18	1.09×10^{51}	1.16×10^{51}	
000301C	2.0404	A	53	BeppoSAX	87.0 ± 4.2	18	1.41×10^{53}	5.82×10^{51}	

Table 1—Continued

GRB	redshift				T_{90}			$E_{\gamma,\text{iso}}$	$L_{\text{p},\text{iso}}$	f	f_{eff}
	(1)	z (2)	method (3)	Ref (4)	Detector (5)	[s] (6)	Ref (7)	[erg cm $^{-2}$] (8)	[erg s $^{-1}$ cm $^{-2}$] (9)	(10)	(11)
000210A	0.846	E	60	BeppoSAX	9.0 ± 1.4	18	1.54×10^{53}	9.74×10^{52}
000131A	4.5 ± 0.015	A	51	Uly/Ko/NE	50	3	1.61×10^{54}	4.14×10^{53}
991216A	1.02	A	49	BeppoSAX	45.0 ± 5.7	18	6.00×10^{53}	3.33×10^{53}
991208A	0.7063 ± 0.0017	E	52	Uly/Ko/NE	60	2	2.66×10^{53}	4.73×10^{52}
990712A	0.4331	E	54	BeppoSAX	38.0 ± 3.2	18	8.21×10^{51}	2.35×10^{51}
990705A	0.8424	E	62	BeppoSAX	32.0 ± 1.4	18	2.49×10^{53}	2.26×10^{52}
990510A	1.619	A	54	BeppoSAX	57.0 ± 3.2	18	1.96×10^{53}	6.68×10^{52}
990506A	1.30658	E	66	BeppoSAX	129.0 ± 1.4	18	8.66×10^{53}	1.00×10^{53}
990308A	BATSE	106 ± 12	1	6.32×10^{52}	5.14×10^{52}
990123A	1.6004	A	50	BeppoSAX	61.0 ± 2.8	18	3.90×10^{54}	5.75×10^{53}
981226A	1.11 ± 0.06	P	83	BeppoSAX	17.0 ± 5.8	18	5.50×10^{51}	7.40×10^{50}
980703A	0.966	E	45	BeppoSAX	76.0 ± 10.2	18	1.33×10^{53}	1.17×10^{52}
980613A	1.0969	E	69	BeppoSAX	42.0 ± 22.1	18	5.94×10^{51}	1.99×10^{51}
980519A	BeppoSAX	33.0 ± 3.2	18	1.64×10^{53}	2.55×10^{53}
980425A	0.0085	E	46	BeppoSAX	22.0 ± 4.5	18	9.40×10^{47}	4.71×10^{46}
980329A	3.5	P	64	BeppoSAX	19.0 ± 2.2	18	2.41×10^{54}	5.18×10^{53}
980326A	BeppoSAX	312.0 ± 8.1	18	1.77×10^{52}	1.73×10^{52}
971214A	3.42	E	47	BeppoSAX	6.0 ± 3.2	18	2.87×10^{53}	9.80×10^{52}
970828A	0.9578	E	55	BATSE	146.59	5	3.00×10^{53}	2.45×10^{52}
970508A	0.835	A	44	BeppoSAX	14.0 ± 3.6	18	8.12×10^{51}	2.82×10^{51}
970228A	0.695 ± 0.002	E	48	BeppoSAX	56.0 ± 3.2	18	2.75×10^{52}	1.57×10^{52}
SGRB											
130603B	0.356	E	246	Swift	0.18	42	2.02×10^{51}	4.15×10^{52}
101224A	Swift	0.2	42	2.34×10^{50}	4.62×10^{50}	1.63	1.63 ± 0.43	
101219A	0.718	E	198	Swift	0.6	42	4.49×10^{51}	6.00×10^{52}	2.75	2.75 ± 0.45	
100816A	0.8048	E	275	Swift	2.9	42	7.93×10^{51}	9.02×10^{51}	2.62	1.52 ± 0.03	
100625A	0.452 ± 0.002	HA	234	Swift	0.33	42	9.17×10^{50}	1.65×10^{51}	2.63	2.63 ± 0.26	
100206A	0.4068	E	217	Swift	0.12	42	5.81×10^{50}	7.86×10^{50}	2.70	2.70 ± 0.26	
100117A	0.92	E	195	Swift	0.3	42	1.32×10^{51}	2.22×10^{51}	2.28	2.28 ± 0.21	
091109B	Swift	0.27	21	6.87×10^{51}	1.04×10^{52}	4.93	4.93 ± 0.65	
090515A	Swift	0.04	21	2.90×10^{49}	9.94×10^{50}	2.58	2.58 ± 0.32	
090510A	0.903	E	165	Swift	5.66	21	2.83×10^{52}	5.57×10^{52}	5.00	5.00 ± 0.55	
090426A	2.609	HA	164	Swift	1.24	21	5.50×10^{51}	1.88×10^{52}	2.61	1.48 ± 0.15	
090305A	Swift	0.35	21	2.17×10^{51}	3.68×10^{51}	1.48	1.48 ± 0.16	
080905A	0.1218	E	193	Swift	1.02	21	4.30×10^{49}	3.05×10^{49}	1.85	1.85 ± 0.15	
080503A	Swift	0.32 ± 0.07	17	1.97	1.53 ± 0.18	
080123A	0.495	...	181	Swift	0.04	21	7.43×10^{50}	2.09×10^{50}	
071227A	0.383	E	132	Swift	$1.8/100$	40	1.04×10^{51}	3.16×10^{51}	3.00	2.80 ± 0.23	
070809A	0.2187	E	139	Swift	1.28	21	3.18×10^{49}	4.08×10^{49}	1.42	1.42 ± 0.25	
070724A	0.457	E	126	Swift	0.43	21	3.68×10^{49}	5.88×10^{49}	1.53	1.53 ± 0.12	
070714B	0.923	E	147	Swift	$3/100$	40	8.36×10^{51}	6.15×10^{51}	2.94	2.54 ± 0.34	
070707A	INTEGRAL	0.8	15	6.88×10^{50}	1.03×10^{51}	
070429B	0.904	E	147	Swift	0.49	21	3.99×10^{50}	8.52×10^{50}	1.51	1.51 ± 0.19	
061217A	0.827	E	118	Swift	0.24	21	2.34×10^{51}	1.69×10^{52}	1.74	1.74 ± 0.12	

Table 1—Continued

GRB	redshift			T_{90}			$E_{\gamma,\text{iso}}$	$L_{\text{p},\text{iso}}$	f	f_{eff}
	(1)	(2)	(3)	(4)	Detector	[s]	Ref	[erg cm $^{-2}$]	[erg s $^{-1}$ cm $^{-2}$]	
061210A	0.41	E	108	Swift	0.13/77	41	1.66×10^{51}	1.07×10^{51}	8.13	7.83 ± 0.38
061201A	0.111	E	109	Swift	0.78	21	1.96×10^{50}	1.31×10^{51}	4.67	4.67 ± 0.67
061006A	0.4377	E	118	Swift	0.5/120	40	2.32×10^{51}	1.99×10^{52}	6.01	5.41 ± 0.32
060801A	1.131	E	150	Swift	0.50	21	2.35×10^{52}	8.96×10^{52}	2.19	2.19 ± 0.35
060502B	0.287	E	105	Swift	0.14	21	2.18×10^{50}	3.55×10^{50}	2.33	2.33 ± 0.24
060313A	Swift	0.74	21	1.28×10^{52}	9.44×10^{52}	4.94	4.94 ± 0.43
060121A	HETE-2	2.61 ± 0.1	16	3.91×10^{51}	2.04×10^{52}
051221A	0.5465	E	99	Swift	1.40	21	3.12×10^{51}	6.94×10^{52}	7.00	7.00 ± 0.65
051210A	> 1.4	P	179	Swift	1.27	40	6.27×10^{51}	1.45×10^{52}	1.44	1.44 ± 0.18
050724A	0.258	HA	90	Swift	2.76	41	3.58×10^{50}	1.08×10^{50}	2.50	2.02 ± 0.19
050709A	0.16	E	89	HETE-2	0.22 ± 0.05	13	3.58×10^{49}	5.30×10^{50}
050509B	0.226	HA	87	Swift	0.02	21	6.99×10^{48}	2.20×10^{49}	1.84	1.84 ± 0.29

Note. — Col. (1) GRB name. Col. (2) redshift. Col. (3) Method of redshifts: (A)bsorption from afterglow, (E)mision lines from host galaxy and (P)hotometric redshift. Col. (4) Reference of redshift. Col. (5) Detector of T_{90} . Col. (6) Value of T_{90} . Col. (7) Reference of T_{90} . Col. (8) Isotropic γ -ray energy in rest frame $1 - 10^4$ keV. $z = 2.0$ is assumed for LGRBs without redshifts and $z = 0.5$ is assumed for SGRBs without redshifts. Spectral parameters in Table 2 are used. Col. (9) γ -ray luminosity in rest frame $1 - 10^4$ keV. Col. (10) Amplitude f parameter, $\frac{F_p}{F_b}$. Col. (11) Effective f parameter, the f parameter by assuming a background making T_{90} to be 2 s.

Comments: ^a $z = 0.5$ is assumed for LGRB 020410A, according to the possible detection of SN in Levan et al. (2005).

References. (1) Schaefer et al. (1999); (2) Hurley & Cline (1999); (3) Hurley et al. (2000a); (4) Hurley et al. (2000b); (5) Jimenez et al. (2001); (6) Heise et al. (2001); (7) in't Zand et al. (2002); (8) Hurley et al. (2002b); (9) Ricker et al. (2002); (10) Graziani et al. (2003); (11) Nicastro et al. (2004); (12) Cummings et al. (2005); (13) Villasenor et al. (2005); (14) Golenetskii et al. (2007a); (15) McGlynn et al. (2008); (16) Pélangeon et al. (2008); (17) Perley et al. (2009b); (18) Frontera et al. (2009); (19) Sakamoto et al. (2010); (20) Gruber et al. (2011); (21) Sakamoto et al. (2011b); (22) Golenetskii et al. (2011b); (23) Golenetskii et al. (2011k); (24) Golenetskii et al. (2012); (25) Gruber & Goldstein (2012); (26) Chaplin (2012); (27) Krimm et al. (2012); (28) Gendre et al. (2013); (29) Frederiks et al. (2013); (30) Xiong (2013); (31) Collazzi & Connaughton (2013); (32) Jenke (2013); (33) Younes (2013); (34) Greiner et al. (2014); (35) von Kienlin et al. (2014); (36) Jenke & Xiong (2014); (37) Golenetskii et al. (2014a); (38) Yu & Goldstein (2014); (39) Burns (2014); (40) Lü et al. (2015); (41) Kaneko et al. (2015); (42) Swift GRB table; (43) http://ibas.iasf-milano.inaf.it/IBAS_Results.html; (44) Galama et al. (1997); (45) Djorgovski et al. (1998); (46) Tinney et al. (1998); (47) Kulkarni et al. (1998); (48) Djorgovski et al. (1999); (49) Vreeswijk et al. (1999); (50) Kulkarni et al. (1999); (51) Andersen et al. (2000); (52) Castro-Tirado et al. (2001); (53) Jensen et al. (2001); (54) Vreeswijk et al. (2001); (55) Djorgovski et al. (2001); (56) Möller et al. (2002); (57) Holland et al. (2002); (58) Price et al. (2002a); (59) Price et al. (2002b); (60) Piro et al. (2002); (61) Mirabal et al. (2002); (62) Le Floch et al. (2002); (63) Fruchter et al. (2002); (64) Jaunsen et al. (2003); (65) Masetti et al. (2003); (66) Bloom et al. (2003a); (67) Barth et al. (2003); (68) Castro et al. (2003); (69) Djorgovski et al. (2003); (70) Hjorth et al. (2003b); (71) Greiner et al. (2003); (72) Vreeswijk et al. (2003); (73) Hjorth et al. (2003a); (74) Vreeswijk et al. (2004); (75) Jakobsson et al. (2004); (76) Klose et al. (2004); (77) Soderberg et al. (2004); (78) Prochaska et al. (2004); (79) Gorosabel et al. (2005); (80) Rau et al. (2005); (81) Jakobsson et al. (2005); (82) Berger et al. (2005c); (83) Christensen et al. (2005); (84) Berger et al. (2005a); (85) Chen et al. (2005); (86) Prochaska et al. (2005b); (87) Prochaska et al. (2005a); (88) Quimby et al. (2005); (89) Fox et al. (2005); (90) Berger et al. (2005b); (91) Jakobsson et al. (2006a); (92) Maiorano et al. (2006); (93) Pellizza et al. (2006); (94) Jakobsson et al. (2006b); (95) Soderberg et al. (2006a); (96) Berger et al. (2006); (97) Mirabal et al. (2006); (98) Penprase et al. (2006); (99) Soderberg et al. (2006c); (100) Watson et al. (2006); (101) Price (2006); (102) Cenko et al. (2006a); (103) Berger & Gladders (2006); (104) Bloom et al. (2006a); (105) Bloom et al. (2006b); (106) Perley et al. (2006); (107) Osip et al. (2006); (108) Cenko et al. (2006b); (109) Berger (2006a); (110) Berger (2006b); (111) Kawai et al. (2006); (112) Gal-Yam et al. (2006); (113) Stratta et al. (2007); (114) Vreeswijk et al. (2007); (115) Berger et al. (2007b); (116) Mirabal et al. (2007); (117) Ofek et al. (2007); (118) Berger et al.

(2007d); (119) Ruiz-Velasco et al. (2007); (120) Chary et al. (2007); (121) Prochaska et al. (2007c); (122) Cucchiara et al. (2007c); (123) Jakobsson et al. (2007b); (124) Berger et al. (2007a); (125) Cenko et al. (2007b); (126) Cucchiara et al. (2007b); (127) Thoene et al. (2007); (128) Prochaska et al. (2007b); (129) Cenko et al. (2007a); (130) Jakobsson et al. (2007a); (131) Cucchiara et al. (2007a); (132) Berger et al. (2007c); (133) Wiersema et al. (2008); (134) Fox et al. (2008); (135) Perley et al. (2008d); (136) Perley et al. (2008c); (137) Cucchiara & Fox (2008); (138) Perley et al. (2008b); (139) Perley et al. (2008a); (140) Berger et al. (2008b); (141) Cucchiara et al. (2008a); (142) Berger et al. (2008a); (143) D'Elia et al. (2008a); (144) D'Elia et al. (2008b); (145) Berger & Rauch (2008); (146) Cucchiara et al. (2008b); (147) Cenko et al. (2008b); (148) Ferrero et al. (2009); (149) Perley et al. (2009c); (150) Berger (2009); (151) Greiner et al. (2009); (152) Fynbo et al. (2009); (153) Cucchiara et al. (2009b); (154) Xu et al. (2009); (155) Cucchiara et al. (2009a); (156) Chornock et al. (2009d); (157) Perley et al. (2009a); (158) de Ugarte Postigo et al. (2009c); (159) Fugazza et al. (2009); (160) Chornock et al. (2009c); (161) Chornock et al. (2009a); (162) Berger & Fox (2009); (163) Chornock et al. (2009b); (164) Levesque et al. (2009); (165) Rau et al. (2009); (166) de Ugarte Postigo et al. (2009b); (167) Thoene et al. (2009); (168) Malesani et al. (2009b); (169) Cenko et al. (2009); (170) Wiersema et al. (2009); (171) Fatkhullin et al. (2009); (172) Malesani et al. (2009a); (173) de Ugarte Postigo et al. (2009a); (174) Jakobsson et al. (2009); (175) Cucchiara et al. (2009c); (176) Levan et al. (2009a); (177) Kuin et al. (2009); (178) Tanvir et al. (2009b); (179) Fong et al. (2010); (180) Rau et al. (2010b); (181) Leibler & Berger (2010); (182) Rau et al. (2010a); (183) Groot et al. (2010); (184) Chornock et al. (2010b); (185) Vergani et al. (2010); (186) Cucchiara & Fox (2010); (187) Goldoni et al. (2010); (188) Cenko et al. (2010); (189) Afonso et al. (2010); (190) Chornock et al. (2010a); (191) Tanvir et al. (2010a); (192) Flores et al. (2010); (193) Rowlinson et al. (2010); (194) Krühler et al. (2011a); (195) Fong et al. (2011); (196) Cenko et al. (2011c); (197) Sparre et al. (2011b); (198) Chornock & Berger (2011); (199) Chornock et al. (2011b); (200) Sparre et al. (2011a); (201) Cenko et al. (2011a); (202) Milne & Cenko (2011); (203) Cenko et al. (2011b); (204) de Ugarte Postigo et al. (2011a); (205) de Ugarte Postigo et al. (2011b); (206) Piranomonte et al. (2011); (207) Cucchiara et al. (2011a); (208) Tanvir et al. (2011); (209) Cabrera Lavers et al. (2011); (210) Levan et al. (2011); (211) Wiersema et al. (2011); (212) Chornock et al. (2011a); (213) Cucchiara et al. (2011b); (214) Götz et al. (2011); (215) Jakobsson et al. (2012); (216) Milvang-Jensen et al. (2012); (217) Perley et al. (2012a); (218) Tello et al. (2012); (219) Kruehler et al. (2012); (220) Cucchiara (2012); (221) Tanvir et al. (2012c); (222) Xu et al. (2012); (223) Greiner et al. (2012); (224) Cucchiara et al. (2012); (225) Tanvir & Ball (2012); (226) Tanvir et al. (2012a); (227) Thoene et al. (2012); (228) Sanchez-Ramirez et al. (2012); (229) Hartoog et al. (2012); (230) Knust et al. (2012); (231) Tanvir et al. (2012b); (232) Perley et al. (2012b); (233) Fynbo et al. (2012); (234) Fong et al. (2013); (235) Chornock et al. (2013a); (236) Kelly et al. (2013); (237) Perley et al. (2013); (238) Cucchiara & Fumagalli (2013); (239) Tanvir et al. (2013a); (240) Kruehler et al. (2013); (241) de Ugarte Postigo et al. (2013a); (242) Flores et al. (2013); (243) Tanvir et al. (2013c); (244) Cucchiara & Tanvir (2013); (245) Sanchez-Ramirez et al. (2013); (246) Cucchiara et al. (2013); (247) Cenko et al. (2013); (248) Smette et al. (2013); (249) Tanvir et al. (2013d); (250) Cucchiara & Perley (2013); (251) de Ugarte Postigo et al. (2013c); (252) Chornock et al. (2013b); (253) Rau et al. (2013); (254) Xu et al. (2013a); (255) de Ugarte Postigo et al. (2013b); (256) Hartoog et al. (2013); (257) Goldoni et al. (2013); (258) Cucchiara & Cenko (2013); (259) Hunt et al. (2014); (260) Jeong et al. (2014b); (261) Rossi et al. (2014); (262) Levan et al. (2014a); (263) Malesani et al. (2014b); (264) Jeong et al. (2014a); (265) Chornock et al. (2014c); (266) Tanvir et al. (2014a); (267) Tanvir et al. (2014b); (268) Tanvir et al. (2014c); (269) Perley (2014); (270) Malesani et al. (2014a); (271) Chornock et al. (2014a); (272) Chornock et al. (2014b); (273) de Ugarte Postigo et al. (2014a); (274) Volnova et al. (2014); (275) Krühler et al. (2015); (276) Cenko et al. (2015); (277) Stanway et al. (2015); (278) van der Horst et al. (2015); (279) Cano et al. (2015); (280) Perley et al. (2016); (281) Keck GRB Host project;

Table 2. prompt

GRB	Detector fluence/flux	Γ	α	β	E_p [keV] (6)	fluence S_γ		peak flux $F_p(P_p)$		reference (11)
			(3)	(4)		(5)	[10^{-7} erg cm $^{-2}$] (7)	Band (8)	(9)	
140606B	Fermi	...	$-1.24^{+0.05}_{-0.05}$	$-2.20^{+0.52}_{-0.52}$	554^{+165}_{-165}	75.9 ± 0.4	10 – 1000	13.2 ± 0.3^P	10 – 1000	103
140518A	Swift	-1.89	$-0.98^{+0.64}_{-0.53}$...	$47.9^{+12.7}_{-7.1}$	10 ± 1	15 – 150	1.0 ± 0.1^P	15 – 150	107
140515A	Swift	1.78 ± 0.13	$-0.98^{+0.55}_{-0.55}$...	$56.4^{+31.3}_{-9.9}$	5.9 ± 0.6	15 – 150	0.9 ± 0.1^P	15 – 150	107
140512A	Fermi	1.45 ± 0.04	$-1.22^{+0.02}_{-0.02}$	$-3.2^{+1.6}_{-1.6}$	682^{+70}_{-70}	293 ± 0	10 – 1000	11.0 ± 0.3^P	10 – 1000	103, 107
140508A	Fermi	...	$-1.19^{+0.02}_{-0.02}$	$-2.36^{+0.10}_{-0.10}$	263^{+14}_{-14}	614 ± 1	10 – 1000	66.8 ± 1.0^P	10 – 1000	103
140506A	Fermi	1.68 ± 0.16	$-1.18^{+0.11}_{-0.11}$	$-2.3^{+0.4}_{-7.7}$	197^{+32}_{-32}	65.9 ± 1.2	10 – 1000	15.7 ± 0.7^P	10 – 1000	103, 107
140430A	Swift	2.00 ± 0.22	11 ± 2	15 – 150	2.5 ± 0.2^P	15 – 150	107
140428A	Swift	1.54 ± 0.26	3.4 ± 0.6	15 – 150	0.6 ± 0.2^P	15 – 150	107
140423A	Fermi	1.33 ± 0.06	$-0.58^{+0.12}_{-0.12}$	$-1.83^{+0.05}_{-0.05}$	121^{+15}_{-15}	180 ± 1	10 – 1000	2.99 ± 0.20^P	10 – 1000	103, 107
140419A	KW	1.21 ± 0.04	$-0.63^{+0.36}_{-0.22}$	$-2.3^{+0.4}_{-2.5}$	293 ± 84	580^{+280}_{-190}	20 – 10000	347^{+18}_{-19}	20 – 10000	105, 107
140318A	Swift	1.35 ± 0.28	2.9 ± 0.5	15 – 150	0.5 ± 0.2^P	15 – 150	107
140311A	Swift	1.67 ± 0.23	23 ± 3	15 – 150	1.3 ± 0.5^P	15 – 150	107
140304A	Fermi	1.29 ± 0.08	$-0.80^{+0.22}_{-0.22}$	$-2.35^{+0.43}_{-0.43}$	123^{+27}_{-27}	24.3 ± 0.3	10 – 1000	2.69 ± 0.22^P	10 – 1000	103, 107
140301A	Swift	1.96 ± 0.28	4.4 ± 0.8	15 – 150	0.7 ± 0.2^P	15 – 150	107
140226A	KW	...	-1.1 ± 0.1	...	414 ± 79	56 ± 11	20 – 10000	78.6 ± 1.7	20 – 10000	104
140213A	Fermi	1.80 ± 0.04	$-1.13^{+0.03}_{-0.03}$	$-2.26^{+0.05}_{-0.05}$	$86.6^{+3.6}_{-3.6}$	212 ± 0	10 – 1000	36.9 ± 0.5^P	10 – 1000	103, 107
140206A	Fermi	1.51 ± 0.03	$-0.06^{+0.10}_{-0.10}$	$-2.35^{+0.07}_{-0.07}$	120^{+5}_{-5}	155 ± 0	10 – 1000	17.4 ± 0.5^P	10 – 1000	103, 107
140114A	Swift	2.06 ± 0.09	32 ± 1	15 – 150	0.9 ± 0.1^P	15 – 150	107
131231A	Fermi	...	-1.21 ± 0.01	-2.3 ± 0.03	178 ± 4	1519 ± 1	10 – 1000	378.8 ± 0.6^P	10 – 1000	103
131227A	Swift	1.36 ± 0.12	8.4 ± 0.6	15 – 150	1.1 ± 0.2^P	15 – 150	107
131117A	Swift	1.81 ± 0.18	$-0.17^{+1.61}_{-1.10}$...	$44.4^{+10.4}_{-6.9}$	2.5 ± 0.4	15 – 150	0.7 ± 0.1^P	15 – 150	107
131108A	Fermi	...	$-0.91^{+0.02}_{-0.02}$	$-2.46^{+0.15}_{-0.15}$	367^{+17}_{-17}	356 ± 1	10 – 1000	19.7 ± 0.4^P	10 – 1000	103
131105A	Fermi	1.45 ± 0.11	$-1.26^{+0.02}_{-0.02}$	-2.33 ± 0.33	265^{+17}_{-17}	237 ± 1	10 – 1000	8.4 ± 0.3^P	10 – 1000	103, 107
131103A	Swift	1.97 ± 0.19	8.2 ± 1.0	15 – 150	1.5 ± 0.3^P	15 – 150	107
131030A	KW	1.30 ± 0.03	-0.71 ± 0.12	-2.95 ± 0.28	177 ± 10	660 ± 40	20 – 10000	3100 ± 10	20 – 10000	101, 107
131011A	Fermi	...	-0.88 ± 0.08	-2.08 ± 0.17	218 ± 32	88.8 ± 0.6	10 – 1000	4.67 ± 0.26	10 – 1000	103
131004A	Fermi	1.81 ± 0.11	$-1.36^{+0.17}_{-0.17}$	$-22.1^{+0.0}_{-0.0}$	118^{+29}_{-29}	5.1 ± 0.2	10 – 1000	6.8 ± 0.3^P	10 – 1000	103, 107
130925A	Fermi	2.05 ± 0.04	$-1.39^{+0.02}_{-0.02}$	$-2.40^{+0.14}_{-0.14}$	$15.4^{+3.7}_{-3.7}$	6.3 ± 0.3	10 – 1000	2.47 ± 0.27^P	10 – 1000	103, 107
130907A	KW	1.17 ± 0.02	-0.91 ± 0.02	-2.42 ± 0.07	394 ± 11	7900 ± 500	20 – 10000	5220 ± 10	20 – 10000	100, 107
130831A	KW	1.93 ± 0.05	-1.51 ± 0.1	-2.8 ± 0.1	67 ± 4	76 ± 4	20 – 10000	325 ± 3	20 – 10000	99, 107
130702A	Fermi	-2.49 ± 0.03	10.4 ± 1.1	57.2 ± 1.2	10 – 1000	7.03 ± 0.86^P	10 – 1000	103
130701A	KW	1.58 ± 0.04	-1.1 ± 0.1	...	89 ± 4	58 ± 2	20 – 10000	343 ± 4	20 – 10000	98, 107
130612A	Fermi	2.00 ± 0.25	$-1.01^{+2.14}_{-2.14}$	$-2.23^{+0.15}_{-0.15}$	$26.4^{+6.8}_{-6.8}$	6.8 ± 0.6	10 – 1000	3.6 ± 0.2^P	10 – 1000	103, 107

Table 2—Continued

GRB	Detector fluence/flux	Γ	α	β	E_p [keV]	fluence S_γ		peak flux $F_p(P_p)$		reference	
(1)	(2)	(3)	(4)	(5)	(6)	[10^{-7} erg cm $^{-2}$]	Band	Band	(9)	(10)	(11)
130610A	Fermi	1.27 ± 0.08	$-1.58^{+0.08}_{-0.08}$...	271^{+111}_{-111}	35.4 ± 0.5	$10 - 1000$	2.86 ± 0.25^P	$10 - 1000$	103, 107	
130606A	KW	1.52 ± 0.12	-1.14 ± 0.15	...	294^{+90}_{-50}	44 ± 8	$20 - 10000$	2.6 ± 0.2^P	$15 - 150$	97, 107	
130604A	Swift	1.51 ± 0.12	14 ± 1	$15 - 150$	0.8 ± 0.2^P	$15 - 150$	107	
130528A	Fermi	1.55 ± 0.09	$-1.08^{+0.05}_{-0.05}$	-2.6 ± 0.3	122^{+7}_{-7}	110 ± 1	$10 - 1000$	5.7 ± 0.3^P	$10 - 1000$	103, 107	
130518A	Fermi	...	$-0.91^{+0.02}_{-0.02}$	$-2.25^{+0.07}_{-0.07}$	398^{+15}_{-15}	945 ± 1	$10 - 1000$	45.4 ± 0.4^P	$10 - 1000$	103	
130511A	Swift	1.35 ± 0.31	2.2 ± 0.4	$15 - 150$	1.3 ± 0.2^P	$15 - 150$	107	
130505A	KW/Swift	1.18 ± 0.07	-0.69 ± 0.04	-2.03 ± 0.03	631 ± 31	3130 ± 60	$20 - 10000$	$^{3}690 \pm 30$	$20 - 10000$	94, 95, 107	
130427B	Swift	1.64 ± 0.15	15 ± 1	$15 - 150$	3.0 ± 0.4^P	$15 - 150$	107	
130427A	Fermi	1.21 ± 0.02	-0.958 ± 0.006	-4.17 ± 0.16	1028 ± 8	24619 ± 12	$10 - 1000$	1051 ± 2^P	$10 - 1000$	93, 103, 107	
130420A	Fermi	2.18 ± 0.05	$-1.13^{+0.12}_{-0.12}$...	$57.3^{+3.1}_{-3.1}$	115 ± 2	$10 - 1000$	5.4 ± 0.5^P	$10 - 1000$	103, 107	
130418A	KW	2.12 ± 0.09	157 ± 25	$20 - 1200$	$^{8}2.5 \pm 0.4$	$20 - 1200$	92	
130408A	KW	1.28 ± 0.26	-0.4 ± 0.2	-2.3 ± 0.2	211 ± 29	120 ± 20	$20 - 10000$	$^{3}52 \pm 5$	$20 - 10000$	91, 107	
130215A	Fermi	1.59 ± 0.14	$-1.19^{+0.11}_{-0.11}$	$-1.59^{+0.04}_{-0.04}$	257^{+130}_{-130}	185 ± 3	$10 - 1000$	3.5 ± 0.3^P	$10 - 1000$	103, 107	
130131B	Swift	1.15 ± 0.20	3.4 ± 0.4	$15 - 150$	1.0 ± 0.2^P	$15 - 150$	107	
121229A	Swift	2.43 ± 0.46	4.6 ± 1.3	$15 - 150$	0.1 ± 0.0^P	$15 - 150$	107	
121211A	Fermi	2.36 ± 0.26	$-0.27^{+0.37}_{-0.37}$...	100^{+15}_{-15}	6.4 ± 0.4	$10 - 1000$	2.37 ± 0.24^P	$10 - 1000$	103, 107	
121209A	Swift	1.43 ± 0.08	29 ± 1	$15 - 150$	3.4 ± 0.3^P	$15 - 150$	107	
121201A	Swift	1.90 ± 0.21	7.8 ± 1.0	$15 - 150$	0.8 ± 0.1^P	$15 - 150$	107	
121128A	Fermi	1.32 ± 0.18	$-1.00^{+0.06}_{-0.06}$	-3.36 ± 0.48	$76.3^{+3.0}_{-3.0}$	93.0 ± 1.1	$10 - 1000$	17.9 ± 0.5^P	$10 - 1000$	103, 107	
121027A	Swift	1.82 ± 0.09	20 ± 1	$15 - 150$	1.3 ± 0.2^P	$15 - 150$	107	
121024A	Swift	1.41 ± 0.22	11 ± 1	$15 - 150$	1.3 ± 0.2^P	$15 - 150$	107	
120922A	Fermi	2.00 ± 0.08	$-0.62^{+0.73}_{-0.73}$	$-2.23^{+0.09}_{-0.09}$	$36.6^{+6.7}_{-6.7}$	82.1 ± 1.7	$10 - 1000$	3.4 ± 0.3^P	$10 - 1000$	103, 107	
120909A	Fermi	1.39 ± 0.06	$-0.83^{+0.08}_{-0.08}$	$-1.92^{+0.09}_{-0.09}$	195^{+25}_{-25}	98.5 ± 1.5	$10 - 1000$	3.0 ± 0.2^P	$10 - 1000$	103, 107	
120907A	Fermi	1.73 ± 0.25	$-0.81^{+0.31}_{-0.31}$...	122^{+34}_{-34}	8.1 ± 0.4	$10 - 1000$	4.3 ± 0.4^P	$10 - 1000$	103, 107	
120815A	Swift	2.29 ± 0.23	4.9 ± 0.7	$15 - 150$	2.2 ± 0.3^P	$15 - 150$	107	
120811C	Fermi	1.99 ± 0.06	$-0.71^{+0.27}_{-0.27}$	$-2.85^{+0.32}_{-0.32}$	$55.6^{+5.3}_{-5.3}$	34.5 ± 2.1	$10 - 1000$	7.7 ± 0.5^P	$10 - 1000$	103, 107	
120805A	Swift	1.20 ± 0.28	8.2 ± 1.4	$15 - 150$	0.37 ± 0.2^P	$15 - 150$	107	
120802A	Swift	1.84 ± 0.10	$-1.22^{+0.50}_{-0.44}$...	$57.3^{+29.9}_{-9.4}$	19 ± 3	$15 - 150$	3.0 ± 0.2^P	$15 - 150$	107	
120729A	Fermi	1.62 ± 0.08	...	$-1.62^{+0.04}_{-0.04}$...	50.8 ± 0.5	$10 - 1000$	5.2 ± 0.3^P	$10 - 1000$	103, 107	
120724A	Swift	2.43	$-0.75^{+1.69}_{-1.06}$...	$26.7^{+7.5}_{-25.5}$	6.8 ± 1.1	$15 - 150$	0.6 ± 0.2^P	$15 - 150$	107	
120722A	Swift	1.90 ± 0.25	12 ± 2	$15 - 150$	1.0 ± 0.3^P	$15 - 150$	107	
120716A	Fermi	...	$-0.76^{+0.12}_{-0.12}$	$-1.84^{+0.03}_{-0.03}$	$85.1^{+10.1}_{-10.1}$	144 ± 0	$10 - 1000$	8.6 ± 0.3^P	$10 - 1000$	103	
120714B	Swift	1.52 ± 0.17	12 ± 1	$15 - 150$	0.4 ± 0.1^P	$15 - 150$	107	

Table 2—Continued

GRB	Detector fluence/flux	Γ	α	β	E_p [keV]	fluence S_γ		peak flux $F_p(P_p)$		reference	
(1)	(2)	(3)	(4)	(5)	(6)	[10^{-7} erg cm $^{-2}$]	Band	Band	(9)	(10)	(11)
120712A	Fermi	1.36 ± 0.08	44.3 ± 0.5	10 – 1000	3.5 ± 0.2^P	10 – 1000	103, 107	
120711A	Fermi	...	$-0.98^{+0.01}_{-0.01}$	$-2.80^{+0.09}_{-0.09}$	1318^{+45}_{-45}	1942 ± 2	10 – 1000	26.7 ± 0.6^P	10 – 1000	103	
120624B	Fermi	1.17 ± 0.03	$-0.92^{+0.01}_{-0.01}$	$-2.22^{+0.07}_{-0.07}$	637^{+24}_{-24}	1916 ± 1	10 – 1000	17.7 ± 0.3^P	10 – 1000	103, 107	
120422A	Swift	1.19 ± 0.24	2.3 ± 0.4	15 – 150	0.6 ± 0.2^P	15 – 150	107	
120404A	Swift	1.85 ± 0.13	16 ± 1	15 – 150	1.2 ± 0.2^P	15 – 150	107	
120327A	Swift	1.52 ± 0.06	36 ± 1	15 – 150	3.9 ± 0.2^P	15 – 150	107	
120326A	Fermi	1.99	$-0.67^{+0.19}_{-0.19}$	$-2.33^{+0.09}_{-0.09}$	$43.9^{+3.9}_{-3.9}$	32.6 ± 0.5	10 – 1000	7.7 ± 0.3^P	10 – 1000	103, 107	
120224A	Swift	2.25 ± 0.36	2.4 ± 0.5	15 – 150	0.9 ± 0.2^P	15 – 150	107	
120211A	Swift	1.50 ± 0.22	8.1 ± 1.2	15 – 150	0.5 ± 0.2^P	15 – 150	107	
120119A	Fermi	1.38 ± 0.04	$-0.96^{+0.03}_{-0.03}$	$-2.37^{+0.09}_{-0.09}$	183^{+7}_{-7}	386 ± 1	10 – 1000	16.9 ± 0.4^P	10 – 1000	103, 107	
120118B	Fermi	2.08 ± 0.11	$-0.30^{+0.29}_{-0.29}$	$-2.55^{+0.15}_{-0.15}$	$43.1^{+3.9}_{-3.9}$	26.6 ± 0.5	10 – 1000	2.83 ± 0.23^P	10 – 1000	103, 107	
111229A	Swift	1.85 ± 0.33	3.4 ± 0.7	15 – 150	1.0 ± 0.2^P	15 – 150	107	
111228A	Fermi	2.27 ± 0.06	$-1.58^{+0.08}_{-0.08}$	$-2.44^{+0.06}_{-0.06}$	$26.5^{+1.3}_{-1.3}$	181 ± 0	10 – 1000	20.8 ± 0.4^P	10 – 1000	103, 107	
111225A	Swift	1.70 ± 0.15	13 ± 1.2	15 – 150	0.7 ± 0.1^P	15 – 150	107	
111215A	Swift	1.70 ± 0.18	45 ± 5	15 – 150	0.5 ± 0.2^P	15 – 150	107	
111211A	AGILE	2.77 ± 0.17	92.0 ± 8.0	20 – 1200	15	20 – 60	87, 88	
111209A	KW	1.48 ± 0.03	-1.31 ± 0.09	...	310 ± 53	4860 ± 610	20 – 1400	0.5 ± 0.1^P	15 – 150	86, 107	
111129A	Swift	2.56 ± 0.38	1.8 ± 0.4	15 – 150	0.9 ± 0.2^P	15 – 150	107	
111123A	Swift	1.68 ± 0.07	73 ± 3	15 – 150	0.9 ± 0.1^P	15 – 150	107	
111107A	Fermi	1.49 ± 0.14	9.1 ± 0.3	10 – 1000	2.28 ± 0.35^P	10 – 1000	103, 107	
111008A	KW	2.02 ± 0.09	$-1.36^{+0.24}_{-0.21}$...	149^{+52}_{-28}	90 ± 9	20 – 10000	$^{5}14 \pm 3$	20 – 10000	85	
111005A	Swift	2.03 ± 0.27	6.2 ± 1.1	15 – 150	1.1 ± 0.3^P	15 – 150	107	
110918A	KW	...	-1.2 ± 0.1	$-2^{+0.03}_{-0.04}$	150^{+20}_{-17}	7500 ± 200	20 – 10000	$^{2}8700 \pm 400$	20 – 10000	84	
110818A	Fermi	1.58 ± 0.11	$-1.11^{+0.17}_{-0.17}$	$-1.76^{+0.10}_{-0.10}$	183^{+85}_{-85}	51.5 ± 0.3	10 – 1000	2.79 ± 0.27^P	10 – 1000	103, 107	
110808A	KW	2.32 ± 0.43	-1.13 ± 0.08	...	2960^{+1217}_{-796}	160 ± 20	20 – 10000	$^{2}1100 \pm 200$	20 – 10000	82, 107	
110801A	KW/Swift	1.84 ± 0.10	$-1.7^{+0.22}_{-0.15}$...	140^{+1270}_{-50}	73^{+17}_{-9}	15 – 1200	1.1 ± 0.2^P	15 – 150	83, 107	
110731A	Fermi	1.15 ± 0.05	$-0.87^{+0.03}_{-0.03}$	$-2.44^{+0.16}_{-0.16}$	319^{+19}_{-19}	228 ± 0	10 – 1000	20.9 ± 0.5^P	10 – 1000	103, 107	
110726A	Swift	1.86	$-0.64^{+0.96}_{-0.78}$...	$46.5^{+15.6}_{-8.1}$	2.2 ± 0.3	15 – 150	1.0 ± 0.2^P	15 – 150	107	
110715A	KW	1.63	$-1.23^{+0.09}_{-0.08}$	$-2.7^{+0.2}_{-0.5}$	120^{+12}_{-11}	230 ± 20	20 – 10000	$^{3}110 \pm 10$	20 – 10000	81, 107	
110709B	KW	1.29 ± 0.04	$-1^{+0.14}_{-0.13}$...	278^{+43}_{-32}	260 ± 20	20 – 5000	110 ± 10	20 – 5000	80, 107	
110503A	KW	1.26 ± 0.07	$-0.98^{+0.09}_{-0.08}$	$-2.7^{+0.2}_{-0.5}$	219^{+20}_{-19}	260 ± 20	20 – 5000	$^{3}110 \pm 10$	20 – 5000	79, 107	
110422A	KW	1.34 ± 0.00	-0.65 ± 0.06	$-2.96^{+0.14}_{-0.19}$	152 ± 5	856 ± 2	20 – 2000	$^{3}120 \pm 15$	20 – 2000	78, 107	
110213B	KW/MAXI	...	-1.52 ± 0.25	...	123 ± 19	177 ± 16	20 – 1400	$0.83^{+0.02}_{-0.53}$	2 – 20	77, 106	

Table 2—Continued

GRB	Detector fluence/flux	Γ	α	β	E_p [keV]	fluence S_γ		peak flux $F_p(P_p)$		reference	
(1)	(2)	(3)	(4)	(5)	(6)	[10^{-7} erg cm $^{-2}$]	Band	Band	(9)	(10)	(11)
110213A	Fermi	1.83 ± 0.12	$-1.42^{+0.09}_{-0.09}$	$-2.13^{+0.09}_{-0.09}$	$74.7^{+13.1}_{-13.1}$	93.7 ± 0.5	10 – 1000	17.8 ± 0.5^P	10 – 1000	103, 107	
110205A	KW	1.80 ± 0.04	-1.52 ± 0.14	...	222 ± 74	366 ± 35	20 – 1200	$^{_8}5.1 \pm 0.7$	20 – 1200	76, 107	
110128A	Fermi	1.31 ± 0.30	$-1.26^{+0.25}_{-0.25}$...	192^{+112}_{-112}	14.2 ± 1.0	10 – 1000	1.55 ± 0.19^P	10 – 1000	103, 107	
110106B	Fermi	1.76 ± 0.11	$-0.94^{+0.16}_{-0.16}$...	129^{+20}_{-20}	41.1 ± 0.6	10 – 1000	2.77 ± 0.27^P	10 – 1000	103, 107	
101225A	Swift	1.82 ± 0.32	19 ± 4	15 – 150	0.028 ± 0.005^P	15 – 150	107	
101219B	Fermi	1.56 ± 0.16	$-1.37^{+0.72}_{-0.72}$	$-2.26^{+0.14}_{-0.14}$	$56.4^{+6.6}_{-6.6}$	39.9 ± 0.5	10 – 1000	2.00 ± 0.18^P	10 – 1000	103, 107	
100906A	Fermi	1.78 ± 0.03	$-0.90^{+0.13}_{-0.13}$	$-1.86^{+0.03}_{-0.03}$	$69.7^{+10.1}_{-10.1}$	232 ± 0	10 – 1000	14.5 ± 0.4^P	10 – 1000	103, 107	
100901A	Swift	1.52 ± 0.21	21 ± 3	15 – 150	0.8 ± 0.2^P	15 – 150	107	
100814A	Fermi	1.47 ± 0.04	$-0.37^{+0.10}_{-0.10}$	$-2.43^{+0.21}_{-0.21}$	135^{+10}_{-10}	149 ± 0	10 – 1000	4.6 ± 0.3^P	10 – 1000	103, 107	
100728B	Fermi	1.55 ± 0.14	$-0.78^{+0.17}_{-0.17}$	$-1.98^{+0.14}_{-0.14}$	109^{+22}_{-22}	33.4 ± 0.6	10 – 1000	6.2 ± 0.3^P	10 – 1000	103, 107	
100728A	Fermi	1.18 ± 0.02	-0.64 ± 0.02	-2.7 ± 0.14	290 ± 8	1279 ± 6	10 – 1000	$^{_5}10.5 \pm 0.3^P$	10 – 1000	103, 107	
100724A	Swift	1.92 ± 0.21	1.6 ± 0.2	15 – 150	1.9 ± 0.2^P	15 – 150	107	
100621A	KW	1.90 ± 0.03	-1.7 ± 0.13	...	95^{+18}_{-13}	360 ± 40	20 – 2000	$^{_5}17 \pm 1.3$	20 – 2000	73, 107	
100615A	Fermi	1.87 ± 0.04	$-0.90^{+0.18}_{-0.18}$	$-1.80^{+0.03}_{-0.03}$	$53.3^{+9.9}_{-9.9}$	87.2 ± 0.8	10 – 1000	8.3 ± 0.2^P	10 – 1000	103, 107	
100606A	KW	1.35 ± 0.10	-1.05 ± 0.14	...	945^{+551}_{-266}	390 ± 50	20 – 2000	$^{_5}25 \pm 2.5$	20 – 2000	72, 107	
100518A	INTEGRAL	$1.28^{+0.05}_{-0.05}$	$5.2^{+4.4}_{-3.8}$	20 – 200	0.80 ± 0.20^P	20 – 200	102	
100513A	Swift	1.62 ± 0.14	14 ± 1	15 – 150	0.6 ± 0.1^P	15 – 150	107	
100508A	Swift	1.23 ± 0.25	7.0 ± 1.1	15 – 150	0.4 ± 0.2^P	15 – 150	107	
100425A	Swift	2.42 ± 0.32	4.7 ± 0.9	15 – 150	1.4 ± 0.2^P	15 – 150	107	
100424A	Swift	1.83 ± 0.13	15 ± 1	15 – 150	0.4 ± 0.1^P	15 – 150	107	
100418A	Swift	2.16 ± 0.25	3.4 ± 0.5	15 – 150	1.0 ± 0.2^P	15 – 150	107	
100414A	Fermi	...	-0.624 ± 0.014	-3.54 ± 0.48	663 ± 16	885 ± 2	10 – 1000	21.9 ± 0.24	10 – 1000	103	
100316D	Swift	2.29 ± 0.41	3.0 ± 0.8	15 – 150	0.1 ± 0.0^P	15 – 150	107	
100316B	Swift	2.23 ± 0.18	2.0 ± 0.2	15 – 150	1.3 ± 0.1^P	15 – 150	107	
100302A	Swift	1.72 ± 0.19	3.1 ± 0.4	15 – 150	0.5 ± 0.1^P	15 – 150	107	
100219A	Swift	1.33 ± 0.25	3.7 ± 0.6	15 – 150	0.4 ± 0.1^P	15 – 150	107	
091208B	Fermi	$1.762^{+0.107}_{-0.109}$	$-0.15^{+0.39}_{-0.39}$	$-1.90^{+0.04}_{-0.04}$	$38.5^{+5.8}_{-5.8}$	61.9 ± 1.9	10 – 1000	20.6 ± 0.3^P	10 – 1000	75, 103	
091127A	Fermi	2.05 ± 0.07	$-1.26^{+0.07}_{-0.07}$	$-2.22^{+0.02}_{-0.02}$	$35.5^{+1.5}_{-1.5}$	207 ± 0	10 – 1000	68.2 ± 0.5^P	10 – 1000	103, 107	
091109A	Swift	$1.306^{+0.254}_{-0.245}$	16.4 ± 2.2	15 – 150	0.99 ± 0.30	15 – 150	75	
091029A	Swift	1.88 ± 0.07	$-1.46^{+0.28}_{-0.27}$...	$61.3^{+25.0}_{-9.1}$	24 ± 1	15 – 150	1.8 ± 0.1^P	15 – 150	107	
091024A	Fermi	1.20 ± 0.08	$-1.32^{+0.08}_{-0.08}$...	1730^{+901}_{-901}	85.6 ± 0.6	10 – 1000	4.2 ± 0.3^P	10 – 1000	103, 107	
091020A	Fermi	1.53 ± 0.07	$-1.26^{+0.06}_{-0.06}$	$-4.0^{+11.1}_{-11.1}$	244^{+36}_{-36}	83.5 ± 1.5	10 – 1000	6.8 ± 0.3^P	10 – 1000	103, 107	
091018A	Konus-RF	2.31 ± 0.06	$-1.53^{+0.59}_{-0.39}$	< -2.44	28^{+10}_{-16}	$14.4^{+1.9}_{-1.6}$	20 – 1000	$^{_5}4.32^{+0.97}_{-0.94}$	20 – 1000	66, 107	

Table 2—Continued

GRB	Detector fluence/flux	Γ	α	β	E_p [keV]	fluence S_γ		peak flux $F_p(P_p)$		reference
			(3)	(4)		(6)	[10^{-7} erg cm $^{-2}$]	Band	(9)	
(1)	(2)	(3)	(4)	(5)	(6)	(7)	(8)	(9)	(10)	(11)
091003A	Fermi	...	$-1.07^{+0.02}_{-0.02}$	$-2.23^{+0.11}_{-0.11}$	367^{+26}_{-26}	233 ± 0	$10 - 1000$	29.2 ± 0.5^P	$10 - 1000$	103
090927A	Fermi	1.80 ± 0.20	3.0 ± 0.2	$10 - 1000$	3.3 ± 0.2^P	$10 - 1000$	103, 107
090926B	Fermi	1.50 ± 0.00	$-0.13^{+0.12}_{-0.12}$	$-3.2^{+0.3}_{-0.3}$	$82.5^{+3.0}_{-3.0}$	107 ± 1	$10 - 1000$	4.6 ± 0.2^P	$10 - 1000$	103, 107
090926A	Fermi	...	$-0.86^{+0.01}_{-0.01}$	$-2.40^{+0.04}_{-0.04}$	339^{+5}_{-5}	1465 ± 3	$10 - 1000$	81.4 ± 0.4^P	$10 - 1000$	103
090902B	Fermi	...	$-1.01^{+0.00}_{-0.00}$...	1054^{+17}_{-17}	2217 ± 3	$10 - 1000$	76.9 ± 0.4^P	$10 - 1000$	103
090814A	Swift	$1.836^{+0.184}_{-0.193}$	12.7 ± 1.6	$15 - 150$	0.43 ± 0.18	$15 - 150$	75
090812A	KW/Swift	1.24 ± 0.05	-1.03 ± 0.07	...	572^{+251}_{-159}	261 ± 34	$15 - 1400$	3.6 ± 0.2^P	$15 - 150$	71, 107
090809A	Swift	$1.349^{+0.258}_{-0.254}$	3.7 ± 0.6	$15 - 150$	0.86 ± 0.19	$15 - 150$	75
090726A	Swift	2.25 ± 0.19	8.6 ± 1.0	$15 - 150$	0.7 ± 0.2^P	$15 - 150$	107
090715B	KW	$1.582^{+0.065}_{-0.065}$	$-1.1^{+0.40}_{-0.34}$...	134^{+56}_{-30}	93^{+15}_{-11}	$20 - 2000$	${}^59 \pm 2.5$	$20 - 2000$	70, 75
090709A	KW	$1.209^{+0.025}_{-0.025}$	-0.85 ± 0.08	$-2.7^{+0.2}_{-0.3}$	298 ± 27	910 ± 7	$20 - 3000$	${}^539 \pm 6$	$20 - 3000$	69, 75
090618A	Fermi	1.58 ± 0.02	$-1.13^{+0.01}_{-0.01}$	$-2.22^{+0.02}_{-0.02}$	146^{+3}_{-3}	2684 ± 4	$10 - 1000$	68.7 ± 1.1^P	$10 - 1000$	103, 107
090530A	Swift	1.61 ± 0.17	11 ± 1	$15 - 150$	2.5 ± 0.3^P	$15 - 150$	107
090529A	Swift	2.00 ± 0.3	6.8 ± 1.7	$15 - 150$	0.4 ± 0.1^P	$15 - 150$	107
090519A	Fermi	1.02 ± 0.20	$-0.95^{+0.10}_{-0.10}$...	1618^{+883}_{-883}	57.3 ± 0.6	$10 - 1000$	1.49 ± 0.16^P	$10 - 1000$	103, 107
090516A	Fermi	1.84 ± 0.11	$-1.52^{+0.05}_{-0.05}$	$-2.30^{+0.27}_{-0.27}$	142^{+26}_{-26}	172 ± 0	$10 - 1000$	4.4 ± 0.2^P	$10 - 1000$	103, 107
090424A	Fermi	1.53 ± 0.03	$-1.04^{+0.02}_{-0.02}$	$-2.76^{+0.12}_{-0.12}$	153^{+3}_{-3}	463 ± 0	$10 - 1000$	109 ± 0^P	$10 - 1000$	103, 107
090423A	Fermi	1.81 ± 0.09	$-0.59^{+0.50}_{-0.50}$	$-2.67^{+0.74}_{-0.74}$	$66.0^{+16.2}_{-16.2}$	8.2 ± 0.7	$10 - 1000$	1.62 ± 0.21^P	$10 - 1000$	103, 107
090418A	KW/Swift	$1.335^{+0.066}_{-0.066}$	-1.3 ± 0.09	...	610^{+554}_{-215}	179 ± 21	$15 - 1200$	1.58 ± 0.27	$15 - 150$	68, 75
090417B	Swift	$1.821^{+0.134}_{-0.138}$	22.5 ± 1.8	$15 - 150$	0.18 ± 0.09	$15 - 150$	75
090407A	Swift	1.73 ± 0.29	11 ± 2	$15 - 150$	0.6 ± 0.1^P	$15 - 150$	107
090328A	Fermi	...	$-1.09^{+0.02}_{-0.02}$	$-2.37^{+0.18}_{-0.18}$	639^{+45}_{-45}	420 ± 0	$10 - 1000$	17.2 ± 0.3^P	$10 - 1000$	103
090323A	Fermi	...	$-1.29^{+0.01}_{-0.01}$	$-2.44^{+0.17}_{-0.17}$	632^{+40}_{-40}	1180 ± 1	$10 - 1000$	12.6 ± 0.2^P	$10 - 1000$	103
090313A	Swift	1.91 ± 0.29	14 ± 2	$15 - 150$	0.8 ± 0.3^P	$15 - 150$	107
090205A	Swift	2.15 ± 0.23	1.9 ± 0.3	$15 - 150$	0.5 ± 0.1^P	$15 - 150$	107
090201A	KW	1.41 ± 0.04	$-0.97^{+0.10}_{-0.09}$	$-2.8^{+0.29}_{-0.92}$	158^{+13}_{-12}	672^{+47}_{-54}	$20 - 2000$	${}^373^{+12}_{-13}$	$20 - 2000$	67, 107
090113A	Fermi	1.60 ± 0.10	$-1.20^{+0.19}_{-0.19}$	$-2.06^{+0.29}_{-0.29}$	137^{+57}_{-57}	15.7 ± 0.5	$10 - 1000$	3.8 ± 0.2^P	$10 - 1000$	103, 107
090102A	Fermi	1.36 ± 0.08	$-0.95^{+0.02}_{-0.02}$...	421^{+18}_{-18}	279 ± 0	$10 - 1000$	11.2 ± 0.2^P	$10 - 1000$	103, 107
081222A	Fermi	1.41 ± 0.04	$-0.86^{+0.05}_{-0.05}$	$-2.31^{+0.12}_{-0.12}$	142^{+9}_{-9}	118 ± 0	$10 - 1000$	12.8 ± 0.2^P	$10 - 1000$	103, 107
081221A	Fermi	1.75 ± 0.03	$-0.90^{+0.02}_{-0.02}$	$-3.9^{+0.5}_{-0.5}$	$86.9^{+1.4}_{-1.4}$	300 ± 0	$10 - 1000$	25.4 ± 0.3^P	$10 - 1000$	103, 107
081210A	Swift	1.42 ± 0.14	18 ± 2	$15 - 150$	2.5 ± 0.2^P	$15 - 150$	107
081203A	KW	$1.426^{+0.060}_{-0.060}$	$-1.33^{+0.27}_{-0.20}$...	578^{+2398}_{-290}	305^{+140}_{-89}	$20 - 3000$	2.47 ± 0.19	$15 - 150$	63, 75
081121A	Fermi	1.09 ± 0.11	$-0.43^{+0.13}_{-0.13}$	$-2.09^{+0.09}_{-0.09}$	160^{+16}_{-16}	152 ± 2	$10 - 1000$	7.7 ± 0.4^P	$10 - 1000$	103, 107

Table 2—Continued

GRB	Detector fluence/flux	Γ	α	β	E_p [keV]	fluence S_γ		peak flux $F_p(P_p)$		reference
						[10^{-7} erg cm $^{-2}$]	Band	Band	Band	
(1)	(2)	(3)	(4)	(5)	(6)	(7)	(8)	(9)	(10)	(11)
081118A	Swift	2.10 ± 0.16	12 ± 1	15 – 150	0.6 ± 0.2^P	15 – 150	107
081109A	Fermi	$1.608^{+0.085}_{-0.085}$	$-0.67^{+1.85}_{-1.85}$	$-1.65^{+0.03}_{-0.03}$	$32.4^{+38.3}_{-38.3}$	65.5 ± 0.6	10 – 1000	2.64 ± 0.16^P	10 – 1000	75, 103
081029A	Swift	1.43 ± 0.18	21 ± 2	15 – 150	0.5 ± 0.2^P	15 – 150	107
081028A	Swift	1.25 ± 0.38	37 ± 2	15 – 150	0.5 ± 0.1^P	15 – 150	107
081008A	Fermi	1.69 ± 0.07	$-1.01^{+0.12}_{-0.12}$	$-2.09^{+0.21}_{-0.21}$	166^{+36}_{-36}	103 ± 1	10 – 1000	2.66 ± 0.16^P	10 – 1000	103, 107
081007A	Swift	2.51 ± 0.20	7.1 ± 0.8	15 – 150	2.6 ± 0.4^P	15 – 150	107
080928A	Fermi	1.77 ± 0.12	...	$-1.80^{+0.06}_{-0.06}$	$17.9^{+28.3}_{-28.3}$	11.6 ± 0.4	10 – 1000	3.2 ± 0.2^P	10 – 1000	103, 107
080916C	Fermi	...	$-1.08^{+0.01}_{-0.01}$	$-2.15^{+0.07}_{-0.07}$	661^{+45}_{-45}	602 ± 0	10 – 1000	13.7 ± 0.3^P	10 – 1000	103
080916A	Fermi	$1.546^{+0.046}_{-0.046}$	$-0.82^{+0.13}_{-0.13}$	$-1.78^{+0.05}_{-0.05}$	106^{+19}_{-19}	78.1 ± 0.8	10 – 1000	4.5 ± 0.3^P	10 – 1000	75, 103
080913A	KW/Swift	1.20 ± 0.15	$-0.82^{+0.75}_{-0.53}$...	121^{+232}_{-39}	$8.5^{+6.0}_{-2.2}$	15 – 1000	1.4 ± 0.2^P	15 – 150	62, 107
080905B	Fermi	$1.657^{+0.142}_{-0.144}$	$-0.86^{+0.22}_{-0.22}$	$-2.29^{+0.65}_{-0.65}$	181^{+60}_{-60}	29.1 ± 0.4	10 – 1000	2.32 ± 0.23^P	10 – 1000	75, 103
080810A	Fermi	1.34 ± 0.06	$-1.19^{+0.04}_{-0.04}$...	909^{+184}_{-184}	108 ± 0	10 – 1000	3.6 ± 0.2^P	10 – 1000	103, 107
080805A	Swift	1.53 ± 0.07	25 ± 1	15 – 150	1.1 ± 0.1^P	15 – 150	107
080804A	Fermi	1.19 ± 0.09	$-0.52^{+0.09}_{-0.09}$	$-1.90^{+0.08}_{-0.08}$	217^{+24}_{-24}	91.3 ± 1.1	10 – 1000	3.8 ± 0.2^P	10 – 1000	103, 107
080721A	KW	1.11 ± 0.08	$-0.933^{+0.106}_{-0.084}$	$-2.43^{+0.24}_{-0.42}$	485^{+67}_{-59}	838^{+62}_{-60}	20 – 5000	${}^3196 \pm 31$	20 – 5000	61, 107
080710A	Swift	1.47 ± 0.23	14 ± 2	15 – 150	1.0 ± 0.2^P	15 – 150	107
080707A	Swift	1.77 ± 0.19	5.2 ± 0.6	15 – 150	1.0 ± 0.1^P	15 – 150	107
080607A	KW	1.31 ± 0.04	$-1.06^{+0.09}_{-0.08}$	$-2.57^{+0.18}_{-0.26}$	394^{+58}_{-54}	893^{+52}_{-47}	20 – 4000	${}^2269 \pm 54$	20 – 4000	60, 107
080605A	KW	1.32 ± 0.03	-1.02 ± 0.08	$-2.58^{+0.31}_{-0.84}$	246^{+23}_{-18}	302^{+13}_{-12}	20 – 2000	${}^2160 \pm 33$	20 – 2000	59, 107
080604A	Swift	1.78 ± 0.18	8.0 ± 0.9	15 – 150	0.4 ± 0.1^P	15 – 150	107
080603B	KW	$1.731^{+0.061}_{-0.061}$	$-0.94^{+1.21}_{-0.75}$...	85^{+91}_{-30}	$45.0^{+15.3}_{-9.0}$	20 – 1000	${}^515.1^{+4.0}_{-3.8}$	20 – 1000	58, 75
080603A	INTEGRAL	1.6 ± 0.2	11 ± 2	20 – 200	0.5^P	20 – 200	89
080602A	KW	1.43 ± 0.13	$79.2^{+14.7}_{-14.5}$	20 – 1000	${}^519.2 \pm 5.8$	20 – 1000	57, 107
080520A	Swift	2.90 ± 0.51	0.55 ± 0.17	15 – 150	0.5 ± 0.1^P	15 – 150	107
080517A	Swift	1.54 ± 0.33	5.6 ± 1.2	15 – 150	0.6 ± 0.2^P	15 – 150	107
080515A	Swift	2.19 ± 0.16	$-0.39^{+1.19}_{-0.95}$...	$33.5^{+4.6}_{-6.2}$	20 ± 3	15 – 150	3.9 ± 0.7^P	15 – 150	107
080430A	Swift	1.73 ± 0.09	12 ± 1	15 – 150	2.6 ± 0.2^P	15 – 150	107
080413B	Swift	$1.742^{+0.058}_{-0.058}$	$-1.230^{+0.256}_{-0.241}$...	$77.67^{+24.35}_{-10.84}$	32.5 ± 1.2	15 – 150	14.0 ± 0.6	15 – 150	75
080413A	Suzaku/Swift	$1.529^{+0.052}_{-0.052}$	-1.2 ± 0.1	...	170^{+80}_{-27}	48^{+4}_{-12}	15 – 150	4.8 ± 0.2	15 – 150	56, 75
080411A	KW	1.75 ± 0.03	$-1.51^{+0.04}_{-0.05}$...	259^{+35}_{-27}	629^{+31}_{-29}	20 – 2000	${}^3128 \pm 16$	20 – 2000	55, 107
080330A	Swift	2.53 ± 0.45	3.4 ± 0.8	15 – 150	0.9 ± 0.2^P	15 – 150	107
080325A	Swift	1.68 ± 0.17	49 ± 4	15 – 150	1.4 ± 0.6^P	15 – 150	107
080319C	KW	$1.285^{+0.068}_{-0.068}$	-1.01 ± 0.13	$-1.87^{+0.15}_{-0.63}$	307^{+141}_{-92}	150^{+34}_{-21}	20 – 4000	${}^533.5^{+7.9}_{-7.0}$	20 – 4000	54, 75

Table 2—Continued

GRB	Detector fluence/flux	Γ	α	β	E_p [keV]	fluence S_γ			peak flux $F_p(P_p)$		reference
						(6)	[10^{-7} erg cm $^{-2}$]	Band	(9)	Band	
(1)	(2)	(3)	(4)	(5)	(7)	(8)	(12)	(13)	(14)	(15)	
080319B	KW	$1.051^{+0.019}_{-0.019}$	$-0.822^{+0.014}_{-0.012}$	$-3.87^{+0.44}_{-1.09}$	651^{+13}_{-14}	5720^{+140}_{-130}	20 – 7000	3217 ± 21	20 – 7000	53, 75	
080310A	Swift	2.32 ± 0.16	23 ± 2	15 – 150	1.3 ± 0.2^P	15 – 150	107	
080210A	Swift	1.77 ± 0.12	18 ± 1	15 – 150	1.6 ± 0.2^P	15 – 150	107	
080207A	Swift	1.56 ± 0.06	$-1.25^{+0.24}_{-0.23}$...	124^{+180}_{-32}	61 ± 2	15 – 150	1.0 ± 0.3^P	15 – 150	107	
080129A	Swift	1.34 ± 0.26	8.9 ± 1.4	15 – 150	0.2 ± 0.1^P	15 – 150	107	
071122A	Swift	1.77 ± 0.31	5.8 ± 1.1	15 – 150	0.4 ± 0.2^P	15 – 150	107	
071117A	KW	1.57 ± 0.06	$-1.53^{+0.15}_{-0.16}$...	278^{+236}_{-79}	$58.4^{+3.0}_{-24.0}$	20 – 1000	$366.6^{+11.3}_{-29.5}$	20 – 1000	49, 107	
071112C	Swift	1.09 ± 0.07	30 ± 4	15 – 150	8 ± 1^P	15 – 150	107	
071031A	Swift	2.42 ± 0.29	9.0 ± 1.3	15 – 150	0.5 ± 0.1^P	15 – 150	107	
071021A	Swift	1.70 ± 0.21	13 ± 2	15 – 150	0.7 ± 0.1^P	15 – 150	107	
071020A	KW	1.11 ± 0.05	$-0.65^{+0.27}_{-0.32}$...	322^{+80}_{-53}	$77.1^{+3.9}_{-47.6}$	20 – 2000	$360.4^{+11.2}_{-38.8}$	20 – 2000	48, 107	
071010B	KW	$1.966^{+0.043}_{-0.044}$	$-1.25^{+0.74}_{-0.49}$	$-2.65^{+0.29}_{-0.49}$	52^{+10}_{-14}	$47.8^{+9.5}_{-31.2}$	20 – 1000	$38.9^{+2.3}_{-6.0}$	20 – 1000	47, 75	
071010A	Swift	$2.238^{+0.320}_{-0.365}$	2.02 ± 0.44	15 – 150	0.45 ± 0.17	15 – 150	75	
071003A	KW	1.36 ± 0.07	-0.97 ± 0.07	...	799^{+124}_{-100}	532^{+30}_{-67}	20 – 4000	3122^{+19}_{-22}	20 – 4000	46, 107	81
070810A	Swift	$2.055^{+0.124}_{-0.128}$	6.7 ± 0.5	15 – 150	1.26 ± 0.16	15 – 150	75	
070802A	Swift	1.79 ± 0.27	2.8 ± 0.5	15 – 150	0.4 ± 0.1^P	15 – 150	107	
070721B	Swift	$1.238^{+0.107}_{-0.106}$	35.6 ± 2.3	15 – 150	1.57 ± 0.25	15 – 150	75	
070714A	Swift	$2.563^{+0.195}_{-0.207}$	1.55 ± 0.16	15 – 150	0.94 ± 0.09	15 – 150	75	
070612A	Swift	$1.640^{+0.092}_{-0.092}$	108 ± 6	15 – 150	1.49 ± 0.33	15 – 150	75	
070611A	Swift	1.66 ± 0.22	3.91 ± 0.57	15 – 150	0.82 ± 0.21^P	15 – 150	107	
070529A	Swift	1.34 ± 0.16	25.70 ± 2.45	15 – 150	1.43 ± 0.36^P	15 – 150	107	
070521A	KW	1.33 ± 0.04	-0.93 ± 0.12	...	222^{+27}_{-21}	181^{+6}_{-31}	20 – 1000	$341.2^{+7.8}_{-10.7}$	20 – 1000	44, 107	
070518A	Swift	2.11 ± 0.25	1.62 ± 0.24	15 – 150	0.68 ± 0.13^P	15 – 150	107	
070508A	KW	1.34 ± 0.02	-0.81 ± 0.07	...	188 ± 8	397^{+7}_{-23}	20 – 1000	$383.0^{+10.3}_{-11.1}$	20 – 1000	43, 107	
070506A	Swift	1.73 ± 0.17	2.10 ± 0.23	15 – 150	0.96 ± 0.13^P	15 – 150	107	
070419B	Swift	$1.651^{+0.050}_{-0.050}$	74.6 ± 1.9	15 – 150	1.16 ± 0.15	15 – 150	75	
070419A	Swift	$2.372^{+0.234}_{-0.257}$	6.7 ± 1.0	15 – 150	< 0.07	15 – 150	75	
070411A	Swift	1.72 ± 0.10	27.00 ± 1.55	15 – 150	0.91 ± 0.13^P	15 – 150	107	
070328A	KW	1.24 ± 0.04	$-0.99^{+0.13}_{-0.11}$	$-1.99^{+0.18}_{-0.40}$	496^{+172}_{-117}	595^{+105}_{-76}	20 – 6000	$545.7^{+10.7}_{-9.1}$	20 – 6000	42, 107	
070318A	Swift	1.42 ± 0.08	24.80 ± 1.12	15 – 150	1.76 ± 0.15^P	15 – 150	107	
070306A	Swift	1.66 ± 0.10	53.80 ± 2.86	15 – 150	4.07 ± 0.21^P	15 – 150	107	
070224A	Swift	2.42 ± 0.30	3.05 ± 0.51	15 – 150	0.34 ± 0.11^P	15 – 150	107	
070223A	Swift	1.85 ± 0.12	17.00 ± 1.20	15 – 150	0.69 ± 0.15^P	15 – 150	107	

Table 2—Continued

GRB (1)	Detector fluence/flux (2)	Γ (3)	α (4)	β (5)	E_p [keV] (6)	fluence S_γ			peak flux $F_p(P_p)$		reference (11)
						[10^{-7} erg cm $^{-2}$] (7)	Band (8)	Band (9)	Band (10)		
070208A	Swift	1.94 ± 0.36	4.45 ± 1.01	15 – 150	0.90 ± 0.22^P	15 – 150	107	
070129A	Swift	2.01 ± 0.15	29.80 ± 2.67	15 – 150	0.55 ± 0.12^P	15 – 150	107	
070125A	KW	...	$-1.10^{+0.10}_{-0.09}$	$-2.08^{+0.10}_{-0.15}$	367^{+65}_{-51}	1740^{+180}_{-150}	20 – 10000	$^{3}225^{+36}_{-34}$	20 – 10000	41	
070110A	Swift	1.58 ± 0.12	16.20 ± 1.08	15 – 150	0.60 ± 0.12^P	15 – 150	107	
070103A	Swift	1.95 ± 0.21	3.38 ± 0.46	15 – 150	1.04 ± 0.15^P	15 – 150	107	
061222B	Swift	$1.956^{+0.127}_{-0.131}$	22.7 ± 1.8	15 – 150	0.87 ± 0.23	15 – 150	75	
061222A	KW	$1.324^{+0.038}_{-0.038}$	$-0.94^{+0.14}_{-0.13}$	$-2.41^{+0.28}_{-1.21}$	283^{+59}_{-42}	266^{+43}_{-23}	20 – 2000	$^{3}56.5^{+14.2}_{-11.9}$	20 – 2000	40, 75	
061202A	Swift	1.58 ± 0.07	34.20 ± 1.33	15 – 150	2.51 ± 0.17^P	15 – 150	107	
061126A	RHESSI	1.32 ± 0.06	$-0.95^{+0.29}_{-0.23}$...	935 ± 360	200 ± 2.21	30 – 2000	9.76 ± 0.38^P	15 – 150	38, 107	
061121A	KW	1.41 ± 0.03	$-1.32^{+0.04}_{-0.05}$...	606^{+90}_{-72}	567^{+30}_{-50}	20 – 5000	$^{3}128^{+16}_{-19}$	20 – 5000	37, 107	
061110B	Swift	$0.991^{+0.155}_{-0.151}$	13.5 ± 1.2	15 – 150	0.43 ± 0.11	15 – 150	75	
061110A	Swift	$1.643^{+0.116}_{-0.118}$	11.3 ± 0.8	15 – 150	0.29 ± 0.10	15 – 150	75	
061021A	KW	1.30 ± 0.06	$-1.22^{+0.12}_{-0.14}$...	777^{+549}_{-237}	134^{+11}_{-47}	20 – 2000	$^{5}37.2^{+5.3}_{-16.2}$	20 – 2000	36, 107	
061007A	KW	1.03 ± 0.03	-0.70 ± 0.04	$-2.61^{+0.15}_{-0.21}$	399^{+19}_{-18}	2490^{+170}_{-120}	20 – 10000	$^{3}195^{+31}_{-24}$	20 – 10000	35, 107	
060927A	Swift	1.61 ± 0.08	$-0.81^{+0.38}_{-0.35}$...	$70.7^{+19.4}_{-9.6}$	11.30 ± 0.68	15 – 150	2.70 ± 0.17^P	15 – 150	107	
060926A	Swift	2.54 ± 0.23	2.19 ± 0.25	15 – 150	1.09 ± 0.14^P	15 – 150	107	
060923B	Swift	$2.474^{+0.228}_{-0.247}$	4.9 ± 0.6	15 – 150	0.74 ± 0.19	15 – 150	75	
060923A	Swift	$1.695^{+0.220}_{-0.227}$	8.8 ± 1.3	15 – 150	1.07 ± 0.21	15 – 150	75	
060912A	Swift	$1.729^{+0.080}_{-0.080}$	13.50 ± 0.62	15 – 150	$^{5}8.58 \pm 0.44^P$	15 – 150	75, 107	
060908A	Swift	1.32 ± 0.06	$-0.93^{+0.26}_{-0.24}$...	147^{+138}_{-37}	28.00 ± 1.11	15 – 150	3.03 ± 0.25^P	15 – 150	107	
060906A	Swift	2.03 ± 0.11	22.10 ± 1.36	15 – 150	1.97 ± 0.28^P	15 – 150	107	
060904B	Swift	$1.604^{+0.135}_{-0.137}$	16.5 ± 1.4	15 – 150	2.10 ± 0.20	15 – 150	75	
060814A	KW	1.53 ± 0.03	$-1.43^{+0.15}_{-0.16}$...	257^{+122}_{-58}	269^{+12}_{-79}	20 – 1000	$^{5}21.3^{+2.9}_{-5.5}$	20 – 1000	33, 107	
060805A	Swift	$2.105^{+0.356}_{-0.404}$	0.73 ± 0.19	15 – 150	0.22 ± 0.09	15 – 150	75	
060729A	Swift	1.75 ± 0.14	26.10 ± 2.11	15 – 150	1.17 ± 0.13^P	15 – 150	107	
060719A	Swift	1.91 ± 0.11	15.00 ± 0.91	15 – 150	2.16 ± 0.20^P	15 – 150	107	
060714A	Swift	1.93 ± 0.11	28.30 ± 1.67	15 – 150	1.28 ± 0.13^P	15 – 150	107	
060707A	Swift	1.67 ± 0.13	$-0.42^{+0.67}_{-0.59}$...	$61.9^{+15.0}_{-8.2}$	16.00 ± 1.51	15 – 150	1.01 ± 0.23^P	15 – 150	107	
060614A	KW	2.02 ± 0.04	$-1.57^{+0.12}_{-0.14}$...	302^{+214}_{-85}	409^{+18}_{-34}	20 – 2000	$^{3}45.0^{+7.2}_{-15.3}$	20 – 2000	32, 107	
060607A	Swift	$1.450^{+0.073}_{-0.073}$	25.6 ± 1.1	15 – 150	1.27 ± 0.12	15 – 150	75	
060605A	Swift	1.55 ± 0.20	6.97 ± 0.90	15 – 150	0.46 ± 0.12^P	15 – 150	107	
060604A	Swift	2.01 ± 0.42	4.02 ± 1.06	15 – 150	0.34 ± 0.13^P	15 – 150	107	
060602A	Swift	$1.219^{+0.162}_{-0.159}$	16.1 ± 1.6	15 – 150	0.37 ± 0.18	15 – 150	75	

Table 2—Continued

GRB	Detector fluence/flux	Γ	α	β	E_p [keV]	fluence S_γ			peak flux $F_p(P_p)$		reference
						[10^{-7} erg cm $^{-2}$]	Band	(7)	Band	(10)	
(1)	(2)	(3)	(4)	(5)	(6)	(7)	(8)	(9)	(10)	(11)	
060526A	Swift	2.01 ± 0.24	12.60 ± 1.65	15 – 150	1.67 ± 0.18^P	15 – 150	107	
060522A	Swift	1.56 ± 0.15	11.40 ± 1.11	15 – 150	0.55 ± 0.15^P	15 – 150	107	
060512A	Swift	2.48 ± 0.30	2.32 ± 0.40	15 – 150	0.88 ± 0.20^P	15 – 150	107	
060510B	Swift	$1.767^{+0.074}_{-0.074}$	39.8 ± 1.6	15 – 150	0.45 ± 0.10	15 – 150	75	
060505A	Swift	1.29 ± 0.28	9.44 ± 1.71	15 – 150	2.65 ± 0.63^P	15 – 150	107	
060502A	Swift	$1.429^{+0.073}_{-0.073}$	23.3 ± 1.0	15 – 150	1.69 ± 0.20	15 – 150	75	
060418A	Swift	1.70 ± 0.06	83.30 ± 2.53	15 – 150	6.52 ± 0.35^P	15 – 150	107	
060319A	Swift	2.33 ± 0.25	2.64 ± 0.34	15 – 150	1.09 ± 0.14^P	15 – 150	107	
060306A	Swift	1.80 ± 0.10	21.30 ± 1.18	15 – 150	5.97 ± 0.35^P	15 – 150	107	
060223A	Swift	$1.689^{+0.111}_{-0.113}$	6.7 ± 0.5	15 – 150	1.00 ± 0.14	15 – 150	75	
060218A	Swift	2.26 ± 0.17	15.70 ± 1.52	15 – 150	0.25 ± 0.11^P	15 – 150	107	
060210A	Swift	1.53 ± 0.09	76.60 ± 4.09	15 – 150	2.72 ± 0.28^P	15 – 150	107	
060206A	Swift	1.66 ± 0.07	$-1.12^{+0.32}_{-0.30}$...	$80.7^{+38.8}_{-14.0}$	8.31 ± 0.42	15 – 150	2.79 ± 0.17^P	15 – 150	107	
060204B	Swift	$1.417^{+0.082}_{-0.082}$	$-0.785^{+0.391}_{-0.358}$...	$98.39^{+60.89}_{-19.90}$	29.3 ± 1.8	15 – 150	1.03 ± 0.14	15 – 150	75	∞
060202A	Swift	1.71 ± 0.13	21.30 ± 1.65	15 – 150	0.51 ± 0.17^P	15 – 150	107	∞
060124A	KW	1.84 ± 0.19	$-1.29^{+0.14}_{-0.11}$	$-2.25^{+0.27}_{-0.88}$	285^{+63}_{-56}	143^{+28}_{-24}	20 – 2000	${}^326.6^{+7.4}_{-6.9}$	20 – 2000	30, 107	
060123A	Swift	1.9 ± 0.6	3	15 – 150	0.04^P	15 – 150	107	
060115A	Swift	1.71 ± 0.11	$-0.74^{+0.12}_{-0.1}$	$-1.81^{+0.12}_{-0.21}$	$94.6^{+21.4}_{-17.6}$	17.10 ± 1.50	15 – 150	0.87 ± 0.12^P	15 – 150	52, 107	
060111A	Swift	$1.621^{+0.064}_{-0.065}$	$-0.882^{+0.303}_{-0.282}$...	$73.90^{+16.92}_{-9.13}$	12.0 ± 0.6	15 – 150	1.33 ± 0.14	15 – 150	75	
051117B	Swift	$1.539^{+0.297}_{-0.307}$	1.75 ± 0.37	15 – 150	0.38 ± 0.12	15 – 150	75	
051111A	Swift	1.32 ± 0.06	40.80 ± 1.34	15 – 150	2.66 ± 0.21^P	15 – 150	107	
051109B	Swift	$1.964^{+0.224}_{-0.240}$	$-0.230^{+1.569}_{-1.173}$...	$39.69^{+11.37}_{-7.47}$	2.26 ± 0.42	15 – 150	0.35 ± 0.11	15 – 150	75	
051109A	KW/Swift	$1.505^{+0.201}_{-0.201}$	$-1.25^{+0.44}_{-0.59}$...	161^{+224}_{-58}	$40.0^{+3.0}_{-34.0}$	20 – 500	$5.8^{+0.3}_{-4.9}$	20 – 500	25, 75	
051022A	HETE-2/KW	...	$-1.01^{+0.02}_{-0.03}$	$-1.95^{+0.25}_{-0.14}$	213^{+18}_{-18}	2610^{+60}_{-110}	20 – 2000	${}^3100.0 \pm 13.0$	20 – 2000	24, 52	
051016B	Swift	$2.320^{+0.210}_{-0.226}$	1.70 ± 0.22	15 – 150	0.81 ± 0.12	15 – 150	75	
051008A	Swift	1.13 ± 0.05	$-0.975^{+0.078}_{-0.086}$...	865^{+178}_{-136}	50.90 ± 1.45	15 – 150	${}^55.44 \pm 0.35^P$	15 – 150	23, 107	
051006A	Swift	1.51 ± 0.17	13.40 ± 1.41	15 – 150	1.62 ± 0.30^P	15 – 150	107	
051001A	Swift	2.05 ± 0.15	17.40 ± 1.47	15 – 150	0.49 ± 0.11^P	15 – 150	107	
050922C	HETE-2/KW	$1.356^{+0.056}_{-0.056}$	$-0.83^{+0.23}_{-0.26}$...	130^{+51}_{-27}	73.0 ± 5.0	20 – 2000	${}^445.0 \pm 7.0$	20 – 2000	21, 22, 75	
050915A	Swift	$1.363^{+0.166}_{-0.165}$	8.4 ± 0.9	15 – 150	0.73 ± 0.13	15 – 150	75	
050908A	Swift	1.88 ± 0.17	4.83 ± 0.51	15 – 150	0.70 ± 0.14^P	15 – 150	107	
050904A	Swift	1.25 ± 0.07	48.30 ± 1.80	15 – 150	0.62 ± 0.17^P	15 – 150	107	
050826A	Swift	1.16 ± 0.31	4.13 ± 0.72	15 – 150	0.38 ± 0.13^P	15 – 150	107	

Table 2—Continued

GRB	Detector fluence/flux	Γ	α	β	E_p [keV]	fluence S_γ [10^{-7} erg cm $^{-2}$]	Band	peak flux $F_p(P_p)$		reference
(1)	(2)	(3)	(4)	(5)	(6)	(7)	(8)	(9)	(10)	(11)
050824A	Swift	2.76 ± 0.38	2.66 ± 0.52	15 – 150	0.50 ± 0.15^P	15 – 150	107
050822A	Swift	2.37 ± 0.14	24.60 ± 1.72	15 – 150	2.24 ± 0.22^P	15 – 150	107
050820A	Swift	1.25 ± 0.12	34.40 ± 2.42	15 – 150	2.45 ± 0.23^P	15 – 150	107
050819A	Swift	2.71 ± 0.29	3.50 ± 0.55	15 – 150	0.38 ± 0.12^P	15 – 150	107
050814A	Swift	1.80 ± 0.17	20.10 ± 2.20	15 – 150	0.71 ± 0.25^P	15 – 150	107
050802A	Swift	1.54 ± 0.13	20.00 ± 1.57	15 – 150	2.75 ± 0.44^P	15 – 150	107
050730A	Swift	1.53 ± 0.11	23.80 ± 1.52	15 – 150	0.55 ± 0.14^P	15 – 150	107
050714B	Swift	$2.406^{+0.270}_{-0.302}$	$-0.416^{+1.927}_{-1.433}$...	$28.71^{+7.26}_{-28.70}$	5.3 ± 1.0	15 – 150	0.34 ± 0.16	15 – 150	75
050525A	KW	1.78 ± 0.00	-1.1 ± 0.05	...	84.1 ± 1.7	206 ± 2	20 – 1000	87 ± 7	20 – 1000	18, 20, 107
050505A	Swift	1.41 ± 0.12	24.90 ± 1.79	15 – 150	1.85 ± 0.31^P	15 – 150	107
050502A	INTEGRAL	...	$-1.07^{+0.13}_{-0.13}$...	190^{+122}_{-58}	$13.9^{+1.1}_{-4.0}$	20 – 200	2.00	20 – 200	51, 102
050416A	Swift	$3.180^{+0.285}_{-0.319}$	$-0.972^{+2.279}_{-1.012}$...	$13.67^{+7.93}_{-12.56}$	4.1 ± 0.6	15 – 150	1.99 ± 0.19	15 – 150	75
050408A	HETE-2	...	$-1.76^{+0.09}_{-0.06}$	$-2.2^{+0.16}_{-0.28}$	$25.9^{+10.5}_{-7.3}$	19	30 – 400	17, 52
050401A	KW	1.40 ± 0.07	-1.15 ± 0.16	-2.65 ± 0.31	132 ± 16	193 ± 4	20 – 2000	24.5 ± 1.2	20 – 2000	16, 107 ∞
050319A	Swift	2.02 ± 0.19	13.10 ± 1.48	15 – 150	1.52 ± 0.21^P	15 – 150	107 \blacktriangleleft
050318A	Swift	1.90 ± 0.10	$-1.03^{+0.45}_{-0.41}$...	$49.2^{+9.4}_{-5.9}$	10.80 ± 0.77	15 – 150	3.16 ± 0.20^P	15 – 150	107
050315A	Swift	2.11 ± 0.09	32.20 ± 1.46	15 – 150	1.93 ± 0.22^P	15 – 150	107
050223A	INTEGRAL	$1.44^{+0.06}_{-0.06}$	< 15.7	20 – 200	0.69 ± 0.16^P	15 – 150	102, 107
050219A	Swift	$1.305^{+0.056}_{-0.056}$	$-0.122^{+0.300}_{-0.282}$...	$90.63^{+11.32}_{-7.77}$	40.8 ± 1.6	15 – 150	3.1 ± 0.3	15 – 150	75
050215B	HETE-2	$2.173^{+0.209}_{-0.223}$...	$-2.2^{+0.4}_{-0.6}$	$17.6^{+6.1}_{-12.8}$	$1.7^{+2.5}_{-1.3}$	30 – 400	0.45 ± 0.10	15 – 150	15, 75
050126A	Swift	1.34 ± 0.15	8.38 ± 0.80	15 – 150	0.71 ± 0.17^P	15 – 150	107
041219A	INTEGRAL	...	$-1.48^{+0.14}_{-0.11}$	$-2.01^{+0.05}_{-0.08}$	156^{+88}_{-54}	$867.3^{+5.4}_{-128.9}$	20 – 200	36.0	20 – 200	51, 102
041006A	HETE-2	...	$-1.3^{+0.05}_{-0.05}$...	$47.7^{+3}_{-2.7}$	70	30 – 400	13, 52
040924A	HETE-2/KW	...	$-1.03^{+0.09}_{-0.09}$...	$41.1^{+2.3}_{-2.3}$	27.3 ± 1.2	20 – 500	33.3 ± 3.5	20 – 500	12, 52
040912A	HETE-2	...	$-1.17^{+1.54}_{-0.62}$	$-2.49^{+0.24}_{-0.4}$	$14.16^{+3.32}_{-4.32}$	4	30 – 400	11, 52
031203A	INTEGRAL	$1.51^{+0.03}_{-0.03}$	$-1.18^{+0.1}_{-0.09}$...	$148.2^{+32.45}_{-23.91}$	$10.6^{+2.7}_{-3.0}$	20 – 200	2.50	20 – 200	51, 52, 102
030528A	HETE-2	...	$-1.33^{+0.15}_{-0.12}$	$-2.65^{+0.29}_{-0.98}$	$31.84^{+4.67}_{-4.97}$	$119.00^{+7.60}_{-7.80}$	2 – 400	17.89 ± 1.57^P	2 – 400	14
030429A	HETE-2	...	$-1.12^{+0.25}_{-0.22}$...	$35.04^{+11.75}_{-7.90}$	$8.54^{+1.48}_{-1.32}$	2 – 400	3.79 ± 0.79^P	2 – 400	14
030329A	HETE-2	...	$-1.26^{+0.01}_{-0.02}$	$-2.28^{+0.05}_{-0.06}$	$67.86^{+2.31}_{-2.15}$	$1630.00^{+14.00}_{-13.00}$	2 – 400	450.88 ± 24.68^P	2 – 400	14
030328A	HETE-2	...	$-1.14^{+0.03}_{-0.03}$	$-2.09^{+0.19}_{-0.40}$	$126.30^{+13.89}_{-13.10}$	$369.50^{+14.00}_{-14.20}$	2 – 400	11.64 ± 0.85^P	2 – 400	14
030323A	HETE-2	$1.62^{+0.24}_{-0.25}$	$12.30^{+3.68}_{-3.43}$	2 – 400	3.86 ± 2.11^P	2 – 400	14
030226A	HETE-2	...	$-0.89^{+0.17}_{-0.15}$...	$97.12^{+26.98}_{-17.06}$	$56.12^{+6.14}_{-6.14}$	2 – 400	2.69 ± 0.57^P	2 – 400	14
030115A	HETE-2	...	$-1.28^{+0.14}_{-0.13}$...	$82.79^{+52.82}_{-22.26}$	$23.05^{+3.98}_{-3.23}$	2 – 400	8.13 ± 1.38^P	2 – 400	14

Table 2—Continued

GRB	Detector fluence/flux	Γ	α	β	E_p [keV]	fluence S_γ			peak flux $F_p(P_p)$		reference
						[10^{-7} erg cm $^{-2}$]	(7)	Band (8)	(9)	Band (10)	
(1)	(2)	(3)	(4)	(5)	(6)	(7)	(8)	(9)	(10)	(11)	
021211A	HETE-2	...	$-0.86^{+0.10}_{-0.09}$	$-2.18^{+0.14}_{-0.25}$	$45.56^{+7.84}_{-6.23}$	$35.34^{+2.07}_{-2.06}$	2 – 400	29.97 ± 1.74^P	2 – 400	14	
021004A	HETE-2	...	$-1.01^{+0.19}_{-0.17}$...	$79.79^{+53.35}_{-22.97}$	$25.45^{+6.85}_{-5.04}$	2 – 400	2.69 ± 0.50^P	2 – 400	14	
020903A	HETE-2	$-2.62^{+0.42}_{-0.55}$	$2.6^{+1.4}_{-0.8}$	$0.95^{+0.62}_{-0.33}$	2 – 400	2.78 ± 0.67^P	2 – 400	14	
020819B	HETE2/Ulysses	...	-0.9 ± 0.2	$-2^{+0.2}_{-0.5}$	50^{+18}_{-12}	78	25 – 100	7	25 – 100	6, 52	
020813A	HETE-2	...	$-0.94^{+0.03}_{-0.03}$	$-1.57^{+0.03}_{-0.04}$	$142.10^{+14.05}_{-12.91}$	$978.70^{+12.70}_{-12.80}$	2 – 400	32.31 ± 2.07^P	2 – 400	14	
020427A	BepoSAX	-2.1 ± 0.26	2.8 ± 2.8	5.8 ± 0.4	2 – 28	0.3 ± 0.04	2 – 28	8	
020410A	BepoSAX/Konus	...	-1.8	...	180	280	15 – 1000	71	15 – 1000	9	
020405A	BepoSAX	2.00 ± 0.13	422 ± 24	40 – 700	32.1 ± 1.9	40 – 700	65	
020331A	HETE-2	...	$-0.79^{+0.13}_{-0.12}$...	$91.57^{+20.99}_{-14.09}$	$69.40^{+8.45}_{-7.45}$	2 – 400	3.65 ± 0.51^P	2 – 400	14	
020322A	BepoSAX	2.34 ± 0.24	8.5 ± 0.8	40 – 700	2.24 ± 0.24	40 – 700	65	
020305A	HETE2/Ulysses	...	$-0.86^{+0.13}_{-0.11}$...	143^{+49}_{-30}	104	30 – 400	64.7	25 – 100	5, 7	
020127A	HETE-2	...	$-1.03^{+0.14}_{-0.13}$...	$104.00^{+47.00}_{-24.10}$	$27.22^{+4.43}_{-3.63}$	2 – 400	8.12 ± 1.50^P	2 – 400	14	
020124A	HETE-2	...	$-0.79^{+0.15}_{-0.14}$	$-2.6^{+0}_{-0.65}$	$86.93^{+18.11}_{-12.45}$	$81.04^{+8.86}_{-7.70}$	2 – 400	9.38 ± 1.77^P	2 – 400	14	
011211A	BepoSAX	1.00 ± 0.39	13.5 ± 2.2	40 – 700	0.35 ± 0.08	40 – 700	65 ∞	
011121A	BepoSAX	1.22 ± 0.17	983 ± 77	40 – 700	65.9 ± 5.3	40 – 700	65 ζ	
011030A	BappoSAX	1.84 ± 0.17	12	2 – 26	0.075	2 – 26	28	
010921A	BepoSAX	2.30 ± 0.24	$-1.55^{+0.08}_{-0.07}$...	$88.63^{+21.76}_{-13.79}$	134 ± 17	40 – 700	10.4 ± 1.6	40 – 700	14, 65	
010222A	BepoSAX	1.57 ± 0.16	-1.35 ± 0.19	-1.64 ± 0.02	> 358	925 ± 28	40 – 700	86.0 ± 2.0	40 – 700	3, 65	
000926A	BepoSAX	0.78 ± 0.78	2.60 ± 0.70	40 – 700	2.16 ± 0.87	40 – 700	65	
000911A	KW	...	-0.84	-2.43	365	2300	15 – 8000	200	15 – 8000	4	
000418A	BepoSAX	134 ± 10	2.00 ± 0.70	40 – 700	1.00 ± 0.36	40 – 700	64, 65	
000301C	BepoSAX	1.79 ± 0.15	83.5 ± 5.3	40 – 700	1.13 ± 0.09	40 – 700	65	
000210A	BepoSAX	1.44 ± 0.16	480 ± 37	40 – 700	164.5 ± 13.1	40 – 700	65	
000131A	BATSE	...	$-0.91^{+0.20}_{-0.15}$	$-2.02^{+0.18}_{-0.32}$	168^{+17}_{-15}	418	20 – 2000	26.7 ± 4.1	30 – 10000	2, 10	
991216A	BATSE	...	-1.2 ± 0.01	-2.22 ± 0.02	382 ± 6	1750 ± 5	20 – 2000	614 ± 12	30 – 10000	10, 90	
991208A	Ulysses	1.68 ± 0.19	490	25 – 100	51	25 – 100	1	
990712A	BepoSAX	1.36 ± 0.18	-1.88 ± 0.07	-2.48 ± 0.56	65.0 ± 10.5	65.0 ± 3.0	40 – 700	13.0 ± 1.0	40 – 700	3, 65	
990705A	BepoSAX	1.40 ± 0.14	-1.05 ± 0.21	-2.2 ± 0.1	188 ± 15	750 ± 80	40 – 700	37.0 ± 1.0	40 – 700	3, 65	
990510A	BepoSAX	1.98 ± 0.13	-1.23 ± 0.05	-2.7 ± 0.4	161 ± 16	190 ± 20	40 – 700	24.7 ± 2.1	40 – 700	3, 65	
990506A	BATSE	1.48 ± 0.13	-1.17 ± 0.01	-2.62 ± 0.07	341 ± 5	1690 ± 10	20 – 2000	93.6 ± 2.0	30 – 10000	10, 65, 90	
990308A	BATSE	...	-0.77 ± 0.14	-2.41 ± 0.41	234 ± 31	58.9 ± 6.2	20 – 2000	11.9 ± 3.8	40 – 700	65, 90	
990123A	BepoSAX	1.21 ± 0.13	-0.89 ± 0.08	-2.45 ± 0.97	780 ± 61	3000 ± 400	40 – 700	170 ± 50	40 – 700	3, 65	
981226A	BepoSAX	2.38 ± 0.35	5.8 ± 0.8	40 – 700	0.37 ± 0.07	40 – 700	65	

Table 2—Continued

GRB	Detector fluence/flux	Γ	α	β	E_p [keV]	fluence S_γ		peak flux $F_p(P_p)$		reference	
(1)	(2)	(3)	(4)	(5)	(6)	[10^{-7} erg cm $^{-2}$]	Band	Band	(9)	(10)	(11)
980703A	BATSE	1.64 ± 0.38	-1.2 ± 0.05	-1.93 ± 0.06	281 ± 32	398 ± 9	20 – 2000	26.4 ± 5.1	30 – 10000	10, 65, 90	
980613A	BeppoSAX	0.59 ± 0.35	-1.43 ± 0.24	-2.7 ± 0.6	92.6 ± 42.5	10.0 ± 2.0	40 – 700	1.60 ± 0.40	40 – 700	3, 65	
980519A	BATSE	...	-1.47 ± 0.06	-2.23 ± 0.26	252 ± 40.9	132 ± 8	20 – 2000	29.8	50 – 300	2, 90	
980425A	BATSE	1.90 ± 0.24	-1.41 ± 0.09	-2.82 ± 0.73	136 ± 12.7	45.1 ± 4.18	20 – 2000	1.71 ± 0.27	40 – 700	65, 90	
980329A	BeppoSAX	1.74 ± 0.14	-0.64 ± 0.14	-2.2 ± 0.8	236 ± 37	650 ± 50	40 – 700	31.0 ± 1.0	40 – 700	3, 65	
980326A	BeppoSAX	1.85 ± 0.21	-1.23 ± 0.21	-2.48 ± 0.31	35.5 ± 18.0	7.5 ± 1.5	40 – 700	2.45 ± 0.15	40 – 700	3, 65	
971214A	BeppoSAX	...	-0.76 ± 0.17	-2.7 ± 1.1	154 ± 30	88.0 ± 9.0	40 – 700	6.8 ± 0.7	40 – 700	3	
970828A	BATSE	...	$-0.45^{+0.06}_{-0.06}$	$-2.06^{+0.08}_{-0.10}$	379^{+15}_{-16}	960	20 – 2000	59.3 ± 3.4	30 – 10000	2, 10	
970508A	BeppoSAX	1.51 ± 0.18	-1.71 ± 0.10	-2.2 ± 0.25	79.0 ± 23.4	18.0 ± 3.0	40 – 700	3.4 ± 0.1	40 – 700	3, 65	
970228A	BeppoSAX	1.92 ± 0.14	-1.54 ± 0.08	-2.5 ± 0.4	115 ± 37	110 ± 10	40 – 700	37.0 ± 1.0	40 – 700	3, 65	
SGRB											
130603B	KW	0.82 ± 0.07	-0.73 ± 0.15	...	660 ± 100	66 ± 7	20 – 10000	$^{2}1000 \pm 200$	20 – 10000	96, 107	
101224A	Fermi	1.05 ± 0.26	$-0.74^{+0.43}_{-0.43}$	$-1.85^{+0.12}_{-0.12}$	229^{+157}_{-157}	1.91 ± 0.27	10 – 1000	1.31 ± 0.21^P	10 – 1000	103, 107	
101219A	KW	0.63 ± 0.09	$-0.22^{+0.30}_{-0.25}$...	490^{+103}_{-79}	36 ± 5	20 – 10000	$^{2}280 \pm 80$	20 – 10000	74, 107	∞
100816A	Fermi	1.17 ± 0.06	$-0.23^{+0.09}_{-0.09}$	$-2.30^{+0.09}_{-0.09}$	126^{+7}_{-7}	36.5 ± 0.5	10 – 1000	15.6 ± 0.2^P	10 – 1000	103, 107	
100625A	Fermi	0.90 ± 0.10	$-0.60^{+0.15}_{-0.15}$...	486^{+80}_{-80}	11.0 ± 0.6	10 – 1000	4.9 ± 0.3^P	10 – 1000	103, 107	
100206A	Fermi	0.63 ± 0.17	$-0.33^{+0.16}_{-0.16}$	$-2.33^{+0.45}_{-0.45}$	460^{+92}_{-92}	8.7 ± 0.2	10 – 1000	2.62 ± 0.14^P	10 – 1000	103, 107	
100117A	Fermi	0.88 ± 0.22	313^{+71}_{-71}	4.2 ± 0.7	10 – 1000	1.59 ± 0.13^P	10 – 1000	103, 107	
091109B	Swift	$0.710^{+0.132}_{-0.128}$	1.95 ± 0.16	15 – 150	1.96 ± 0.19	15 – 150	75	
090515A	Swift	1.41 ± 0.24	$-0.15^{+1.27}_{-1.00}$...	$79.8^{+94.0}_{-19.3}$	0.2 ± 0.03	15 – 150	5.7 ± 0.9^P	15 – 150	107	
090510A	Fermi	0.98 ± 0.20	$-0.86^{+0.03}_{-0.03}$	$-2.58^{+0.29}_{-0.29}$	4301^{+483}_{-483}	33.7 ± 0.4	10 – 1000	9.1 ± 0.2^P	10 – 1000	103, 107	
090426A	Swift	1.93 ± 0.22	1.8 ± 0.3	15 – 150	2.4 ± 0.3^P	15 – 150	107	
090305A	Swift	$0.769^{+0.367}_{-0.336}$	0.75 ± 0.14	15 – 150	0.85 ± 0.19	15 – 150	75	
080905A	Fermi	$0.795^{+0.251}_{-0.233}$...	$-2.35^{+0.67}_{-0.67}$	311^{+87}_{-87}	8.5 ± 0.5	10 – 1000	2.34 ± 0.14^P	10 – 1000	75, 103	
080503A	Swift	2.00 ± 0.13	20 ± 1	15 – 150	0.9 ± 0.1^P	15 – 150	107	
080123A	Swift	2.15 ± 0.54	5.7 ± 1.7	15 – 150	1.8 ± 0.4^P	15 – 150	107	
071227A	KW	0.99 ± 0.22	-0.7	...	1000	16.0 ± 2.0	20 – 1300	$^{3}35.0 \pm 11.0$	20 – 1300	50, 107	
070809A	Swift	1.69 ± 0.22	1.0 ± 0.1	15 – 150	1.2 ± 0.2^P	15 – 150	107	
070724A	Swift	$1.861^{+0.296}_{-0.324}$	0.31 ± 0.07	15 – 150	0.34 ± 0.09	15 – 150	75	
070714B	Swift	$1.398^{+0.218}_{-0.219}$	7.2 ± 1.0	15 – 150	2.7 ± 0.2^P	15 – 150	75, 107	
070707A	INTEGRAL	1.19 ± 0.14	$-0.57^{+0.43}_{-0.59}$...	427^{+374}_{-144}	2.10	20 – 200	2.10	20 – 200	45, 51	
070429B	Swift	$1.645^{+0.220}_{-0.227}$	0.65 ± 0.10	15 – 150	0.73 ± 0.12	15 – 150	75	
061217A	Swift	0.86 ± 0.30	0.42 ± 0.07	15 – 150	1.49 ± 0.24^P	15 – 150	107	

Table 2—Continued

GRB	Detector fluence/flux	Γ	α	β	E_p [keV]	S_γ $[10^{-7} \text{ erg cm}^{-2}]$	Band	peak flux $F_p(P_p)$		reference
(1)	(2)	(3)	(4)	(5)	(6)	(7)	(8)	(9)	(10)	(11)
061210A	Swift	1.56 ± 0.28	11.10 ± 1.76	15 – 150	5.31 ± 0.47^P	15 – 150	107
061201A	KW	0.81 ± 0.15	$-0.36^{+0.40}_{-0.65}$...	873^{+458}_{-284}	$53.3^{+7.0}_{-44.4}$	20 – 3000	2319^{+72}_{-272}	20 – 3000	39, 107
061006A	KW	1.72 ± 0.17	$-0.62^{+0.18}_{-0.21}$...	664^{+227}_{-144}	$35.7^{+3.1}_{-19.2}$	20 – 2000	2213^{+41}_{-120}	20 – 2000	34, 107
060801A	Swift	0.47 ± 0.24	0.80 ± 0.10	15 – 150	1.27 ± 0.16^P	15 – 150	107
060502B	Swift	$0.985^{+0.205}_{-0.198}$	0.49 ± 0.06	15 – 150	0.62 ± 0.12	15 – 150	75
060313A	KW	0.70 ± 0.07	$-0.60^{+0.19}_{-0.22}$...	922^{+306}_{-177}	142^{+10}_{-85}	20 – 2000	2700^{+100}_{-430}	20 – 2000	31, 107
060121A	HETE-2/KW	...	$-0.51^{+0.55}_{-0.60}$	$-2.39^{+0.27}_{-1.41}$	104^{+134}_{-77}	$47.1^{+4.4}_{-37.1}$	20 – 1000	3164^{+18}_{-132}	20 – 1000	29
051221A	KW	$1.394^{+0.055}_{-0.055}$	$-1.08^{+0.13}_{-0.14}$...	402^{+93}_{-72}	$32.0^{+1.0}_{-17.0}$	20 – 2000	1460^{+20}_{-250}	20 – 2000	26, 75
051210A	Swift	1.06 ± 0.28	0.85 ± 0.14	15 – 150	0.75 ± 0.12^P	15 – 150	107
050724A	Swift	1.89 ± 0.22	9.98 ± 1.20	15 – 150	3.26 ± 0.30^P	15 – 150	107
050709A	HETE-2	...	-0.7 ± 0.2	...	83^{+18}_{-12}	4 ± 0.4	2 – 400	51 ± 5	2 – 400	19, 27
050509B	Swift	$1.275^{+0.405}_{-0.399}$	0.07 ± 0.02	15 – 150	0.18 ± 0.10	15 – 150	75

Note. — Col. (1) GRB name. Col. (2) Detector of fluence and/or peak flux. Col. (3) Spectral Index of power law fitting. Col. (4-6) Spectral parameters of Band function. Col. (7) γ -ray Fluence S_γ , in unit of $10^{-7} \text{ erg cm}^{-2}$. Col. (8) The observational energy band of the fluence in col. (7). Col. (9) γ -ray 1 second peak flux F_p , in unit of $10^{-7} \text{ erg s}^{-1} \text{ cm}^{-2}$, or peak photon flux P_p , in unit of photons $\text{s}^{-1} \text{ cm}^{-2}$ (with superscript p). (1-7) Fluxes from Konus-Wind are not 1 second peak flux. 1. 0.004 s; 2. 0.016 s; 3. 0.064 s; 4. 0.128 s; 5. 0.256 s; 6. 0.5 s; 7. 2.944 s; 8. 3 s. Col. (10) The observational energy band of the flux in col. (9). Col. (11) Reference of prompt emission properties.

References. (1) Hurley et al. (2000c); (2) Jimenez et al. (2001); (3) Amati et al. (2002); (4) Price et al. (2002b); (5) Hurley et al. (2002a); (6) Hurley et al. (2002b); (7) Barraud et al. (2003); (8) Amati et al. (2004); (9) Nicastro et al. (2004); (10) Yonetoku et al. (2004); (11) Butler et al. (2004); (12) Golenetskii et al. (2004); (13) Galassi et al. (2004); (14) Sakamoto et al. (2005a); (15) Nakagawa et al. (2005); (16) Golenetskii et al. (2005b); (17) Sakamoto et al. (2005b); (18) Golenetskii et al. (2005c); (19) Boer et al. (2005); (20) Golenetskii et al. (2005a); (21) Crew et al. (2005); (22) Golenetskii et al. (2005d); (23) Golenetskii et al. (2005e); (24) Golenetskii et al. (2005f); (25) Golenetskii et al. (2005g); (26) Golenetskii et al. (2005h); (27) Villasenor et al. (2005); (28) Galli & Piro (2006); (29) Golenetskii et al. (2006b); (30) Golenetskii et al. (2006c); (31) Golenetskii et al. (2006d); (32) Golenetskii et al. (2006e); (33) Golenetskii et al. (2006f); (34) Golenetskii et al. (2006j); (35) Golenetskii et al. (2006g); (36) Golenetskii et al. (2006h); (37) Golenetskii et al. (2006a); (38) Bellm et al. (2006); (39) Golenetskii et al. (2006i); (40) Pal'Shin (2006); (41) Golenetskii et al. (2007a); (42) Golenetskii et al. (2007b); (43) Golenetskii et al. (2007i); (44) Golenetskii et al. (2007c); (45) Golenetskii et al. (2007d); (46) Golenetskii et al. (2007e); (47) Golenetskii et al. (2007f); (48) Golenetskii et al. (2007g); (49) Golenetskii et al. (2007j); (50) Golenetskii et al. (2007h); (51) Foley et al. (2008); (52) Pé langeon et al. (2008); (53) Golenetskii et al. (2008a); (54) Golenetskii et al. (2008b); (55) Golenetskii et al. (2008c); (56) Ohno et al. (2008); (57) Golenetskii et al. (2008d); (58) Golenetskii et al. (2008e); (59) Golenetskii et al. (2008f); (60) Golenetskii et al. (2008g); (61) Golenetskii et al. (2008h); (62) Pal'Shin et al. (2008); (63) Golenetskii et al. (2008i); (64) Nava et al. (2008); (65) Frontera et al. (2009); (66) Golenetskii et al. (2009a); (67) Golenetskii et al. (2009d); (68) Pal'Shin et al. (2009a); (69) Golenetskii et al. (2009b); (70) Golenetskii et al. (2009c); (71) Pal'Shin et al. (2009b); (72) Golenetskii et al. (2010a); (73) Golenetskii et al. (2010b); (74) Golenetskii et al. (2010c); (75) Sakamoto et al. (2011b); (76)

Golenetskii et al. (2011a); (77) Golenetskii et al. (2011b); (78) Golenetskii et al. (2011c); (79) Golenetskii et al. (2011d); (80) Golenetskii et al. (2011e); (81) Golenetskii et al. (2011f); (82) Golenetskii et al. (2011g); (83) Sakamoto et al. (2011a); (84) Golenetskii et al. (2011h); (85) Golenetskii et al. (2011i); (86) Golenetskii et al. (2011j); (87) Lazzarotto et al. (2011); (88) Golenetskii et al. (2011k); (89) Guidorzi et al. (2011); (90) Goldstein et al. (2013); (91) Golenetskii et al. (2013e); (92) Golenetskii et al. (2013f); (93) Golenetskii et al. (2013g); (94) Golenetskii et al. (2013h); (95) Frederiks (2013); (96) Golenetskii et al. (2013i); (97) Golenetskii et al. (2013j); (98) Golenetskii et al. (2013a); (99) Golenetskii et al. (2013b); (100) Golenetskii et al. (2013c); (101) Golenetskii et al. (2013d); (102) Bošnjak et al. (2014); (103) Gruber et al. (2014); (104) Golenetskii et al. (2014a); (105) Golenetskii et al. (2014b); (106) Serino et al. (2014); (107) GRBtable;

|
∞
∞
|

Table 3. sfr

Table 3—Continued

GRB	z	Instrument (Spectrum)	log M_*		SFR		sSFR [Gyr $^{-1}$]	[X/H]		A_V		reference
			[M $_{\odot}$]	method	[M $_{\odot}$ yr $^{-1}$]	method		(9)	method	(11)	(12)	
(1)	(2)	(3)	(4)	(5)	(6)	(7)	(8)	(9)	(10)	(11)	(12)	(13)
130610A	2.092	VLT/UVES	0
130606A	5.913	VLT/X-Shooter	-1.3 ± 0.4	A/Si	74
130604A	1.06	Gemini	0
130528A	1.25	GTC/OSIRIS	6.8	[OII]	0	hostSED	67
130518A	2.49	GTC/OSIRIS	0
130511A	1.3033	Gemini/GMOS	0
130505A	2.27	Gemini/GMOS	> -1.42	A/Fe	79
130427B	2.78	VLT/X-Shooter	0
130427A	0.3401	VLT/X-Shooter	9 ± 0.2	SED	0.34 $^{+0.20}_{-0.06}$	H α	0.34	-0.120 $^{+0.12}_{-0.13}$	E	0.20 $^{+0.63}_{-0.20}$	Balmer	58, 77
130420A	1.297	GTC/OSIRIS	0
130418A	1.217	VLT/X-Shooter//GROND	0
130408A	3.757	VLT/X-Shooter//GROND	< 9.6	UV	...	-1.24 ± 0.12	A/S	79, 81
130215A	0.597	Shane/KAST	0
130131B	2.5393	VLT/X-Shooter	8.0 $^{+13.4}_{-5.0}$	[OIII]	06 77
121229A	2.707	VLT/X-Shooter	0
121211A	1.023	Keck I/LRIS	0
121209A	2.1	VLT/X-Shooter	0
121201A	3.3830	VLT/X-Shooter	30 $^{+68}_{-21}$	[OII]	77
121128A	2.20	Gemini/GMOS	0
121027A	1.7732	VLT/X-Shooter	24 $^{+41}_{-15}$	[OIII]	77
121024A	2.3012	VLT/X-Shooter	9.9 $^{+0.2}_{-0.3}$	SED	37 $^{+4}_{-4}$	H α	4.66	-0.280 $^{+0.11}_{-0.12}$	E	0.00 $^{+0.40}_{-0.00}$	Balmer	77, 86
120922A	3.1	< 7.5	UV	81
120909A	3.93	VLT/X-Shooter	24.7	UV	...	-0.66 ± 0.11	A/S	79, 81
120907A	0.970	GTC/OSIRIS	0
120815A	2.3587	VLT/X-Shooter	< 10	line_width	2.3 $^{+2.7}_{-1.0}$	H α	...	-0.93 ± 0.13	A/Zn	0.20 $^{+1.13}_{-0.20}$	Balmer	52, 77, 79
120811C	2.671	GTC/OSIRIS	0
120805A	3.1	VLT/X-Shooter	39.0 $^{+9.5}_{-8.3}$	UV	81
120802A	3.796	Gemini/GMOS	0
120729A	0.80	Gemini/GMOS	8.3 ± 0.2	SED	6 $^{+25}_{-4.0}$	SED	30.07	66
120724A	1.48	Gemini/GMOS	0
120722A	0.9590	VLT/X-Shooter	22 $^{+4}_{-4}$	H α	...	-0.210 $^{+0.10}_{-0.10}$	E	1.52 $^{+0.17}_{-0.17}$	Balmer	77
120716A	2.486	VLT/X-Shooter	> -1.76	A/Fe	79
120714B	0.3985	VLT/X-Shooter	0.27 $^{+0.07}_{-0.05}$	H α	...	-0.300 $^{+0.11}_{-0.11}$	E	0.33 $^{+0.27}_{-0.27}$	Balmer	77

Table 3—Continued

Table 3—Continued

GRB	z	Instrument (Spectrum)	log M_*		SFR		sSFR [Gyr $^{-1}$]	[X/H]		Av		reference
			[M $_{\odot}$]	method	[M $_{\odot}$ yr $^{-1}$]	method		(9)	method	(11)	method	
(1)	(2)	(3)	(4)	(5)	(6)	(7)	(8)	(9)	(10)	(11)	(12)	(13)
110213A	1.46	Bok/BC	0
110205A	2.22	FLWO/FAST	> -0.82	A/S	79
110128A	2.339	VLT/X-Shooter	0
110106B	0.618	Gemini/GMOS	0
101225A	0.847	Gemini/GMOS	0
101219B	0.55185	VLT/X-Shooter	0
100906A	1.727	Gemini/GMOS	0
100901A	1.408	Gemini/GMOS	0
100814A	1.4392	VLT/X-Shooter	3.2 $^{+2.9}_{-0.7}$	H α	0.27 $^{+0.86}_{-0.27}$	Balmer	77
100728B	2.106	VLT/X-Shooter	0
100728A	1.5670	VLT/X-Shooter	14.5 $^{+60.6}_{-8.0}$	H α	0.76 $^{+2.29}_{-0.76}$	Balmer	77
100724A	1.2890	VLT/X-Shooter	3.2 $^{+5.1}_{-1.4}$	H α	...	-0.490 \pm 0.1	E/KK04	0.80 $^{+1.23}_{-0.80}$	Balmer	77, 88
100621A	0.5426	VLT/X-Shooter	8.98 $^{+0.14}_{-0.10}$	SED	8.7 $^{+0.8}_{-0.8}$	H α	9.11	-0.170 $^{+0.10}_{-0.10}$	E	0.17 $^{+0.10}_{-0.10}$	Balmer	35, 77
100615A	1.3978	VLT/X-Shooter	8.6 $^{+13.9}_{-4.4}$	H α	...	-0.290 $^{+0.12}_{-0.13}$	E	1.59 $^{+1.26}_{-0.93}$	Balmer	77
100606A	1.5545	VLT/X-Shooter	4.9 $^{+12.9}_{-1.8}$	H α	...	0.020 $^{+0.19}_{-0.21}$	E	0.17 $^{+1.99}_{-0.17}$	Balmer	77
100518A	4	< 0.5	UV	81
100513A	4.772	Gemini/GMOS	6.0	UV	81
100508A	0.5201	VLT/X-Shooter	2.6 $^{+0.7}_{-0.5}$	H α	...	-0.010 $^{+0.10}_{-0.10}$	E	0.96 $^{+0.30}_{-0.30}$	Balmer	77
100425A	1.755	VLT/X-Shooter	-0.96 \pm 0.42	A/Fe	79
100424A	2.4656	VLT/X-Shooter	21 $^{+20}_{-8}$	H β	...	-0.760 $^{+0.25}_{-0.18}$	E	0.43 $^{+0.60}_{-0.43}$	Balmer	77
100418A	0.6235	VLT/X-Shooter	9.54 $^{+0.28}_{-0.03}$	SED	4.2 $^{+1.0}_{-0.8}$	H α	1.21	-0.170 $^{+0.10}_{-0.10}$	E	0.56 $^{+0.20}_{-0.23}$	Balmer	51, 77
100414A	1.368	Gemini/GMOS	0
100316D	0.0592	Magellan/Clay	8.95	SED	1.7	H α	1.91	-0.390 \pm 0.1	E/PP04	0	Balmer	32, 39, 78
100316B	1.180	VLT/X-Shooter	2.5 \pm 0.2	[OII]	...	-0.290	E/KK04	0 $^{+0.05}_{-0.00}$	Balmer	88
100302A	4.813	2010GCN..10466...1C/GRBtablez	0
100219A	4.6667	VLT/X-Shooter	5.1	UV	...	-0.900 \pm 0.5	A/O	0.13 \pm 0.05	hostSED	60, 81
091208B	1.0633	Keck I/HIRES	0
091127A	0.4904	VLT/X-Shooter	8.3	SED	0.37 $^{+0.10}_{-0.07}$	H α	1.85	-0.620 $^{+0.18}_{-0.20}$	E	0.53 $^{+0.30}_{-0.27}$	Balmer	36, 77
091109A	3.076	VLT/FORS2	4.2	UV	81
091029A	2.752	Gemini/GMOS	0.00 $^{+0.04}_{-0.00}$	AGSED	34
091024A	1.092	Gemini/GMOS	0
091020A	1.71	NOT/ALFOSC	0
091018A	0.9710	VLT/X-Shooter	9.52 $^{+0.08}_{-0.10}$	SED	1.29 $^{+3.46}_{-0.32}$	H α	0.39	0.090 $^{+0.18}_{-0.19}$	E	0.20 $^{+1.86}_{-0.20}$	Balmer	76, 77

Table 3—Continued

GRB	z	Instrument (Spectrum)	log M_*		SFR		sSFR [Gyr $^{-1}$]	[X/H]		A_V		reference
			[M $_{\odot}$] (4)	method (5)	[M $_{\odot}$ yr $^{-1}$] (6)	method (7)		(9)	method (10)	[mag] (11)	method (12)	
(1)	(2)	(3)										(13)
091003A	0.8969	Gemini/GMOS	0
090927A	1.37	VLT/FORS2	0
090926B	1.2427	VLT/X-Shooter	10.1 $^{+0.4}_{-0.5}$	SED	26 $^{+19}_{-11}$	H α	2.07	-0.350 $^{+0.15}_{-0.17}$	E	2.09 $^{+0.66}_{-0.60}$	Balmer	35, 77
090926A	2.1062	VLT/FORS2	-1.89	A/S	< 0.10	AGSED	27, 33
090902B	1.822	Gemini/GMOS	0.05 \pm 0.05	AGSED	33
090814A	0.696	VLT/FORS2	0.05 $^{+0.14}_{-0.05}$	AGSED	34
090812A	2.452	VLT/FORS2	> -1.64	A/Si	0.41 $^{+0.04}_{-0.09}$	AGSED	34, 79
090809A	2.737	VLT/X-Shooter	-0.57 \pm 0.10	A/Si	79
090726A	2.71	SAO RAS6m/SCORPIO	0
090715B	3.00		WHT/ISIS	0
090709A	1.7	...	9.98 $^{+0.21}_{-0.08}$	SED	8.0 $^{+4.1}_{-4.1}$	SED	0.84	1.40 $^{+0.12}_{-0.38}$	hostSED	59
090618A	0.54	Lick/KAST	0
090530A	1.266	VLT/X-Shooter	0
090529A	2.625	VLT/FORS2	0
090519A	3.85	VLT/FORS2	< 2.0	UV	0.01 $^{+0.19}_{-0.01}$	AGSED	34, 81
090516A	4.109	VLT/FORS2	20.4	UV	...	> -1.36	A/Si	79, 81
090424A	0.544	VLT/FORS2	9.38 $^{+0.17}_{-0.19}$	SED	0.56 \pm 0.24	Hab	0.23	-0.260	E	56, 76
090423A	8.23	VLT/ISAAC	0
090418A	1.608	Lick3m/KAST	0
090417B	0.345	Gemini/GMOS	9.54 $^{+0.04}_{-0.06}$	SED	0.5 $^{+0.3}_{-0.3}$	SED	0.14	0.87 $^{+0.12}_{-0.08}$	hostSED	59
090407A	1.4478	VLT/X-Shooter	10.18 $^{+0.17}_{-0.14}$	SED	13.8 $^{+18.8}_{-6.7}$	H α	0.91	0.160 $^{+0.13}_{-0.13}$	E	2.29 $^{+1.13}_{-0.86}$	Balmer	59, 77
090328A	0.7357	VLT/FORS1	9.24	SED	4.8	[OII]	2.76	0.22 $^{+0.06}_{-0.18}$	AGSED	22
090323A	3.5832	VLT/X-Shooter	11.2 \pm 0.75	SED	24 $^{+53}_{-17}$	[OII]	0.15	0.67 \pm 0.34	A/S	0.14 $^{+0.04}_{-0.03}$	AGSED	22, 49, 77, 82
090313A	3.375	VLT/X-Shooter	< 14.2	UV	...	-1.7 \pm 0.3	A/Fe	0.42 $^{+0.06}_{-0.05}$	AGSED	34, 81, 82
090205A	4.6497	VLT/FORS1	< 10.7	...	4.2 \pm 0.98	Lya	...	> -0.57	A/S	24
090201A	2.1000	VLT/X-Shooter	48 $^{+30}_{-14}$	H α	0.36 $^{+0.63}_{-0.36}$	Balmer	77
090113A	1.7494	VLT/X-Shooter	17.9 $^{+10.1}_{-4.8}$	H α	0.03 $^{+0.73}_{-0.03}$	Balmer	77
090102A	1.547	NOT/ALFOSC	0.45 $^{+0.06}_{-0.08}$	AGSED	34
081222A	2.77	Gemini/GMOS	0.00 $^{+0.03}_{-0.00}$	AGSED	34
081221A	2.2590	VLT/X-Shooter	10.57 $^{+0.13}_{-0.14}$	SED	35 $^{+106}_{-22}$	H α	0.94	1.03 $^{+1.82}_{-1.03}$	Balmer	59, 77
081210A	2.0631	VLT/X-Shooter	15.3 $^{+111.7}_{-7.0}$	H β	0.43 $^{+2.02}_{-0.43}$	Balmer	77
081203A	2.05	Swift/UVOT	0
081121A	2.512	Magellan/Clay	0.00 $^{+0.03}_{-0.00}$	AGSED	34

Table 3—Continued

Table 3—Continued

Table 3—Continued

Table 3—Continued

GRB	z	Instrument (Spectrum)	log M_*		SFR		sSFR [Gyr $^{-1}$]	[X/H]		A_V		reference
			[M $_{\odot}$]	method	[M $_{\odot}$ yr $^{-1}$]	method		(9)	method	[mag]	method	
(1)	(2)	(3)	(4)	(5)	(6)	(7)	(8)	(9)	(10)	(11)	(12)	(13)
060526A	3.2213	VLT/FORS1	< 9.28	IR	< 0.4	UV	...	-0.57 ± 0.25	A/S	< 0.07	AGSED	25, 31, 38, 81
060522A	5.11	Keck/LRIS	0
060512A	0.4428	Keck/LRIS	0.47 ± 0.05	AGSED	31
060510B	4.9	Gemini/GMOS	12.0	UV	...	> -0.84	A/S	79, 81
060505A	0.0889	VLT/FORS	9.41 ± 0.01	SED	0.43	H α	0.17	-0.250	E	0.53 ± 0.08	Balmer	19, 20
060502A	1.5026	Gemini/GMOS	0.51 $^{+0.12}_{-0.10}$	AGSED	31
060418A	1.4901	Magellan/MIKE	-1.65	A/Si	< 0.06	AGSED	13, 31
060319A	1.172	Keck/LRIS	10.33 $^{+0.15}_{-0.07}$	SED	8.3 $^{+6.9}_{-4.3}$	SED	0.39	0.91 $^{+0.24}_{-0.24}$	hostSED	59
060306A	1.5597	VLT/X-Shooter	9.90 $^{+0.09}_{-0.05}$	SED	17.6 $^{+83.6}_{-11.0}$	H α	2.22	1.46 $^{+2.29}_{-1.33}$	Balmer	59, 77
060223A	4.406	Keck/LRIS	1.1	UV	...	> -1.8	A/S	79, 81
060218A	0.03351	VLT/FORS1	7.78 ± 0.08	SED	0.05	H α	0.83	-0.560	E	0.00 ± 0.02	Balmer	19, 20
060210A	3.9122	Gemini/GMOS	10.14 ± 0.32	IR	45.5	UV	3.30	> -0.83	A/Si	38, 79, 81
060206A	4.0559	Lick/KAST	< 9.32	IR	1.2	UV	...	> -0.74	A/S	< 0.04	AGSED	31, 38, 79, 81
060204B	2.3393	VLT/X-Shooter	78 $^{+85}_{-34}$	H α	1.13 $^{+0.96}_{-0.76}$	Balmer	67
060202A	0.785	Keck/LRIS	9.04 $^{+0.20}_{-0.04}$	SED	5.8 $^{+1.1}_{-2.0}$	SED	5.29	1.00 $^{+0.10}_{-0.20}$	hostSED	67
060124A	2.3	Keck/LRIS	0.08 ± 0.03	AGSED	31
060123A	0.56	Keck/LRIS	0
060115A	3.5328	VLT/FORS1	< 9.41	IR	2.1	UV	...	> -1.53	A/S	38, 79, 81
060111A	2.32	Keck/LRIS	0
051117B	0.4805	VLT/X-Shooter	4.7 $^{+4.9}_{-2.2}$	H α	...	0.310 $^{+0.16}_{-0.16}$	E	2.39 $^{+0.90}_{-0.80}$	Balmer	77
051111A	1.55	Keck/HIRES	30	UV	9
051109B	0.080	Keck/LRIS	0
051109A	2.346	Hobby-Eberly/MLRS	< 0.14	AGSED	31
051022A	0.8061	BTA/SCORPIO	10.42 ± 0.18	SED	60 $^{+12}_{-10}$	H α	2.28	-0.200 $^{+0.09}_{-0.09}$	E	1.86 $^{+0.17}_{-0.13}$	Balmer	19, 77
051016B	0.9358	VLT/X-Shooter	10.2 $^{+2.6}_{-2.0}$	H α	...	-0.420 $^{+0.15}_{-0.20}$	E	0.17 $^{+0.23}_{-0.17}$	Balmer	77
051008A	2.77	...	9.69 $^{+1.43}_{-0.08}$	SED	72.1 $^{+25.5}_{-54.4}$	SED	14.72	0.85 $^{+0.07}_{-0.58}$	hostSED	59
051006A	1.059	VLT/FORS2	0
051001A	2.4295	VLT/X-Shooter	110 $^{+124}_{-59}$	H α	1.92 $^{+0.93}_{-0.93}$	Balmer	77
050922C	2.1992	VLT/UVES	-1.88 ± 0.14	A/S	0.07 ± 0.02	AGSED	31, 79
050915A	2.5275	VLT/X-Shooter	10.56 $^{+0.19}_{-0.12}$	SED	196 $^{+1563}_{-174}$	H β	5.40	2.78 $^{+2.02}_{-1.99}$	Balmer	59, 77
050908A	3.3467	VLT/FORS1	< 9.30	IR	0.7	UV	38, 81
050904A	6.295	Subaru/FOCAS	< 10.0	SED	> -1.0	A/S	0.01 ± 0.02	AGSED	19, 21, 79
050826A	0.296	MDM2.4m/CCDS	9.79 ± 0.11	SED	9.13	[OII]	1.48	0.140	E/R23	0.1 $^{+0.2}_{-0.1}$	linefit	19, 26, 43

Table 3—Continued

GRB	z	Instrument (Spectrum)	log M_*		SFR		sSFR [Gyr $^{-1}$]	[X/H]		A_V		reference
			[M $_{\odot}$]	method	[M $_{\odot}$ yr $^{-1}$]	method		(9)	method	[mag]	method	
(1)	(2)	(3)	(4)	(5)	(6)	(7)	(8)	(9)	(10)	(11)	(12)	(13)
050824A	0.8277	VLT/X-Shooter	1.20 $^{+0.30}_{-0.26}$	H α	...	-0.580 $^{+0.18}_{-0.20}$	E	0.00 $^{+0.23}_{-0.00}$	Balmer	77
050822A	1.434	VLT/FORS1	0
050820A	2.61469	VLT/UVES	9.25 $^{+1.2}_{-0.2}$	SED	-0.76 \pm 0.13	A/S	0.18 $^{+0.01}_{-0.01}$	AGSED	18, 31, 79
050819A	2.5042	VLT/X-Shooter	22 $^{+426}_{-15}$	H β	1.13 $^{+2.78}_{-1.13}$	Balmer	77
050814A	5.3	...	9.93 \pm 0.46	IR	38
050802A	1.7102	NOT/ALFOSC	0.06 \pm 0.02	AGSED	31
050730A	3.96855	VLT/UVES	< 9.41	IR	< 0.3	UV	...	-1.96 \pm 0.11	A/S	0.16 $^{+0.03}_{-0.02}$	AGSED	31, 38, 79, 81
050714B	2.4383	VLT/X-Shooter	12.9 $^{+14.0}_{-5.3}$	H α	0.70 $^{+0.93}_{-0.70}$	Balmer	77
050525A	0.6063	VLT/X-Shooter	8.1 $^{+0.6}_{-0.6}$	SED	0.07 $^{+0.21}_{-0.05}$	H α	0.56	0.33 $^{+2.06}_{-0.33}$	Balmer	76, 77
050505A	4.2748	Keck/LRIS	< 3.5	Lya	...	> -1.2	A/S	8, 79
050502A	3.793	Keck/HIRES	< 9.30	IR	< 6.5	UV	38, 81
050416A	0.6542	Keck/LRIS	9.84 \pm 0.74	SED	4.5 $^{+1.6}_{-1.2}$	H α	0.65	-0.230 $^{+0.11}_{-0.11}$	E	1.62 $^{+0.36}_{-0.36}$	Balmer	19, 77
050408A	1.2356	Magellan /Clay	0
050401A	2.8983	VLT/FORS2	> -1.07	A/Zn	0.57	AGSED	10, 79
050319A	3.2425	NOT/AIFOSC	9.78 \pm 0.51	IR	19.7	UV	3.27	> -0.77	A/S	0.07 $^{+0.04}_{-0.03}$	AGSED	31, 38, 79, 81
050318A	1.4436	Magellan / Baade	0.53 $^{+0.06}_{-0.06}$	AGSED	31
050315A	1.9500	VLT/FORS	0.58 \pm 0.17	Lya	47
050223A	0.584	VLT/FORS1	9.73 \pm 0.36	SED	1.65	H β	0.31	-1.190 $/-$ 0.030	E	> 2	Balmer	6, 19
050219A	0.211	VLT/X-Shooter	9.98	SED	0.06 $^{+0.01}_{-0.02}$	[OII]	0.01	69
050215B	2.62	Keck/LRIS	0
050126A	1.29002	Keck/NIRC	0
041219A	0.31	...	9.7	SED	42
041006A	0.716	Gemini/GMOS	8.66 \pm 0.87	SED	0.34	[OII]	0.74	0.00 $^{+0.53}_{-0.00}$	hostSED	19, 59
040924A	0.858	VLT/FORS2	9.20 \pm 0.37	SED	0.85	H β	0.54	-0.460 $^{+0.20}_{-0.30}$	E	0.0 $^{+1.2}_{-0.0}$	linefit	19, 43
040912A	1.563	VLT/FORS2	6.3 \pm 0.4	[OII]	12
031203A	0.1055	Magellan/IMACS	8.82 \pm 0.43	SED	12.68	H α	19.19	-0.670	E	0.28 \pm 0.04	Balmer	19, 20
030528A	0.782	VLT/FORS2	8.82 \pm 0.39	SED	9.96	H β	15.08	-0.590	E	0.0 $^{+0.8}_{-0.0}$	linefit	19, 43
030429A	2.658	VLT/FORS1	0.15	Lya	...	> -1.13	A/Si	4, 79
030329A	0.1685	VLT/FORS2	7.74 \pm 0.06	SED	0.11	H α	2.00	-0.720	E	0.24 \pm 0.05	Balmer	19, 20
030328A	1.5216	VLT/FORS1	8.83 \pm 0.52	SED	3.20	UV	4.73	1.06 $^{+0.26}_{-0.29}$	hostSED	19, 59
030323A	3.3736	VLT/FORS2	< 9.23	IR	1.12 \pm 0.09	Lya	...	> -1.32	A/S	3, 38, 79
030226A	1.986	Keck/ESI	> -1.28	A/Fe	79
030115A	2	...	10.87	SED	1.6	UV	0.02	64

Table 3—Continued

Table 3—Continued

GRB	z	Instrument (Spectrum)	$\log M_*$		SFR		sSFR [Gyr $^{-1}$]	[X/H]		A_V		reference
			[M $_{\odot}$]	method	[M $_{\odot}$ yr $^{-1}$]	method		(8)	(9)	method	(11)	method
(1)	(2)	(3)	(4)	(5)	(6)	(7)	(8)	(9)	(10)	(11)	(12)	(13)
980703A	0.966	Keck/LRIS	9.33 ± 0.36	SED	7.03	H β	3.29	$-1.090 / -0.550$	E	0.14 ± 0.53	Balmer	19, 20
980613A	1.0969	Keck/LRIS	8.49 ± 0.21	SED	4.70	[OII]	15.21	0.500000	hostSED	19, 29
980519A	0
980425A	0.0085	VLT/FORS2	9.21 ± 0.52	SED	0.21	H α	0.13	-0.530	E	$1.9^{+0.1}_{-0.1}$	linefit	19, 43
980329A	3.5	5.1	UV	81
980326A	0
971214A	3.42	Keck/LRIS	9.59 ± 0.40	SED	11.40	UV	2.93	$1.35^{+0.18}_{-0.10}$	hostSED	19, 59
970828A	0.9578	Keck/LRIS	9.19 ± 0.36	SED	0.87	[OII]	0.56	$2.13^{+0.10}_{-0.09}$	hostSED	19, 59
970508A	0.835	Keck/LRIS	8.52 ± 0.10	SED	1.14	[OII]	3.44	$0.84^{+0.76}_{-0.19}$	hostSED	19, 59
970228A	0.695	Keck/LRIS	8.65 ± 0.05	SED	0.53	[OII]	1.19	$-0.220^{+0.15}_{-0.24}$	E	$0.0^{+0.7}_{-0.0}$	linefit	19, 43
SGRB												
130603B	0.356	GTC/OSIRIS	9.23	SED	4.85	H α	2.86	-0.240 ± 0.17	E	1.2	Balmer	62
101224A	0
101219A	0.718	Gemini/GMOS	9.15	SED	16 ± 0.4	[OII]	11.33	1.5	hostSED	15
100816A	0.8048	VLT/X-Shooter	58^{+51}_{-26}	H α	...	$0.060^{+0.16}_{-0.18}$	E	$4.38^{+0.80}_{-0.73}$	Balmer	77
100625A	0.452	Magellan/Clay	9.66	SED	< 0.3	[OII]	55
100206A	0.4068	Keck I/LRIS	10.7	SED	30	line/SED	0.60	$0.120^{+0.10}_{-0.12}$	E/PP04	1.8 ± 0.2	line/SED	48
100117A	0.92	Gemini/GMOS	10.3	SED	0.1	[OII]	0.01	29, 37
091109B	0
090515A	11.2	SED	29
090510A	0.903	VLT/FORS	9.7	SED	0.6	[OII]	0.12	$0.7^{+0.2}_{-0.4}$	hostSED	22, 29
090426A	2.609	Keck I/LRIS	10.81	...	14.4 ± 2	UV	0.22	30, 89
090305A	0
080905A	0.1218	VLT/FORS1	0
080503A	0
080123A	0.495	...	10.1	SED	29
071227A	0.383	VLT/FORS2	10.4	SED	0.6	[OII]	0.02	-0.190 ± 0.3	E	1.50000	hostSED	16, 29
070809A	0.2187	Keck/LRIS	11.4	SED	29
070724A	0.457	Gemini/GMOS	10.1	SED	2.5	[OII]	0.20	0.210	E	17, 29
070714B	0.923	Keck/LRIS	9.4	SED	0.4	[OII]	0.16	17, 29
070707A	0
070429B	0.904	Keck/LRIS	10.4	SED	1.1	[OII]	0.04	17, 29
061217A	0.827	Magellan	9.1	SED	2.5	[OII]	1.99	17, 29

Table 3—Continued

GRB	z	Instrument (Spectrum)	log M_*		SFR		sSFR [Gyr $^{-1}$]	[X/H]		A_V		reference
			[M $_{\odot}$]	method	[M $_{\odot}$ yr $^{-1}$]	method		(9)	method	[mag]	method	
(1)	(2)	(3)	(4)	(5)	(6)	(7)	(8)	(9)	(10)	(11)	(12)	(13)
061210A	0.41	Keck/LRIS	9.6	SED	1.2	[OII]	0.30	0.110	E	17, 29
061201A	0.111	Magellan	0
061006A	0.4377	Gemini/GMOS	10.43 ± 0.23	SED	0.17	UV	0.01	-0.090	E	17, 19
060801A	1.131	Gemini/GMOS	9.1	SED	6.1	[OII]	4.85	17, 29
060502B	0.287	Keck/LRIS	0
060313A	0
060121A	0
051221A	0.5465	Gemini/GMOS	8.61 ± 0.64	SED	2.11	H β	5.18	-1.090 / -0.100	E	19
051210A	1.4	...	8.8	SED	29
050724A	0.258	Gemini/GMOS	10.64 ± 0.05	SED	18.76	UV	0.43	19
050709A	0.16	VLT/FORS2	8.66 ± 0.07	SED	0.14	H α	0.31	-0.190	E	17, 19
050509B	0.226	Keck/DEIMOS	11.08 ± 0.03	SED	16.87	UV	0.14	19

Note. — Col. (1) GRB name. Col. (2) redshift. Col. (3) The instrument which obtained the optical spectrum. Col. (4-5) Stellar mass M_* and the methods which derive it. Col. (6-7) Star formation rate and the methods which derive it. Col. (8) Specific SFR, SFR/ M_* . Col. (9-10) Metallicity and the methods which derive it. (E)mission line and (A)bsorption line. Col. (11-12) Extinction and the methods which derive it. Col. (13) Reference.

References. (1) Fynbo et al. (2002); (2) Fynbo et al. (2003); (3) Vreeswijk et al. (2004); (4) Jakobsson et al. (2004); (5) Vreeswijk et al. (2006); (6) Pellizza et al. (2006); (7) Jakobsson et al. (2006b); (8) Berger et al. (2006); (9) Penprase et al. (2006); (10) Watson et al. (2006); (11) Della Valle et al. (2006); (12) Stratta et al. (2007); (13) Prochaska et al. (2007a); (14) Cenko et al. (2008a); (15) Prochaska et al. (2008); (16) D'Avanzo et al. (2009); (17) Berger (2009); (18) Chen et al. (2009); (19) Savaglio et al. (2009); (20) Han et al. (2010); (21) Zafar et al. (2010); (22) McBreen et al. (2010); (23) Castro-Tirado et al. (2010); (24) D'Avanzo et al. (2010); (25) Thöne et al. (2010); (26) Levesque et al. (2010a); (27) Rau et al. (2010b); (28) Tanvir et al. (2010c); (29) Leibler & Berger (2010); (30) Levesque et al. (2010b); (31) Schady et al. (2010); (32) Chornock et al. (2010c); (33) Schulze et al. (2011); (34) Greiner et al. (2011); (35) Krühler et al. (2011b); (36) Vergani et al. (2011); (37) Fong et al. (2011); (38) Laskar et al. (2011); (39) Levesque et al. (2011); (40) De Cia et al. (2011); (41) Cano et al. (2011); (42) Götz et al. (2011); (43) Mannucci et al. (2011); (44) Guidorzi et al. (2011); (45) Basa et al. (2012); (46) De Cia et al. (2012); (47) Milvang-Jensen et al. (2012); (48) Perley et al. (2012a); (49) Savaglio et al. (2012); (50) Svensson et al. (2012); (51) Niino et al. (2012); (52) Krühler et al. (2013); (53) de Ugarte Postigo et al. (2013d); (54) Zauderer et al. (2013); (55) Fong et al. (2013); (56) Jin et al. (2013); (57) Kelly et al. (2013); (58) Xu et al. (2013b); (59) Perley et al. (2013); (60) Thöne et al. (2013); (61) Elliott et al. (2013b); (62) de Ugarte Postigo et al. (2014b); (63) D'Elia et al. (2014); (64) Hunt et al. (2014); (65) Schulze et al. (2014); (66) Cano et al. (2014); (67) Jeong et al. (2014b); (68) Fynbo et al. (2014); (69) Rossi et al. (2014); (70) Sparre et al. (2014); (71) Morgan et al. (2014); (72) Olivares E. et al. (2015); (73) Schady et al. (2015); (74) Hartoog et al. (2015); (75) Melandri et al. (2015); (76) Vergani et al. (2015); (77) Krühler et al. (2015); (78) Michalowski et al. (2015); (79) Cucchiara et al. (2015); (80) Hashimoto et al. (2015); (81) Greiner et al. (2015); (82) Arabsalmani et al. (2015); (83) Stanway et al. (2015); (84) van der Horst et al. (2015); (85) Kohn et al. (2015); (86) Friis et al. (2015); (87) Cano et al. (2015); (88) Piranomonte et al. (2015); (89) GHOST;

Table 4. offset

GRB	z	Instrument (Image)	P_{cc}	R_{50} ["]	R_{50} [kpc]	n	R_{off} ["]	R_{off} [kpc]	r_{off} [R_{50}]	F_{light}	reference
(1)	(2)	(3)	(4)	(5)	(6)	(7)	(8)	(9)	(10)	(11)	(12)
140606B	0.384	0
140518A	4.707	0
140515A	6.32	HST	0.014	$0.12^{+0.05}_{-0.04}$	$0.680^{+0.27}_{-0.23}$...	0.210 ± 0.070	1.21 ± 0.40	1.776	...	47
140512A	0.725	0
140508A	1.027	0
140506A	0.8893	0
140430A	1.6019	0
140428A	4.7	0
140423A	3.26	0
140419A	3.956	0
140318A	1.02	0
140311A	4.954	0
140304A	5.283	0
140301A	1.4155	0
140226A	1.98	0
140213A	1.2079	0
140206A	2.739	0
140114A	3	0
131231A	0.6427	0
131227A	5.3	0
131117A	4.042	0
131108A	2.4	0
131105A	1.6854	0
131103A	0.5960	0
131030A	1.293	0
131011A	1.874	0
131004A	0.717	0
130925A	0.3483	HST	...	0.48	2.400	...	0.120	0.595	0.248	...	38, 43
130907A	1.238	0
130831A	0.4791	0
130702A	0.145	Keck/LRIS	...	0.700*	1.785	...	0.600	1.530	0.857	...	34, 49
130701A	1.1548	0
130612A	2.006	0

Table 4—Continued

GRB	z	Instrument (Image)	P_{cc}	R_{50} ["]	R_{50} [kpc]	n	R_{off} ["]	R_{off} [kpc]	r_{off} [R_{50}]	F_{light}	reference
(1)	(2)	(3)	(4)	(5)	(6)	(7)	(8)	(9)	(10)	(11)	(12)
130610A	2.092	0
130606A	5.913	HST	0.014	0.190 ± 0.020	1.14 ± 0.10	...	0.060 ± 0.020	0.36 ± 0.12	0.314	...	47
130604A	1.06	0
130528A	1.25	0
130518A	2.49	0
130511A	1.3033	0
130505A	2.27	0
130427B	2.78	0
130427A	0.3401	HST	...	0.400*	1.954	...	0.83 ± 0.03	4.1 ± 0.1	2.075	...	41
130420A	1.297	0
130418A	1.217	0
130408A	3.757	0
130215A	0.597	0
130131B	2.5393	0
121229A	2.707	0
121211A	1.023	0
121209A	2.1	0
121201A	3.3830	0
121128A	2.20	0
121027A	1.7732	0
121024A	2.3012	0
120922A	3.1	0
120909A	3.93	0
120907A	0.970	0
120815A	2.3587	0
120811C	2.671	0
120805A	3.1	0
120802A	3.796	0
120729A	0.80	0
120724A	1.48	0
120722A	0.9590	0
120716A	2.486	0
120714B	0.3985	0

Table 4—Continued

GRB	z	Instrument (Image)	P_{cc}	R_{50} ["]	R_{50} [kpc]	n	R_{off} ["]	R_{off} [kpc]	r_{off} $[R_{50}]$	F_{light}	reference
(1)	(2)	(3)	(4)	(5)	(6)	(7)	(8)	(9)	(10)	(11)	(12)
120712A	4.1745	0
120711A	1.405	0
120624B	2.1974	VLT	...	< 0.190	< 1.60	32
120422A	0.2826	Magellan	...	1.000	4.299	...	1.900	8.167	1.900	...	29
120404A	2.876	0
120327A	2.813	0
120326A	1.798	0
120224A	1.1	0
120211A	2.4	0
120119A	1.7291	HST	0.003	0.202	1.752	...	0.012 ± 0.017	0.104 ± 0.147	0.059 ± 0.086	1.000	48
120118B	2.9428	0
111229A	1.3805	0
111228A	0.7164	0
111225A	2.012	0
111215A	2.06	HST	...	0.250*	2.143	...	0.310*	2.657	1.240	...	45
111211A	0.4786	0
111209A	0.6770	HST	...	0.06	0.400	...	0.011 ± 0.038	0.079 ± 0.272	0.198	...	40
111129A	1.0796	0
111123A	3.1513	0
111107A	2.893	0
111008A	4.9898	0
111005A	0.0133	6.300*	1.712	...	3.500*	0.951	0.555	...	44
110918A	0.9843	GROND	0.010	1.30	10.600	...	1.48	12.000	1.132	...	31
110818A	3.3609	0
110808A	1.3490	0
110801A	1.858	0
110731A	2.83	HST	0.005	0.121	0.977	...	0.182 ± 0.010	1.47 ± 0.08	1.50 ± 0.09	0.029	48
110726A	1.036	0
110715A	0.82	0
110709B	2.09	HST	0.111	0.073	0.625	...	0.067 ± 0.323	0.57 ± 2.76	0.92 ± 4.43	0.055	48
110503A	1.613	0
110422A	1.770	0
110213B	1.083	0

Table 4—Continued

GRB	z	Instrument (Image)	P_{cc}	R_{50} ["]	R_{50} [kpc]	n	R_{off} ["]	R_{off} [kpc]	r_{off} [R_{50}]	F_{light}	reference
(1)	(2)	(3)	(4)	(5)	(6)	(7)	(8)	(9)	(10)	(11)	(12)
110213A	1.46	0
110205A	2.22	0
110128A	2.339	0
110106B	0.618	0
101225A	0.847	HST	...	< 0.040	< 0.34	...	0.016 ± 0.020	0.124 ± 0.156	0.365	...	40
101219B	0.55185	0
100906A	1.727	0
100901A	1.408	0
100814A	1.4392	0
100728B	2.106	0
100728A	1.5670	0
100724A	1.2890	0
100621A	0.5426	HST	0.002	0.262	1.688	...	0.045 ± 0.069	0.290 ± 0.444	0.172 ± 0.263	0.914	48
100615A	1.3978	HST	0.034	0.083	0.716	...	0.246 ± 0.320	2.12 ± 2.76	2.96 ± 3.85	0.051	48
100606A	1.5545	0
100518A	4	0
100513A	4.772	0
100508A	0.5201	0
100425A	1.755	0
100424A	2.4656	0
100418A	0.6235	0
100414A	1.368	0
100316D	0.0592	HST	0.879	48
100316B	1.180	0
100302A	4.813	0
100219A	4.6667	GTC/OSIRIS	...	1.400*	9.408	...	0.40 ± 0.30	2.69 ± 2.02	0.286	...	37
091208B	1.0633	0
091127A	0.4904	HST	0.011	0.411	2.509	...	0.221 ± 0.049	1.35 ± 0.30	0.54 ± 0.12	0.833	48
091109A	3.076	0
091029A	2.752	0
091024A	1.092	0
091020A	1.71	0
091018A	0.9710	0

Table 4—Continued

GRB	z	Instrument (Image)	P_{cc}	R_{50} ["]	R_{50} [kpc]	n	R_{off} ["]	R_{off} [kpc]	r_{off} [R_{50}]	F_{light}	reference
(1)	(2)	(3)	(4)	(5)	(6)	(7)	(8)	(9)	(10)	(11)	(12)
091003A	0.8969	0
090927A	1.37	0
090926B	1.2427	NTT	0.018	< 0.60	< 5.1	27
090926A	2.1062	0
090902B	1.822	0
090814A	0.696	0
090812A	2.452	0
090809A	2.737	0
090726A	2.71	0
090715B	3.00	0
090709A	1.7	HST	0.010	0.256	2.222	...	0.283 ± 0.036	2.46 ± 0.31	1.10 ± 0.14	0.461	48
090618A	0.54	HST	0.020	0.519	3.335	...	0.69 ± 0.05	4.5 ± 0.3	1.33 ± 0.09	0.260	48
090530A	1.266	0
090529A	2.625	0
090519A	3.85	0
090516A	4.109	0
090424A	0.544	HST	0.005	0.407	2.625	...	0.41 ± 0.04	2.62 ± 0.24	1.00 ± 0.09	0.740	48
090423A	8.23	0
090418A	1.608	HST	0.009	0.214	1.858	...	0.096 ± 0.211	0.83 ± 1.83	0.45 ± 0.98	0.367	48
090417B	0.345	HST	0.006	< 0.91	< 4.5	...	0.88 ± 1.00	4.3 ± 4.9	0.966	...	26, 36
090407A	1.4478	HST	0.026	0.336	2.905	...	0.172 ± 0.410	1.49 ± 3.54	0.51 ± 1.22	0.245	48
090328A	0.7357	GROND	0.140	1.035	23
090323A	3.5832	0
090313A	3.375	0
090205A	4.6497	VLT/FORS1	0.40 ± 0.30	2.69 ± 2.02	24
090201A	2.1000	0
090113A	1.7494	0
090102A	1.547	HST	0.090 ± 0.060	0.78 ± 0.52	22
081222A	2.77	0
081221A	2.2590	HST	0.013	0.409	3.462	...	0.39 ± 0.07	3.3 ± 0.6	0.95 ± 0.18	0.761	48
081210A	2.0631	0
081203A	2.05	0
081121A	2.512	HST	0.010	0.198	1.644	...	0.262 ± 0.122	2.17 ± 1.01	1.32 ± 0.61	0.197	48

Table 4—Continued

GRB	z	Instrument (Image)	P_{cc}	R_{50} ["]	R_{50} [kpc]	n	R_{off} ["]	R_{off} [kpc]	r_{off} [R_{50}]	Flight	reference
(1)	(2)	(3)	(4)	(5)	(6)	(7)	(8)	(9)	(10)	(11)	(12)
081118A	2.58	0
081109A	0.9785	VLT	0.002	< 0.200	< 1.62	27
081029A	3.8479	0
081028A	3.038	0
081008A	1.967	HST	0.066	0.236	2.032	...	1.66 ± 0.03	14.3 ± 0.2	7.0 ± 0.1	0.000	48
081007A	0.5295	HST	0.011	0.277	1.762	...	0.111 ± 0.029	0.71 ± 0.18	0.40 ± 0.10	0.792	48
080928A	1.6919	HST	0.035	0.442	3.836	...	1.71 ± 0.03	14.8 ± 0.3	3.9 ± 0.1	0.009	48
080916C	4.35	0
080916A	0.6887	HST	0.004	0.240	1.728	...	0.011 ± 0.061	0.079 ± 0.439	0.046 ± 0.254	0.930	48
080913A	6.7	0
080905B	2.3739	0
080810A	3.3604	0
080805A	1.5052	HST	0.010	0.275	2.383	...	0.47 ± 0.05	4.0 ± 0.4	1.69 ± 0.17	0.517	48
080804A	2.2059	0
080721A	2.5914	0
080710A	0.8454	0
080707A	1.2322	HST	0.005	0.263	2.236	...	0.089 ± 0.054	0.76 ± 0.46	0.34 ± 0.20	0.836	48
080607A	3.0368	HST	0.036	0.419	3.317	...	0.68 ± 0.24	5.4 ± 1.9	1.62 ± 0.57	0.177	48
080605A	1.6408	HST	0.002	0.198	1.719	...	0.081 ± 0.031	0.70 ± 0.27	0.41 ± 0.16	0.820	48
080604A	1.4171	0
080603B	2.6892	0
080603A	1.688	HST	0.003	0.202	1.753	...	0.089 ± 0.030	0.77 ± 0.26	0.44 ± 0.15	0.880	48
080602A	1.8204	0
080520A	1.5457	HST	0.011	0.223	1.934	...	0.47 ± 0.18	4.1 ± 1.6	2.10 ± 0.82	0.117	48
080517A	0.089	WHT	...	1.70 ± 0.80	2.83 ± 1.33	1.5	3.00 ± 1.20	5.0 ± 2.0	1.764	...	46
080515A	2.47	0
080430A	0.767	HST	0.011	0.282	2.118	...	0.108 ± 0.049	0.81 ± 0.37	0.38 ± 0.17	0.645	48
080413B	1.1012	0
080413A	2.4330	0
080411A	1.0301	0
080330A	1.5119	0
080325A	1.78	HST	0.017	0.443	3.840	...	0.70 ± 0.07	6.0 ± 0.7	1.57 ± 0.17	0.134	48
080319C	1.9492	HST	0.023	0.638	5.498	...	0.85 ± 0.05	7.4 ± 0.4	1.34 ± 0.08	0.599	48

Table 4—Continued

GRB	z	Instrument (Image)	P_{cc}	R_{50} ["]	R_{50} [kpc]	n	R_{off} ["]	R_{off} [kpc]	r_{off} [R_{50}]	F_{light}	reference
(1)	(2)	(3)	(4)	(5)	(6)	(7)	(8)	(9)	(10)	(11)	(12)
080319B	0.9382	HST	0.015	0.147	1.179	...	0.215 ± 0.118	1.72 ± 0.95	1.46 ± 0.80	0.598	48
080310A	2.4274	0
080210A	2.6419	0
080207A	2.0856	HST	0.047	0.683	5.846	...	0.77 ± 0.44	6.6 ± 3.7	1.13 ± 0.64	0.207	48
080129A	4.349	0
071122A	1.14	HST	0.009	0.393	3.298	...	0.075 ± 0.053	0.63 ± 0.45	0.191 ± 0.134	0.951	48
071117A	1.3308	0
071112C	0.8227	HST	0.016	0.398	3.065	...	0.202 ± 0.027	1.55 ± 0.21	0.51 ± 0.07	0.774	48
071031A	2.692	0
071021A	2.4515	Keck	0.006	0.48 ± 0.50	4.0 ± 4.2	36
071020A	2.1462	0
071010B	0.947	HST	0.004	0.257	2.067	...	0.109 ± 0.025	0.88 ± 0.20	0.42 ± 0.10	0.825	48
071010A	0.98	0
071003A	1.60435	0
070810A	2.17	0
070802A	2.4538	HST	0.014	0.348	2.903	...	0.132 ± 0.048	1.10 ± 0.40	0.38 ± 0.14	0.692	48
070721B	3.6298	HST	0.011	0.057	0.425	...	0.045 ± 0.054	0.34 ± 0.40	0.79 ± 0.94	0.211	48
070714A	1.58	0
070612A	0.617	0
070611A	2.0394	0
070529A	2.4996	0
070521A	2.0865	HST	0.072	0.90 ± 1.40	7.7 ± 12.0	36
070518A	1.161	0
070508A	0.82	HST	0.027	0.592	4.554	...	0.42 ± 0.03	3.3 ± 0.3	0.71 ± 0.06	0.517	48
070506A	2.3090	0
070419B	1.9586	0
070419A	0.9705	0
070411A	2.9538	0
070328A	2.0627	0
070318A	0.8401	HST	0.005	0.205	1.590	...	0.109 ± 0.060	0.84 ± 0.47	0.53 ± 0.29	0.781	48
070306A	1.4965	HST	0.002	0.209	1.810	...	0.090 ± 0.045	0.78 ± 0.39	0.43 ± 0.21	0.798	48
070224A	1.9922	0
070223A	1.6295	0

Table 4—Continued

GRB	z	Instrument (Image)	P_{cc}	R_{50} ["]	R_{50} [kpc]	n	R_{off} ["]	R_{off} [kpc]	r_{off} $[R_{50}]$	F_{light}	reference
(1)	(2)	(3)	(4)	(5)	(6)	(7)	(8)	(9)	(10)	(11)	(12)
070208A	1.165	HST	0.005	0.368	3.100	...	0.099 ± 0.040	0.83 ± 0.34	0.269 ± 0.108	0.928	48
070129A	2.3384	0
070125A	1.547	Keck	HST	3.200	27.753
070110A	2.3523	0
070103A	2.6208	0
061222B	3.355	0
061222A	2.088	HST	0.005	0.193	1.652	...	0.044 ± 0.044	0.38 ± 0.38	0.228 ± 0.229	0.955	48
061202A	2.2543	0
061126A	1.1588	Keck	< 1.00	< 8.4	19
061121A	1.3145	0
061110B	3.4344	HST	0.008	0.104	0.791	...	0.061 ± 0.030	0.46 ± 0.23	0.59 ± 0.29	0.393	48
061110A	0.7578	HST	0.007	0.176	1.316	...	0.135 ± 0.040	1.01 ± 0.30	0.77 ± 0.23	0.419	48
061021A	0.3453	0
061007A	1.2622	HST	0.013	0.373	3.181	...	0.022 ± 0.103	0.188 ± 0.878	0.059 ± 0.277	0.778	48
060927A	5.4636	0
060926A	3.2090	0
060923B	1.5094	0
060923A	2.6	HST	0.038	0.696	5.735	...	0.291 ± 0.066	2.40 ± 0.54	0.42 ± 0.10	0.980	48
060912A	0.9362	HST	0.017	0.713	5.715	...	0.65 ± 0.15	5.2 ± 1.2	0.92 ± 0.21	0.525	48
060908A	1.8836	0
060906A	3.6856	0
060904B	0.7029	0
060814A	1.9223	HST	0.003	0.36 ± 0.40	3.1 ± 3.5	36
060805A	2.3633	0
060729A	0.5429	HST	0.011	0.308	1.984	...	0.34 ± 0.04	2.18 ± 0.27	1.10 ± 0.14	0.246	48
060719A	1.5318	HST	0.006	0.246	2.133	...	0.206 ± 0.081	1.79 ± 0.70	0.84 ± 0.33	0.581	48
060714A	2.7108	0
060707A	3.4246	0
060614A	0.125	HST	0.003	0.329	0.739	...	0.36 ± 0.01	0.80 ± 0.03	1.08 ± 0.04	0.459	48
060607A	3.0749	0
060605A	3.773	HST	0.026	0.109	0.802	...	0.183 ± 0.117	1.35 ± 0.86	1.68 ± 1.07	0.103	48
060604A	2.1355	0
060602A	0.787	0

Table 4—Continued

GRB	z	Instrument (Image)	P_{cc}	R_{50} ["]	R_{50} [kpc]	n	R_{off} ["]	R_{off} [kpc]	r_{off} [R_{50}]	F_{light}	reference
(1)	(2)	(3)	(4)	(5)	(6)	(7)	(8)	(9)	(10)	(11)	(12)
060526A	3.2213	0
060522A	5.11	HST	0.300	1.930	28
060512A	0.4428	0
060510B	4.9	0
060505A	0.0889	HST	0.009	1.195	1.988	...	4.3 ± 0.0	7.2 ± 0.1	3.6 ± 0.0	0.987	48
060502A	1.5026	HST	0.007	0.162	1.403	...	0.051 ± 0.023	0.44 ± 0.20	0.32 ± 0.14	0.689	48
060418A	1.4901	HST	0.019	0.118	1.022	...	0.40 ± 0.01	3.5 ± 0.0	3.4 ± 0.0	0.000	48
060319A	1.172	Keck	0.028	1.22 ± 0.90	10.3 ± 7.6	36
060306A	1.5597	Keck	0.037	0.80 ± 1.30	6.9 ± 11.3	36
060223A	4.406	HST	0.026	0.211	1.455	...	0.112 ± 0.178	0.77 ± 1.23	0.53 ± 0.84	0.292	48
060218A	0.03351	HST	0.002	0.606	0.405	...	0.174 ± 0.045	0.116 ± 0.030	0.286 ± 0.075	0.872	48
060210A	3.9122	0
060206A	4.0559	HST	0.035	0.091	0.650	...	0.292 ± 0.128	2.09 ± 0.92	3.2 ± 1.4	0.032	48
060204B	2.3393	0
060202A	0.785	Keck	0.029	1.53 ± 1.10	11.6 ± 8.3	36
060124A	2.3	HST	0.011	0.172	1.452	...	0.132 ± 0.091	1.11 ± 0.77	0.77 ± 0.53	0.427	48
060123A	0.56	0
060115A	3.5328	HST	0.030	0.125	0.942	...	0.280 ± 0.065	2.11 ± 0.49	2.24 ± 0.52	0.081	48
060111A	2.32	0
051117B	0.4805	0
051111A	1.55	0
051109B	0.080	0
051109A	2.346	0
051022A	0.8061	HST	0.002	0.334	2.554	...	0.171 ± 0.124	1.31 ± 0.95	0.51 ± 0.37	0.556	48
051016B	0.9358	HST	0.004	0.228	1.827	...	0.257 ± 0.194	2.06 ± 1.55	1.13 ± 0.85	0.329	48
051008A	2.77	Keck	0.058	0.68 ± 1.20	5.5 ± 9.7	36
051006A	1.059	0
051001A	2.4295	0
050922C	2.1992	0
050915A	2.5275	Keck	0.010	0.82 ± 0.18	6.8 ± 1.5	36
050908A	3.3467	HST	0.005	0.068	0.522	...	0.037 ± 0.055	0.284 ± 0.422	0.54 ± 0.80	0.316	48
050904A	6.295	HST	0.013	$0.12^{+0.03}_{-0.03}$	$0.680^{+0.16}_{-0.18}$...	0.130 ± 0.040	0.75 ± 0.23	1.101	...	47
050826A	0.296	MDM	0.000	0.400	1.777	18

Table 4—Continued

GRB	z	Instrument (Image)	P_{cc}	R_{50} ["]	R_{50} [kpc]	n	R_{off} ["]	R_{off} [kpc]	r_{off} [R_{50}]	F_{light}	reference
(1)	(2)	(3)	(4)	(5)	(6)	(7)	(8)	(9)	(10)	(11)	(12)
050824A	0.8277	HST	0.021	0.402	3.102	...	0.47 ± 0.05	3.6 ± 0.4	1.18 ± 0.13	0.324	48
050822A	1.434	0
050820A	2.61469	HST	0.010	0.116	0.955	...	0.44 ± 0.01	3.6 ± 0.1	3.8 ± 0.1	0.606	48
050819A	2.5042	0
050814A	5.3	0
050802A	1.7102	0
050730A	3.96855	0
050714B	2.4383	0
050525A	0.6063	HST	0.005	0.119	0.809	...	0.028 ± 0.007	0.190 ± 0.048	0.235 ± 0.057	0.914	48
050505A	4.2748	0
050502A	3.793	0
050416A	0.6542	HST	0.001	0.160	1.127	...	0.037 ± 0.013	0.261 ± 0.092	0.232 ± 0.081	0.896	48
050408A	1.2356	HST	0.008	0.278	2.364	...	0.152 ± 0.029	1.29 ± 0.25	0.55 ± 0.10	0.724	48
050401A	2.8983	HST	0.006	0.170	1.364	...	0.082 ± 0.051	0.66 ± 0.41	0.48 ± 0.30	0.799	48
050319A	3.2425	0
050318A	1.4436	0
050315A	1.9500	HST	0.006	0.236	2.034	...	0.114 ± 0.056	0.98 ± 0.48	0.48 ± 0.24	0.693	48
050223A	0.584	0
050219A	0.211	VLT	0.008	1.300	4.493	3.3	4.600	15.899	3.539	...	39
050215B	2.62	0
050126A	1.29002	0
041219A	0.31	0
041006A	0.716	HST	0.012	0.298	2.179	1.1	0.35 ± 0.01	2.57 ± 0.06	1.18 ± 0.03	...	48
040924A	0.858	HST	0.003	0.188	1.468	1.1	0.286 ± 0.015	2.23 ± 0.12	1.52 ± 0.08	0.783	48
040912A	1.563	0
031203A	0.1055	CTIO	0.068 ± 0.057	0.132 ± 0.110	11
030528A	0.782	0
030429A	2.658	Magellan/PANIC	...	0.400*	3.280	...	1.000	8.199	2.500	...	21
030329A	0.1685		HST	0.006	0.20	0.575	1.8	0.991	16
030328A	1.5216	0
030323A	3.3736	HST	0.060	0.14	1.039	1	0.140	1.072	1.032	0.862	10, 16
030226A	1.986	0
030115A	2	HST	0.060	0.560	4.815	1.9	0.863	16, 17

Table 4—Continued

GRB	z	Instrument (Image)	P_{cc}	R_{50} ["]	R_{50} [kpc]	n	R_{off} ["]	R_{off} [kpc]	r_{off} [R_{50}]	F_{light}	reference
(1)	(2)	(3)	(4)	(5)	(6)	(7)	(8)	(9)	(10)	(11)	(12)
021211A	1.006	HST	0.007	0.11	0.911	1.1	0.758	16
021004A	2.3351	HST	0.006	0.12	1.011	1	0.280	2.357	2.331	1.000	15, 16
020903A	0.251	HST	0.006	0.20	0.799	1.6	0.958	16
020819B	0.41	Keck/ESI	...	1.35 ± 0.05	7.4 ± 0.3	...	3.00 ± 0.10	16.5 ± 0.6	2.222	...	14
020813A	1.255	HST	0.008	0.14	1.190	1	0.880	16
020427A	...	HST	0.006	0.46 ± 0.08	3.955	0.7	0.090 ± 0.145	0.774	0.196	...	8, 17
020410A ^a	...	HST	0.006	0.240	1.481	1.4	0.973	16, 17
020405A	0.6908	HST	0.010	0.93	6.682	0.587	16
020331A	...	HST	0.007	0.080	0.688	1	1.000	16, 17
020322A	...	HST	0.090	0.282	16
020305A	2.8	HST	0.006	0.150	1.214	1.4	0.070	0.567	0.467	0.911	12, 16, 17
020127A	1.9	HST	...	0.290	2.504	1	17
020124A	3.198	0
011211A	2.14	HST	0.006	0.18	1.503	1	0.500	4.266	2.838	0.953	1, 16
011121A	0.36	HST	0.016	0.65	3.291	2.6	0.900	4.563	1.387	0.511	9, 16
011030A	3	HST	0.008	0.230	1.827	0.3	0.34 ± 0.06	2.69 ± 0.48	1.474	...	8, 17
010921A	0.4509	HST	0.015	0.26	1.542	1.0	0.33 ± 0.03	1.89 ± 0.19	1.227	0.439	3, 16
010222A	1.47688	HST	0.013	0.19	1.603	1	0.044 ± 0.006	0.38 ± 0.05	0.238	0.927	7, 16
000926A	2.0379	HST	0.013	0.67	5.726	0.8	0.032 ± 0.004	0.275 ± 0.035	0.048	1.000	6, 16
000911A	1.0585	Keck	...	< 0.40	< 3.3	...	0.080 ± 0.100	0.66 ± 0.83	0.200	...	4, 13
000418A	1.1181	HST	0.150	0.096 ± 0.027	0.80 ± 0.23	0.7	0.023 ± 0.064	0.192 ± 0.535	0.239 ± 0.670	0.454	2, 16
000301C	2.0404	HST	0.006	0.066 ± 0.028	0.57 ± 0.24	1	0.069 ± 0.007	0.59 ± 0.06	1.05 ± 0.46	0.512	2, 16
000210A	0.846	VLT	0.016	1.000	7.773	5
000131A	4.5	HST	0.100	0.48	3.313	0.8	0.491	16
991216A	1.02	HST	0.030	0.40 ± 0.04	3.3 ± 0.4	1.7	0.36 ± 0.03	2.94 ± 0.26	0.90 ± 0.13	0.825	2, 16
991208A	0.7063	HST	0.073	0.048 ± 0.026	0.35 ± 0.19	2.2	0.196 ± 0.097	1.43 ± 0.71	4.1 ± 3.0	0.940	2, 16
990712A	0.4331	HST	0.012	0.282 ± 0.026	1.60 ± 0.15	1.7	0.049 ± 0.080	0.279 ± 0.455	0.174 ± 0.284	0.971	2, 16
990705A	0.8424	HST	0.015	1.15 ± 0.03	8.9 ± 0.2	1	0.87 ± 0.05	6.8 ± 0.4	0.76 ± 0.04	...	2
990510A	1.619	HST	0.006	0.167 ± 0.041	1.45 ± 0.36	1	0.066 ± 0.009	0.57 ± 0.08	0.40 ± 0.11	0.794	2, 16
990506A	1.30658	HST	0.044	0.090 ± 0.027	0.77 ± 0.23	1.0	0.297 ± 0.459	2.54 ± 3.93	3.3 ± 5.2	...	2
990308A	...	HST	0.32	0.213 ± 0.028	1.831	1	1.04 ± 0.36	8.959	4.9 ± 1.8	...	2
990123A	1.6004	HST	0.005	0.40 ± 0.03	3.5 ± 0.2	1.6	0.67 ± 0.00	5.8 ± 0.0	1.67 ± 0.12	0.113	2, 16
981226A	1.11	HST	0.018	0.34 ± 0.03	2.81 ± 0.25	1.2	0.75 ± 0.33	6.3 ± 2.7	2.23 ± 1.00	...	2

Table 4—Continued

GRB	z	Instrument (Image)	P_{cc}	R_{50} ["]	R_{50} [kpc]	n	R_{off} ["]	R_{off} [kpc]	r_{off} [R_{50}]	F_{light}	reference
(1)	(2)	(3)	(4)	(5)	(6)	(7)	(8)	(9)	(10)	(11)	(12)
980703A	0.966	HST	0.035	0.169 ± 0.026	1.37 ± 0.21	1.0	0.112 ± 0.063	0.91 ± 0.51	0.66 ± 0.39	0.557	2, 16
980613A	1.0969	HST	0.075	0.227 ± 0.031	1.89 ± 0.26	1.6	0.089 ± 0.076	0.74 ± 0.63	0.39 ± 0.34	0.416	2, 16
980519A	...	HST	0.050	0.43 ± 0.04	3.731	1	1.10 ± 0.10	9.466	2.54 ± 0.33	0.848	2, 16
980425A	0.0085	HST	0.010	18.7 ± 0.0	3.3 ± 0.0	...	12.6 ± 0.1	2.19 ± 0.01	0.67 ± 0.00	...	2
980329A	3.5	HST	0.040	0.245 ± 0.033	1.85 ± 0.25	0.9	0.037 ± 0.049	0.280 ± 0.370	0.151 ± 0.202	0.794	2, 16
980326A	...	HST	0.033	0.043 ± 0.028	0.370	...	0.130 ± 0.068	1.118	3.0 ± 2.5	1.000	2, 16
971214A	3.42	HST	0.150	0.226 ± 0.031	1.72 ± 0.24	1.2	0.139 ± 0.070	1.06 ± 0.53	0.61 ± 0.32	0.535	2, 16
970828A	0.9578	HST	0.070	0.296 ± 0.089	2.39 ± 0.72	0.7	0.47 ± 0.51	3.8 ± 4.1	1.60 ± 1.78	...	2
970508A	0.835	HST	0.007	0.089 ± 0.026	0.69 ± 0.20	1.2	0.011 ± 0.011	0.085 ± 0.085	0.123 ± 0.129	1.000	2, 16
970228A	0.695	HST	0.009	0.34 ± 0.03	2.49 ± 0.22	1	0.43 ± 0.03	3.1 ± 0.2	1.24 ± 0.15	...	2
SGRB											
130603B	0.356	HST	...	1.000	5.033	3.81	1.05 ± 0.04	5.3 ± 0.2	1.05 ± 0.04	0.35	35
101224A	...	NOT	0.50 ± 3.20	3.085	42
101219A	0.718	< 3.4	< 24.9	33
100816A	0.8048	0
100625A	0.452	< 3.4	< 19.8	33
100206A	0.4068	Gemini/Keck	0.020	2.500	13.690	0.58	4.0 ± 3.3	21.9 ± 18.1	1.600	...	30
100117A	0.92	HST	...	0.290	2.313	4.95	0.170 ± 0.040	1.36 ± 0.32	0.59 ± 0.13	0.54	35
091109B	...	HST	11.7 ± 0.0	72.2 ± 0.2	35
090515A	...	HST	...	0.900	5.552	2.95	14.0 ± 0.0	86.2 ± 0.1	15.5 ± 0.0	0	35
090510A	0.903	HST	...	0.950	7.536	1.27	1.33 ± 0.37	10.6 ± 2.9	1.40 ± 0.39	0	35
090426A	2.609	HST	...	0.210	1.729	0.89	0.060 ± 0.030	0.49 ± 0.25	0.286 ± 0.140	0.82	35
090305A	...	HST	...	0.360	2.221	0.57	0.43 ± 0.03	2.65 ± 0.24	1.20 ± 0.08	0.3	35
080905A	0.1218	HST	...	1.800	3.955	1.00	8.3 ± 0.1	18.2 ± 0.2	4.6 ± 0.1	0	35
080503A	...	HST	...	0.260	1.604	0.32	0.90 ± 0.03	5.6 ± 0.2	3.5 ± 0.1	0	35
080123A	0.495	0
071227A	0.383	HST	...	0.910	4.800	1.05	2.98 ± 0.05	15.7 ± 0.3	3.3 ± 0.1	0	35
070809A	0.2187	HST	...	0.610	2.168	3.03	5.6 ± 0.5	20.0 ± 1.6	9.2 ± 0.8	0	35
070724A	0.457	HST	...	0.630	3.696	0.92	0.94 ± 0.03	5.5 ± 0.2	1.49 ± 0.04	0.23	35
070714B	0.923	HST	...	0.340	2.714	0.76	1.55 ± 0.11	12.4 ± 0.9	4.6 ± 0.3	0	35
070707A	...	HST	...	0.360	2.221	0.89	0.40 ± 0.03	2.47 ± 0.24	1.11 ± 0.08	0	35
070429B	0.904	HST	...	0.650	5.158	2.15	< 1.46	< 11.6	< 2.25	...	35
061217A	0.827	0

Table 4—Continued

GRB	z	Instrument (Image)	P_{cc}	R_{50} ["]	R_{50} [kpc]	n	R_{off} ["]	R_{off} [kpc]	r_{off} [R_{50}]	F_{light}	reference
(1)	(2)	(3)	(4)	(5)	(6)	(7)	(8)	(9)	(10)	(11)	(12)
061210A	0.41	0
061201A	0.111	HST	...	1.090	2.209	1.03	16.2 ± 0.0	32.9 ± 0.1	14.9 ± 0.0	0	35
061006A	0.4377	HST	...	0.650	3.719	0.7	0.230 ± 0.043	1.32 ± 0.25	0.35 ± 0.07	0.63	25
060801A	1.131	0
060502B	0.287	0
060313A	...	HST	...	0.230	1.419	1.3	0.284 ± 0.062	1.75 ± 0.50	1.24 ± 0.23	0	25
060121A	...	HST	...	0.670	4.133	1.4	0.119 ± 0.046	0.73 ± 0.37	0.178 ± 0.070	0.41	25
051221A	0.5465	HST	...	0.390	2.521	0.9	0.30 ± 0.03	1.95 ± 0.19	0.77 ± 0.08	0.65	25
051210A	1.4	HST	...	0.630	5.433	1.0	4.2 ± 1.7	36.2 ± 14.7	6.7 ± 2.7	...	25
050724A	0.258	HST	...	0.978	3.936	2.9	0.67 ± 0.02	2.68 ± 0.08	0.68 ± 0.02	0.33	25
050709A	0.16	HST	...	0.640	1.771	0.6	1.36 ± 0.00	3.8 ± 0.0	2.13 ± 0.01	0.09	25
050509B	0.226	HST	...	5.653	20.600	5.6	17.8 ± 3.4	64.8 ± 12.4	3.1 ± 0.6	...	25

Note. — Col. (1) GRB name. Col. (2) redshift. Col. (3) The instrument which obtained the optical image. Col. (4) Probability of Chance Coincidence. Col. (5-6) Half light radius in unit of arcsec and kpc. Col. (7) Sérsic index $\Sigma(r) = \Sigma_e \exp\{-k_n[(r/r_e)^{1/n} - 1]\}$. Col. (8-9) Offset of GRB from the center of host galaxy, in unit of arcsec and kpc. Col. (10) Normalized offset $r_{\text{off}} = R_{\text{off}}/R_{50}$. Col. (11) The fraction of area within host galaxy which is brighter than the GRB region. 1.0 indicates GRB is in the brightest region of the host and 0.0 indicates GRB is in the faintest region of the host. Col. (12) Reference.

^a. $z = 0.5$ is assumed for GRB 020410A, according to the possible detection of SN in Levan et al. (2005).

References. (1) Burud et al. (2001); (2) Bloom et al. (2002); (3) Price et al. (2002a); (4) Price et al. (2002b); (5) Piro et al. (2002); (6) Castro et al. (2003); (7) Galama et al. (2003); (8) Bloom et al. (2003b); (9) Greiner et al. (2003); (10) Vreeswijk et al. (2004); (11) Cobb et al. (2004); (12) Gorosabel et al. (2005); (13) Masetti et al. (2005); (14) Jakobsson et al. (2005); (15) Fynbo et al. (2005); (16) Fruchter et al. (2006); (17) Wainwright et al. (2007); (18) Mirabal et al. (2007); (19) Perley et al. (2008d); (20) Cenko et al. (2008a); (21) Chen et al. (2009); (22) Levan et al. (2009b); (23) McBreen et al. (2010); (24) D'Avanzo et al. (2010); (25) Fong et al. (2010); (26) Holland et al. (2010); (27) Krühler et al. (2011b); (28) Tanvir et al. (2012d); (29) Levesque et al. (2012); (30) Perley et al. (2012a); (31) Elliott et al. (2013a); (32) de Ugarte Postigo et al. (2013d); (33) Fong et al. (2013); (34) Kelly et al. (2013); (35) Fong & Berger (2013); (36) Perley et al. (2013); (37) Thöne et al. (2013); (38) Greiner et al. (2014); (39) Rossi et al. (2014); (40) Levan et al. (2014a); (41) Levan et al. (2014b); (42) Tunnicliffe et al. (2014); (43) Schady et al. (2015); (44) Michałowski et al. (2015); (45) Dominik et al. (2015); (46) Stanway et al. (2015); (47) McGuire et al. (2015); (48) Blanchard et al. (2016); (49) Toy et al. (2016);

Table 5: Statistical results of properties for consensus LGRB/SGRB definition.

Name	Consensus L/S							
	No. LGRB	value	No. SGRB	value	P_{KS}	Overlap range	LGRB in overlap (%)	SGRB in overlap (%)
$\log T_{90}$ (s)	369	1.70 ± 0.60	34	-0.30 ± 0.57	3.e-26	(0.11,0.75)	7	20
z	351	1.64 ± 1.30	25	0.45 ± 0.51	8.e-11	(0.11,2.61)	72	100
$\log E_{\text{iso}}$ (erg)	369	52.7 ± 1.0	33	51.1 ± 0.9	5.e-14	(48.8,52.5)	36	100
$\log L_{\text{iso}}$ (erg s $^{-1}$)	366	52.1 ± 1.1	33	51.3 ± 1.1	7.e-03	(49.3,53.0)	78	100
α	196	-1.01 ± 0.34	16	-0.60 ± 0.25	2.e-07	(-1.08,-0.15)	55	100
$\log E_p$ (keV)	202	2.17 ± 0.47	18	2.66 ± 0.43	2.e-04	(1.90,3.5)	73	94
$\log f$	224	0.13 ± 0.22	29	0.41 ± 0.22	1.e-07	(0.15,0.91)	43	100
f_{eff}	214	1.11 ± 0.30	29	2.28 ± 1.76	2.e-20	(1.42,4.8)	7	79
$\log \text{SFR}$ ($M_{\odot} \text{ yr}^{-1}$)	149	0.70 ± 0.85	16	0.32 ± 0.80	8.e-02	(-1.00,1.76)	88	100
$\log \text{sSFR}$ (Gyr $^{-1}$)	77	-0.03 ± 0.67	14	-0.51 ± 0.97	2.e-02	(-2.20,1.05)	90	92
$\log M_*$ (M_{\odot})	101	9.5 ± 0.8	22	10.1 ± 0.8	1.e-01	(8.6,11.4)	86	100
[X/H]	134	-0.59 ± 0.60	9	-0.09 ± 0.25	7.e-04	(-0.59,0.21)	47	100
$\log R_{50}$ (kpc)	128	0.26 ± 0.32	24	0.57 ± 0.29	4.e-04	(0.15,1.03)	69	91
$\log R_{\text{off}}$ (kpc)	136	0.25 ± 0.55	28	1.02 ± 0.62	1.e-04	(-0.31,1.44)	83	82
$\log r_{\text{off}} (=R_{\text{off}}/R_{50})$	117	-0.07 ± 0.44	24	0.20 ± 0.51	2.e-02	(-0.75,0.85)	93	87
F_{light}	99	0.69 ± 0.31	20	0.09 ± 0.27	7.e-05	(0.00,0.82)	65	100
$z < 1.4$								
$\log T_{90}$ (s)	158	1.61 ± 0.70	33	-0.31 ± 0.57	1.e-22	(0.15,0.75)	11	21
z	140	0.83 ± 0.36	24	0.45 ± 0.30	1.e-03	(0.11,1.13)	72	100
$\log E_{\text{iso}}$ (erg)	158	52.2 ± 1.2	32	51.1 ± 0.9	2.e-06	(48.8,52.5)	57	100
$\log L_{\text{iso}}$ (erg s $^{-1}$)	156	51.5 ± 1.3	32	51.3 ± 1.1	8.e-01	(49.3,53.0)	81	100
α	90	-1.13 ± 0.37	16	-0.60 ± 0.25	2.e-07	(-1.08,-0.15)	40	100
$\log E_p$ (keV)	94	2.11 ± 0.53	18	2.66 ± 0.43	3.e-04	(1.90,3.5)	70	94
$\log f$	84	0.18 ± 0.29	28	0.41 ± 0.22	8.e-05	(0.15,0.91)	47	100
f_{eff}	82	1.15 ± 0.44	28	2.33 ± 1.77	4.e-16	(1.42,4.8)	9	78
$\log \text{SFR}$ ($M_{\odot} \text{ yr}^{-1}$)	78	0.38 ± 0.79	16	0.32 ± 0.80	1.e+00	(-1.00,1.76)	88	100
$\log \text{sSFR}$ (Gyr $^{-1}$)	55	-0.08 ± 0.68	14	-0.51 ± 0.97	2.e-02	(-2.20,1.05)	90	92
$\log M_*$ (M_{\odot})	72	9.3 ± 0.8	22	10.1 ± 0.8	4.e-02	(8.6,11.4)	80	100
[X/H]	53	-0.39 ± 0.31	9	-0.09 ± 0.25	1.e-02	(-0.59,0.21)	73	100
$\log R_{50}$ (kpc)	78	0.32 ± 0.33	23	0.57 ± 0.28	4.e-03	(0.15,1.03)	73	91
$\log R_{\text{off}}$ (kpc)	79	0.25 ± 0.58	27	1.02 ± 0.58	2.e-04	(-0.13,1.22)	77	62
$\log r_{\text{off}} (=R_{\text{off}}/R_{50})$	69	-0.12 ± 0.44	23	0.20 ± 0.49	1.e-02	(-0.75,0.69)	91	82
F_{light}	55	0.79 ± 0.24	19	0.00 ± 0.24	2.e-07	(0.05,0.65)	36	47

Table 6: Statistical results of properties for T90 defined LGRB/SGRB.

Name	T90 L/S							
	No. LGRB	value	No. SGRB	value	P_{KS}	Overlap range	LGRB in overlap (%)	SGRB in overlap (%)
$\log T_{90}$ (s)	371	1.70 ± 0.60	32	-0.31 ± 0.50	2.e-27	(0.30,0.26)	0	0
z	352	1.63 ± 1.31	24	0.46 ± 0.60	6.e-08	(0.11,2.61)	73	100
$\log E_{\text{iso}}$ (erg)	371	52.7 ± 1.0	31	51.0 ± 0.9	5.e-15	(48.8,52.4)	35	100
$\log L_{\text{iso}}$ (erg s $^{-1}$)	368	52.1 ± 1.1	31	51.2 ± 1.0	1.e-03	(49.3,53.0)	80	100
α	198	-1.01 ± 0.34	14	-0.60 ± 0.32	3.e-06	(-1.36,-0.15)	84	92
$\log E_p$ (keV)	204	2.17 ± 0.48	16	2.66 ± 0.35	3.e-04	(1.90,3.00)	71	100
$\log f$	226	0.14 ± 0.22	27	0.36 ± 0.23	2.e-06	(0.14,0.91)	45	92
f_{eff}	216	1.12 ± 0.40	27	2.19 ± 1.78	5.e-18	(1.38,5.0)	10	88
$\log \text{SFR}$ ($M_{\odot} \text{ yr}^{-1}$)	150	0.71 ± 0.86	15	0.40 ± 0.70	5.e-02	(-1.00,1.48)	78	100
$\log \text{sSFR}$ (Gyr^{-1})	78	-0.04 ± 0.68	13	-0.22 ± 1.00	2.e-01	(-2.20,1.05)	89	84
$\log M_*$ (M_{\odot})	103	9.5 ± 0.8	20	10.1 ± 0.9	2.e-01	(8.6,11.4)	86	95
[X/H]	133	-0.61 ± 0.61	10	-0.19 ± 0.26	1.e-02	(-0.59,0.21)	43	80
$\log R_{50}$ (kpc)	131	0.27 ± 0.32	21	0.57 ± 0.30	3.e-03	(0.15,1.03)	70	90
$\log R_{\text{off}}$ (kpc)	139	0.25 ± 0.55	25	0.74 ± 0.68	6.e-04	(-0.56,1.44)	91	76
$\log r_{\text{off}} (=R_{\text{off}}/R_{50})$	120	-0.05 ± 0.43	21	0.20 ± 0.60	3.e-02	(-1.32,0.85)	99	85
F_{light}	102	0.65 ± 0.32	17	0.09 ± 0.34	4.e-03	(0.00,1.00)	100	100
$z < 1.4$								
$\log T_{90}$ (s)	161	1.59 ± 0.70	30	-0.37 ± 0.49	1.e-23	(0.30,0.26)	0	0
z	142	0.83 ± 0.36	22	0.45 ± 0.32	1.e-03	(0.11,1.29)	85	100
$\log E_{\text{iso}}$ (erg)	161	52.2 ± 1.2	29	51.0 ± 0.9	4.e-08	(48.8,52.4)	57	100
$\log L_{\text{iso}}$ (erg s $^{-1}$)	159	51.5 ± 1.3	29	51.2 ± 1.0	5.e-01	(49.3,53.0)	83	100
α	92	-1.13 ± 0.38	14	-0.60 ± 0.32	4.e-06	(-1.36,-0.15)	75	92
$\log E_p$ (keV)	96	2.11 ± 0.54	16	2.66 ± 0.35	3.e-04	(1.90,3.00)	66	100
$\log f$	86	0.18 ± 0.29	26	0.36 ± 0.23	8.e-04	(0.14,0.91)	50	92
f_{eff}	84	1.15 ± 0.61	26	2.28 ± 1.80	4.e-13	(1.38,5.0)	17	88
$\log \text{SFR}$ ($M_{\odot} \text{ yr}^{-1}$)	80	0.36 ± 0.81	14	0.40 ± 0.72	1.e+00	(-1.00,1.48)	87	100
$\log \text{sSFR}$ (Gyr^{-1})	57	-0.08 ± 0.69	12	-0.22 ± 1.04	2.e-01	(-2.20,1.05)	89	83
$\log M_*$ (M_{\odot})	75	9.3 ± 0.8	19	10.1 ± 0.9	3.e-02	(8.6,11.4)	81	94
[X/H]	53	-0.35 ± 0.31	9	-0.19 ± 0.27	9.e-02	(-0.59,0.21)	67	77
$\log R_{50}$ (kpc)	82	0.33 ± 0.33	19	0.57 ± 0.30	3.e-02	(0.15,1.03)	74	89
$\log R_{\text{off}}$ (kpc)	83	0.28 ± 0.58	23	1.06 ± 0.58	5.e-04	(0.12,1.22)	59	52
$\log r_{\text{off}} (=R_{\text{off}}/R_{50})$	73	-0.12 ± 0.45	19	0.33 ± 0.46	7.e-03	(-0.45,0.69)	75	73
F_{light}	59	0.78 ± 0.28	15	0.00 ± 0.25	4.e-05	(0.00,0.65)	40	93

Table 7: Statistical results of Simulated 1D distributions.

Name	Consensus L/S					T90 L/S				
	N(LGRB)	value	N(SGRB)	value	P_{KS}	N(LGRB)	value	N(SGRB)	value	P_{KS}
$\log T_{90}$ (s)	359	1.67 ± 0.57	41	-0.13 ± 0.61	5.e-30	365	1.67 ± 0.57	35	-0.30 ± 0.50	1.e-29
z	380	1.75 ± 1.38	20	0.44 ± 0.31	5.e-09	378	1.75 ± 1.38	22	0.46 ± 0.46	6.e-08
$\log E_{\text{iso}}$ (erg)	363	52.6 ± 1.0	37	51.0 ± 1.0	7.e-14	370	52.6 ± 1.0	30	50.9 ± 0.9	4.e-16
$\log L_{\text{iso}}$ (erg s $^{-1}$)	368	52.2 ± 1.1	32	51.2 ± 1.2	3.e-04	370	52.2 ± 1.1	30	51.2 ± 1.2	3.e-04
α	367	-1.03 ± 0.33	33	-0.60 ± 0.17	7.e-15	369	-1.01 ± 0.33	31	-0.62 ± 0.30	2.e-12
$\log E_p$ (keV)	362	2.19 ± 0.49	38	2.69 ± 0.41	4.e-10	365	2.19 ± 0.50	35	2.66 ± 0.33	1.e-09
$\log f$	358	0.12 ± 0.22	42	0.36 ± 0.21	1.e-12	356	0.12 ± 0.22	44	0.30 ± 0.21	1.e-12
f_{eff}	346	1.11 ± 0.32	54	2.54 ± 1.84	4.e-38	352	1.11 ± 0.46	48	2.19 ± 1.92	2.e-32
$\log \text{SFR}$ (M $_{\odot}$ yr $^{-1}$)	364	0.83 ± 0.86	36	0.08 ± 0.72	3.e-03	367	0.80 ± 0.87	33	0.40 ± 0.67	1.e-02
$\log \text{sSFR}$ (Gyr $^{-1}$)	345	-0.03 ± 0.71	55	-0.51 ± 0.92	3.e-08	339	-0.04 ± 0.71	61	0.13 ± 0.93	2.e-04
$\log M_{*}$ (M $_{\odot}$)	327	9.5 ± 0.8	73	9.7 ± 0.8	2.e-05	336	9.5 ± 0.8	64	9.7 ± 0.8	2.e-04
[X/H]	375	-0.59 ± 0.62	25	-0.19 ± 0.23	4.e-09	367	-0.59 ± 0.62	33	-0.19 ± 0.24	3.e-08
$\log R_{50}$ (kpc)	342	0.28 ± 0.30	58	0.57 ± 0.29	6.e-10	344	0.28 ± 0.30	56	0.36 ± 0.32	9.e-08
$\log R_{\text{off}}$ (kpc)	347	0.21 ± 0.53	53	0.72 ± 0.66	4.e-06	349	0.24 ± 0.52	51	0.72 ± 0.74	9.e-06
$\log r_{\text{off}} (=R_{\text{off}}/R_{50})$	326	-0.04 ± 0.44	74	0.20 ± 0.44	4.e-07	329	-0.04 ± 0.42	71	0.17 ± 0.57	1.e-05
F_{light}	326	0.69 ± 0.30	74	0.09 ± 0.25	4.e-19	330	0.69 ± 0.31	70	0.30 ± 0.28	2.e-11
$z < 1.4$										
$\log T_{90}$ (s)	323	1.48 ± 0.66	77	-0.30 ± 0.55	0.e+00	336	1.41 ± 0.66	64	-0.30 ± 0.43	0.e+00
z	341	0.81 ± 0.37	59	0.45 ± 0.33	3.e-05	342	0.82 ± 0.37	58	0.46 ± 0.36	7.e-05
$\log E_{\text{iso}}$ (erg)	313	52.2 ± 1.1	87	51.3 ± 1.0	2.e-10	325	52.2 ± 1.1	75	51.0 ± 0.9	2.e-15
$\log L_{\text{iso}}$ (erg s $^{-1}$)	310	51.4 ± 1.3	90	51.3 ± 1.1	3.e-01	317	51.4 ± 1.3	83	51.2 ± 1.0	4.e-02
α	339	-1.18 ± 0.36	61	-0.70 ± 0.19	1.e-28	346	-1.13 ± 0.37	54	-0.70 ± 0.25	9.e-27
$\log E_p$ (keV)	339	2.16 ± 0.49	61	2.63 ± 0.45	9.e-11	348	2.15 ± 0.51	52	2.69 ± 0.36	3.e-11
$\log f$	304	0.17 ± 0.32	96	0.34 ± 0.21	1.e-16	301	0.18 ± 0.32	99	0.29 ± 0.21	2.e-14
f_{eff}	306	1.15 ± 0.50	94	2.28 ± 1.88	0.e+00	304	1.15 ± 0.62	96	2.19 ± 1.84	0.e+00
$\log \text{SFR}$ (M $_{\odot}$ yr $^{-1}$)	318	0.38 ± 0.81	82	0.08 ± 0.61	6.e-06	323	0.32 ± 0.81	77	0.40 ± 0.58	6.e-02
$\log \text{sSFR}$ (Gyr $^{-1}$)	317	-0.08 ± 0.69	83	-0.52 ± 0.89	7.e-13	325	-0.12 ± 0.70	75	-0.22 ± 0.95	8.e-05
$\log M_{*}$ (M $_{\odot}$)	309	9.3 ± 0.7	91	9.6 ± 0.8	2.e-03	315	9.3 ± 0.7	85	9.3 ± 0.8	3.e-03
[X/H]	331	-0.39 ± 0.28	69	-0.09 ± 0.19	4.e-21	326	-0.35 ± 0.29	74	-0.19 ± 0.20	4.e-12
$\log R_{50}$ (kpc)	313	0.35 ± 0.33	87	0.60 ± 0.34	5.e-11	321	0.37 ± 0.32	79	0.57 ± 0.40	6.e-06
$\log R_{\text{off}}$ (kpc)	300	0.31 ± 0.57	100	1.02 ± 0.56	2.e-14	312	0.34 ± 0.56	88	0.74 ± 0.70	3.e-11
$\log r_{\text{off}} (=R_{\text{off}}/R_{50})$	293	-0.18 ± 0.43	107	0.20 ± 0.51	4.e-13	305	-0.17 ± 0.43	95	0.33 ± 0.52	2.e-11
F_{light}	296	0.78 ± 0.23	104	0.09 ± 0.25	2.e-32	300	0.78 ± 0.26	100	0.23 ± 0.25	5.e-24

Table 8: Statistical results of 2D.

	T90					z					α					E_p (keV)				
	No.	angle	P_{KS}	ρ_s	P_s	No.	angle	P_{KS}	ρ_s	P_s	No.	angle	P_{KS}	ρ_s	P_s	No.	angle	P_{KS}	ρ_s	P_s
$M_*(M_\odot)$	101/22	87	4.e-15	2.e-01	1.e-01	94/20	111	1.e-04	5.e-01	3.e-07	60/10	100	2.e-05	3.e-01	2.e-02	63/11	86	6.e-04	1.e-01	4.e-01
SFR (M_\odot yr $^{-1}$)	149/16	80	7.e-12	3.e-01	2.e-03	149/16	87	4.e-05	5.e-01	4.e-11	74/9	101	4.e-05	3.e-01	5.e-03	77/10	94	8.e-04	1.e-01	3.e-01
sSFR (yr $^{-1}$)	77/14	68	2.e-10	1.e-01	3.e-01	77/14	18	1.e-02	2.e-01	7.e-02	48/7	87	8.e-04	-1.e-01	4.e-01	51/8	92	4.e-04	-1.e-01	4.e-01
[X/H]	134/9	115	3.e-08	-8.e-02	4.e-01	134/9	104	1.e-05	-6.e-01	7.e-14	65/7	46	2.e-04	-3.e-01	4.e-02	68/7	31	2.e-03	-1.e-01	3.e-01
R_{50} (kpc)	128/24	115	8.e-19	-1.e-01	2.e-01	113/17	147	3.e-06	-2.e-01	7.e-02	74/12	75	2.e-07	5.e-02	7.e-01	79/14	26	6.e-06	8.e-02	5.e-01
R_{off} (kpc)	136/28	104	1.e-20	-5.e-02	6.e-01	124/19	107	2.e-08	-1.e-02	9.e-01	75/15	71	5.e-09	2.e-01	1.e-01	79/17	60	5.e-05	8.e-02	5.e-01
$r_{\text{off}} (= R_{\text{off}}/R_{50})$	117/24	84	9.e-17	9.e-03	9.e-01	106/17	110	4.e-06	9.e-02	4.e-01	65/12	73	3.e-06	2.e-01	1.e-01	69/14	74	1.e-04	-2.e-02	9.e-01
F_{light}	99/20	46	3.e-15	-8.e-02	4.e-01	89/14	62	9.e-07	-4.e-01	4.e-04	55/11	106	4.e-07	-2.e-01	1.e-01	58/13	139	7.e-05	-3.e-01	3.e-02
	$L_{p,\text{iso}}$					$E_{\gamma,\text{iso}}$					f					f_{eff}				
	No.	angle	P_{KS}	ρ_s	P_s	No.	angle	P_{KS}	ρ_s	P_s	No.	angle	P_{KS}	ρ_s	P_s	No.	angle	P_{KS}	ρ_s	P_s
$M_*(M_\odot)$	100/22	169	1.e-02	2.e-01	2.e-02	101/22	102	1.e-07	3.e-01	2.e-03	49/19	84	1.e-03	-3.e-01	3.e-02	48/19	75	6.e-11	-4.e-01	6.e-03
SFR (M_\odot yr $^{-1}$)	147/16	158	9.e-03	3.e-01	1.e-03	149/16	103	6.e-06	4.e-01	8.e-06	87/14	98	3.e-05	-3.e-01	3.e-03	83/14	90	2.e-10	-4.e-01	4.e-04
sSFR (yr $^{-1}$)	76/14	6	1.e-02	5.e-02	7.e-01	77/14	78	2.e-04	9.e-02	4.e-01	37/12	112	2.e-02	-1.e-01	4.e-01	36/12	101	1.e-07	-3.e-01	9.e-02
[X/H]	134/9	1	3.e-04	-4.e-01	4.e-07	134/9	113	5.e-06	-4.e-01	2.e-06	81/7	51	4.e-06	-6.e-02	6.e-01	74/7	30	1.e-06	-5.e-02	7.e-01
R_{50} (kpc)	126/23	173	1.e-05	-4.e-02	7.e-01	128/23	137	5.e-10	-8.e-02	4.e-01	62/20	20	4.e-05	6.e-02	7.e-01	59/20	87	4.e-12	4.e-02	8.e-01
R_{off} (kpc)	134/27	166	3.e-06	6.e-02	5.e-01	136/27	111	1.e-11	3.e-02	7.e-01	73/24	71	1.e-06	-2.e-02	8.e-01	69/24	86	3.e-14	1.e-01	3.e-01
$r_{\text{off}} (= R_{\text{off}}/R_{50})$	115/23	154	9.e-04	9.e-02	3.e-01	117/23	108	2.e-09	8.e-02	4.e-01	61/20	68	5.e-05	-5.e-02	7.e-01	58/20	84	5.e-12	1.e-01	4.e-01
F_{light}	98/19	7	4.e-05	-2.e-01	1.e-01	99/19	41	7.e-10	-2.e-01	6.e-02	53/16	100	2.e-04	2.e-01	2.e-01	50/16	87	4.e-10	9.e-03	1.e+00

|